EXAMINING THE INTEGRITY OF THE BLOOD-BRAIN BARRIER (BBB) AND THE USE OF LYSOPHOSPHATIDIC ACID (LPA) TO MODULATE THE BARRIER PROPERTIES

By

NGOC H. ON

A Thesis
Submitted to the Faculty of Graduate Studies of
The University of Manitoba
in Partial Fulfillment of the Requirements for the Degree of

DOCTOR OF PHILOSOPHY

Department of Pharmacology and Therapeutics
Faculty of Medicine
University of Manitoba
Winnipeg, MB, Canada

ABSTRACT

INTRODUCTION: The blood brain barrier (BBB), formed by the brain capillary endothelial cells separating the blood from the brain. Furthermore, the brain endothelial cells also express numerous transporter systems which help regulate and maintain the brain microenvironment. The protective function of the BBB and their transporter systems under pathological disease states, including brain tumor, can be an obstacle for the entry of therapeutic agents to the brain.

OBJECTIVES: The current study set out to characterize brain tumor-induced alterations of the BBB of a mouse brain tumor model. Studies were performed to address changes in BBB permeability to P-gp dependent solutes using Rhodamine (R800). Furthermore, the use of lysophosphatidic acid (LPA) to modulate BBB permeability was also examined in healthy mice and tumor-bearing mice.

METHODS: Tumors were induced by injecting Lewis Lung carcinoma (3LL) cells into the right hemisphere of female Balb/c mice. Changes in BBB permeability were assessed at various stages of tumor development, using both gadolinium contrast-enhanced agent (Gad) and ^{3}H-mannitol. Functional activity of P-gp in the BBB was examined in adult mice following i.v. injection of R800 in the presence and absence of GF120918 (a P-gp inhibitor). Alterations in BBB permeability were characterized in healthy and tumor-bearing mice using a small (Gad) and large (IRdye800cw PEG) vascular permeability agent as well as R800 (changes in P-gp mediated permeability).

RESULTS: Median mouse survival following 3LL injection was 17 days. The BBB was largely intact during tumor development with disruptions observed at the later stages of tumor development as indicated by Gad permeability. By inhibiting the function of P-gp with GF120918, the distribution of R800 in the brain increased by 4-fold. The enhancement effect of LPA on BBB permeability occurs within 3-6 minutes of injection with the barrier being restored back to its normal function within 20 minutes. Furthermore, an increased in brain penetration of IRdye800ce PEG and R800 were observed following LPA injection in both healthy and tumo-bearing mice.

CONCLUSION: These studies provide the initial proof of concept for the use of BBB modulators including LPA and GF120918 to enhance drug delivery to the brain and the tumor sites.

ACKNOWLEGEMENTS

I would like to take the opportunity to extend my sincere gratitude to the following of people who have shaped me into the person that I am today:

To my supervisor, Dr. Donald Miller:

Thank you for taking a chance on me. I remembered coming to your lab years ago with no laboratory experience and you were always there providing all the necessary help despite your busy schedule. Your dedication and support for your students is beyond my expectations. Not only you are my 'scientific father' but you will always be one of the most influential people in my life. The experiences in your lab will forever be cherished in my memory. Once again, thank you for your patience, encouragements, and the wonderful years in your lab.

To my committee members, Dr. Fiona Parkinson, Dr. David Eisenstat, and Dr. James Peeling:

Thank you for your thoughtful inputs to make this project a complete success. I would also like to extend my appreciation for all the time you've spent on writing my reference letters.

To the Pharmacology & Therapeutics staff members:

I would like to express my gratitude to all the staff members in our department for helping me throughout the years. Your knowledge and wisdom will forever be with me.

To all the teachers that I've encountered from elementary to high school:

Thank you for your wisdom, knowledge, and above all, challenging me to reach my potentials.

To my friends and lab mates:

Thank you for your moral support, companionship and making the lab environment more enjoyable through your gossips. Special thank to a special friend (EM) for always being there listening to my problems, and making sure that I got home safely from my late nights at school.

To my family in Vietnam (especially my Grandma and my Aunt):

Thank you for your support and encouragement. Although we are separated by thousands of miles, your undying love provided me the courage and motivation to pursue my dreams.

To my mother, the most important person in my life:

Words cannot express how much you mean to me. Thank you for not given up on me and taking a chance in life so that I could have the opportunity to achieve my dreams. You are always there for me, believing in me, and supporting my decisions. You taught me the importance of higher education and encouraged me to pursue my dreams. Thank you for helping me get where I am today.

To the funding agency:

I would also like to acknowledge The Manitoba Health Research Council (MHRC) for providing me with financial support over the last 4 years.

Dedicated to

my mother…..

"There are only two mistakes one can make along the road to truth; not going all the way, and not starting."

Buddha

TABLE OF CONTENTS

LIST OF TABLES

LIST OF FIGURES

LIST OF COPYRIGHTED MATERIALS

Balayssac, D., N. Authier, A. Cayre, and F. Coudore. 2005. Does inhibition of P-glycoprotein lead to drug-drug interactions? Toxicology Letters 156 (3) (Apr 28): 319-29.
Permission obtained from Elsevier License (August 14, 2012).

On, N. H., F. Chen, M. Hinton, and D. W. Miller. 2011. Assessment of P-glycoprotein activity in the blood-brain barrier (BBB) using near infrared fluorescence (NIRF) imaging techniques. Pharmaceutical Research (May 20).
Permission obtained from Springer License (August 14, 2012).

LIST OF ABBREVIATIONS

A-B	Apical to Basolateral
AB	Assay Buffer
ABC	ATP-Binding Cassette
ATP	Adenosine Triphosphate
B-A	Basolateral to Apical
BBB	Blood-Brain Barrier
BBS	Brain Buffer Solution
BCRP	Breast Cancer-Resistance Protein
BCSFB	Blood Cerebral Spinal Fluid Barrier
BMEC	Brain Microvessel Endothelial Cells
BSA	Bovine Serum Albumin
BTB	Blood-Tumor Barrier
C1P	Ceramide-1-Phosphate
CNS	Central Nervous System
CSF	Cerebral Spinal Fluid
CVO	Circumventricular Organs
DMEM	Dulbecco's Modified Eagle's Medium
DMSO	Dimethyl Sulfoxide
ECM	Extracellular Matrix
EDG	Endothelial Differentiation Gene
ER	Efflux Ratio
FBS	Fetal Bovine SerumFDX
FDX	Fluorescence Dextran

FOV	Field of View
Gad	Gadolinium Contrast Enhanced-Agent
GFAP	Glial Fibrillary Acidic Protein
GF120918	Elacridor
G.I	Gastrointestinal Tract
GLUT	Glucose Transporter Proteins
GPCR	G-Protein Coupled Receptor
GSH	Reduced Gluthathione
HBMEC	Human Brain Microvessel Endothelial Cell
H & E	Hematoxylin and Eosin
HER-2	Epidermal Growth Factor Receptor-2
HRP	Horse Radish Peroxidase
IACUC	Institutional Animal Care and Use Committee
JAM	Junctional Adhesion Molecules
3LL	Lewis Lung Carcinoma Cells
LPA	Lysophosphatidic Acid
LPAR	Lysophosphatidic Acid Receptors
LPP	Lipid Phosphate Phosphatase
MCT	Monocarboxylate Transporter
MDCK	Madin-Darby Canine Kidney Epithelial Cells
PAC	Paclitaxel
MRI	Magnetic Resonance Imaging
MRP	Multidrug-Resistance-Associated Proteins
NIRF	Near Infrared Fluorescence Imaging
OATP	Organic Anion Transporting Polypeptide

OAT	Organic Anion Transporter
PA	Pilocytic Astrocytoma
PBS	Phosphate Buffer Saline
PBT	Primary Brain Tumor
PEG	Poly(ethylene) Glycol
PET	Positron Emission Tomography
P-gp	P-glycoprotein
PVDF	Polyvinylidene Fluoride
ROI	Regions of Interest
R123	Rhodamine123
R800	Rhodamine800
RT-PCR	Real-Time Polymerase Chain Reaction
S1P	Sphingosine-1-Phosphate
SDS	Sodium Dodecyl Sulfate
SGLT	Sodium Glucose Cotransporter
SLC	Solute Carrier
SLCO	Solute Carrier Organic Anion Transporter Family
TAT	T-Type Amino Acid Transporter
TER	Transcellular Electrical Resistance
VE	Vascular Endothelial
VZG-1	Ventricular Zone-1
WBRT	Whole-Brain Radiotherapy
WHO	World Health Organization
WT	Wild-Type
ZO	Zonula Occludens

CHAPTER 1: THE PHYSICAL AND ANATOMICAL STRUCTURES OF THE BLOOD-BRAIN BARRIER (BBB) AND POTENTIAL IMPACT ON BRAIN TUMOR TREATMENT.

1.1. Introduction

Brain tumors are defined as a collection of neoplasms resulting from uncontrolled growth of cells in the brain. While each neoplasm has its own distinct biology, brain tumors are generally classified as either primary or secondary (metastatic) tumors based on the origin of the transformed cell. Within primary brain tumors, further classification also exists based on general locations, with intracranial tumors being defined as tumors that arise from the brain tissues, while extracranial tumors, including meningioma and lymphoma, are defined as tumors that originate from non-brain tissue. For most intracranial tumors, the clinical presentation, diagnosis, and treatment approach are similar (DeAngelis LM 2001, 114). The neurological symptoms of brain tumors can be classified as focal or generalized. Generalized symptoms consist of headache, although nausea and vomiting are also common when the tumor reaches its final stage reflecting the increase in intracranial pressure. Focal symptoms are defined by the intracranial locations of the tumors which usually include hemiparesis and aphasias. Generally, magnetic resonance imaging and computed tomography are employed for clinical diagnosis of brain tumor. Once the diagnosis is made, the treatment options included surgery, radiation, and chemotherapy (DeAngelis LM 2001, 114). The poor prognosis for both primary and metastatic brain tumors underlies the need for more effective treatment strategies for this disease.

1.1.1. Primary brain tumors:

Recent statistics estimate that roughly 52,000 new cases of primary brain tumors (PBT) are diagnosed in America each year (Vargo 2011, S50-62). Some of these tumors are benign (noncancerous), and can usually be removed with minimal risk of re-occurence. In contrast, malignant brain tumors, which are often difficult to completely remove and have a high rate of re-occurence, interfere with the vital functions of the brain, ultimately resulting in death. The

incidence of malignant PBT is slightly lower than that of benign PBT, with an occurrence rate of 6 and 9 per 100,000 people, respectively. The overall incidence of PBT is slighter higher in females than males with 17.2/100,000 vs 15.8/100,000. However, malignant PBT occurs more often in men than women at a rate of 7.6/100,000 vs 5.4/100,000 (Vargo 2011, S50-62). Primary tumors can form in almost any type of tissue or cell within the brain. The tumors are named after the type of cell that they originated from (Table 1.1 provides a histological classification of primary tumors). The prevalence of the various types of PBT vary as a function of age with embryonal or primitive neuroectodermal, and low grade glioma being the most common in children, while meningioma and malignant glioma being the most common among adults.

Primitive neuroectodermal (embryonal) tumors are referred to as small cell malignant neoplasms of the central nervous system (CNS). One of the most common and extensively studied CNS embryonal tumors is medulloblastoma. Medulloblastoma is considered as one of the most common tumors in children under the age of 15 with an estimated incidence of 0.5 per 100,000 children being affected (Vogel and Fuller 2003, 387-398). It is a malignant tumor originating in the cerebellum. There are several subtypes of medulloblastoma classified based on the morphologic pattern of the cells. In addition to the original medulloblastoma which consists of Homer Wright Rosettes and enfilades, the World Health Organization (WHO) recognizes four additional variants of medulloblastoma based on their morphological appearances and patterns. These include desmoplastic medulloblastoma, large-cell or anaplastic medulloblastoma, melanotic medulloblastoma, and medullomyoblastoma (Vogel and Fuller 2003, 387-398). Another common PBT that occurs in children is low grade glioma. Pediatric low grade gliomas can be further subclassified based on their localization and histological subtypes (Pfister, Hartmann, and Korshunov 2009, 1375-1386). One of the most common childhood

gliomas is pilocytic astrocytoma (PA) occurring at a rate of 15-20% of all brain tumors in children. The WHO has considered PA as a low grade (grade I) glioma due to their noninfiltrative properties, and circumscribed and benign appearances. They usually have a very favorable prognosis with 10- year survival rates of 96% (Pfister, Hartmann, and Korshunov 2009, 1375-1386). Cyst formation is also common in these tumors and is often used as a diagnostic feature. They are typically found in the cerebellar hemisphere, but on some occasions, they can also be localized in the hypothalamic/optic pathways, thalamic region, cerebral hemispheres, brainstem, and spinal cord (Pfister, Hartmann, and Korshunov 2009, 1375-1386). PA tumor cells show biphasic, piloid patterns containing histopathological markers such as Rosenthal fibers and eosinophilic granular bodies/proteins.

Meningiomas are usually benign tumors that originated from arachnoid cap cells. These cells form the outer lining of the arachnoid membrane (Bertalanffy et al. 2006, 30-35). Meningiomas are considered to be the second most common primary brain tumor in adults, and account for 13.4 to 40% of all extracranial tumors (Bertalanffy et al. 2006, 30-35). These tumors affect roughly 4 people per 100,000 per year with the median age at diagnosis being approximately 63 years-old. Approximately 80% of all meningiomas are considered to be benign; however, the clinical progression of the disease can be difficult to predict due to recurrence of the disease despite complete surgical resection. The main cause for the recurrence is unknown; however, it has been speculated that the presence of a microscopic amounts of the tumor foci left behind after resection of the tumor mass re-establishes the tumor growth (Mawrin and Perry 2010, 379-391). The remaining 20% of meningiomas are considered malignant and are comprised of both atypical and anaplastic high grade meningiomas. These tumors are more aggressive and are associated with higher morbidity and mortality. Atypical meningioma is

considered a grade II tumor according to the WHO classification system with considerably higher risk of recurrence than benign meningiomas (approximately 8-fold). Furthermore, mortality rate for atypical meningioma is also higher compared to age and sex matched controls (Mawrin and Perry 2010, 379-391). The more severe form of meningioma (WHO grade III) is anaplastic meningioma which, although less frequent in occurrence, has a much higher risk of death with reported average survival rates of less than 2 years (Mawrin and Perry 2010, 379-391).

Malignant gliomas are the most common primary brain tumors in adults, with glioblastoma multiforme being the most prevalent and most aggressive, accounting for roughly 51.4% of all malignant gliomas (Preusser et al. 2011, 9-21). The infiltrative and aggressive nature of glioblastoma corresponds to grade IV astrocytoma which is the highest grade and most aggressive PBT in accordance to the WHO criteria. The annual diagnosed incidence of glioblastoma is approximately 3-5 people per 100,000 with higher occurrences in the European population than the African and Asian population (Preusser et al. 2011, 9-21). Glioblastomas can virtually affect anyone regardless of age or sex; however, they are more frequent in the older population with a median age of 64 years. In younger patients (median age 45), secondary glioblastoma (glioblastoma progressed gradually from a lower grade glioma) is more common while children are rarely affected by glioblastoma. The overall median survival rate for patients with glioblastoma is only 15 months; however aggressive therapy and supportive care can extend the survival rate to 22 months (Preusser et al. 2011, 9-21). The etiology of glioblastoma is largely unknown; however there are established risk factors including exposure to high doses of radiation and genetic predisposition enhances the risk of glioblastoma. Furthermore, several studies also indicated that neural stem or progenitor cells can initiate malignant gliomas by

enhancing the rate of mutation; thus, more differentiated cell types are less susceptible to these malignant transformations (Preusser et al. 2011, 9-21)

Table 1.1: Classification of primary brain tumors. Adapted from DeAngelis LM 2001, 114.

Neuroepithelial Tissue Tumors	Meningeal Tumors	Primary CNS Lymphomas	Germ Cell Tumors	Tumors of Sellar Region
Astrocytic Tumors *-Astrocytoma* *-Anaplastic astrocytoma* *-Glioblastoma multiforme* *-Pilocytic astrocytoma* *-Pleomorphic xanthoastrocytoma* *-Subependymal giant-cell astrocyma*	Meningioma Hemangiopericytoma Melanocytic tumor Hemangioblastoma		Germinoma Embryonal carcinoma Yolk-sac tumor (endodermal-sinus tumor) Choriocarcinoma Teratoma Mixed-germ-cell tumors	Pituitary adenoma Pituitary carcinoma Craniopharyngioma
Oligodendroglial tumor *-Oligodendroglioma* *-Anaplastic oligodendroglioma*				
Mixed Gliomas *-Oligoastrocytoma* *-Anaplastic oligoastocytoma*				
Ependymal tumors *-Ependymomas* *-Anaplastic ependymoma* *-Myxopapillary ependymoma* *-Subependymoma*				
Choroid Plexus Tumors *-Choroid plexus papilloma* *-Choroid plexus carcinoma*				
Neuronal & Mixed neuronal-glial tumors *-Gangliocytoma* *-Dysembryoplastic neuroepithelial tumor* *-Ganglioglioma* *-Anaplastic ganglioglioma* *-Central neurocytoma*				
Pineal Parenchymal tumors *-Pineocytoma* *-Pineoblastoma*				
Embryonal tumors -Medulloblastoma -Primitive neuroectodermal tumors				

1.1.2. Metastatic Brain Tumors:

Metastatic brain tumors, also known as secondary brain tumors, originate from systemic organs and migrate to sites within the brain. The incidence of metastatic brain tumors in adults is significantly higher than that of primary tumors (approximately 10 times higher). About 10-16% of cancer patients will eventually develop brain metastasis during the course of the disease (Walbert and Gilbert 2009, 299-306). The incidence of metastatic brain tumors varies substantially depending on the primary site of the cancer. For instance, lung, breast, and skin cancer have the highest incidence of brain metastasis, while cancers at other sites, such as the prostate, stomach, liver and ovary rarely metastasize to the brain (Giglio and Gilbert 2010, 50-59; Kamar and Posner 2010, 217-235). Furthermore, even among those tumors most likely to metastasize to the brain, there can be substantial differences in metastatic potential. For example, non small-cell lung carcinoma (NSCLC) is more likely to metastasize to the brain than small-cell lung carcinoma (SCLC) (Postmus and Smit 1999, 753-759). Similarly, a higher incidence of brain metastasis are more likely to develop among those breast cancer patients whose tumors overexpress human epidermal growth factor receptor 2 (HER-2) compared to patients whose breast tumors are HER-2 negative (Kamar and Posner 2010, 217-235). For metastasis to occur, the tumor cells have to leave the primary tumor sites by migrating through the basement membrane and then through the endothelial cells in order to enter the circulation. Within the circulation, the cells must evade the immune system and resist sheer physical stress of the circulation system and eventually stop at the distal organs. At the distal organ (secondary organs) the cells must exit the circulation system and cope with the stress of new, hostile environments, proliferate, and successfully grow into the metastatic lesion (Steeg and Theodorescu 2008, 206-219). In 1889, Stephan Paget formulated the seed and soil hypothesis

for tumor metastasis. The seed and soil hypothesis suggests that the occurrence of tumors at secondary sites is dependent not only on the tumor cells ("seed") but also on the proper microenvironment of the secondary sites ("soil") (Mendoza and Khanna 2009, 1452-1462). The specific site of the second metastasis is determined by the interaction between the tumor cells and the local microenvironment rather than the anatomical location of the primary site relative to the secondary sites (Mendoza and Khanna 2009, 1452-1462).

Despite the differences in the origin of the primary tumors, once the cancer cells metastasize to the brain, the prognosis is similar. The median survival for metastatic brain tumor patients is only 2.7 months. Even choosing the best cohort, those with controlled systemic disease, early detection and 65 year-old or younger, the median survival is only 7 months (Viani et al. 2007, 53). Furthermore, the incidence of metastatic brain tumor will increase over time due to more effective systemic treatments which result in longer overall survival for these patients (Walbert and Gilbert 2009, 229-306). Factor in the likelihood of increased incidence of metastatic; there is a clear need for improved treatment strategies to enhance not only survival time but also quality of life of patients with metastatic brain tumors.

1.2. Diagnosis and Treatment of Brain Tumors:

The primary diagnostic technique used in suspected cases of neurological diseases including brain tumors is magnetic resonance imaging (MRI) both with and without contrast enhanced agent to establish the initial lesion (Kamar and Posner 2010, 217-235). Contrast agents are used with MRI to enhance the visualization of internal organs. Gadolinium-based compounds are the most commonly employed for this purpose. They enhance the visualization of the images by altering the relaxation time of the tissues and the body cavities where they are present. They accomplish this through the shortening of the T1 relaxation time of the nearby

protons causing an increase rate of emission from a high energy state to a low energy state. The contrast agents can be administered systemically or orally depending on the organ of interest. Oral administration is useful for gastrointestinal (G.I) tract scanning while intravascular administration is helpful for imaging other organs. Not all contrast-enhancing lesions indicate metastatic brain tumors (Kamar and Posner 2010, 217-235). If subsequent concerns about the diagnoses are raised, then stereotatic needle biopsy can be considered to reveal additional information about the tumor.

Treatment strategies for metastatic brain tumors depend on the size of the tumor, number of metastases and the location within the brain (Carrubba and Vitaz 2009, 707-711). Patients with one, two or three lesions that are less than 3 cm in size are more suited to focal therapy such as surgery or stereotactic radiosurgery. Basal ganglia and cerebellar metastasis in particular are ideal candidates for radiosurgery (Kamar and Posner 2010, 217-235). Larger tumors and/or multiple metastatic sites are ideally treated with whole-brain radiation therapy. Other factors including the age of the patient, performance status (scoring systems used to quantify the general well-being and daily life of cancer patients in order to determine if chemotherapy is suitable or dosage adjustment is required), clinical symptoms, and the extent of the disease can significantly determine the type of treatment a patient receives (Elaimy et al. 2011, 69). Another factor to consider when designing options for treating metastatic brain tumors is histology of the tumors. This histological history of the tumor cells includes such things as morphology, and sensitivity to radiation and chemotherapy at the primary tumor site. Histological examination of the tumor can provide information concerning the sensitivity of the tumor to radiation and chemotherapeutic agents. As tumors arising from the same organ can metastasize differently in the brain with respect to location, histological evaluation can also

provide potential clues as to where lesions will most likely occur in the brain. Thus histological factors can be used to guide treatment options (Kamar and Posner 2010, 217-235).

Due to the variation of factors that can impact on treatment response, it has been suggested that the treatment for each patient should be individualized. Recursive partitioning analysis (RPA) has been formulated based on the pretreatment prognostic characteristics and treatment related variables in order to decide the appropriateness of the treatment (Gaspar et al. 1997, 745-751). Recursive partitioning analysis is a statistical method that examines multiple variables to create a predictive model from which a treatment decision tree can be created. Recursive partitioning methods have become popular and widely applicable tools for non-parametric regression and classification in many scientific fields. In the case of brain tumors, highly technical and invasive surgery has been associated with improved intracranial control and survival rate; however, it is unclear if these results are attributed to therapy alone or due to the process of patient selection. Recursive partitioning analysis has confirmed performance status and active extracranial disease as major indicators of outcome following the treatments (Gaspar et al. 1997, 745-751).

Implementation of local treatment strategies including surgery, radiosurgery, as well as whole-brain radiotherapy (WBRT) are effective to control local tumor, and reduce the risk of neurological death (Peereboom 2005, S54-65; discusssion S1-4). However, despite significant advances, many of these techniques are still very limited in their ability to influence survival. For example, the average survival time for patients with no treatment is only one month, while treatment with WBRT extends survival to four months and combining WBRT with local therapy results in a maximum of 10 months. If these treatment options fail or are not applicable, then chemotherapy is the next line of treatment for brain tumors (Cruz-Munoz and Kerbel 2011, 123-

130). There are several chemotherapeutic agents that have activity against systemic cancers that are known to metastasize to the brain. However, systemic use of chemotherapeutic agents to treat metastatic brain tumor has produced limited therapeutic responses. Many of the current therapeutic agents with activity against primary systemic tumors are large, water-soluble molecules that have poor blood brain barrier (BBB) penetration (Table 1.2 from (Peereboom 2005, S54-65; discusssion S1-4). Thus, therapeutic drug concentration in the brain might be difficult to achieve using standard delivery methods (Peereboom 2005, S54-65; discusssion S1-4). A number of chemotherapeutic drugs (roughly 2%) that are small in size (MW < 400 Da) with high lipid solubility have also been used to control brain metastases of certain histologies with little to no success (Table1.3 from (Peereboom 2005, S54-65; discusssion S1-4)). This too may be attributable to poor BBB penetration due to active efflux transporters expressed within the endothelial cells of the BBB.

The role of the BBB in the limited effectiveness of chemotherapeutic agents in treating brain tumors is a topic of considerable debate. Conventional wisdom was that the BBB within the tumor region (also known as blood-tumor barrier (BTB)) is disrupted and permeable to agents that would otherwise be unable to penetrate (Stewart 1994, 121-139). However, experimental data from our laboratory suggested that this disruption only occurred at the intermediate and late stages of tumor development when the tumor size is large. During the initial stage of tumor growth, the BBB was still intact and capable of limiting drug penetration into the brain and tumor sites. Even when the BBB is compromised in the intermediate and late stages of tumor growth, the majority of the disruption is localized at the center of the tumor while the periphery of the tumor is virtually impermeable resulting in subtherapeutic doses of drugs delivered to tissues surrounding the tumors. Along with this subtherapeutic drug delivery

is a net movement of drug down its concentration gradient from areas of the tumor, where drug concentrations are high, to normal brain tissue, where drug concentrations are low. In this regard, the normal brain tissue and the cerebrospinal fluid can act to effectively remove the drugs from the tumor region in a process known as the “sink” effect, thus reducing the amount of drug available at the tumor site.

An additional factor influencing chemotherapeutic drug concentrations in the brain and brain tumor is the presence of influx and efflux transporters within the BBB. In fact, the presence of efflux transporter such as P-glycoprotein (P-gp) in the BBB can reduce the accumulation of drugs in the brain. *In vitro* studies studies using the Madin-Darby Canine Kidney multidrug resistance (MDCK MDR) cell line and as well as *ex vivo* using near infrared fluorescence imaging techniques, have shown that the presence of functional P-gp reduces the accumulation of their substrates in the brain by 4-fold (On et al. 2011). If the chemotherapeutic drug happens to be a substrate for efflux transporters within the brain, then its accumulation in the brain will be significantly reduced. Clearly, both the physiological and the anatomical properties of the BBB play a critical role in the accumulation and distribution of drugs in the brain. Therapeutic doses of drugs can be achieved within the brain and tumor regions when the properties of the barrier are modified resulting in better tumor response.

Table 1.2: Chemotherapeutic agents used to treat systemic cancers that are known to metastasize to the brain. Adapted from Peereboom 2005, S54-65; discusssion S1-4.

Breast	Small cell lung cancer	Non-small cell lung cancer	Melanoma
Doxorubicin	Paclitaxel	Cisplatin	Dacarbazine
Epirubicin	Docetaxel	Carboplatin	Temozolomide
Paclitaxel	Gemcitabine	Paclitaxel	Interleukin-2
Docetaxel	Vinorelbine	Docetaxel	Combination Therapy
Capecitabine	Etoposide	Vinorelbine	
Vinorelbine	Ifosfamide	Etoposide	
Gemcitabine	Cyclophosphamide	Irinotecan	
Trastuzumab	Topotecan	Gemcitabine	
Combination therapy	Irinotecan	Vinblastine	
	Combination Therapy	Mitomycin	
		Ifosfamide	
		Pemetrexed	
		Gefitinib	
		Erlotinib	
		Combination Therapy	

Table 1.3: Permeability of chemotherapeutic agents in brain capillary. Adapted from Peereboom 2005, S54-65; discusssion S1-4.

High	Intermediate	Low
Nimustine	Temozolomide	Doxorubicin
Carmustine	Cytarabine	Vincristine
Lomustine	Topotecan	Taxanes
Procarbazine	Hydroxyurea	Gemcitabine
Thiotepa	Etoposide/Tenoposide	
	Cisplatin/Carboplatin	
	Irinotecan	
	Bleomycin	
	Methotrexate	

1.3. Blood-Brain Barrier (BBB)

1.3.1. Discovery of Blood-Brain Barrier:

The discovery of the barrier separating the blood from the brain began over a century ago during the late 1880s when Paul Ehrlich systemically injected trypan blue into an animal and discovered that virtually all the organs were stained with the dye except the brain and spinal cord ((Ehrlich Paul 1885, 69-72). Ehrlich originally attributed these findings to a lack of brain tissue affinity for the dye. However, one of Ehrlich's students, Edwin E. Goldmann, injected trypan blue into the cerebrospinal fluid (CSF) and observed that the brain was readily stained with the dye while tissues outside of the brain were virtually unstained. These studies provided the first evidence suggesting that there was a cellular barrier that existed between the blood and the brain (Goldmann EE 1909, 192-265). Interestingly, Goldman initially believed the BBB was localized within the choroid plexus instead of the brain microvasculature. Additional studies performed systemically using variety of compounds provided the evidence for the existence of a discrete barrier separating the blood from the CNS (Stern L. and Gautier R. 1921, 138-192). In these studies, Stern and Gautier systemically injected pharmacologically active substances into cats, dogs, rabbits and guinea pigs, and then qualitatively tested for the presence of the compounds in the CSF after certain time points. From the experiments, they found that substances such as bromide, morphine, and atropine were present in the CSF and induced neurological effects on the animals. On the contrary, substances such as iodide, ferrocyanide, salicylate, epinephrine, and fluorescein did not accumulate in the CSF. However, these substances were able to induce neurological effects when injected directly into the subarachnoid space of the brain. Based on the studies, they concluded that there was a barrier

separating the blood from the brain and that this barrier restricted the movement of substances into and out of the brain.

Though these studies helped established the existence of an anatomical barrier separating the blood and brain extracellular environment, the exact cellular structure(s) responsible for the formation of the barrier had not been identified. It was postulated that either the capillary endothelial cells or the perivascular astrocytic foot processes that surrounded the brain capillaries formed the anatomical structures of the BBB. The advancement of the electron microscope provided the resolution required to make the distinction. Using horseradish peroxidase (an electron dense protein with molecular weight of 40 KDa) as a macromolecular tracer, Reese found that the protein was virtually impermeable to the tight junction of the endothelial cells. These studies provided evidence that the endothelial cells within the capillaries of the brain provided the cellular barrier to solute entry into the brain (Reese and Karnovsky 1967, 207-217). It should be noted that while the vast majority of the brain capillaries have reduced permeability, there are localized areas within the brain where capillary permeability is not as restricted (Ueno 2007, 1199-1206). The circumventricular organs (CVO) found in near the third and fourth ventricle region of the brain have endocrine functions secreting hormones into the blood stream that influence peripheral tissue responses (Ueno 2007, 1199-1206). Unlike other regions of the brain, the capillaries lining the CVOs are more permeable allowing diffusion of hormones and other macromolecules into the bloodstream. The other capillaries within the brain that have no barrier function are the fenestrated capillaries within the choroid plexus (Vorbrodt and Dobrogowska 2003, 221-242). The choroid plexus is made of extensive network of capillaries which is surrounded by a single layer of epithelial cells forming the blood cerebral spinal fluid barrier (BCSFB) and is involved in the

production and secretion of CSF (Wolburg and Paulus 2010, 75-88). The complex junctions of the BBB and the BCSFB play an essential role in protecting the brain from xenobiotic substances; however, under pathological conditions, these protective barriers can be an obstacle for the pharmacological treatments of CNS disorders.

1.3.2. Physiology and Anatomy of the Blood-Brain Barrier:

At the cellular level, the BBB is formed by the continuous endothelial cells, associated astrocytic foot processes and a sparse scattering of pericytes as shown in Figure 1.1. The brain endothelial cells with their tight junctions and adherens junctions, low pinocytic activity and absence of fenestrations provide the physical cellular barrier (Reese and Karnovsky 1967, 207-217). Under normal conditions, the tight junctional complex formed between the brain capillary endothelial cells prevents the paracellular diffusion of water-soluble molecules between the blood and the brain. These morphological properties result in a capillary bed with low permeability to hydrophilic compounds. Indeed, hydrophilic compounds with molecular weights greater than 600 Da are generally considered to have little appreciable paracellular diffusion in the BBB (Banks 2009, S3).

The brain vascular endothelium is surrounded by a layer of astrocytic endfoot processes which also contribute to the restrictive nature of the barrier (Abbott 2002, 629-638). Although the astrocytes themselves do not physically restrict the passage of solutes in the BBB, they contribute to the barrier properties by releasing various growth factors that either tighten or loosen the BBB. This was elegantly demonstrated in the studies of Stewart and Wiley in which an avascular fragment of young quail brain was transplanted into coelomic cavities of a 3-day old chick embryo. After 18 days of incubation, the capillaries formed in the grafted brain tissue consisted of endothelial cells linked by tight junctions. Furthermore, these cells also had high

mitochondria densities and few pinocytic vesicles (Stewart and Wiley 1981, 183-192). These studies convincingly demonstrated the importance of the brain microenvironment in the formation of the BBB and the importance of astrocytic cells on the differentiation and development of BBB phenotypes. The inductive factors that mediate the interactions between endothelial and astroglial cells are still unknown (Haseloff et al. 2005, 25-39). However, it has been speculated that these inductive factors are small in size since each has to diffuse through a basement membrane at the capillaries and venules ends. Closely associated with the abluminal surface of the capillary basement membrane are the pericyte cells. The precise function of pericytes is not fully known, but studies suggest that the pericytes maintain the integrity of the BBB (Balabanov and Dore-Duffy 1998, 637-644; Kamouchi et al. 2011). Evidence supporting this is the recent tri-culture BBB model consisting of endothelial cells, astrocytes, and pericytes which produced significantly higher transendothelial electrical resistance as compared to models incorporating endothelial cells and astrocytes (Wilhelm, Fazakas, and Krizbai 2011, 113-128).

The cells that form the BBB are anchored by an extracellular matrix. The extracellular matrix (ECM) within the CNS has unique composition and organization. The extracellular matrix contains little to no fibrous proteins including collegen types I and III and very minute amounts of glycosaminoglycan chains (Engelhardt and Sorokin 2009, 497-511). In fact, the extracellular matrix within the CNS is mainly composed of basement membranes and the meninges (Baeten and Akassoglou 2011). The basement membrane contained in the brain and spinal cord appears thin and tightly interwoven around a protein sheet roughly 20-200nm thick as can be seen under a scanning electron microscope (Baeten and Akassoglou 2011). It also contains laminins, collagen type IV, heparin sulfate proteoglycans, and the nidogens which exist in several isoforms

(Baeten and Akassoglou 2011). These proteins can combine to form biochemically and functionally different basement membranes. Within the neurovascular unit, the basement membrane also contains minor components that contribute to the overall structure and function of the barriers including osteonectin (BM40, SPARC), fibulin 1 and fibulin 2, collagen types VIII, XV, XVIII and thrombospondin 1 and 2 (Timpl 1989, 487-502). There are several receptors found on the basement membrane of the endothelial cells and astrocyte endfeet. These receptors anchor the cell layers to their respective basement membrane and provide a physical link between the ECM and cytoskeleton. Furthermore, they also regulate many signal transduction pathways including focal adhesion kinase/c-Jun N-terminal kinases (FAK/JNK), Ras/ERK (MAP kinase), and small GTPases such as Rho, Rac, and CD42, allowing the cells to adapt to changes in microenvironment (Baeten and Akassoglou 2011).

The brain capillaries are structurally and functionally different from capillaries formed in the other organs. At the capillaries and post capillary venules, the selectiveness and permissiveness of the endothelial cell monolayer within the CNS is dependent on the tight junctions that connect adjacent endothelial cells. The tight junctions consist of various adhesion proteins including occludins, claudins and junctional adhesion molecules (JAM) that form a complex transmembrane network within the CNS microvessels (Ueno 2007, 1199-1206). Claudin is a family of integral membrane tight junction proteins with at least 24 members that are vital for the formation of tight junctions in endothelial and epithelial cells. The protein itself is distributed in all tissues; however, both claudin-5 and claudin-3 are specifically expressed within the endothelial cells of the BBB (Wolburg et al. 2003, 586-592). In addition, there are several cytoplasmic proteins such as zonula occludens (ZO)-1 and ZO-2, cingulin, AF-6 and 7H6 proteins which are connected to the actin cytoskeleton and play a crucial role in the formation of the

tight junctions in the brain endothelial cells by linking the integral membrane proteins to the cells (Engelhardt and Sorokin 2009, 497-511; Hawkins and Davis 2005, 173-185).

Brain endothelial cells of the BBB are tightly connected by protein complexes that form tight and adherens junctions (Figure 1.2). The adherens junctions are mainly composed of vascular endothelial (VE)-cadherin proteins which use Ca^{2+} to mediate cell-cell interactions between the extracellular domains of proteins. The cytoplasmic domain of VE-cadherin binds to another protein called β-catenin which in turn binds to the actin cytoskeleton to stabilize the adheren junctions. Vascular endothelial-cadherin is less involved in the regulation of paracellular diffusion of molecules across the BBB; however, it can indirectly regulate permeability of the barrier by inducing the expression of claudin-5 which in turn regulates the diffusion of small molecules across the barrier (Engelhardt and Sorokin 2009, 497-511). Furthermore, the β-catenin from the adheren junction complexes also influences BBB permeability by inducing the expression of claudin-3 (Engelhardt and Sorokin 2009, 497-511). The tight junctions and the adheren junctions are separated by protein molecules including PECAM-1 and CD99. These proteins per se do not participate in maintaining BBB integrity, but are important for the restoration of the barrier properties following injury. In fact, mutations in the PECAM-1 gene did not affect the integrity of the BBB but severely impaired the reanealing process of the barrier under pathological conditions (Graesser et al. 2002, 383-392).

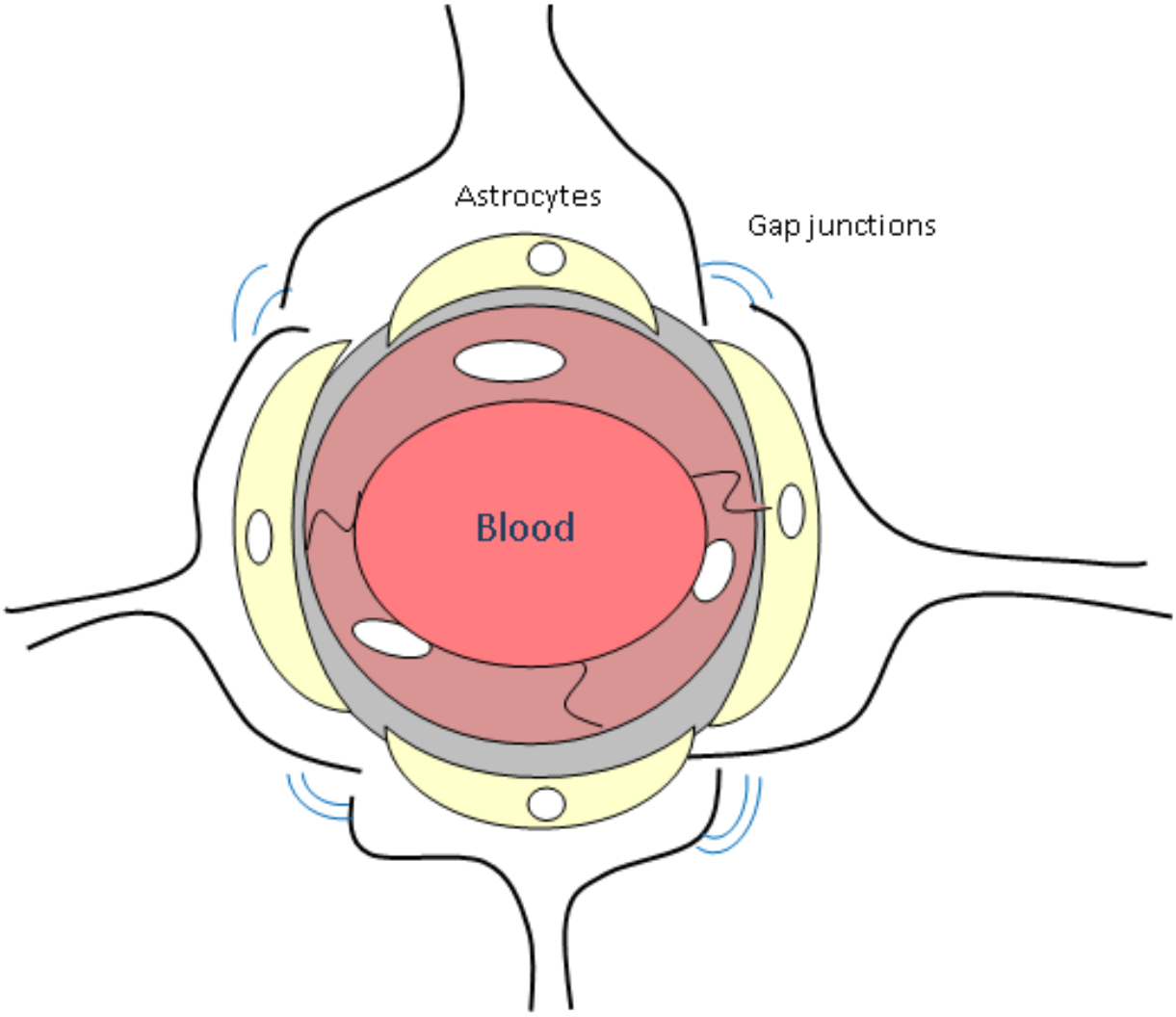

Figure 1.1: Neurovascular Unit of the blood brain barrier consists of the endothelial cells (pink) surrounded by basement membrane (gray), pericytes (yellow) and astrocyte foot processes. The tight junctions (black lines) formed between two endothelial cells restrict the paracellular diffusion of compounds. Adapted from Abbott et al. 2010, 13-25.

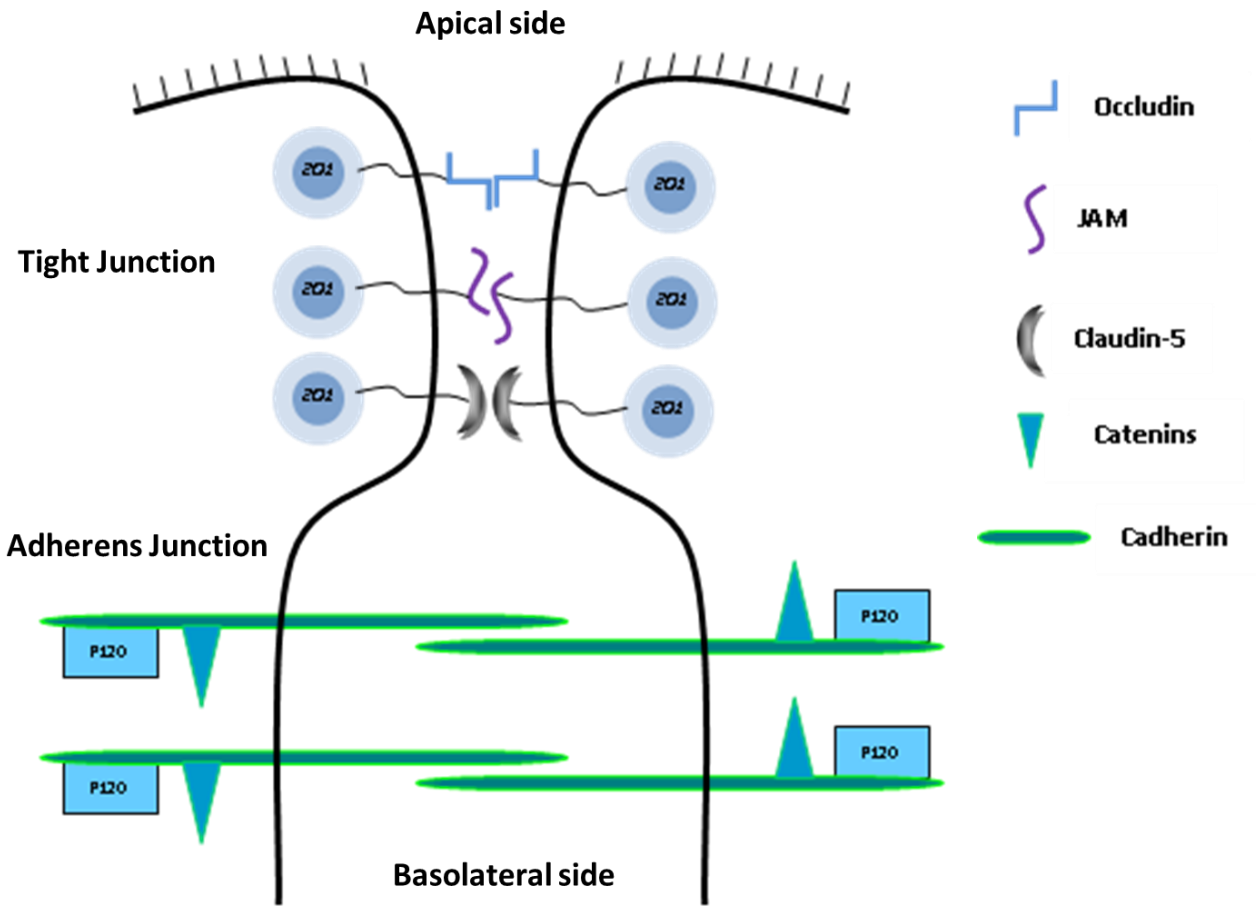

Figure 1.2: Schematic representation of proteins that are involved in the formation of the tight junction and adherens junctions in brain microvessel endothelial cells. Adapted from Abbott et al. 2010, 13-25.

1.4. Blood-Brain Barrier (BBB) Transporters:

The tight junction complex that connects brain microvascular endothelial cells serves as a physical barrier preventing the paracellular diffusion of endogenous and exogenous compounds. The presence of tight junctions is essential for maintaining the proper ion levels in the brain extracellular fluid required for neuronal transmission. However, paracellular diffusion of nutrients and metabolites between the blood and the extracellular compartment of the brain is also highly restricted. Consequently, the uptake of essential molecules, such as glucose and amino acids, to meet the metabolic requirements of the brain occurs through specific transporter proteins located on the plasma membrane of the endothelial cells. In addition to uptake transporters, the brain endothelial cells also express numerous efflux transporters (Hermann and Bassetti 2007, 128-134). Efflux transporters are also expressed in numerous organs including the intestines, liver, kidneys, and the placenta. Many of these transporters are members of the ATP-binding cassette (ABC) protein family. They utilize energy from adenosine triphosphate (ATP) hydrolysis to actively remove compounds from the cells against a concentration gradient. In terms of cancer therapy, efflux transporters in the endothelial cells can significantly reduce the accumulation of chemotherapeutic drugs in the brain, further reducing the amount of drugs in the brain and brain tumor sites. Factors influencing the BBB permeability of drugs include physiochemical properties of the drugs such as charge, lipophilicity, molecular weight, as well as potential transport via uptake and efflux transporters with the endothelial cells of the BBB (Pajouhesh and Lenz 2005, 541-553). From a drug transport perspective, the organic anion-transporting polypeptide 1A2 (OATP1A2/SLO1A2), organic anion transporter 3 (OAT3/SLC22A8), monocarboxylate transporter 1 (MCT1/SLC16A1), P-glycoprotein (P-gp; MDR1/ABCB1), breast-cancer-resistance protein (BCRP/ABCG2) and multidrug-resistance-

associated proteins 1-9(MRP1-9/ABCC1-9) (Urquhart and Kim 2009, 1063-1070) would appear to be critical determinants of brain penetration. The proposed localization of these transporters in both the BBB and BCSF barrier are shown in Figure 1.3. Each individual transporter is discussed in greater detail below.

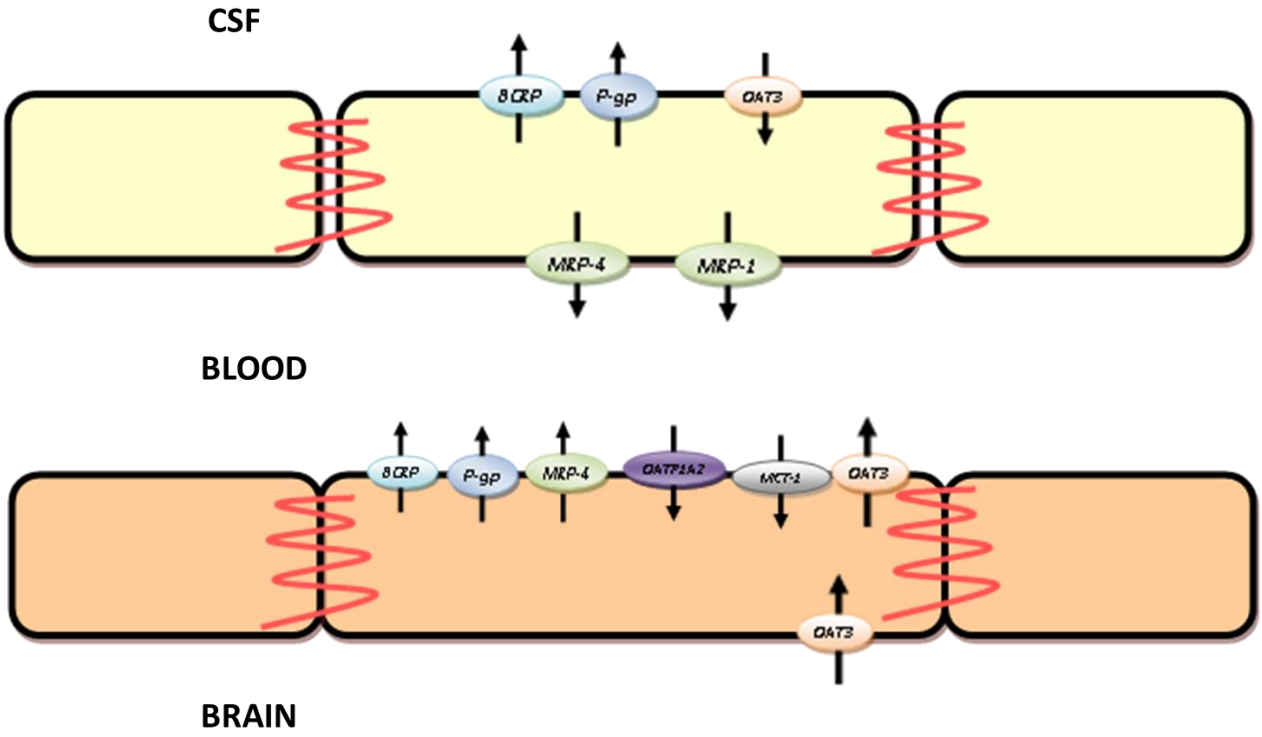

Figure 1.3: The localization of transporters in the blood brain barrier (BBB) and blood cerebral spinal fluid barrier (BCSFB) of CNS. Adapted from Urquhart and Kim 2009, 1063-1070.

1.4.1. Organic Anion Transporting Polypeptide (OATP):

Organic anion transporting polypeptides (OATPs) transport a wide variety of amphipathic organic compounds across the plasma membrane in a sodium independent manner. In addition to some xenobiotics and an increasing number of pharmaceutical drugs, OATPs also mediate the movement of bile salts, anionic peptides, steroid conjugates and thyroid

hormones (Gao et al. 1999, 1255-1264). At the protein level, the nomenclature for the OATPs follows that used for the cytochrome P450 enzymes in which the family grouping is designated by an Arabic numbering system, followed by alphabetical designation of sub-family, followed by the Arabic numbering of the gene product (Hagenbuch and Meier 2004, 653-665). Within the same OATP family there is more than 40% amino acid sequence identity, while OATPs within the same sub-family share at least 60% amino acid sequence identity (Hagenbuch and Meier 2004, 653-665). Genes encoding the various OATPs follow the solute carrier (SLC) nomenclature. Genes within the SLC group include ion-coupled transporters and exchangers (Hagenbuch and Meier 2004, 653-665). There are currently more than 40 different families within the SLC group. The OATPs are members of the solute carrier organic anion transporter family (SLCO) (Meier-Abt, Mokrab, and Mizuguchi 2005, 213-227). SLCO genes contain numerous sequence variations including single nucleotide polymorphisms that can alter the pharmacokinetics of selected drugs through alterations in the activity of the corresponding OATPs (Kalliokoski and Niemi 2009, 693-705).

There are currently 11 different OATPs known to be expressed in humans (OATP1A2, 1B1, 1B3, 1C1, 2A1, 2B1, 3A1, 4A1, 4C1, 5A1, and 6A1) (Hagenbuch and Meier 2004, 653-665). The first discovered human member of the OATP family was OATP1A2 (Kalliokoski and Niemi 2009, 693-705). At the protein level, OATP1A2 (previously designated OATP-A) is expressed in many organs including the liver, intestine, kidney, lung, testes, and the brain. Northern blot analysis indicates a high level of OATP1A2 mRNA in the central nervous system (Kullak-Ublick et al. 1995, 1274-1282). This transporter is localized within the frontal cortex of the brain and specifically confined to the endothelial cells of the BBB (Gao et al. 1999, 1255-1264). The presence of OATP1A2 on the luminal side of the BBB suggests that the brain utilizes this

transporter to allow nutrients and therapeutic drugs to enter the CNS (Gao et al. 1999, 1255-1264).

An additional OATP transporter found within the endothelial cells of the BBB is OATP1A4. OATP1A4 is a homolog of hepatic organic anion transporter OATP1A1. Similar to other OATPs this BBB transporter exhibits broad substrate specificities especially for amphipathic compounds. Furthermore, this transporter is mainly concentrated in both the liver and the brain (Gao et al. 1999, 1255-1264). Rat brain analysis using immunohistochemical staining showed that OATP1A4 is localized on both the apical and basolateral side of the endothelial cells of the BBB and thus, mediates the uptake of compounds from both the brain and the blood compartments (Ose et al. 2010, 168-176). The remaining OATPs are predominantly expressed at non-CNS sites such as the liver and intestinal epithelium.

1.4.2. Organic Anion Transporter (OAT):

Organic anion transporters (OATs) belong to the SLC22A gene family. Similarly to OATPs, OATs transport a broad range of chemically unrelated endogenous and exogenous compounds. There are at least 10 families of OATs designated by Arabic numbers (eg. OAT1). OAT1 is predominantly expressed in the kidney although a very small amount is also found in the brain particularly concentrated in regions such as cortex, hypothalamus, hypocampus and cerebellum (Burckhardt and Burckhardt 2011, 29-104). This transporter is known to interact with a broad range of drugs including antibiotics (penicillins, benzylpenicillin and carbenicillin), antineoplastics (methotrexate) and even cholesterol lowering drugs including the statins and fibrates such as fluvastatin, pravastatin, and bezafibrate, respectively (Burckhardt and Burckhardt 2011, 29-104). OAT2, on the other hand, is predominantly expressed in the liver and very little is found in the kidney and brain. The expression level of this transporter in a particular

tissue can vary between gender and species (Buist et al. 2002, 145-151). For instance, in the adult male rat, the mRNA for OAT2 expression is greater in the liver than the kidney, and the opposite is true for the adult female rat where the mRNA level in the kidney is greater than in the liver (Buist et al. 2002, 145-151). However, this phenomenon has not been observed in humans. Moreover, the expression level of OAT2 is also influenced by hepatocyte nuclear factors and endogenous gas molecules including nitric oxide (Aoki et al. 2008, 1882-1887; Popowski et al. 2005, 1629-1638). Given a similar molecular structure to OAT1, OAT2 also mediates the transport of a broad range of biological and exogenous molecules. For instance, OAT2 also affects the distribution and elimination of cholesterol lowering drugs including statins, antibiotics such as cephalosporins, and antineoplastic drugs like 5-fluorouracil (Burckhardt and Burckhardt 2011, 29-104). From a CNS standpoint, OAT3 appears to be the most important family, with Northern blot analysis indicating OAT3 expression in the kidney, liver, skeletal muscles, adrenal glands, and brain (Burckhardt and Burckhardt 2011, 29-104). Within the CNS, OAT3 is primarily localized in the brain capillaries and epithelial cells of the choroid plexus, specifically on the basolateral side of the plasma membrane of the cells (Kikuchi et al. 2003, 51-58). OAT3 is also inducible with regulation by various endogenous factors such as hepatic nuclear factors, protein kinase C and cyclic AMP being reported (Burckhardt and Burckhardt 2011, 29-104). Furthermore, impairment of kidney or liver functions also affects the expression of OAT3 in their respective locations (Brandoni et al. 2006, 673-682; Villar et al. 2005, 2704-2713). The primary function of OAT3 at the BBB and the choroid plexus is to remove compounds from the brain into the blood stream. In particular, acidic metabolites derived from neurotransmitter and hormone metabolism are the main endogenous compounds that interact with OAT3. Drugs including ACE inhibitors, angiotensin II receptor blockers, and various statins

are known to interact with OAT3 with high affinity. Diuretics and antibiotics bind to OAT3 with moderate affinity, while both quinolones and antiviral drugs bind with low affinity (Burckhardt and Burckhardt 2011, 29-104). As OAT3 interacts with a large number of drugs, it is highly likely that drug-drug interactions may take place during the transport of compounds between the blood and the tissues by competitively binding to OAT3 transporters. The other OATs (OAT4, OAT5, OAT7-OAT10) have little if any expression in the CNS and carry out important elimination processes in the kidney and liver (Burckhardt and Burckhardt 2011, 29-104). Interestingly, OAT6 is found in the nasal epithelia but not in the major organs such as kidney, liver or brain. The exact location within the nasal epithelium is unknown; however, it was postulated that OAT6 is involved in odorant detection (Kaler et al. 2006, 872-876).

1.4.3. Glucose Transporters (GLUT):

Glucose is the major source of energy for most mammalian cells, particularly in the brain. Despite the high dependence of the brain on glycolysis, the source of glucose comes entirely from the blood and is dependent on passage through the BBB. The entry of glucose into the brain is mediated by facilitative glucose transporter proteins (GLUTs) that are integral membrane proteins consisting of seven genes which encode six proteins designated as GLUT1-7 (Vannucci, Maher, and Simpson 1997, 2-21). Each protein consists of a 12 membrane spanning domain with the N-glycosylation site located extracellularly. Sodium glucose cotransporter (SGLT) is another glucose transporter that contributes to nutrient transport across the brain. SGLT, which transports $2Na^+$/glucose cotransporter and is widely expressed in the intestine and kidney epithelial cells. A small population of SGLT is also located in neurons and in brain endothelial cells (Vemula et al. 2009, 487-495). The functional role of SGLT has not been established in the brain; however, it was speculated that SGLT helped maintain intracellular

glucose levels in the brain under stressful conditions such as hypoglycemia (Vemula et al. 2009, 487-495). The main forms of glucose transporters found within the CNS are sodium independent transporters including GLUT1 and GLUT3; however, other isoforms of glucose transporters are also present in small amounts as shown in Figure 1.4 adapted from (Vannucci, Maher, and Simpson 1997, 2-21). The main glucose transporter in the BBB is GLUT1. It is highly expressed in the blood-tissue barrier including the BBB, blood-retinal barrier and the placental barrier, and blood-CSF barrier (BCSFB) (Pardridge 1999, 556-569; Pardridge, Boado, and Farrell 1990, 18035-18040; Farrell, Yang, and Pardridge 1992, 193-199). As the rate limiting step in glucose utilization in the brain, GLUT1 is highly responsive to metabolic changes within the brain. For example, the level of GLUT1 mRNA and protein level can increase or decrease depending on the ambient concentration of hexose. High concentration of hexose decreases the expression of GLUT1 while low hexose concentration causes an up-regulation of both GLUT1 mRNA and protein levels (Klip et al. 1994, 43-53). Following brain injury such as a stroke and brain tumors, both mRNA and protein levels of GLUT1 and GLUT3 in brain are significantly increased (Vannucci, Maher, and Simpson 1997, 2-21; Bondy, Lee, and Zhou 1992, 305-314; Au et al. 1997, 131-135). It has been suggested that both GLUT1 and GLUT3 are responsible for the malignant transformation of tumor cells which is consistent with increased demand of glucose utilization in tumor cells (Au et al. 1997, 131-135). GLUT1 within the CNS exists as two distinct forms which differ only at the extent of glycosylation (Birnbaum, Haspel, and Rosen 1986, 5784-5788). The 55 KDa GLUT1 is found primarily at the in the endothelial cells of the BBB while the non-vascular, non-glycosylated 45 KDa form is mainly found in neural cells as well as the basolateral plasma membrane of epithelial cells isolated from the choroid plexus (Vannucci, Maher, and Simpson 1997, 2-21). Aside from the prominent expression found in the microvessels and choroid plexus,

GLUT1 has also been detected in small cells with dark stained nuclei characteristic of glia cells (Bondy, Lee, and Zhou 1992, 305-314). Immunohistochemistry staining also showed a positive detection of GLUT1 in astrocytes that are in direct contact with the cerebral microvessels of rat brain slices. Electron microscopy also revealed dense distribution of GLUT1 within the astrocyte foot processes surrounding the microvessels of the gray matter and synaptic contacts (Morgello et al. 1995, 43-54).

Unlike GLUT1, GLUT3 is readily detected in non-vascular regions of the cortex. In situ hybridization studies confirmed that GLUT3 is predominantly expressed in neuronal cells. The functional significance of GLUT3 expression in neurons is demonstrated by in vitro studies in primary cultures of granule neurons and cortical neurons in which a direct correlation between GLUT3 expression and neuronal differentiation was observed (Maher 1995, 459-469). An association between regions of high metabolic activity and GLUT3 expression sparks speculation that glucose utilization is correlated with electrical activity in the synaptic terminals. This is consistent with the high cellular energy requirements for the restoration of the electrochemical gradient following neuronal depolarization (Vannucci, Maher, and Simpson 1997, 2-21).

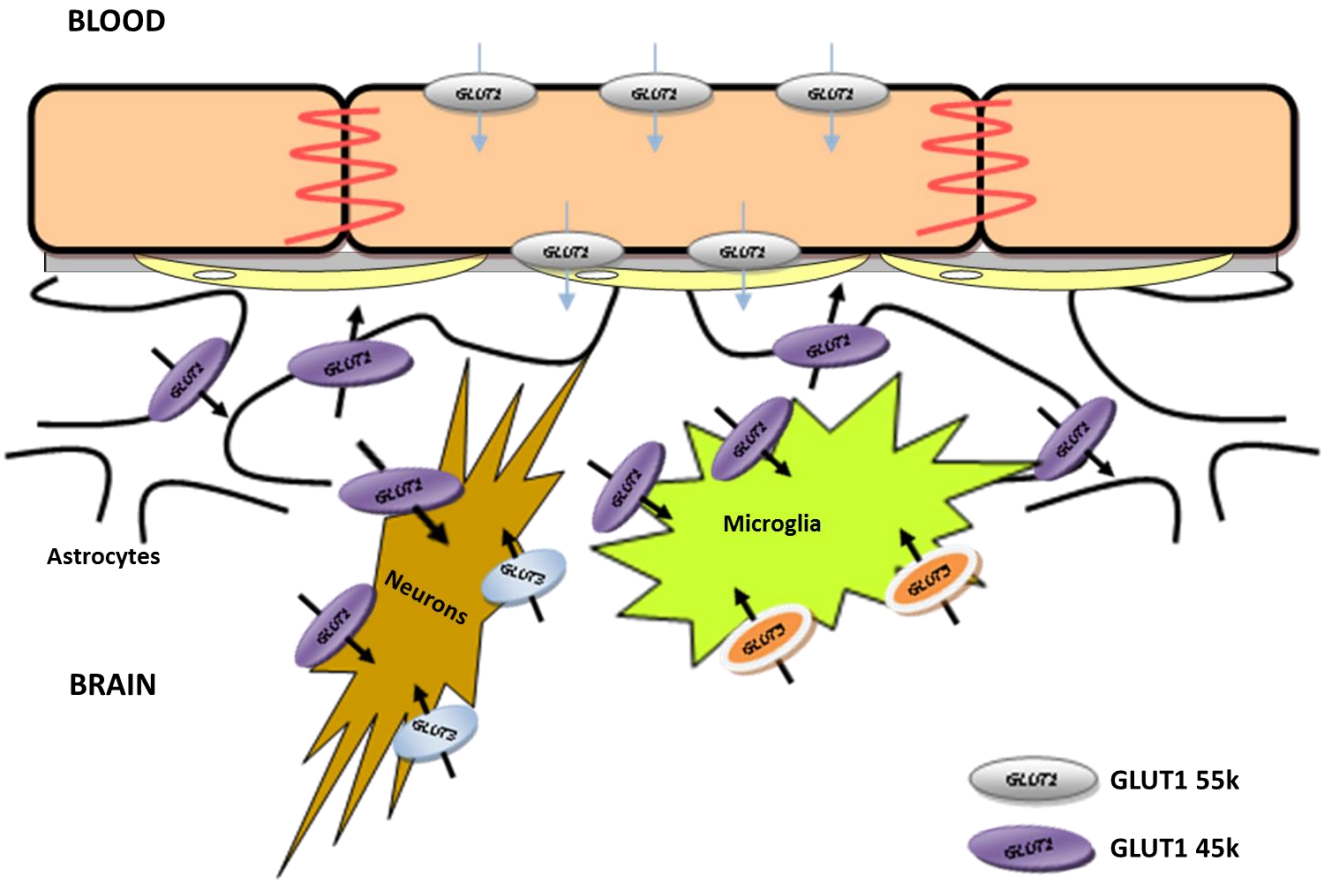

Figure 1.4: Cellular localization of different isoforms of glucose transporter in the CNS. Adapted from Simpson, Carruthers, and Vannucci 2007, 1766-1791.

1.4.4. Monocarboxylate Transporter (MCT):

Monocarboxylic acids, including lactate, pyruvate, and ketones play an important role in energy metabolism within the body. Monocarboxylates such as pyruvates, lactates, and ketone bodies (i.e acetoacetate and β-hydroxybutyarate) can be utilized by neurons, in the absence of glucose, to generate a substantial amount of energy for the brain (Pierre and Pellerin 2005, 1-14). Under pathological and physiological conditions including diabetes, prolonged starvation, hypoglycemia, or even intense exercise, the build-up of lactate provides an energy source which is readily used by the brain (Nybo and Secher 2004, 223-261; Gjedde and Crone 1975, 1165-

1169; Hawkins, Mans, and Davis 1986, E169-78). In addition, monocarboxylates including lactic acid are a metabolic by-product produced and released within the CNS by neurons (Bouzier-Sore et al. 2002, 273-282)(Pellerin 2003, 331-338), astrocytes (Bouzier-Sore et al. 2002, 273-282) and oligodendrocytes (Waniewski and Martin 2004, 209-217). As monocarboxylates are hydrophilic compounds and do not freely cross the BBB, specific transporter systems are required to maintain proper levels of these endogenous metabolic products in the brain (Pierre and Pellerin 2005, 1-14).

Sequence homology indicates that the monocarboxylate transporter family (previous known as SLC16 gene family) consists of 14 members identified as MCT1-9, MCT11-14 and T-type amino acid transporter 1 (TAT1) (Simpson, Carruthers, and Vannucci 2007b, 1766-1791). MCT1-4 is a symporter mediating the co-transport of monocarboxylate and proton in a one to one stoichiometry ratio. Transport is initiated by the binding of the proton followed by the binding of the monocarboxylate, translocation of the monocarboxylate and the proton then occurs across the membrane and finally there is release to the other side of the membrane. The process is reversible with the rate limiting step being the return of the transporter to its original state, then available to bind to another substrate (Pierre and Pellerin 2005, 1-14). MCT1-4 is present in almost all tissues including the muscles, liver, kidney, heart, testes, and brain (Pierre and Pellerin 2005, 1-14; Simpson, Carruthers, and Vannucci 2007a, 1766-1791). MCT1 is found in the muscles, liver, kidney, heart and CNS, while similar localization can be generalized for MCT2 (Pierre and Pellerin 2005, 1-14). MCT3 is exclusively expressed on the basolateral side of the retinal pigment epithelium and MCT4 is highly expressed in the skeletal muscles and also in the brain. Within the CNS, MCT1 was the first monocarboxylic acid transporter identified in the BBB of the endothelial cells and in the ependycytes lining the ventricles (Pierre et al. 2000, 617-627).

Electron microscopy also reveals a small amount of MCT1 in astrocytic end-feet surrounding the capillaries (Leino, Gerhart, and Drewes 1999, 47-54). This was confirmed immunohistochemically using markers such as glial fibrillary acidic protein (GFAP) or S100β (Pierre et al. 2000, 617-627). The presence of MCT1 was found in the cytoplasm of astrocyte and also associated with the plasma membrane (Pierre and Pellerin 2005, 1-14). Conflicting results were generated by separate groups for neuron cells due to different antibodies and species used. Pierred et al 2000 reported that MCT1 was never present in neuron cells of the rat brain whereas Debernardi et al 2003 detected a small amount of MCT1 protein in the mouse cortical brain. In situ hybridization and northern blot analysis revealed the presence of MCT2 in the cortex, hippocampus, and cerebellum of the mouse brain (Vannucci and Simpson 2003, E1127-34). Cultured cortical neurons exhibited MCT2 immunoreactivity at the surface and in the cytoplasm of the cell bodies and neurites, but MCT2 was absent from astrocytes. In fact, MCT2 protein expression was never observed in glial-like cells of the mouse brain, but it was visible in some endothelial cells forming the BBB (Pierre and Pellerin 2005, 1-14; Pierre et al. 2000, 617-627). MCT4, on the other hand, was exclusively expressed in the astrocytes and glial cells of rodent brain. Furthermore, when the hippocampus and the corpus callosum were labeled, the expression of MCT4 was restricted to astrocytes (Pierre and Pellerin 2005, 1-14). MCT8 was recently recognized as thyroid hormone transporter as opposed to monocarboxylate (Friesema et al. 2003, 40128-40135).

1.4.5. ATP-Binding Cassette Transporters (ABC):

The ATP-binding cassette (ABC) superfamily of transporter proteins are responsible for the active transport of a wide variety of compounds including phospholipids, ions, peptides, steroids, polysaccharides, amino acids, organic anions, bile acids, drugs and other xenobiotic

compounds across cellular membranes. There are roughly 48 genes encoding the various human ABC transporters, each is organized into seven subfamilies designated ABCA to ABCG (Tai et al. 2009, 14-24). Over-expression of ABC transporters are the main contributors to the development of multidrug resistance (MDR) in cancer cells. For instance, when the MDR gene that codes for an efflux transporter is being transfected into drug sensitive cells, the transfectant cells become resistant to the drugs that are substrates for the transporters resulting in a decrease in the intracellular concentration of the drugs, there by conferring multidrug resistance (Dantzig, de Alwis, and Burgess 2003, 133-150). MDR in tumor cell lines is often linked to an ATP-dependent decrease in cellular accumulation of drugs namely through p-glycoprotein (p-gp encoded by ABCB1), multidrug resistance proteins (MRP encoded by ABCC), and breast cancer resistance protein (BCRP encoded by ABCG2) drug efflux transporters (Potschka 2010, 118-127). In addition to their function as multidrug resistance proteins, many of these transporters are also expressed in healthy tissues suggesting that they also have a protective function in limiting the accumulation and speeding the elimination of xenobiotic compounds which could result in tissue toxicity (Loscher and Potschka 2005, 86-98). The main ABC proteins that function as drug efflux transporters are described below.

1.4.5.1. ***Multidrug Resistance Protein (MRP):*** The identification and characterization of efflux transporters within the multidrug resistance protein (MRP ABCC) subfamily began in 1992 with the initial cloning of MRP1 from a small cell lung cancer cell line (H69AR) (Cole et al. 1992, 1650-1654). MRPs are efflux transporters requiring ATP hydrolysis for the transport of many biological substrates including glutathione and its conjugates, glucuronides, and cyclic nucleotides. Additionally, many natural or synthetic toxins are also transport substrates for MRPs, thus lowering their accumulation within the cell (Chang 2007, 15-37). The ABCC subfamily

of proteins consists of 9 MRPs (MRP1-9); each protein consists of 2 cytoplasmic nucleotide binding domains (NBDs) and at least two sections of transmembrane spanning domains as illustrated in Figure 1.5 (Chang XB 2007). MRPs are widely expressed in several organs including the liver, kidney, small intestines and the brain. The expression and the sublocalization of MRPs are often cell type specific. For instance, MRP2 and MRP3 are both found in human hepatocytes with MRP2 being specifically localized in the apical side of the membrane, while the majority of MRP3 is found in the basolateral side. Furthermore, with the same respective orientation, MRP2 is also expressed in the kidney, small intestine, bronchi, gallbladder, and placenta where it plays a significant role in the excretion of many phase II conjugation products of drugs or endogenous substrates into the bile, urine, or intestinal lumen (Keppler 2011, 299-323). MRP3 is found in other tissues including cholangiocytes, gall bladder, pancreas, kidney, and the intestines. Likewise, MRP6 is also found in the basolateral side of the both human and rodent hepatocytes and kidneys (Keppler 2011, 299-323). The main form of MRPs being expressed in the CNS included MRP1, 4 and 5 (Zhang Y et al 2004). MRP1 is the predominant isoform found within the endothelial cells forming the BBB based, and it is specifically present on the apical side of the membrane. MRP1 has also been detected in the epithelial cells forming the BCSFB, however, in contrast to the endothelial cells of the BBB, MRP1 is primarily found in the basolateral membrane. However, other laboratory including Miller et al identified MRP2 as the predominant isoform expressed in the BBB using killifish and dogfish shark brain capillaries with confocal microscopy (Miller et al. 2002, R191-8). The reason for the discrepancy of various MRP expressions within the BBB is unknown. One possible explanation for the discrepancy could be related to the difference in reverse transcription-polymerase chain reaction primers or antibodies used to identify various forms of MRP. Alternatively, the expression of MRP within

the BBB could be species specific (Zhang et al. 2004, 449-455). MRP1 is also expressed in peripheral tissues which include the kidneys, lungs, skeletal and cardiac muscles, testes, and the placenta (Chang 2007, 15-37). Unlike other MRPs, there is very little to no MRP1 expression in hepatocytes (Keppler 2011, 299-323). Depending on the cell type, MRP4 can be found in both the apical and basolateral side of the plasma membrane. In the choroid plexus epithelial cells that form the BCSF barrier as well as in the hepatocytes, pancreatic ductal epithelial cells and prostate epithelial cells, there is predominantly a basolateral distribution of MRP4. However, within the endothelial cells forming the BBB, MRP4 is also found on the apical side of the plasma cell membrane, indicating the protein has an important role in limiting the accumulation and distribution of drugs within the CNS (Keppler 2011, 299-323; Zhang et al. 2004, 449-455). In the human brain, MRP5 is mainly concentrated in the astrocytes and neurons although small levels were detected on the luminal side of the endothelial cells forming the BBB (Nies et al. 2004, 349-360). Given the broad spectrum of substrates, MRP members can significantly alter the accumulation, distribution and elimination of drugs. Furthermore, they can also participate in drug-drug interactions which can complicate treatment outcomes. Most MRP subtrates are amphiphilic organic anions with a molecular weight roughly between 300 to 1000 Da (Keppler 2011, 299-323). Organic cations can become substrates for MRPs in the presence of reduced gluthathione (GSH) which is endogenously produced by cells at millimolar concentrations (Loe, Deeley, and Cole 1998, 5130-5136). The presence of GSH can enhance the spectrum of MRPs substrates, and must be taken into consideration when characterizing the functionality of these transporters.

1.4.5.2. ***Breast Cancer Resistance Protein (BCRP):*** Another member of the ABC family of efflux transporters is the breast cancer resistance protein (BCPR). BCRP was originally

discovered in the MCF-7 AdrVp breast cancer cell line after observing that the cells are resistant to chemotherapeutic drugs including mitoxantrone, doxorubicin, and daunorubicin (Nicolazzo and Katneni 2009, 130-147). The gene sequence of the protein was isolated shortly after and was classified as the group G subfamily of ABC transporters. There are at least 5 members of ABCG subfamily identified in humans (ABCG1, ABCG2, ABCG4, ABCG5, and ABCG8). However, the primary form that plays a crucial role in the transport of substances between the blood and the CNS is ABCG2 (Nicolazzo and Katneni 2009, 130-147). The ABCG2 gene is also isolated in other vertebrates including birds, reptiles, and fish with highly conserved sequences across the species (Robey et al. 2009, 3-13). At the protein level, ABCG2 is approximately 72-kDa with 665 amino acids and is considered as a half-transporter as shown in Figure 1.5. Other ABC transporters have two sets of membrane spanning regions (6 transmembrane α-helices) and two nucleotide binding domains (NBD); the G subfamily of protein consists of only one set of membrane spanning domain 6 transmembrane α-helices and only one NBD (Nicolazzo and Katneni 2009, 130-147). In order to function, it is believed that these half-transporters form homodimers (Ozvegy et al. 2001, 111-117).

The expression of ABCG2 is regulated by both endogenous and exogenous factors. The expression of ABCG2 is influenced by various cytokines and growth factors (Robey et al. 2009, 3-13). Yin and colleagues reported the use of transforming growth factor-beta (TGFβ) caused a decrease in ABCG2 gene expression in MCF-7 breast cancer cells. Tumor necrosis factor-alpha or interleukin 1-beta also decreased the mRNA and protein expression of ABCG2 in primary trophoblasts while insulin-like growth factor II increased expression of ABCG2 at the mRNA level (Robey et al. 2009, 3-13). These pro-inflammatory cytokines and endotoxins are upregulated in certain pathological conditions such as infections or inflammation, thus

resulting in a decreased expression of ABCG2 (Hahnova-Cygalova, Ceckova, and Staud 2011, 53-68). The surface expression of ABCG2 protein is believed to be regulated by the protein kinase Akt (Mogi et al. 2003, 39068-39075). Takada et al reported a shift of ABCG2 protein expression from the apical membrane to the intracellular space of the kidney polarized cells after it had been treated with phosphotidylinositol 3-kinase inhibitors LY294002 and wortmanin (Takada et al. 2005, 905-909). This shift in protein expression is correlated with the phosphorylation state of Akt; however, the precise mechanism by which Atk regulates the surface expression of ABCG2 is not clear (Mogi et al. 2003, 39068-39075).

The specific localization of ABCG2 within the CNS is primarily confined to the luminal plasma membrane of the brain microvessel endothelial cells. Given the localization within the BBB and the compounds that are transported by ABCG2, it has been suggested that ABCG2 most likely protects the brain from xenobiotics and toxins similar to other ABC transporters (Nicolazzo and Katneni 2009, 130-147). Furthermore, ABCG2 also plays a role in the accumulation and disposition of various endogenous substrates including sulfate and glucuronide conjugates of estrone and dehydroepiandrosterone (Imai et al. 2003, 610-618; Suzuki et al. 2003, 22644-22649). In addition to endogenous substrates, ABCG2 also binds and recognizes a broad range of structurally-unrelated drugs and xenobiotics (Nicolazzo and Katneni 2009, 130-147). Many of these transport substrates also interact with other ABC transporters including ABCB1 and the ABCC subfamily; thus, the accumulation and distribution of drugs can be significantly altered.

1.4.5.3. ***P-glycoprotein (P-gp):*** P-glycoprotein (P-gp) was the first ABC transporter to be characterized. First identified by Juliano and Ling in 1976 using Chinese hamster ovary cells with selected resistance to colchicine, they discovered that the drug resistance properties of the mutated cells were consistently correlated with a high molecular weight component found in

the plasma membrane with an approximate weight of 170,000 Da (Juliano and Ling 1976, 152-162). They also observed that the component was likely a glycoprotein associated with the plasma membrane of the mutated cells and was consistently absent or expressed at a lower level in the wild-type cells. Furthermore, they also noticed that the mutant cells with high levels of glycoprotein displayed an alter drug permeability; thus, they designated it as "P-glycoprotein" (Juliano and Ling 1976, 152-162). P-gp is also expressed in numerous tissues, including adrenal glands, kidneys, liver, colon, small intestine, heart, testes, peripheral nerves, and the brain. At the BBB, it is the most extensively studied ABC transporter being expressed in the luminal plasma membrane of brain endothelial cells (Dantzig, de Alwis, and Burgess 2003, 133-150). Under normal conditions, the presence of P-gp in the BBB limits a broad range of substances from penetrating the brain tissue. Some notable drug classes with reduced brain penetration due to P-gp efflux at the BBB include anti-epileptics, anti-cancer drugs, anti-histamines and HIV protease inhibitors (Tai et al. 2009, 14-24). Numerous studies using drugs such as cyclosporine, digoxin, domperidone, etoposide, loperamide, ondansetron, taxol and vinblastine have shown the important role of P-gp in the pharmacokinetics of P-gp substrates in multiple parts of the body. Table 1.4 shows some of the drugs that are known substrates for P-gp.

Similar to other ABC transporters, P-gp is a transmembrane protein with a molecular weight of 170KDa formed by two homologous subunits that function as an efflux pump in an ATP-dependent manner (shown in Figure1.5). The protein is assembled in two halves connected by a 75 amino acid linker region. Each half contains 6 transmembrane segments, an intracellular nucleotide binding domain, and both intracellular N and C terminal regions. The exact localization of P-gp had been a subject of some debate with evidence supporting both luminal and abluminal expression of the protein. Luminal P-gp expression had been observed in rat and

mouse brain capillaries (Zhang et al. 2004, 449-455; Beaulieu et al. 1997, 539-544; Tatsuta et al. 1992, 20383-20391). Furthermore, the luminal expression of P-gp has also been isolated in human brain microvessels (Virgintino et al. 2002, 1671-1676; Seetharaman et al. 1998, 1151-1159). In constrast, electron microscope techniques have shown an enhanced expression of P-gp on the abluminal side of the rat brain endothelial cells (Bendayan et al. 2006, 1159-1167). Nevertheless, recent studies using immunoreactivity support the localization of P-gp on the luminal side of the endothelial cells (Roberts et al. 2008, 423-438).

Substrates and Inhibitors of P-gp: Numerous studies have attempted to identify and characterize P-gp substrates. A substrate can be any compound that is capable of binding to the protein and subsequently transported across the lipid bilayer. Unlike conventional transporters, which recognize specific substrates, P-gp recognizes a broad range of compounds and has the capacity to extract its substrates directly from the plasma membrane (Seelig and Landwojtowicz 2000, 31-40). Some of the most common features of P-gp substrates include their lipophilic nature that enables them to cross the lipid bilayer of the cell membrane. Furthermore, many P-gp substrates commonly consist of two aromatic rings and a basic nitrogen atom. These molecules can be uncharged or basic in nature, although some acidic compounds including methotrexate and phenytoin can also bind to P-gp but at a lower rate. Molecules with molecular weight ranges from 300 to 2000 Da are capable of binding to the protein and being transported (Ueda, Taguchi, and Morishima 1997, 151-159). Peptide substrates consisting of 3 to 15 amino acids with molecular weight ranges from 380 to 1880 Da can also interact with P-gp (Ueda, Taguchi, and Morishima 1997, 151-159). Most recently, beta amyloid protein, the component found in amyloid plaques in Alzheimer ’s disease was reported to be a transport substrate of both P-gp but not BCRP (Wijesuriya et al. 2010, 228-238; Kania et al. 2011, 1-11).

One method for overcoming the limited permeability of P-gp transport substrates is to pharmacologically inhibit Pgp. P-glycoprotein inhibitors are themselves non-cytotoxic agents that can be used in combination with P-gp substrates to maintain the intracellular drug concentration. An inhibitor binds to P-gp and prevents the transport of P-gp substrates. There are at least three generations of P-gp inhibitors. The first generation compounds are less potent and non-selective with undesirable side effects at inhibitory concentrations. Examples of first generation inhibitors include the calcium channel blocker, verapamil, and the immunosuppressive agent cyclosporin A. First generation P-gp inhibitors act as competitive inhibitors of P-gp transport (Hollo et al. 1996, 99-104).

The second generation compounds including dexverapamil or dexniguldipine were developed to reduce the toxicity associated with P-gp inhibition. They eliminate the undesirable side effects while retaining the ability to inhibit P-gp. The third generation inhibitors including tariquidar and elacridar are much more specific and more potent than earlier compounds. Unlike the first and second generation of P-gp inhibitors, the third generation of drugs act as non-competitive inhibitors of P-gp, and the compounds themselves are not transported by P-gp (Bauer et al. 2010, 5489-5497). Tables 1.4 and 1.5 summarize the various P-gp inhibitors, respectively (Dantzig, de Alwis, and Burgess 2003, 133-150).

The ability of P-gp to extrude xenobiotics provides protection and detoxification of cells under normal conditions. For example, knock-out mice ($MDR1a^{-/-}$) have been shown to be more sensitive to ivermectin and are susceptible to serious neurotoxicity compared to wild type control mice (Balayssac et al. 2005b, 319-329). Considering the broad range of P-gp substrates and the expression of P-gp in tissues responsible for absorption, distribution and elimination of drugs, it is no surprise that this particular drug efflux transporter can significantly affect the

absorption and distribution of drugs. This is especially true for cancer therapies used in the treatment of brain tumors. The tight junctions of the BBB restrict paracellular diffusion of chemotherapeutic agents into the CNS, while the presence of the various drug efflux transporters, such as P-gp, within the endothelial cells of the BBB reduces transcellular passage of chemotherapeutic agents into the brain and tumor sites.

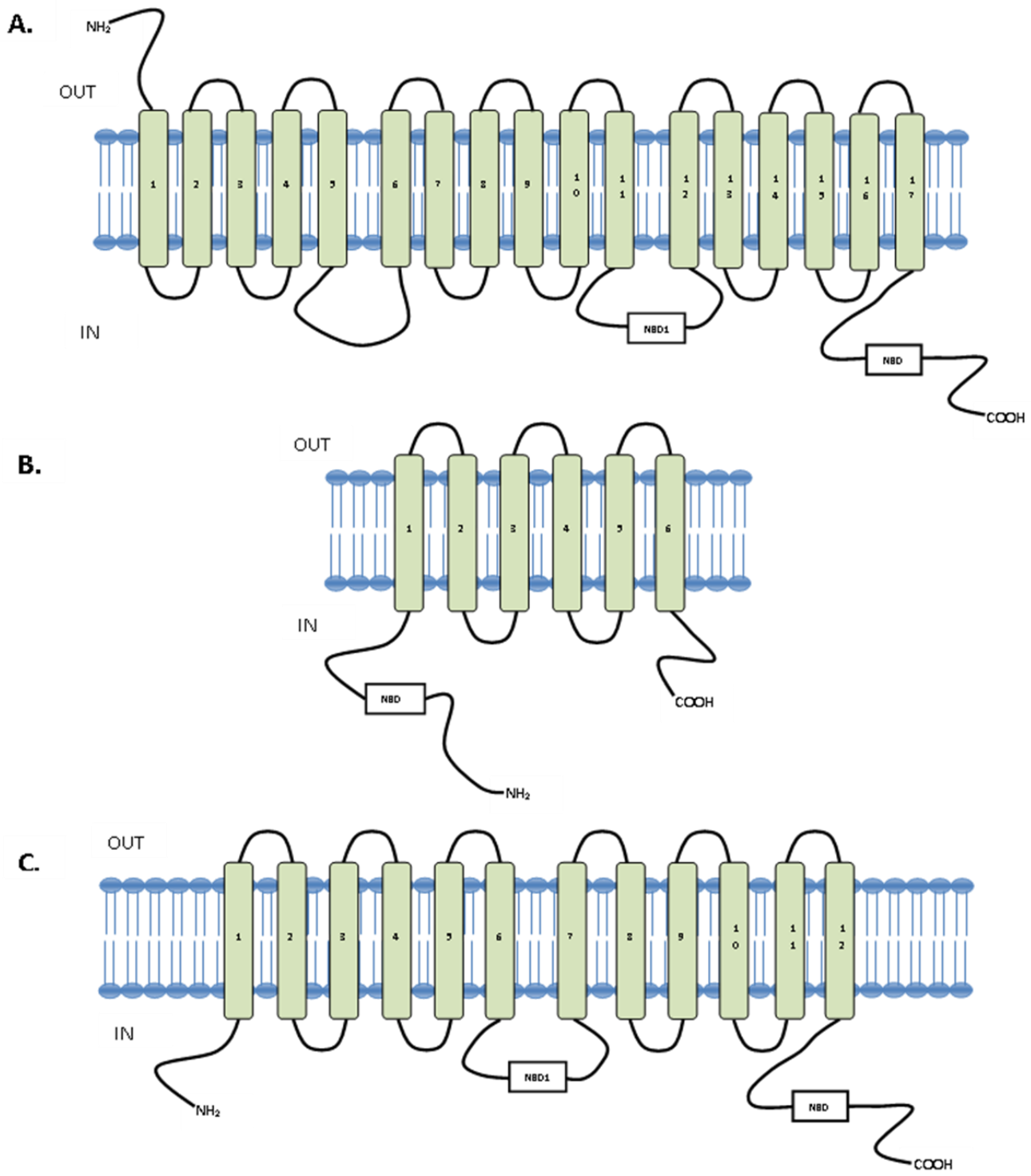

Figure 1.5: Structures of (A) MRP transporter, (B) BCRP transporter, and (C) P-glycoprotein transporter. Adapted from Chang 2007, 15-37; Nicolazzo and Katneni 2009, 130-147.

Table 1.4: Representative compounds that are known to be P-glycoprotein substrates. Adapted from Balayssac et al. 2005, 319-329.

Cancer Drugs	Immuno-suppressive Drugs	Lipid Lowering Agent	Steroids	HIV Protease Inhibitors	Cardiac Drugs	Anti-Diarrheal Drugs	Anti-Gout Agent	Anti-Bacterial Agents	Anti-Helminthic Agent
Doxorubicin	Cyclosporin A	Lovastatin	Aldosterone	Amprenavir	Digoxin	Loperamide	Colchicine	Erythromyccin	Ivermectin
Daunourbicin	FK506		Cortisol	Indinavir	Quinidine	Antiemetics		Rifampin	Abamectin
Vinblastine	Tacrolimus		Corticosterone	Nelfinavir		Domperidone		Valinomycin	
Vincristine			Hydrocortisone	Ritonavir		Ondansetron		Gramicidin	
Vindesine			Dexamethaxone	Saquinavir				Grepafloxacin	
Vinorelbine			Triamcinolone	Lopinavir					
Paclitaxel									
Etoposide									
Teniposide									
Epirubicin									
Irinotecan									
Tamoxifen									
Methotrexate									
Amsacrine									
Imatinib									

Table 1.5: Representative compounds that are known to be P-glycoprotein inhibitors. Adapted from Balayssac et al. 2005, 319-329.

Cyclopropylibenzosuberane	Immunosupp-ressant	Calcuim channel blocker	Progesterone antagonist	Antiarrhythmic agent	Antifungal agent	Acridonecarboxamide derivative	Topoisomerase
LY335979	Cyclosporin A	Verapamil	Mefiprostone (RU486)	Quinidine	Ketoconazole	GG918 (GF120918)	Xenova (XR 5944)
	Valspodar (PSC833)						

1.5. Blood-Brain Barrier (BBB) and Permeability of Chemotherapeutic Agents:

Compared with other endothelial cells forming capillaries in peripheral organs (non-CNS), the brain endothelial cells possess numerous astrocyte processes, mitochondria, junctional complexes, low fenestrae and pinocytic vesicles. All of these characteristics contribute to the ability of the BBB to restrict the diffusion of blood-borne substances from entering the brain (Emerich et al. 2001, 105-123). Although the protective nature of the BBB is essential to maintaining the brain microenvironment in the healthy individuals, under pathological conditions including brain tumors, the presence of the BBB can significantly limit chemotherapeutic agents from gaining access into the brain and the tumor sites. There is a general consensus that most chemotherapeutic agents achieve relatively low concentrations in the normal CNS due to the presence of the BBB and BCSFB (Stewart 1994, 121-139). During the early days of brain tumor chemotherapy, it was difficult to get drugs tested in human brain tumors patients unless there was evidence that the drugs could readily cross the BBB (Stewart 1994, 121-139). Indeed, the quantity of drugs being distributed into the brain is dependent on several factors including physiological variables such as blood flow and membrane integrity, physicochemical properties of the drug such as molecular weight and lipophilicity, and the expression of influx and efflux transporters at the BBB and BCSFB including ABC transporters and OATPs (Motl et al. 2006, 871-903).

1.5.1. Physiological Variables:

In general, when the velocity of blood flow increases, there is also an increase in the diffusion of highly permeable drugs into the brain tissues via passive diffusion, while the penetration of drugs with low permeability will not be affected (Motl et al. 2006, 871-903).

Furthermore, under pathological conditions including brain tumors or temporary disruption of BBB using irradiation and hypertonic chemicals, the integrity of the BBB is compromised resulting in increased drug penetration into the brain.

1.5.2. Physicochemical Properties:

Both the molecular weight of the compounds and their lipophilicity determine the extent of BBB penetration. Molecules with molecular weight <400 Da with high lipophilicity can trasverse the membrane to achieve pharmacologically active concentrations in the brain (Motl et al. 2006, 871-903). However, other factors including the number of hydrogen bond also determine the extent of BBB penetration. Compounds with more than 5 H-bond donors and 10 H-bond acceptors are likely to have poor BBB permeability (Motl et al. 2006, 871-903).

1.5.3. Expression of Influx and Efflux Transporters:

The physiological and physiochemical properties of the drug can significantly affect their distribution in the brain; however in certain compounds, discrepancies between lipophilicity and the extent of BBB penetration have been reported. This phenomenon is attributed to the presence of influx and efflux transporters such as SLC and the ABC gene family located at the BBB and BCSFB (Dantzig, de Alwis, and Burgess 2003, 133-150). Among them, P-gp, is the most extensively studied and has been shown to play an important role in the disposition of anticancer drugs in CNS.

1.6. Blood-Brain Barrier (BBB) and Brain Tumors:

The integrity of the BBB in both primary and metastatic brain tumors has been explored by a number of investigators with conflicting results. In some studies, alterations in the properties of endothelial cells including the disruption of the tight junctions, presence of fenestration and an increase in the number pinocytic vesicles can result in an enhancement of perivascular space, thereby, affecting the movement of compounds across the barrier (Deeken and Loscher 2007, 1663-1674). These findings indicate that the BBB is disrupted in brain tumors and would suggest a very minor role of the BBB in influences the treatment outcomes in brain tumors. However, many clinicians remain convinced of the importance of BBB in brain tumor treatments. Although the BBB is disrupted within the tumor site, the level of disruption can be varied both spatially and temporally. The greatest enhancement of permeability occurs within the tumor core while the BBB remains relatively intact at the proliferating tumor edge (Muldoon et al. 2007, 2295-2305). Furthermore, the level of disruption is also dependent on the stage of cancer development. A recent study from our lab which was also supported by Zhang et al 1992 indicated that the BBB is only disrupted during the intermediate and late stages of tumor development, while the BBB remained relatively intact during the early stage of tumor growth.

1.6.1. Blood-Brain Barrier Permeability in Primary Brain Tumors:

Glioblastoma is one of the most common and most aggressive primary brain tumors affecting approximately 3 in every 100,000 people annually (Nakamura et al. 2011, 77-83). Glioblastomas are angiogenic consisting of new and leaky blood vessels. Indeed, the leaky glioblastoma vasculature can be observed using MRI with the aid of a gadolinium contrast enhanced-agent (Gad) (de Vries et al. 2006, 1199-1209). Therefore, questions arise as to

whether the BBB plays a significant role in the chemotherapeutic treatment of brain tumors as drugs should be able to cross these lesions in a similar manner to MRI contrast agents. The role of the BBB in the delivery of chemotherapeutic agents to the brain had been a topic of considerable debate. Early studies were done by Vick NA et al 1977 using the extracellular protein tracer horseradish peroxidase (molecular weight 44,000) in a virally induced in vivo model of glioma demonstrated discontinuous and enhanced fenestration in tumor endothelium, supporting the leaky nature of the tumor blood vessels. Other clinicians including Steward DJ et al 1994, and Donnelli MG et al 1992 reported that the BBB and the blood-tumor barrier (BTB) were not a factor in determining the quantity of drugs accumulating in the brain (Stewart 1994, 121-139; Donelli, Zucchetti, and D'Incalci 1992, 251-260). However, investigators believed that the BBB and the BTB played a significant role in preventing most chemotherapeutic drugs from reaching the tumor sites resulting in low tumor response. In the case of gliomas with their pleiomorphic characteristics, the central parts of the tumor might not pose a significant problem especially when the tumor can be removed by surgery; however, the major obstacle is the outer rim of the tumors where the malignant cells infiltrate into the surrounding brain with an intact BBB. Within these regions, the efficacy of chemotherapeutic agents depends on their ability to penetrate the BBB sufficiently in order to reach therapeutic levels (de Vries et al. 2006, 1199-1209). This idea was supported by studies done by Wolff et al examining the *in vitro* cytotoxicity of different chemotherapeutic agents in various human, rat, and mouse glioma cells. Even in the most resistant cells, substantial cytotoxicity was observed with chemotherapeutic agents that are normally ineffective in the clinical treatment of brain tumors (Wolff et al. 1999, 481-486). This suggests the resistance of brain tumors to chemotherapeutic agents is due, in large part, to the failure to obtain appropriate therapeutic concentrations of the drugs in the brain.

1.6.2. Blood-Brain Barrier Permeability in Metastatic Brain Tumors:

In contrast to gliomas, brain metastases often form lesions with well defined boundaries consisting of leaky blood vessels due to neovascularization (de Vries et al. 2006, 1199-1209). The extent of this barrier being compromised has been a topic of considerable debate for more than 30 years. Studies conducted by Stewart et al. indicate that tumor cells infiltrating peritumoral brain tissue in humans causes blood vessels to take on some of the structural characteristics of leaky vessels as the tumor progresses (Stewart et al. 1987a, 697-705). These studies indicate that BBB integrity was compromised in the presence of brain tumor. In mouse melanoma brain metastasis model it was observed that Evans blue dye and HRP (horse radish peroxide) leakage through tight junctions increased with time post-inoculation suggesting tumor-associated disruption of the BBB (Cranmer et al. 2005a, 325-356). Many of these morphological studies, however, did not have quantitative data regarding the frequency and distribution of the BBB defects. In general, brain metastases are resistant to most chemotherapeutic agents and this resistance can be due to the inability of drugs to cross the BBB (Zhang et al. 1992, 1115-1124; Fidler et al. 2002a, 53-57). Quantitative techniques including autoradiography have been employed to measure local capillary permeability in metastatic brain tumor models. Based on this technique, Hasewaga H et al 1983 found that BBB permeability of metastatic brain tumors are variable depending on the size, the nature, and the anatomical location of the lesion (Hasegawa et al. 1983, 304-310). Small tumors (usually less than 1mm in diameter) generally showed no increase in capillary permeability; however, as the tumor mass increased, so did the BBB permeability. This change can be explained by the newly formed abnormal blood vessels that disrupte the endothelium cells (Hasegawa et al. 1983, 304-310).

1.7. Blood-Brain Barrier Disruption/Modulation:

Various strategies have been attempted to increase drug delivery to the brain through altering drug penetration through either paracellular or transcellular routes. Disruption of the tight junction complexes in the brain capillary endothelial cells enhances the movement of compounds via paracellular diffusion. This disruption has to be reversible in order to effectively increase the accumulation of compounds in the brain and the tumor sites without producing therapy limiting toxicity. Pharmacological disruption of the BBB has been employed in clinical trials using several methods including intracarotid infusion of mannitol solutions, and modifying the tight junction properties of the BBB by the administration of bradykinin analogues (Kemper et al. 2004, 415-423).

Osmotic disruption of the BBB by the administration of hypertonic solutions causes the shrinkage of endothelial cells and thus disrupts the tight junctions between the endothelial cells (Kemper et al. 2004, 415-423). This increase in intercellular space between the endothelial cells improves the movement of substances between the blood and the brain. However, the major drawback of osmotic disruption is the long recovery period of the BBB which may take up to several hours (Siegal et al. 2000, 599-605). The prolonged period of BBB opening also allows the entry of other substances including albumin and pathogens, which can result in major side effects such as seizures, neuropathological changes including vasogenic edema and inflammation, as well as neurological toxicity (Kemper et al. 2004, 415-423).

Administration of histamine, bradykinin or bradykinin analogues can selectively open the BBB by activating bradykinin B2 receptors located on the endothelial cells (Kroll and Neuwelt 1998, 1083-99; discussion 1099-100; Patel et al. 2009, 35-58) and initiate the second messenger system to disengage the tight junctions formed between the endothelial cells of the BBB. In

contrast to osmotic disruption, the selective opening of the BBB mediated by this receptor system lasted only for 20 minutes (Kemper et al. 2004, 415-423). A study using a glioma rat model demonstrated a significant treatment response when carboplatin was administered in combination with RMP-7 (Cereport^{TM}), a bradykinin analogue. However, a phase II clinical trial in patients with glioma did not show any treatment benefit with Cereport^{TM} (Prados et al. 2003, 96-103). One possible explanation for the failure of Cereport^{TM} can be attributed to a varying level of bradykinin B2 receptor expression in glioma patients eliciting varying amounts of BBB and BTB disruption (Black and Ningaraj 2004, 165-173). Alternatively, the negative results can also be due to the sub-optimal dosage of Cereport^{TM} and/or the differences between the BTB in glioma patients and the models used in preclinical trials (Kemper et al. 2004, 415-423).

An alternative way to modulate tight junction permeability to enhance the brain penetration of hydrophilic drugs and large therapeutic molecules is through the use lysophosphatidic acid (LPA), one of the simplest glycerolphospholipids (Moolenaar, van Meeteren, and Giepmans 2004, 870-881). LPA is known to exist endogenously at a concentration of 2-20uM and it can function as an intracellular signaling molecule that has a broad range of biological responses (Moolenaar, van Meeteren, and Giepmans 2004, 870-881) including cell migration and proliferation, smooth muscle contraction, the assembly of focal adhesions, and stress fiber formation. Pretreatment of LPA on porcine endothelial cells has shown a significant reduction in the transcellular electrical resistance (TER) values which reflects on the increase in tight junction permeability (Schulze et al. 1997, 991-1000) allowing an increased flux of sucrose across the monolayer.

1.8. Statement of the Problem:

The protective function of the BBB along with the presence of P-gp is a major obstacle in treating many CNS disorders including brain tumors. Many of the current chemotherapeutic agents used for the treatment of brain tumors are known to be substrates for P-gp which can affect the accumulation of drugs in the brain and the tumor sites.

The hypothesis for the current dissertation is that an intact BBB with functional P-gp can significantly reduce the accumulation of chemotherapeutic agents in the brain and tumor areas. By modulating the barrier properties either through disrupting the BBB and/or inhibiting the function of P-gp, the amount of drugs penetrating the brain can be increased, resulting in better tumor response.

The main objectives are:

1) To characterize a mouse metastatic brain tumor model.
2) To examine the activity of P-gp using a near infrared probe.
3) To examine the effects of BBB tight junctions on the permeability of both small and large molecules.
4) To examine the effects of BBB tight junctions on the permeability of both small and large molecules in brain tumor mice under conditions when the BBB is reversibly impaired as well as in conditions when P-gp activity is inhibited.

CHAPTER 2: EXAMINATION OF BLOOD–BRAIN BARRIER (BBB) INTEGRITY IN A MOUSE BRAIN TUMOR MODEL.

2.1. INTRODUCTION

The incidence of brain metastases is increasing, with an estimated 170,000 new cases of brain metastasis diagnosed annually in the U.S. (Chan and Loeffler 2001, 105-107). This increase is due in part to superior diagnostic techniques and to better treatment regimens for peripheral tumors, resulting in longer survival times for patients with peripheral tumors and therefore increased risk of developing brain metastasis. Of the solid organ tumors, lung cancer accounts for approximately 50% of brain metastases (Wong and Berkenblit 2004, 68-79). The clinical impact of brain metastases in lung cancer is such that intracranial metastasis is present in an estimated 10-20% of small cell lung cancer patients at initial diagnosis and in 80% of patients at autopsy (Cohen and Matthews 1978, 234-243).

While improvements in both drug design and drug dosing have resulted in significant advances in cancer treatment, brain tumor responsiveness to chemotherapy remains poor (Bart et al. 2000, 449-462). One of the primary reasons for this could be the specialized capillary endothelial cells that form the blood-brain barrier (BBB). An intact BBB represents a challenge to the effective delivery of chemotherapeutic agents. This is due to the tight cellular junctions, reduced pinocytic activity and absence of fenestrations that are characteristic of the brain endothelial cells that form the BBB (Goldstein and Betz 1986, 74-83). Furthermore, the expression of efflux transporters such as P-glycoprotein (P-gp), multidrug-resistance associated protein MRPs, breast cancer resistance protein (BCRP), within the brain microvessel endothelial cells act to further restrict the distribution of chemotherapeutic agents in brain (Loscher and Potschka 2005, 86-98; Loscher and Potschka 2005, 22-76).

It has been suggested that BBB integrity is compromised in brain tumors (Wiranowska et al. 1992, 225-236). However, more recent data suggest that BBB permeability is heterogeneous within the tumor site and is dependent on the stage of tumor development (Wiranowska et al. 1992, 225-236; Fidler et al. 2002b, 53-57). In the present study, a murine brain tumor model was used to comprehensively examine BBB function throughout tumor development. Blood-brain barrier integrity was examined at various stages of tumor development using both vascular permeability tracers as well as magnetic resonance imaging (MRI). The data suggest that the BBB remains intact throughout the early and intermediate stages of tumor development, with significant increases in BBB permeability occurring only during the final stages of tumor progression. Furthermore, expression of the drug efflux transporter protein, P-gp, in cerebral microvascular endothelial cells remained unchanged throughout the time frame examined. These studies indicate that BBB is still an obstacle for delivery of chemotherapeutic agents and highlight the need for approaches that enhance the delivery of chemotherapeutic agents in the brain.

2.2. MATERIALS AND METHODS

2.2.1. Animals and Brain Tumor Model:

Female inbred Balb/c mice were used for the brain tumor model. Mice (15-20 g) were purchased from Charles River Laboratories (Wilmington, MA) and fed a standard laboratory diet *ad libitum*. Mice were anesthetized and placed in a stereotaxic apparatus (Kopf instruments) for intracerebral implantation of the Lewis Lung Carcinoma (3LL) cells. A total of 5000 3LL cells were suspended in 7.5 μl of buffer and injected slowly over a 3-minute period into the right hemisphere at a depth of 4 mm, 2 mm posterior of the bregma and 1 mm lateral of the coronal suture using a 25 μl Hamilton syringe fitted with a 31-gauge beveled needle. Mice were allowed

to recover from anesthesia undisturbed before being returned to their respective cages. All animal studies were done in accordance with protocols approved by the Institutional Animal Care and Use Committee (IACUC) at the University of Manitoba.

2.2.2. Survival Analysis:

Following tumor cell implantation, mice were provided food and water *ad libitum* and monitored daily for signs of tumor growth and progression. Tumor survival studies were performed using humane endpoints including loss of locomotor activity, and weight loss (up to 25%). The survival time was measured from the day of tumor cell implantation to the day of euthanasia or death and median mouse survival time was calculated.

2.2.3. Assessment of Tumor Volume:

For the tumor volume studies, mice were sacrificed on day 7, 10, 12, and 15 post-tumor injection. The brains were removed and fixed with formaldehyde 4 % w/v (Formalde-Fresh®, Fisher Scientific). A series of coronal sections of the brain were made at 1 mm intervals and blocked in paraffin. Brain slices (6 µm) were cut from each serial section using a cryostat, and stained with hematoxylin and eosin (H & E) dye. The H & E stained slices were scanned and tumor volumes determined based on serial slices from the captured images using a computer image analysis system (Image J; NIH, Bethesda, MD). The area analyzed spanned from 5 mm rostral to 5 mm caudal from the site of tumor cell injection.

In separate studies tumor volume was examined within the same mouse at 7, 12, and 15-days post tumor cell implantation using MRI techniques. Mice were anesthetized and secured in a Biospec 7 Tesla (7T)/21 cm spectrometer magnet (Bruker; Karlsruhe, Germany) equipped with Paravision 3.0 software. Coronal images of brain were obtained using T2-weighted spin echo (SE) pulse sequences with the following parameters: repetition time (TR) /

echo time (TE) = 164000/20.00 milliseconds, slice thickness of 0.75 mm, field of view (FOV) = 2.5 x 2.5 cm^2, averages = 12, matrix size = 256 x 256, and resolution of 117 x 117 μm^2. Quantitative analyses of tumor volume were performed by visually locating the tumor lesion on the T2-weighted images and tumor volume was calculated from the selected regions of interest (ROI) from serial slices using Marevisi 3.5 software (Institute for Biodiagnostics, National Research Council, Canada).

2.2.4. Assessment of Blood-Brain Barrier Permeability:

In order to establish the effect of tumor growth on the permeability of the blood-brain barrier (BBB), cerebrovascular leakage of ^{3}H-mannitol, a low molecular weight marker (182.17 Da), and Evans Blue (EB), a high molecular weight marker (approximately 65,000 Da) was evaluated 7, 10, 12, and 15 days after tumor implantation. Mice (n=9) were anesthetized with ketamine (30mg/ml)/xylazine (4mg/ml) and a phosphate buffered saline solution containing ^{3}H mannitol (4 μCi/mouse) and Evans Blue (2% w/v) was administered via bolus tail vein injection. After ten minutes, blood samples were taken, the mouse sacrificed and brain samples removed. The right (tumor-bearing) and left (non-tumor bearing) brain hemispheres were separated and weighed. Capillary depletion was performed as described below.

Vascular integrity within the tumor, at various stages of development, was also assessed using gadolinium contrast enhanced MRI. Vascular integrity of tumor mice and non-tumor mice (control mice) was examined prior to implantation (pre tumor injection) and on day 7, 12, and 15 post injection of tumor cells or vehicle, respectively, using gadolinium (Gad) enhanced MRI. For these studies, T1-weighted images were obtained using the same MRI system described previously with the following parameters: repetition time of 750 msec, an echo time of 11.6 msec, a slice thickness of 0.75 mm, FOV was 2.5 x 2.5 cm^2, averages = 12, matrix size was 256 x

256, and resolution was 117 x 117 μm^2. Two sets of T1-weighted images were obtained. The first scan was done in the absence of Gad enhancement. A second T1-weighted imaging scan was performed following an intravenous bolus injection of 0.4 mmol/kg of Gadolinium diethylenetriamine pentaacetate (Gad). The intensity of Gad enhancement in the brain and at the tumor site was determined by the percent difference in pre and post-Gad images according to the following formula using Paravision 3.0 software:

((Post-Gad T1-weighted images – Pre-Gad T1-weighted images) / Pre-Gad T1-weighted images) x 100

Quantification of Gad was accomplished by manually placing the ROI over the tumor region using Marevisi 3.5 software (Institute for Biodiagnostics, National Research Council, Canada).

2.2.5. Capillary Depletion (These studies were done by Dr. Sanjot Savant):

For the assessment of BBB permeability, determination of angiogenesis, and examination of P-gp expression, capillary depletion was performed as described (Triguero, Buciak, and Pardridge 1990, 1882-1888). Briefly, mice were sacrificed on various days post tumor cell injection (7-15 days). Sham mice receiving only intracranial injections of culture media were sacrificed on day 15 post-media injection. After the brain was removed, the right and left hemispheres were separated and weighed. The hemispheres were homogenized using a glass homogenizer in five times the volume of physiological buffer (HEPES 10mM, NaCl 141mM, KCl 4mM, $CaCl_2$ 2.8 mM, $MgSO_4$ 1mM, NaH_2PO_4 1mM, and D-glucose 10mM) and 13% dextran. The homogenate was then centrifuged at 5400 x g for 15 minutes at 4°C. The pellet containing the brain capillary endothelial cells was carefully separated from the supernatant containing brain parenchyma. Aliquots (200 µl) from both the supernatant and pellet fractions were analyzed using a liquid scintillation counter (Packard 2500 TR/AB) to measure the

radioactivity of ^{3}H-mannitol. The amount of ^{3}H-mannitol in the supernatant can be correlated with the amount of tracer having passed through the BBB. The amount of radiolabeled mannitol retained in the brain capillary pellet was used to assess cerebrovascular volume. In both cases, the radioactivity in supernatant and pellet fractions was normalized based on the total activity present in the blood. The protein content of the resulting capillary pellet from both the tumor-injected right hemisphere and non-tumor containing left hemisphere on days 7, 10, 12, and 15-post tumor injection was determined using the BCA method (Sigma).

2.2.6. Western Blot Analysis of P-glycoprotein (This study was done by Dr. Ryan Mitchell):

Cell lysates from the capillary-enriched pellet and capillary-depleted supernatant were denatured by heating at 95°C for 5 minutes and loaded onto 7.5% polyacrylamide gels (BioRad, Hercules, CA). Electrophoresis of the molecular weight marker and samples was performed under a constant voltage (40 mV) at room temperature for approximately 3 hours. The protein bands were transferred to Millipore polyvinylidene fluoride (PVDF) membranes by applying a constant current of 240 mA for 1 hour at 4°C. Membranes were washed and incubated with 0.3 % Tween-20 and 1 % BSA to block non-specific binding sites on the membrane. The expression of P-gp protein was identified using P-gp antibody (C219) (Kamiya Biomedical, Seattle, WA). The membrane was exposed to primary antibodies overnight at 4°C. After washing, the membrane was incubated with a secondary horseradish peroxidase antimouse Ig antibody (1:1500 dilution; Amersham Life Sciences, Cleveland, OH). The specific protein band was visualized using a chemiluminescence kit (Pierce, Rockford, IL).

2.2.7. Immunohistochemical Detection of P-glycoprotein:

Coronal brain slices (6 μm) were prepared as described above from formalin-fixed and paraffin embedded brain sections and mounted onto glass slides. After drying, slides were submerged in xylene solution to remove paraffin and re-hydrated in a series of 5 minute washes in 100, 90, 80, 70 and 0% ethanol solutions. Formalin cross-links were removed by gently boiling slides in citric acid (4 mg/ml) and sodium citrate (1 mg/ml) solution for 40 minutes. Slides were cooled and rinsed with 5 mM Tris buffer and endogenous peroxidase activity was blocked using 3% H_2O_2 for 10 minutes at room temperature. Brain slices were exposed to blocking buffer (10% goat serum in phosphate buffered saline (PBS) solution with 1% bovine serum albumin) for 30 minutes at room temperature. To minimize non-specific binding of the primary antibody, slides were incubated for an additional 60 minutes at room temperature with a 1:10 dilution of unconjugated goat-anti-mouse IgG in phosphate buffered saline containing 1% bovine serum albumin. Slides were washed and incubated at 4^{O} C overnight in phosphate buffered saline solution containing primary C219 antibody (1:40 dilution). After washing, secondary antibody (biotin-SP-conjugated goat-anti-mouse IgG) was added at a dilution of 1:500 for 20 minutes at room temperature. Slides were washed and incubated for 20 minutes at room temperature with 1:500 dilution of HRP-Streptavidin (Vector Labs; location). Brain slices were stained with DAB and counterstained with haematoxylin.

2.2.8. Statistical Analysis:

Statistical analysis of BBB permeability and cerebral vascular volume was evaluated using the paired Student's t-test. The values of left (non-tumor bearing) hemisphere were compared with the values in right (tumor bearing) hemisphere.

2.3. RESULTS

2.3.1. Survival Studies and Tumor Progression:

All mice injected with 3LL cells developed brain tumors (Figure 2.1). Using humane endpoints in determination of survival time, mice implanted with 3LL tumor cells survived a median of 17 days (Figure 2.1). The progression of the tumor was rapid with 100 % of the mice surviving to 15 days post-tumor cell implantation; however none of the mice survived past day 19 (Figure 2.1). The earliest outward sign of tumor burden typically occurred within 10 days post-innoculation and was manifested as weight loss (< 10% body weight). This was followed by a period of 1-4 days of further weight loss, hunchback posture, and diminished locomotor activity. Based on the survival studies, additional mice were examined for tumor development using both MRI and histochemical analysis. Tumor was consistently evident microscopically 7 days after tumor implantation in mice. Both qualitative (histological) and quantitative (tumor volume estimates) examination of tumor progression indicated a rapidly expanding tumor area in the brain, reaching 1.4 mm^3 and 29.7 mm^3 by day 7 and 12 post-tumor cell implantation, respectively (Figures 2.2). By day 15, there was a widely visible tumor mass present that occupied as much as 75 % of the right brain hemisphere and had reached a volume of approximately 77.3 mm^3 (Figure 2.2). Even at this late stage (i.e. day 15-post tumor cell implantation), notably the histological examination of the brain slices revealed that the tumor mass was restricted to the right hemisphere (Figure 2.3).

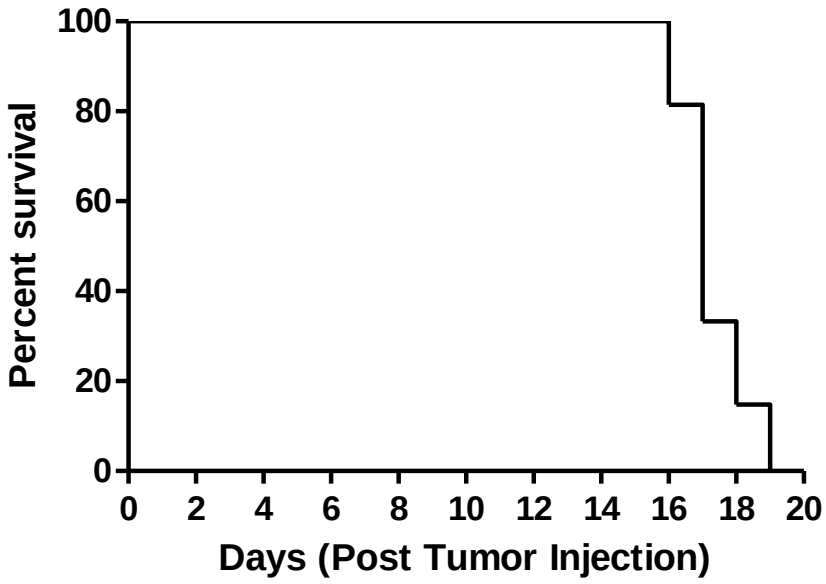

Figure 2.1: Survival studies in tumor injected mouse. All the mice survived until day 15 post tumor injection but none survived past day 19. The mean survival time was day 17 post tumor injection. (n=7).

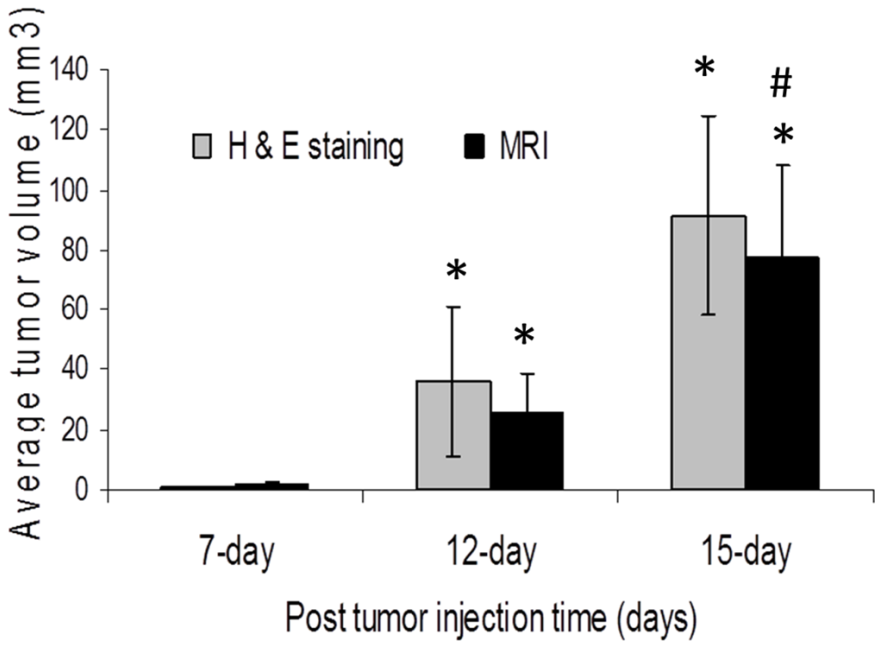

Figure 2.2: Tumor volume on day 7, 12, and 15 post 3-LL tumor cell injection in female Balb/c mice using both H&E staining and T2-weighted MRI. The data are represented as mean ± sem, n=5 for each time point. *p<0.05 compared to day 7 tumor mice within same group; # p<0.05 compared to day 12 tumor mice within same group as assessed by 2-way ANOVA.

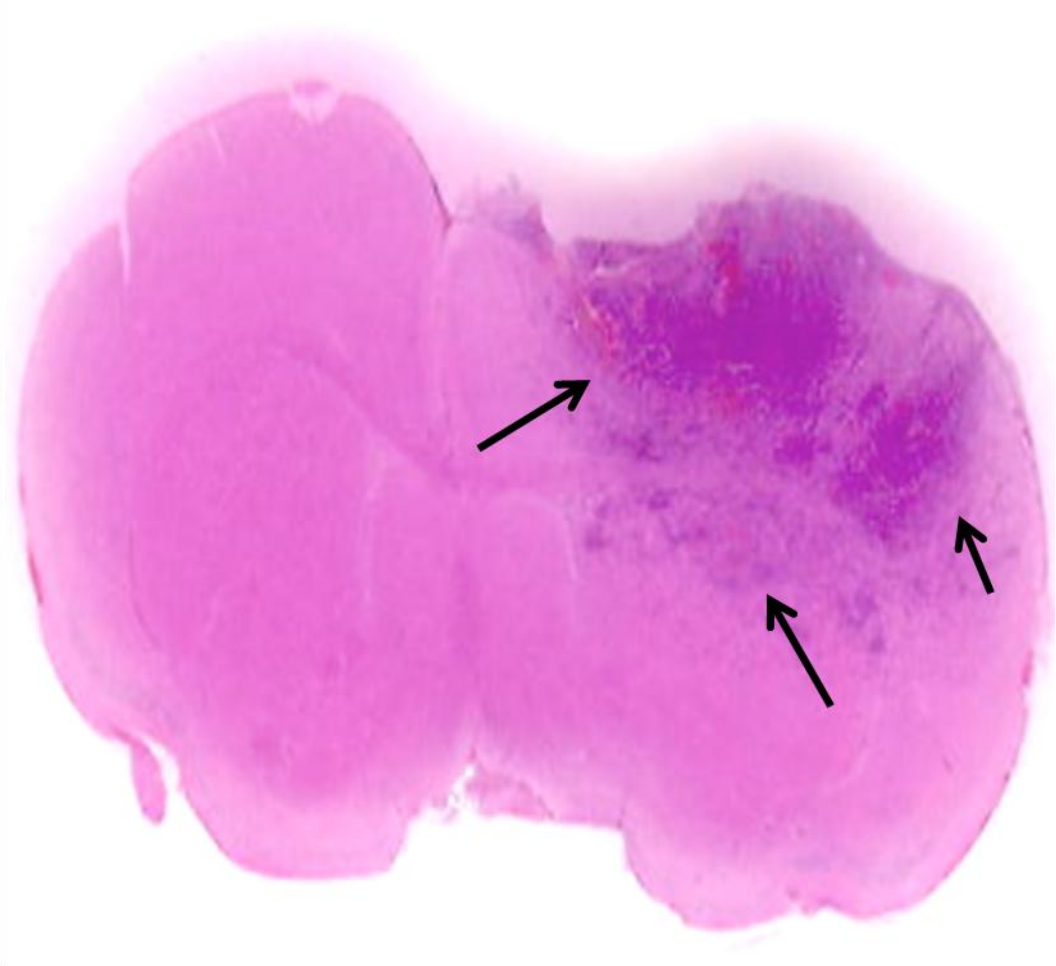

Figure 2.3: H & E stained mouse brain section on day 15-post tumor injection. Arrows indicate the tumor areas. The 3LL tumor cells were restricted to the right hemisphere only. Note that even at this advanced stage, tumor mass is confined to right hemisphere.

2.3.2. Effects of Tumor on Cerebral Vascular Volume:

The impact of tumor growth on cerebral vascular angiogenesis was determined by measuring both the protein and ^{3}H-mannitol content in the capillary pellet from the tumor-bearing right brain hemisphere and the non-tumor bearing left hemisphere at various days during tumor development. At days 7 and 10 post tumor cell implantation, the fraction of administered ^{3}H-mannitol present in the capillary pellet was approximately 0.005 (Table 2.1). Furthermore, there were no differences in ^{3}H-mannitol content in the capillary fractions taken from the right (tumor bearing) versus left (non-tumor bearing) brain hemispheres from day 7 and day 10 mice (Table 2.1). However, by day 12, there was a slight but significant increase in ^{3}H-mannitol content in the capillary fraction from the right hemisphere compared to that observed in the left hemisphere. Differences in radiolabeled mannitol content in the vascular pellet were even greater at day 15 post tumor cell implantation, with an almost two-fold increase in radiolabeled mannitol content from the right hemisphere capillary fraction compared to the left hemisphere (Table 2.1). Qualitatively similar data were observed with protein content in the capillary fractions from the right and left brain hemispheres (Table 2.1).

Table 2.I: Changes in cerebral vascular volume in mice as a function of brain tumor development.

Days post-tumor cell implantation	Brain Hemisphere	Vascular ^{3}H-Mannitol Content[a]	Vascular Protein Content (mg/ml)
7	Right	0.0052± 0.0006	12 ± 4
7	Left	0.0052±0.0003	16 ± 6
10	Right	0.0049± 0.0014	15 ± 1
10	Left	0.0048±0.0008	17 ± 7
12	Right	0.0061±0.0004*	25 ± 3*
12	Left	0.0051±0.0003	16 ± 4
15	Right	0.0081±0.0014*	38 ± 7*
15	Left	0.0043 ±0 .00002	16 ± 2

[a] The content of ^{3}H-mannitol in the brain microvasculature was determined by taking the ratio of radioactivity in the capillary enriched fraction (dpm/mg protein) to that in the blood (dpm/ml).*$p < 0.05$ compared to values in left hemisphere on the same day. (n=7).

2.3.3. Permeability Assessment in Brain and Tumor Microvasculature:

Blood-brain barrier permeability was examined at various stages of tumor development using both small molecule (^{3}H-mannitol) and large molecule (Evans Blue) permeability markers. In the sham operated mice, ^{3}H-mannitol had a brain-to-plasma ratio of approximately 5% in both the right and left brain hemispheres (Figure 2.4). The amount of radiolabeled mannitol present in the left (non-tumor bearing) hemisphere from tumor cell injected mice was similar to that found in the sham operated mice at all time points examined (Figure 2.4). At the earlier time points examined (i.e. days 7 and 10-post tumor cell implantation), there were no significant differences observed in radiolabeled mannitol permeability in the right (tumor-bearing) hemisphere compared to the left hemisphere (Figure 2.4). However, there was a slight but statistically significant increase in ^{3}H-mannitol permeability in the right hemisphere in mice by 12-days post tumor cell implantation (Figure 2.4). By day 15-post tumor cell implantation there was an approximately 2-fold increase in mannitol permeability in the right hemisphere compared to the left hemisphere (Figure 2.4). Despite the increases in ^{3}H-mannitol penetration observed in the tumor bearing portion of the brain, quantitative assessment showed that Evans

Blue accumulation in the capillary depleted fractions from both right and left hemispheres was comparable to the sham mice at all time points examined (data not shown).

Qualitatively similar results were obtained using Gad enhanced MRI to assess BBB integrity. In both the sham operated mice and in the pre-tumor injected mice, no Gad enhancement was observed, indicating there was no vascular damage attributable to the surgical procedure itself (Figure 2.5). Furthermore, the mean Gad enhancement in tumor bearing mice at day 7 was similar to that observed in sham operated mice. However, by day 12 of tumor cell implantation, there was visible leakage observed in all the mice examined. The mean Gad enahncement in the tumor mice at day 12 was approximately 3-fold higher than the control mice (Figure 2.5). An even larger area of Gad leakage was observed by day 15 post tumor cell implantation with a 9-fold greater mean Gad enahcement value in tumor bearing mice compared to control mice (Figure 2.5).

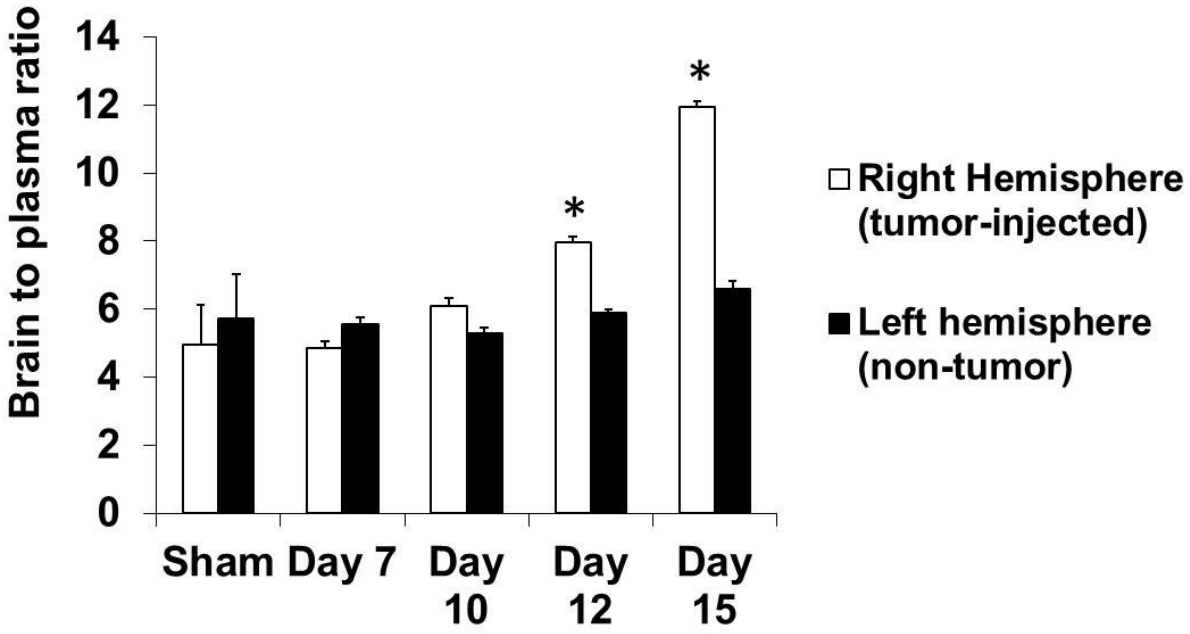

Figure 2.4: Permeability of radiolabelled mannitol across the blood brain barrier in tumor bearing mice. Mice at different stages of tumor development were given i.v. injections of radiolabelled mannitol. Animals were sacrificed and the brain separated into right (tumor-bearing) and left (non-tumor bearing) hemispheres. The data are presented as the brain to plasma ratio of the resulting radioactivity. Each data point is the mean ± sem of at least 9 mice. The student t-test was performed to compare the differences in the tumor bearing right hemisphere and non-tumor bearing left hemisphere on each corresponding day.

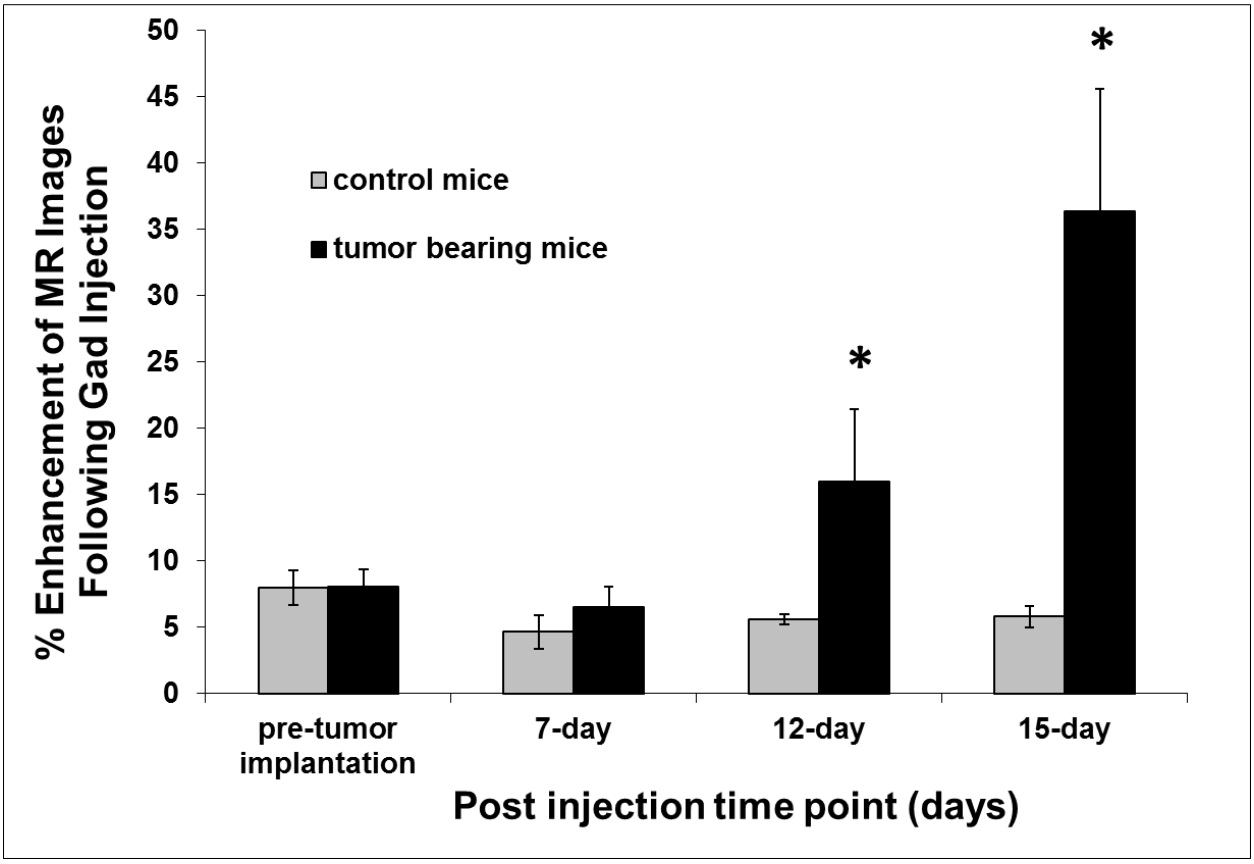

Figure 2.5: The percent enhancement of the MR images after Gad injection at different stages of tumor growth. Mice at different time points after the injection of media (control mice) or 3LL cells (tumor mice) were imaged using Gad-contrast enhanced MRI as a permeability marker. Each data point is the mean $\pm$ sem of at least 4 mice. The student t-test was performed and compared to the control mice at the same time point.

2.3.4. P-glycoprotein Expression:

To examine tumor-dependent alterations in P-gp expression in the microvasculature of the brain, Western blots were performed using capillary enriched fractions of the tumor-injected mouse brains at day 7, 10, 12, and 15 days post-tumor cell inoculation, and in sham mice at day 15 (Figure 2.6). Examination of P-glycoprotein (P-gp) expression in the capillary-enriched fractions indicated no significant differences in P-gp expression in the tumor-containing hemisphere compared to the non-tumor-bearing hemisphere at any of the days examined (Figure 2.6b). Immunhistochemical examination of the brain slices showed strong P-gp staining within the cerebral microvasculature with no apparent difference in P-gp staining in tumor versus non-tumor sections (Figure 2.7).

A.

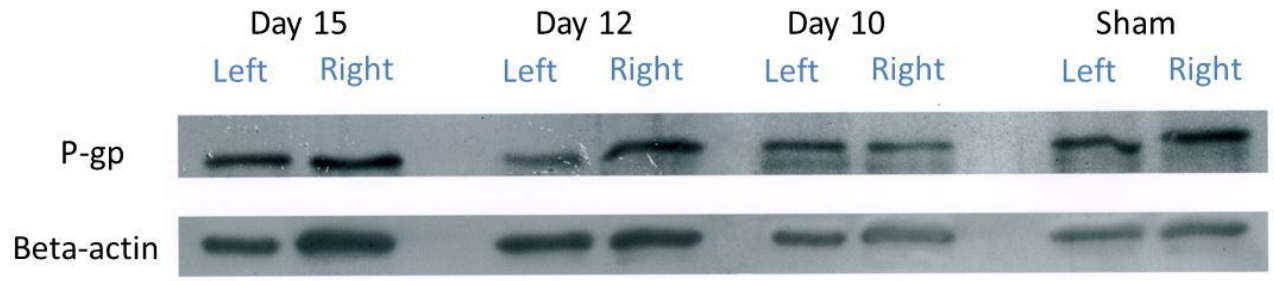

B.

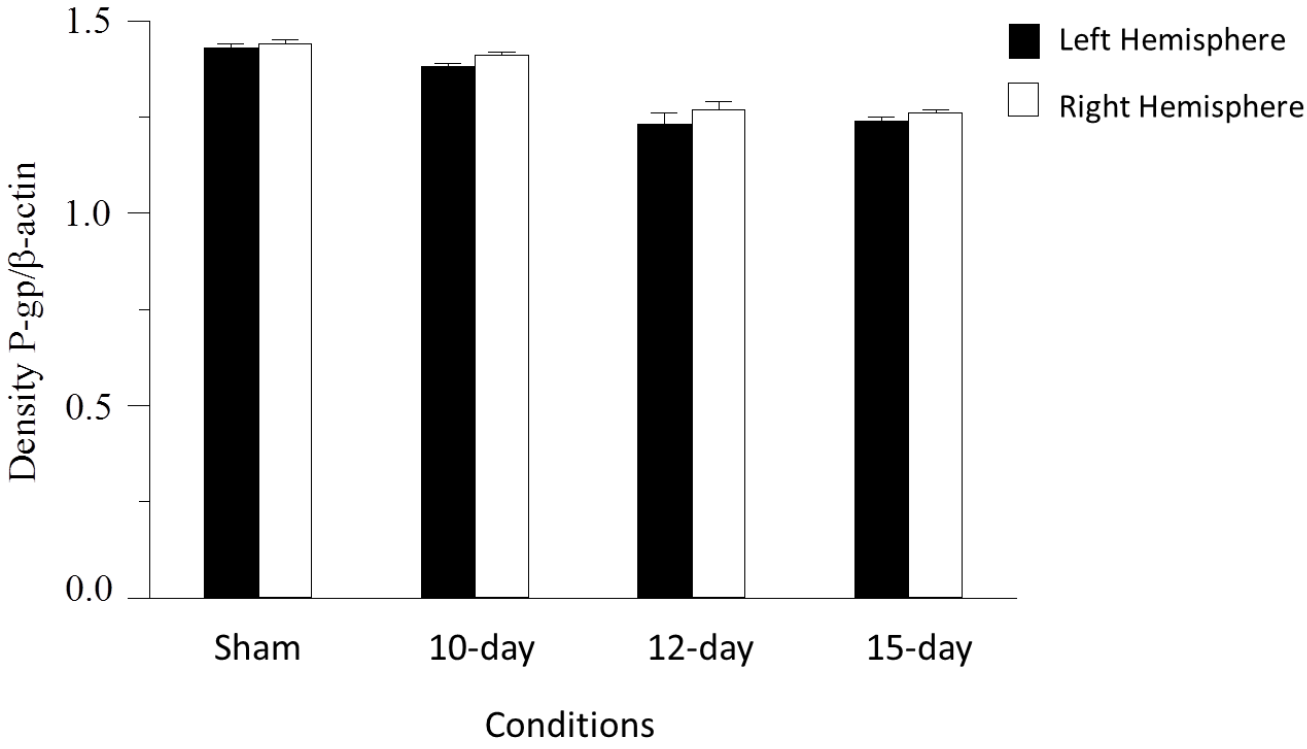

Figure 2.6: Western blot of capillary-enriched fractions from mice implanted with 3LL tumor cells at different times during tumor development. Panel A: Expression of P-gp and beta-actin in the left hemisphere and right hemisphere capillary-enriched fractions from tumor-injected mice on 15, 12 and 10-days post tumor injection. P-gp expression in the left and right hemispheres of sham operated mice (day 15) is also shown. Samples were pooled from 3 mice at each time point. Panel B: Densitometry analysis of the western blot samples for P-gp in capillaries from the left and right brain hemispheres.

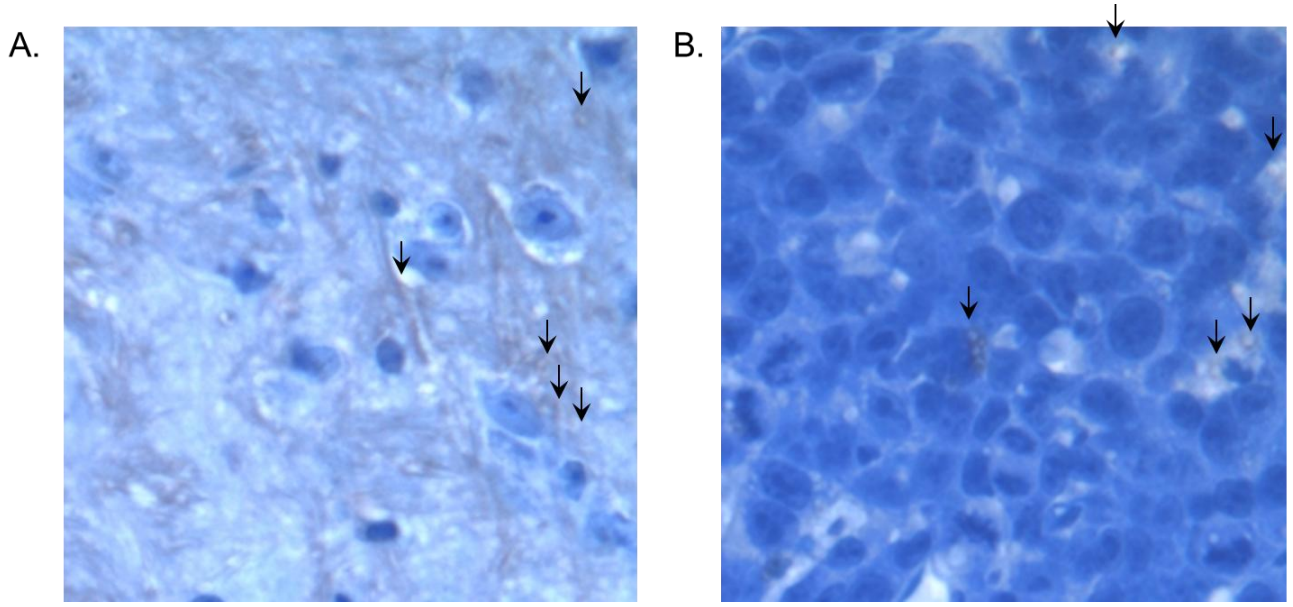

Figure 2.7: Immunohistochemistry of Day 15 mouse brain implanted with 3LL tumor. The arrows indicate the presence of p-glycoprotein, which appears as brown staining. The p-glycoprotein expression is confined to the microvessels and appears to be unchanged in non-tumor (A) and tumor (B) regions of the brain. (Images obtained from the same section of tissue).

2.4. DISCUSSION

The incidence of metastases to the brain is approximately 10% for all cancer patients ((Nayak, Lee, and Wen 2012, 48-54), with lung, breast and melanoma having the highest rate of metastasis ((Giglio and Gilbert 2010, 50-59)(Kamar and Posner 2010, 217-235)). In the case of lung tumor, metastases to the brain is a frequent complication present in 10% of patients at time of diagnosis and in approximately 40% of all lung cancer patients during the course of their disease (Schuette 2004, S253-7). Treatment of lung metastases to the brain has focused primarily on whole brain radiation therapy and surgery (Taimur and Edelman 2003, 342-346), with chemotherapy reserved for clinical trials (Kim et al. 2010, 258-263). While treatment varies depending on the type of cancer and stage of progression, patient prognosis and long-term survival have not improved regardless of treatment options.

The role of the BBB in the limited chemotherapeutic responses of brain tumors remains a fundamental issue. In the clinical setting, studies by Vogelbaum and colleagues measured the extravasation of S100beta, an astrocytic protein, into serum as a potential biomarker for brain tumors. The study consisted of 38 patients with newly diagnosed lung carcinoma and no neurologic symptoms or known history of brain metastasis (Vogelbaum et al. 2005, 817-824). The study demonstrated significantly elevated levels of S100β in serum, which would suggest that BBB integrity is compromised in these patients (Vogelbaum et al. 2005, 817-824). Histological examination of brain samples from patients indicated that tumor cells were infiltrating peritumoral brain tissue caused blood vessels to take on some of the structural characteristics of leaky vessels as tumor progresses (Stewart et al. 1987b, 697-705).

However, there is no clear consensus on BBB permeability within and around the tumor site. Studies by Regina et al., reported that specific morphological characteristics of the BBB

were maintained at the cellular level in brain tumors (Regina et al. 2001, 13-25). Perhaps the most convincing argument for the BBB having a role in the limited effectiveness of chemotherapeutic agents in treating most brain tumors is the observation that the same tumor cell that is resistant to chemotherapeutics when found in the brain, is significantly responsive when located at sites outside the brain (Weiss 1980, 51-81). This is reinforced in the studies by Wolff et al. (Wolff et al. 1999, 481-486) examined the in vitro cytotoxicity of a large panel of chemotherapeutic agents in various human, rat, and mouse glioma cells. Even in the most resistant cells, substantial cytotoxicity was observed with chemotherapeutic agents that are normally ineffective in the clinical treatment of brain tumors. Furthermore, BCNU, an agent commonly used clinically to treat brain tumors was among the least effective of all the chemotherapeutics examined in the in vitro cytotoxicity studies. This suggests the resistance of brain tumors to chemotherapeutic agents is due, in large part, to the failure to obtain appropriate therapeutic concentrations of the drugs in the brain. Indeed, a retrospective evaluation of tumor responsiveness to chemotherapeutic agents found a favorable response to chemotherapy was only around 45% in patients with small cell lung cancer brain metastases. One of the main contributing factors to the low response rate was inaccessibility to anti-cancer agents due to the blood-brain-barrier (BBB) (Stewart et al. 1987b, 697-705). Thus these studies suggest that the BBB remains intact, at least to the extent that significant delivery of chemotherapeutic agents is compromised, and that improving the permeability of chemotherapeutic agents in the BBB may have a substantial impact on the treatment of brain tumors.

The goal of the present study was to evaluate BBB permeability throughout various stages of tumor growth in a murine brain tumor model relevant to metastatic brain tumors. The

model consisted of Lewis Lung carcinoma cells (3LL) implanted directly into the brain of Balb/c mice. In the present study, the resulting brain tumor progressed rapidly with a median survival time of 17 days and none of the mice surviving past 19 days. Histological examination and MRI indicated the tumor progresses as a relatively defined mass with no micrometastases observed. The 3LL tumor cell line is a lung carcinoma originally isolated from the C57BL/6 mouse strain (Talmadge and Fidler 1982, 975-980). However implanting 3LL cells into allogeneic recipients, including Balb/c, is characterized by local tumor development at the site of implantation but no spontaneous metastases to other tissue (Isakov, Feldman, and Segal 1982, 12-32). Interestingly, this is not due to lack of migration of the cells from the primary site, but to immunogenetic restrictions in tumor development within the allogeneic host. Thus intracranial implantation of the 3LL cells into Balb/c mice provided an ideal model to focus on tumor-induced alterations in BBB function and the implications of this from a drug delivery standpoint without concerns about multiple tumor sites within the brain.

The present study examined BBB permeability during various stages of tumor progression using two complimentary methods. The first method used a radiolabeled small molecule tracer, ^{3}H-mannitol and a large macromolecule tracer dye, Evans blue, to assess permeability alterations. For the small molecule tracer, the current study shows that the BBB remains intact early on in tumor progression (up to 10 days post tumor cell implantation), and becomes leaky only after the tumor mass has progressed to approximately 10 mm^3 or more (i.e 12-days post tumor cell implantation and beyond). However, even though BBB integrity to the small hydrophilic vascular permeability agent was significantly altered at the later stages of tumor development, permeability to Evans blue, a dye that binds with high affinity to albumin, remained unchanged. This suggests that although tight junctions are disrupted, the wholesale

breakdown of BBB integrity observed with other CNS pathologies does not occur in this particular brain tumor model.

Similar findings were observed using MRI techniques to monitor BBB permeability during tumor progression. In the present study, Gad contrast agent was used to quantitatively measure BBB changes during tumor progression. There was essentially no Gad enhancement observed in the brain images of the sham-operated mice, indicating that the surgical implantation of tumor cells did not lead to vascular leakage. Likewise, there was no Gad enhancement observed in the brain images of tumor-bearing mice at 7 days post tumor implantation, suggesting no alterations in BBB permeability at this early stage of tumor development. However, there was significant enhancement of the Gad contrast enhancement in the brain images of tumor mice at 12 and 15-days post tumor cell implantation.

Interestingly, the changes in BBB permeability observed in tumors at the later stages of development in the present study occurred along the same time frame as increased angiogenesis within the tumor. At the most advanced stages of tumor development (i.e. day 15) there was an approximately 2-fold increase in cerebral microvasculature volume. This increase coincided with the dramatic enhancement in BBB permeability observed in the tumor regions at day 15. The 3LL tumor metastases to the brain are characterized by increased angiogenesis to support tumor growth (Fathallah-Shaykh et al. 2000, 217-222). This is consistent with other metastatic brain tumor models. For instance, studies indicated that the BBB was intact in the early stages of human metastatic brain tumor growth in nude mice (Zhang et al. 1992, 1115-1124). In these studies in which human breast cancer cells were implanted in the brain, it was observed that the BBB remained intact in tumors smaller than 0.25 mm in diameter, but was leaky in larger metastases (Zhang et al. 1992, 1115-1124). A similar finding of alterations in BBB

permeability as a function of tumor progression has also been demonstrated in studies using a mouse melanoma metastatic brain tumor model (Cranmer et al. 2005b, 325-356). Together these studies highlight the impact of tumor development on BBB permeability.

Gadolinium-contrast enhanced MRI is commonly used clinically to examine BBB integrity and identify brain tumors with enhanced vascular permeability (Essig et al. 2006, 89-106). Additional advantages of using MRI and the Gad to assess BBB permeability in the current study was the ability to monitor permeability changes within the same animal and the ability to examine regional differences in BBB permeability. Thus, while Gad contrast revealed significant leakage within the tumor site, as much as 9-fold enhancement by day 15 post-tumor cell implantation, there was little if any enhancement observed outside of the tumor margins. These findings, together with the radiolabeled mannitol permeability assessments in the right and left hemispheres, suggest that the alterations in BBB permeability observed during later stages of tumor development are confined to regions within the tumor itself. The implication of this finding is that the presence of an intact BBB surrounding the tumor would create a substantial concentration gradient between the tumor and non-tumor regions of the brain. As a result of the concentration gradient, there would be diffusion of the chemotherapeutic agent away from the tumor into non-tumor sites with lower concentration of Gad. Such a phenomenon may in part account for the recent findings of Lockman and colleagues (2010) demonstrating that even in brain tumor models with disrupted BBB function, the resulting concentration of therapeutic agents within the tumor site was sub-optimal for affecting tumor growth. These studies highlight the importance of an intact BBB around the tumor site and suggest the resistance of brain tumors, even relatively leaky brain tumors, to chemotherapeutic

agents may stem from the failure to obtain appropriate therapeutic concentrations of the drugs throughout the brain.

The increases in BBB permeability of radiolabeled mannitol and Gad contrast agent observed in the later stages of brain tumor development reflect a breakdown of the tight junction complexes of the brain endothelial cells that limit paracellular diffusion. However, the expression of drug efflux transporters at the BBB and the BTB may also limit distribution of chemotherapeutic agents in the brain (Rice et al. 2003, 339-343). ABC transporters including P-gp, MRP and BCRP localized at the luminal side of the endothelium are the main contributors to the development of multidrug resistance (MDR) in brain cancer patients.

The most extensively studied drug efflux transporter in the BBB is P-gp. As P-gp transports a variety of drugs, its expression within the brain endothelial cells forming the BBB could impact on a wide range of chemotherapeutic agents (Bachmeier et al. 2005, 1259-1268). Indeed, using a mouse glioblastoma brain tumor model, Fellner and colleagues reported that paclitaxel, a P-gp substrate, did not affect tumor volume. However, co-administration of paclitaxel (intravenous) and PSC833, an inhibitor of P-gp, resulted in significant reductions in tumor volume in treated mice by 90% (Fellner et al. 2002, 1309-1318). Thus, P-gp is an important obstacle preventing paclitaxel entry into the brain, and inhibition of this transporter allows the drug to reach sensitive tumors within the CNS (Fellner et al. 2002, 1309-1318). These findings are consistent with a role for P-gp in the resistance of some brain tumors to chemotherapy agents (Henson, Cordon-Cardo, and Posner 1992, 37-43; Fellner et al. 2002, 1309-1318).

Given the important contribution of P-gp in restricting chemotherapeutic permeability in the BBB, an additional concern is the potential influence of tumor progression on P-gp

expression within the BBB. Recent studies indicate down regulation of drug efflux transporter expression in cerebral vascular cells within the tumor regions of patients with primary central nervous system lymphoma (Sakata et al. 2011, 333-339). In contrast, an increased expression of drug efflux transporters have been reported in other CNS tumors such as ependymomas (Ginguene et al. 2010, 926-935). In the 3-LL brain tumor model used in the present study, P-gp expression was observed throughout brain tumor development. As P-gp was not expressed in the tumor cells, the main source is likely the brain capillary endothelial cells. More importantly, there was no significant difference in P-gp expression in the tumor-bearing and non-tumor bearing cerebral vascular samples at any time point examined. These findings indicate that even though there is a substantial increase in ^{3}H-mannitol and Gad permeability at the later stages of tumor development, suggesting a breakdown of the tight junctions between the brain endothelial cells, P-gp expression remained unchanged. Therefore, from a therapeutic perspective, even at the later stages when BBB permeability is compromised, P-gp is likely to be functional and may limit chemotherapeutic delivery to the tumor site.

In summary, we have successfully established a brain tumor model in mice using 3LL cells. The median survival of the mice with tumors was 17 days and in this model (Figure 2.1), BBB was intact at the initial stages of brain tumor development (Figures 2.4 and 2.5); however, at the later stages as tumor mass increased, the BBB was leaky to small molecules such as mannitol and Gad-contrast agent. There were no changes in P-gp expression within the BBB at any of the time points examined following tumor cell implantation (Figure 2.6). Based on these findings it would appear that modification of BBB permeability either through barrier disruption techniques (Hall et al. 2006, 279-284; Meairs and Alonso 2007, 354-362; Sato et al. 1998, 1135-

41; disc 1141-2) or pharmacological inhibition of drug efflux transporters could have a favorable impact on brain tumor responsiveness to chemotherapeutic agents.

CHAPTER 3: ASSESSMENT OF P-GLYCOPROTEIN ACTIVITY IN THE BLOOD-BRAIN BARRIER (BBB) USING NEAR INFRARED FLUORESCENCE (NIRF) IMAGING TECHNIQUES.

3.1. INTRODUCTION

The delivery of many drugs for the treatment of central nervous system (CNS) disorders is limited by the presence of the blood-brain barrier (BBB). The BBB is comprised of a continuous layer of endothelial cells, associated astrocyte foot-processes and scattered pericytes. However, it is the brain microvessel endothelial cells with highly developed tight-junction complexes, low endocytic activity and the absence of fenestrations (Girardin 2006, 311-321) that provide the physical barrier to the passage of most polar and hydrophilic solutes from the blood into the brain. In addition to restricted paracellular diffusion, the brain microvessel endothelial cells (BMEC) forming the BBB express numerous transporter systems that are essential for maintaining the proper brain microenvironment (Girardin 2006, 311-321; de Boer and Gaillard 2006, 455-462).

P-glycoprotein (P-gp) is a drug efflux transport protein that was originally identified in multidrug resistant cancer cells (Matsuoka et al. 1999, 383-392), but is also found in intestinal, kidney and liver epithelial cells and the BMEC of the BBB (Balayssac et al. 2005a, 319-329). A member of the ATP-binding cassette (ABC) family of proteins, P-gp actively transports a wide variety of drugs out of the cell (Ernst et al. 2010, 540-549). The expression of P-gp and related drug efflux transporter in the BBB has multiple implications on CNS response to drugs. The presence of P-glycoprotein activity in the BBB influences the brain distribution of a large number of therapeutic agents including anticancer drugs, antivirals, antihistamines, antiepileptics and analgesics (Bachmeier et al. 2005, 1259-1268; Lin and Yamazaki 2003, 59-98; Lee et al. 2010, 603-619; Schinkel et al. 1996, 2517-2524). The wide range of drugs with P-gp transporter activity also poses potential problems with regard to drug interactions and unwanted brain penetration of therapeutic agents (Feng et al. 2008, 268-275). A final consideration is the

potential for altered P-gp expression and/or activity in the BBB in response to hypoxia (Callaghan et al. 2008, 365-378), seizure activity (Pekcec et al. 2009, 144-151) or drug exposure itself (Haslam et al. 2008, 246-255). For all the above, the ability to assess P-gp activity has important implications for understanding both drug and pathology induced changes in BBB permeability.

Positron emission tomography (PET) is a powerful imaging tool for assessing CNS function. Application of PET imaging to assess P-gp activity in the BBB has been performed with radiolabeled P-gp substrates including [^{11}C] verapamil, [^{11}C] cloperamide and [^{11}C] N-des-methyl loperamide in human and in animal studies (Dorner et al. 2009, 6073-6082; Langer et al. 2007, 1774-1784). However, the highly specialized facilities and instrumentation required and the costs associated with PET imaging limit its general use. Therefore, alternative imaging techniques applicable to small animal pre-clinical studies are needed. Fluorescence and bioluminescence have been used for imaging studies, although tissue penetration is a major limitation (Choy, Choyke, and Libutti 2003, 303-312; Kaijzel, van der Pluijm, and Lowik 2007, 3490-3497). The development of near infrared fluorescence (NIRF) imaging techniques has emerged as an alternative to PET. The longer emission wavelength allows deeper tissue penetration (up to 2 or more centimeters compared to 1-2 mm with standard fluorescent imaging probes) (Ntziachristos, Bremer, and Weissleder 2003, 195-208). Additionally, background fluorescence in tissue and cells is low in the NIRF range (700-800nm) (Klohs, Wunder, and Licha 2008, 144-151). While there are a growing number of near infrared probes for various applications (Hilderbrand and Weissleder 2010, 71-79), there are no published reports of NIRF imaging agents for P-gp. Development of such probes would greatly facilitate application of NIRF imaging techniques for assessing P-gp function.

The purpose of the present study was to identify a suitable method for examining P-gp activity using NIRF imaging techniques. Rhodamine 800 (R800) is a lipophilic, cationic dye with a chemical structure similar to that of rhodamine 123 (R123), a P-gp substrate (Miller et al. 1996, 301-306). Unlike the other rhodamine dyes, R800 has fluorescence emission properties in the NIRF range (685 to 730 nm wavelength). Based on these properties, R800 was examined as a potential NIRF imaging probe for assessing P-gp activity in the BBB. Results of the present study demonstrate that R800 is indeed a P-gp transport substrate. The initial *in vivo* studies suggest R800 may be a suitable NIRF imaging agent for assessing P-gp activity in the BBB.

3.2. MATERIALS AND METHODS

3.2.1. Materials/Reagents:

Rhodamine 800 was purchased from Exciton Inc. (Dayton, Ohio). The vascular and lymphatic NIRF imaging agent, IRdye 800cw PEG, was obtained from Licor (Omaha, NE). Elacridar (GF120918) was obtained from Toronto Research Chemical Inc. (North York, ON). Dulbecco's Modified Eagle's Medium, standard fetal bovine serum, non-essential amino acid solution, and 1X trypsin were purchased from HyClone (Logan, Utah). Penicillin-streptomycin was supplied by MP Biomedicals (Solon, Ohio). Ketamine hydrochloride and xylazine were purchased from Wyeth (Guelph, ON) and Bayer Inc. (Toronto, ON) respectively. Transwell® polycarbonate membrane inserts (0.4μm pore size; 24 mm diameter) were purchased from Corning Incorporated (Corning, NY). All other reagents and chemicals were purchased from Sigma Chemical Company (St. Louis, MO).

3.2.2. Cell Lines:

Madin-Darby canine kidney epithelial cells (MDCK) were purchased from American Type Tissue Culture Collection (Manassas, VA) and MDCK cells transfected with the human *MDR1*gene were provided by M. Gottesman, National Cancer Institute (Bethesda, MD). The cells were grown in Dulbecco's Modified Eagle's Medium (DMEM) supplemented with 10% standard fetal bovine serum, 1% penicillin-streptomycin and 1% non-essential amino acids. The MDCK*MDR1* were grown in the same media as described above with the addition of (0.2 μM) colchicine to maintain elevated expression of P-glycoprotein. Cells were expanded in 75 cm^2 culture flasks and seeded onto 12-well culture plates or Transwell® inserts at a density of 50,000 cells per cm^2 for uptake and permeability studies, respectively. Cells were grown in a humidified environment of 37°C with 5% CO_2 with media replacement every other day.

3.2.3. Accumulation Studies:

Confluent monolayers of MDCKWT and MDCK*MDR1* cells were grown in a 24-well plate and pre-treated for 30-minutes at 37^O C with 0.5 ml assay buffer (AB, containing in mM; 122 NaCl, 3 KCl, 1.4 $CaCl_2$, 1.2 $MgSO_4$, 25 $NaHCO_3$, 10 HEPES, 10 glucose, and 0.4 K_2HPO_4 at a pH of 7.4) with or without 1μM GF120918. Following pre-treatment, solutions were removed and replaced with assay buffer (AB) containing 3.2μM of R800 with or without 1μM GF120918. Cells were incubated for various time points (15-60 minutes) at 37°C, after which the solutions were aspirated, and the cells were washed 3 times with 0.5 ml/well of ice-cold phosphate buffered saline solution (145 mM NaCl, 3mM NaH_2PO_4, and 7mM Na_2HPO_4) and then solubilized with 0.5 ml/well of 1% Triton-X 100. The amount of R800 in MDCKwt and MDCK*MDR1* cells under control and GF-120918 treated conditions was normalized to the amount of protein present in cell

lysates and determined using an Odyssey Near Infrared Imaging System (LI-COR Biosciences, Lincoln, Nebraska) set on the 700 nm channel.

3.2.4. Bi-Directional Permeability Studies:

Permeability was assessed over a 60 minute period in both MDCKWT and MDCK*MDR1* monolayers in the apical to basolateral (A to B) and basolateral to apical (B to A) directions. The volume of the apical compartment was 1.5 ml and the volume in the basolateral compartment was 2.5 ml. The initial concentration of R800 in the donor compartment was 10 µM. Samples were removed from the donor compartment (10 µl) at the start of the study. Samples were also taken from the receiver compartment (150 µl) at various times over a 60-minute period. In separate studies, bi-directional permeability of R800 was also determined following a 30-minute pre-treatment with the P-gp inhibitor, GF120918 (1.0 µM). All samples removed were replaced with an equal volume of assay buffer, and all permeability studies were performed at 37˚C. Samples were analyzed as described above using the Odyssey near infrared fluorescence imager (LI-COR Bioscience, Lincoln, Nebraska) and the apparent permeability coefficients (P_{app}) were determined based on the following formula:

$P_{app} = dC_r/d_t\ (V_d/A * C_d)$

Where C_r is concentration in the receiver compartment; t is time; V_d is the volume in the donor compartment; A is the area; and C_d is the concentration in the donor compartment at time 0.

The efflux ratio (ER) was determined by dividing the P_{app} for R800 in basolateral to apical (B-A) direction by the P_{app} for R800 in the apical to basolateral (A-B) direction as described previously (32, 33).

3.2.5. P-gp ATPase Assay (These studies were done by Martha Hinton):

R800-induced ATP hydrolysis was assessed using High Five insert cell membranes expressing human MDR1, BCRP and MRP1 (BD Bioscience). A 0.06 mL reaction mixture containing 20 µg membranes, 20 µM verapamil (positive control) or various concentrations of R800 (1-10 µM) and 5 mM MgATP, in buffer containing 50 mM Tris-MES, 2 mM EGTA, 50 mM KCl, 2mM dithiothreitol, and 5 mM sodium azide, was incubated at 37^{o}C for 20 minutes in the presence or absence of sodium orthovanadate (Martin et al. 1997, 765-771). Orthovanadate inhibited P-gp dependent ATP hydrolysis by trapping MgADP in the nucleotide binding site. Thus, ATPase activity measured in the presence of orthovanadate was subtracted from the activity generated without orthovanadate to yield vanadate-sensitive ATPase activity. The reaction was stopped by the addition of 30 µL 10% sodium dodecyl sulfate (SDS) with antifoam A. An additional 20 minutes incubation at 37^{o} C was performed following the addition of 200 µL of 35 mM ammonium molybdate in 15 mM zinc acetate in 10% ascorbic acid (1:4). The liberation of inorganic phosphate resulting from the addition of P-gp transport substrate was detected through absorbance at 630 nm using a Synergy HT plate reader and quantitated by comparing the absorbance to a phosphate standard curve. The EC_{50}, K_m and V_{max} values from the ATPase studies were determined using a sigmoidal dose-response nonlinear regression curve fit of the experimental data performed by GraphPad Prism version 3.02 (GraphPad Software, San Diego, California).

3.2.6. R800 Tissue Distribution in Mice:

Adult female Balb/c mice were obtained from the University of Manitoba breeding colony and maintained in the Central Animal Care Facility under temperature-controlled environment with 12 hours dark/light cycle and unlimited access to food and water. All animal

experiments were approved by the University of Manitoba Animal Care Committee (protocol number 08-0866).

Female Balb/c mice were anesthetized with a cocktail of ketamine and xylazine. Mice were administered R800 (0.032 µmol/kg) either alone or in combination with the vascular permeability marker, IRDye 800cw PEG (0.01µmol/kg), via tail vein injection. To determine the effects of P-gp on R800 and IRDye 800cw PEG tissue accumulation, a separate group of mice received 9 mg/kg of GF120918 via tail vein injection 15 minutes prior to administration of the imaging agents. Previous studies have shown this dose and dosing schedule for GF120918 to produce plasma concentrations of GF120198 above the IC_{50} of the compound throughout the entire period of study. Stock solutions of GF120918 and R800 were prepared in dimethyl sulfoxide (DMSO) and diluted using 70 % ethanol or phosphate buffered saline (PBS) for GF120918 and R800, respectively, so that the final concentration of DMSO was less than 1%. The IRDye 800cw PEG solutions were prepared directly in phosphate buffered saline (PBS). Mice were sacrificed under anesthtetic of ketamine and xylazine at 20 minutes after administration of fluorescent imaging agents via cardiac perfusion with a 10% formaldehyde solution. Blood and tissue samples were collected and prepared for *ex vivo* imaging for R800 and IRDye 800cw PEG fluorescence using an Odyssey Near Infrared Fluorescence Imaging system. Fresh tissue was sectioned into 2 mm thick slices for *ex vivo* analysis. *In vivo* NIRF imaging was performed on both control and GF 120918 treated mice prior to sacrifice to obtain whole animal scans at various times using the Odyssey Near Infrared Fluorescent Imaging system.

3.2.7. Statisical Analysis:

The *in vitro* studies examining R800 accumulation and permeability were analyzed using ANOVA with Student Newman-Keul post-hoc comparison of the means. Changes in R800

fluorescence in the *ex vivo* tissue slice studies were analyzed using Student t-tests. Statistical significance was set at $p < 0.05$ unless otherwise noted.

3.3. RESULTS

3.3.1. ATPase studies:

To examine whether R800 was a P-gp substrate, studies were performed using P-gp, BCRP, and MRP1 membranes (Figure 3.1A). In these studies, hydrolysis of ATP was used as a quantitative index of drug efflux transporter activity. The results from the P-gp ATPase assay showed that R800 produced a clear dose-dependent increase in ATP hydrolysis (Figure 3.1B). The resulting EC_{50} with R800 in the P-gp membrane assay was approximately 7 μM. In contrast, R800 added to the BCRP and MRP1 membrane preparation displayed no clear concentration dependency (Figure 3.1A).

A.

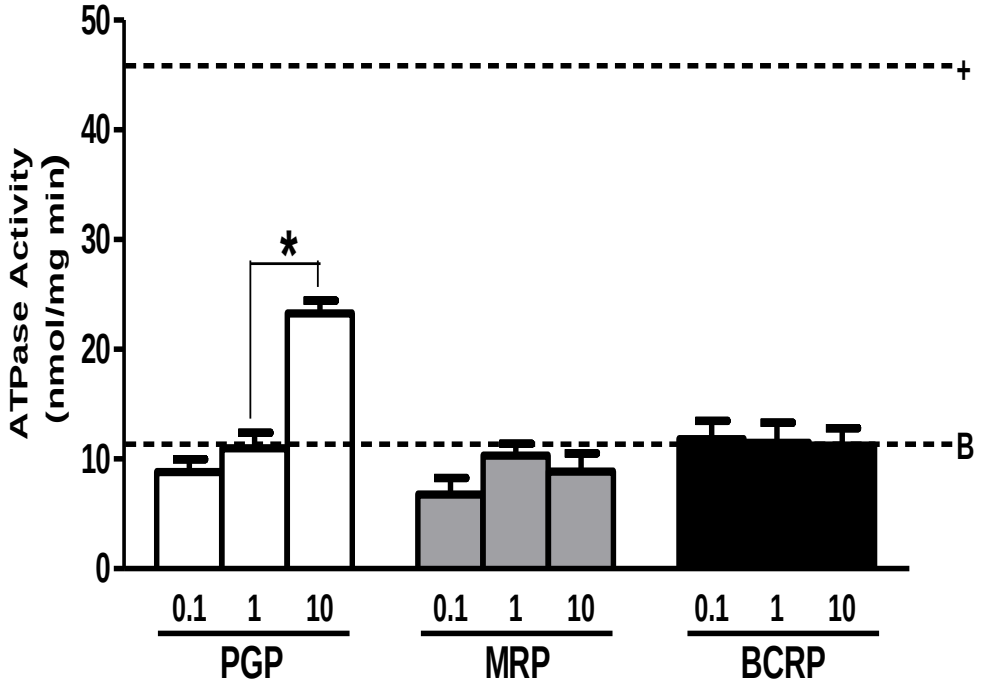

B.

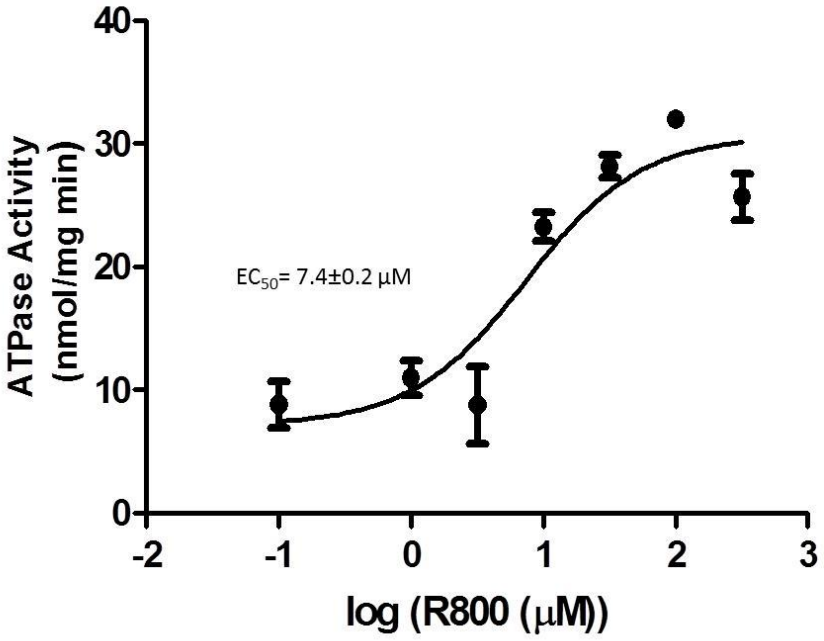

Figure 3.1: Membrane ATPase studies with R800. ATPase activity in P-gp, MRP1 and BCRP membranes following exposure to 0.1, 1 and 10 µM R800 (Panel A). Dashed lines represent basal (non-stimulated) activity (B) and response in P-gp membranes to 20 µM verapamil (+). Extended concentration response curve for R800 in P-gp membrane preparation (Panel B). Values represent the mean ± sem of 4 membrane preparations. * $p < 0.05$ compared to basal activity. Curve fitted using Graphpad Prism software 3.02.

3.3.2. Accumulation and Permeability Studies in MDCKMDR1 Cells:

Accumulation of R800 was examined in both MDCKWT and MDCK*MDR1* cell lines (Figure 3.2A). The accumulation of R800 was significantly lower in the MDCK*MDR1* cells compared to the wild-type cells ($p<0.05$) at all time points examined, with the greatest differences observed at the 45 and 60 minutes time points (Figure 3.2A). Treatment of the MDCK*MDR1* cells with GF120918 resulted in a significant enhancement in R800 accumulation in the cells (Figure 3.2A). Following treatment of the MDCK*MDR1* with GF120918, cellular levels of R800 were comparable to those observed in the MDCKWT cells under normal conditions. Qualitatively similar data were obtained using NIRF microscopy studies with the MDCK*MDR1* cells showing little R800 fluorescence under control conditions (Figure 3.2B), and substantially higher levels of fluorescence following treatment with GF120918 (Figure 3.2C).

The bi-directional transport of R800 was also examined in MDCK*MDR1* monolayers. Under normal conditions (control), permeability was significantly greater in the basolateral to apical (B-A) direction compared to that observed in the apical to basolateral (A-B) direction (Figure 3.3A). As a result, the efflux permeability ratio for R800 was approximately 3 in MDCK*MDR1* monolayers (Figure 3.3B). In contrast, MDCK*MDR1* monolayers treated with GF120918 displayed similar permeability in both the B-A and A-B directions (Figure 3.3A) and had an efflux permeability ratio near 1 (Figure 3.3B).

A.

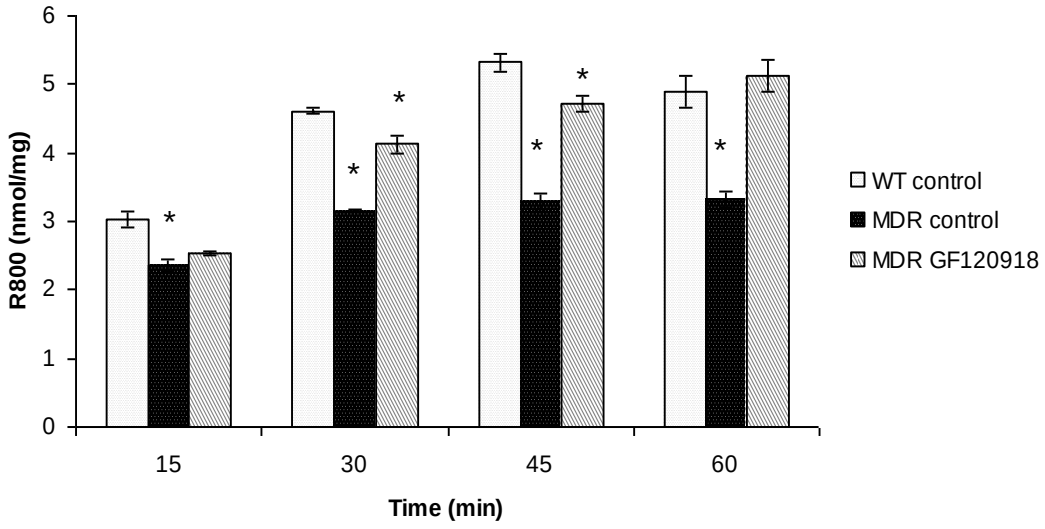

B. **C.**

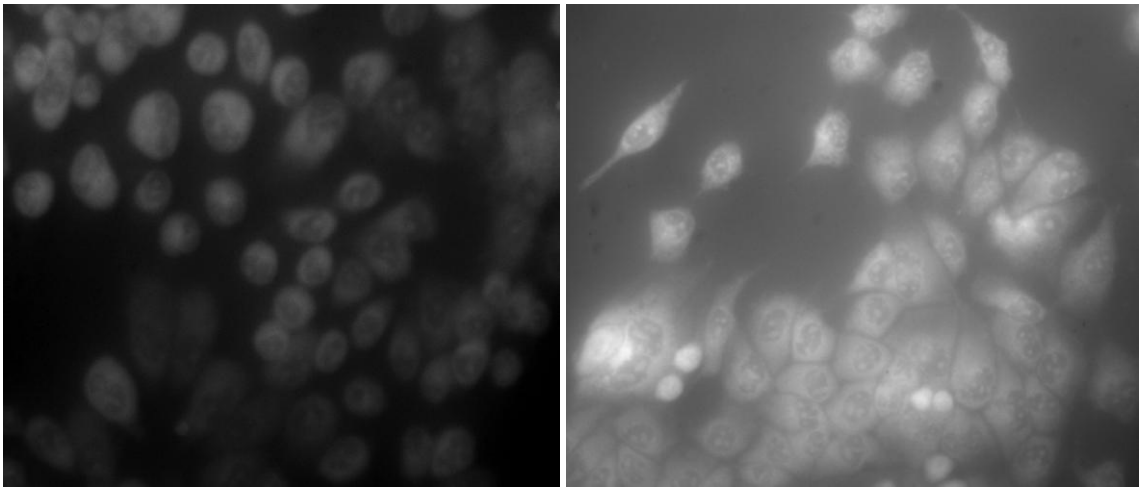

Figure 3.2: Cellular accumulation of R800 in MDCK*wt* and MDCK*MDR1* monolayers. Time-dependent accumulation of R800 in MDCKwt and MDCKMDR1 cells in the absence and presence of 1 µM GF120918 (Panel A). Fluorescence micrographs of R800 in MDCK*MDR1* cells following a 30 minutes exposure to 3.2 µM R800 alone (Panel B) or 3.2 µM R800 together with 1.0 µM GF120918 (Panel C). Values represent the mean ± sem of 3 monolayers per time point and treatment group. * $p < 0.05$ compared WT at the same time point.

A.

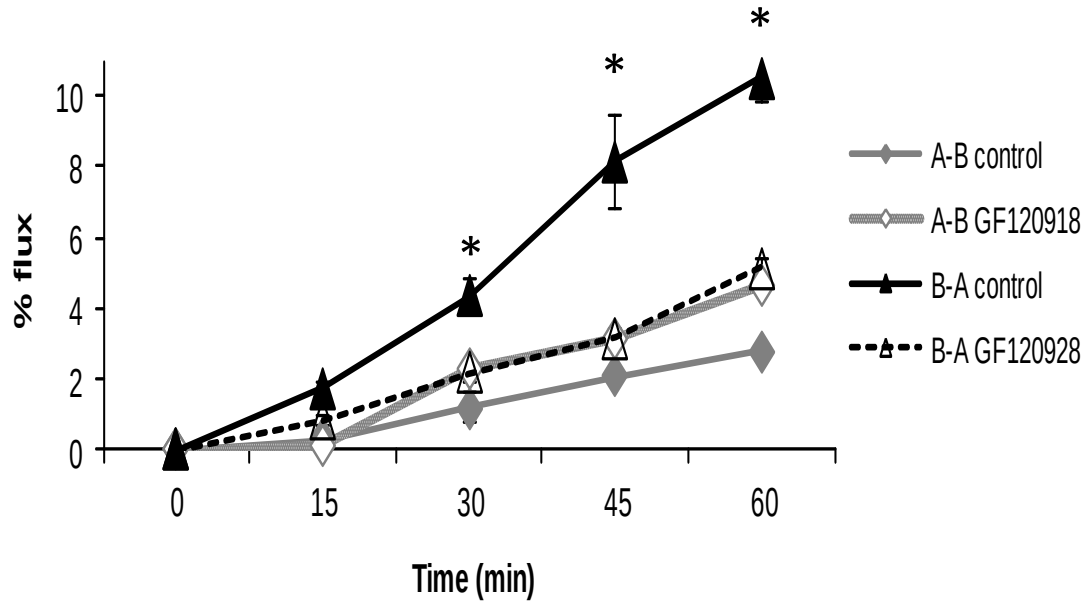

B.

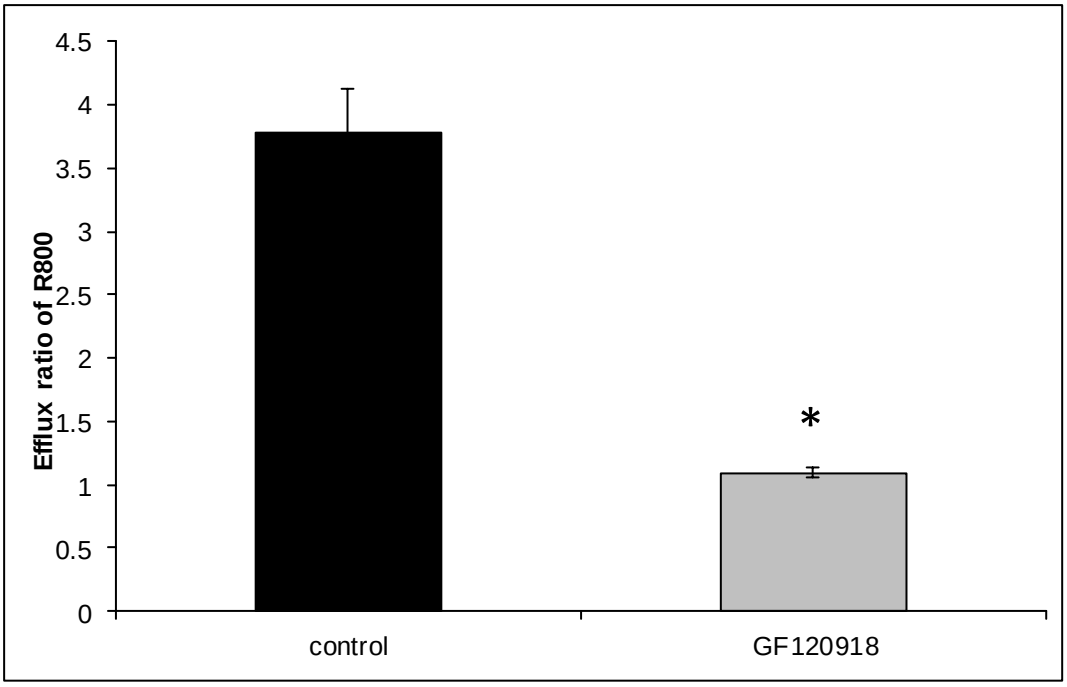

Figure 3.3: R800 permeability studies in MDCK*MDR1* monolayers. Bi-directional permeability studies for R800 in MDCKMDR1 cells in the presence and absence of GF120918 (Panel A). Efflux ratio (ER) values for R800 under control conditions and following treatment with GF 120918 (Panel B). The ER values were based on apparent permeability coefficients determined at 60 minutes. Values represent the mean ± sem of 3 monolayers per treatment group. * $p < 0.05$ compared to A-B control monolayers; * $p < 0.05$ compared to ER in control group.

3.3.3. R800 Tissue Distribution in Mice:

The accumulation of R800 in the brain following systemic administration of the imaging dye was examined in mice under normal conditions and following treatment with P-gp inhibitor (GF120918). Representative brain slices from mice receiving either vehicle (PBS), R800, or R800 with GF120918 pretreatment are shown in Figure 3.4. Under normal conditions, with functional P-gp, R800 accumulation in the brain is negligible, as indicated by the similar fluorescence in brain slices from R800 treated and vehicle injected mice receiving no R800 (Figure 3.4A and 3.4B). Indeed, the only brain regions showing appreciable accumulation of R800 were the ventricles, which showed intense fluorescence following i.v. injection of R800 (Figure 3.4B). In contrast, following pretreatment with GF120918, the amount of R800 accumulating in brain tissue was substantially enhanced compared to both non-treated mice and mice receiving R800 alone (Figure 3.4C). Quantitative assessment of R800 fluorescence in the brain and choroid plexus indicated an approximately 4-fold and 2-fold increase in fluorescence in the GF120918 pretreatment group, respectively, compared to control mice receiving R800 alone (Figure 3.5A). In contrast, the vascular permeability marker IRdye 800cw PEG, showed no appreciable brain accumulation in either control or GF120918 pre-treated mice (Figure 3.6). Whole animal imaging indicated accumulation of R800 in both the liver and kidney within 7 minutes and lasted up to 40 minutes following the injection (Figure 3.7). The accumulation of R800 in the liver was enhanced in mice treated with GF 120918 (Figure 3.7). Similar findings were observed in the *ex vivo* assessment of R800 fluorescence in liver and kidney slices, with a 2-fold enhancement of fluorescence in the liver of GF120918 treated mice (Figure 3.5B). The fluorescence intensity in the kidney was not significantly influenced by GF120918 treatment (Figure 3.5B).

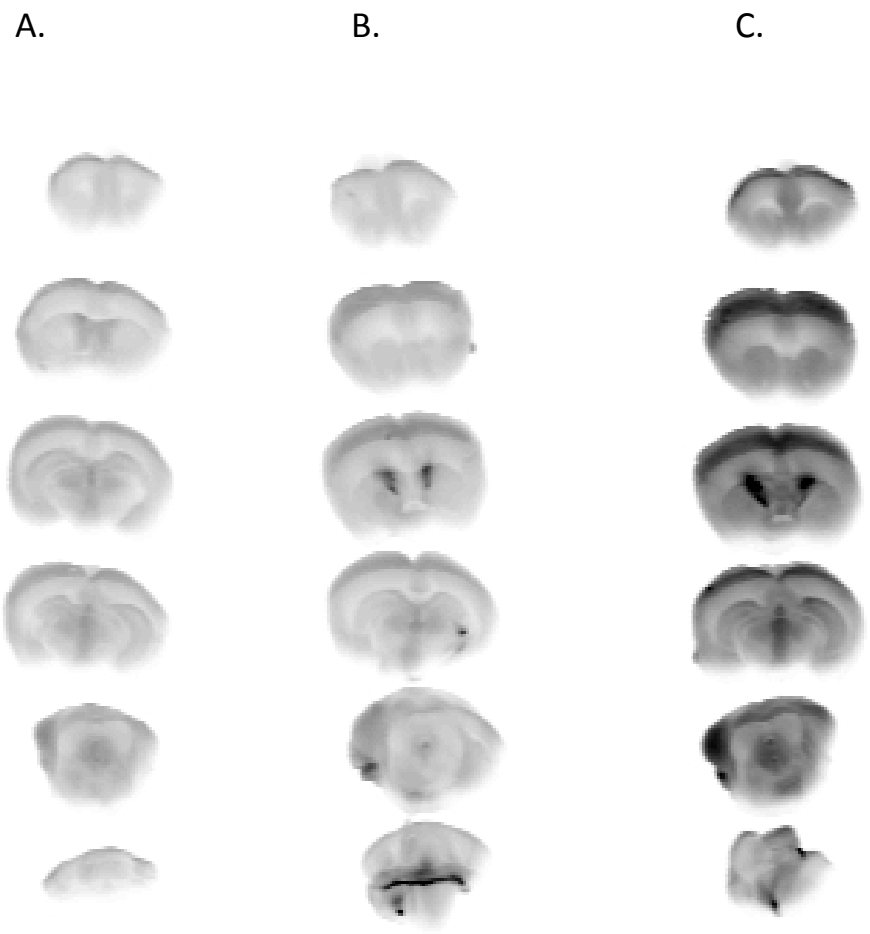

Figure 3.4: Representative serial coronal slices of mouse brain from (A) control, (B) R800 treated (0.032 µmol/kg), (C) GF120918 (9mg/kg) and R800 (0.032 µmol/kg) treated mouse at 20 min post injection. Slices were 2 mm thick and are oriented from the anterior (top) to posterior (bottom) regions with representative of 7 mice. The darker the slice image, the greater the R800 fluorescence.

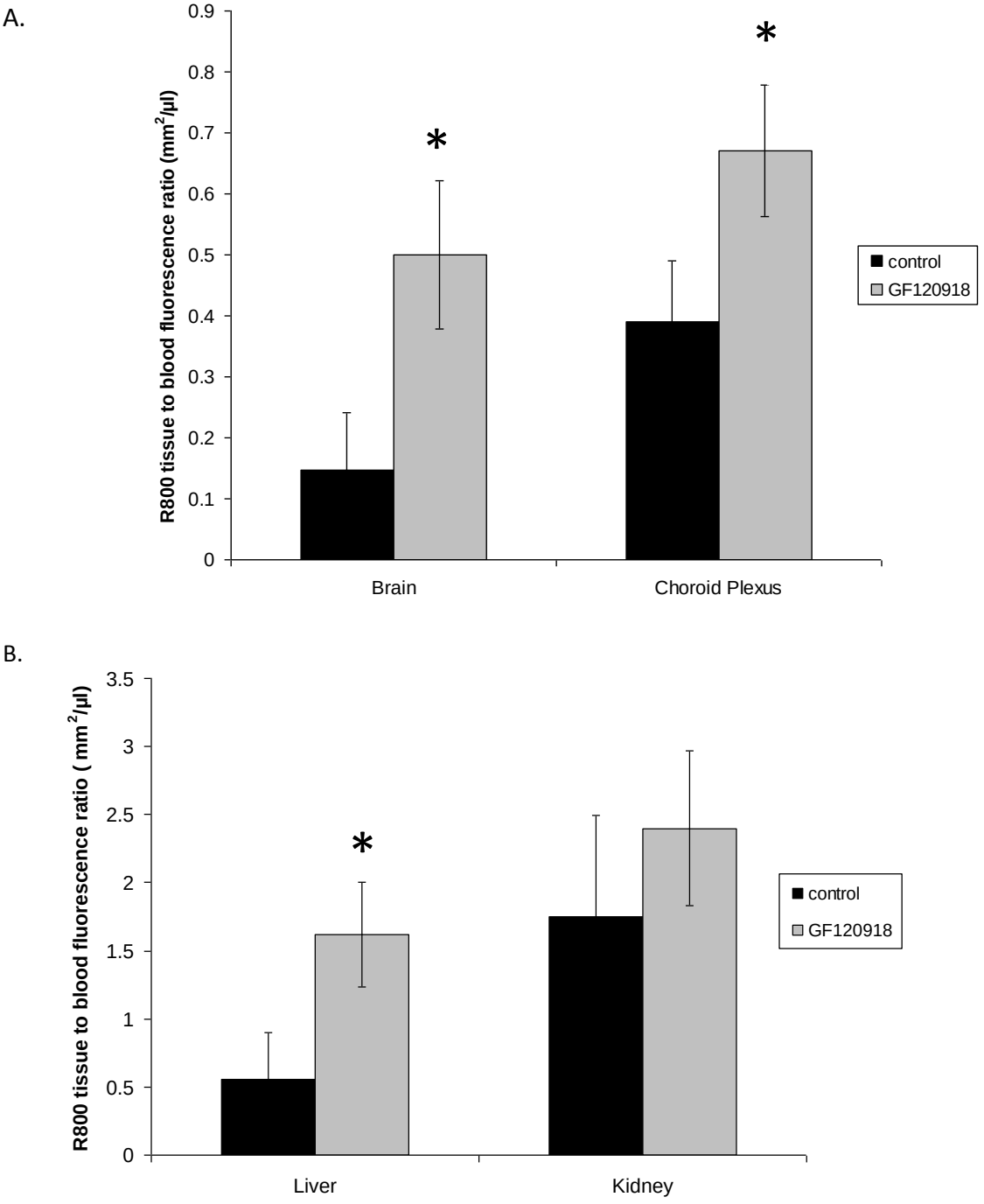

Figure 3.5: Quantitative assessment of R800 fluorescence in the brain and choroid plexus (Panel A), liver and kidney (Panel B) under control conditions (R800 alone) and following pre-treatment with P-gp inhibitor, GF 120918. Fluorescence intensity is presented as tissue to blood ratio. Values represent the mean ± SEM (n = 4) of mice per treatment group. * $p < 0.05$ compared to control mice.

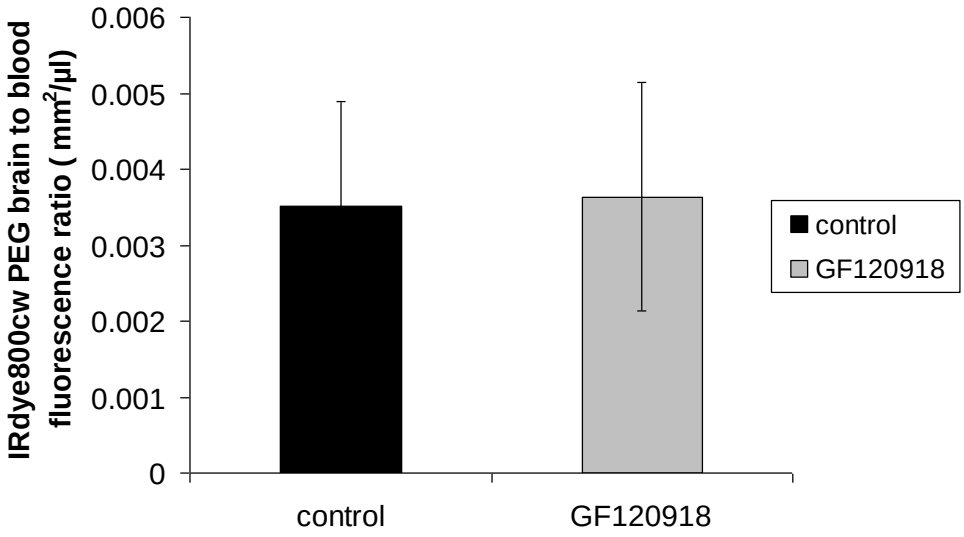

Figure 3.6: Quantitative analysis of IRdye800cw PEG in the brain under control conditions and following pre-treatment with P-gp inhibitor, GF 120918. The total fluorescence from serial coronal brain slices were normalized to the fluorescence intensity of the blood. The values represent the mean ± SEM of (n = 4) mice per treatment group.

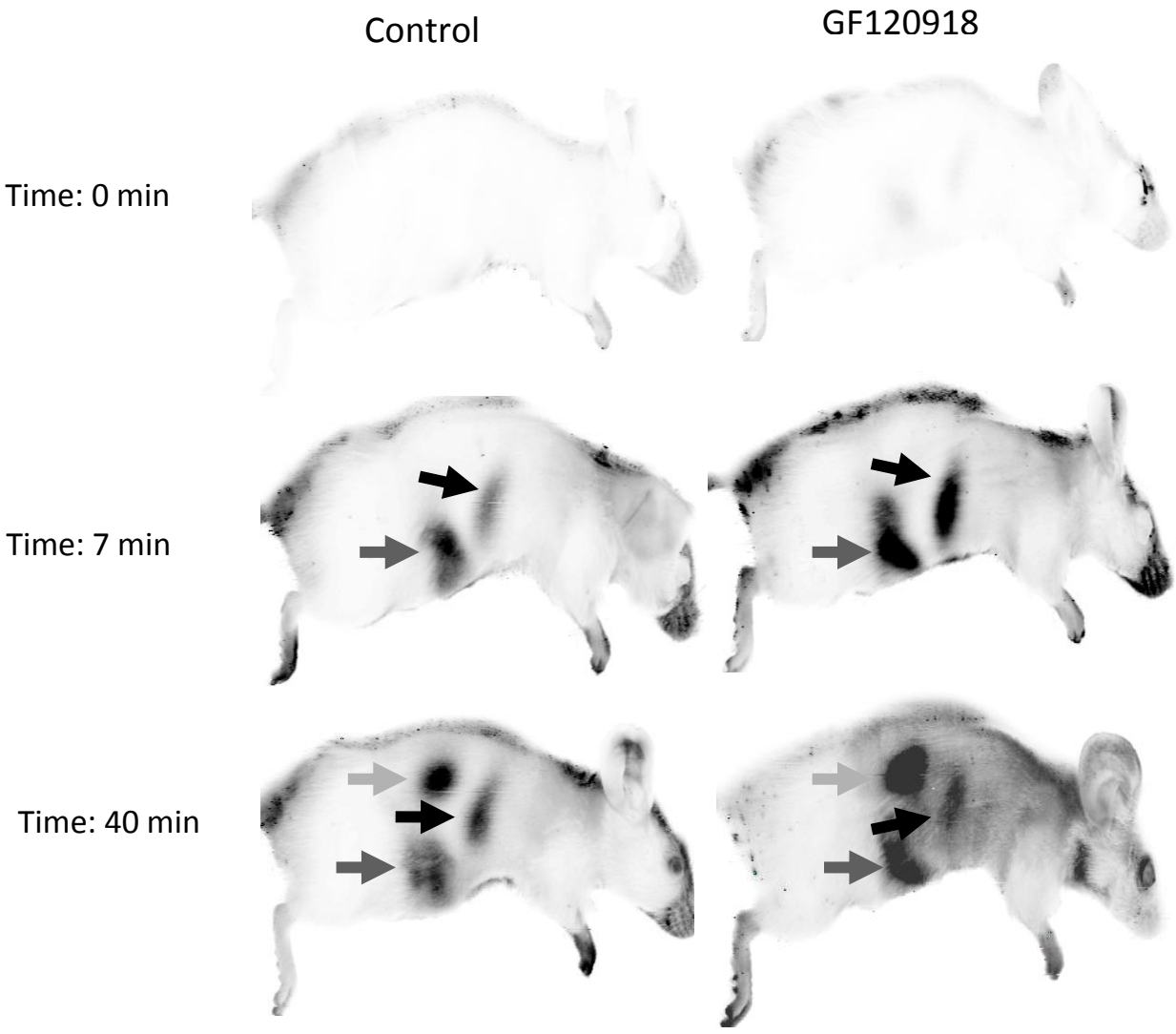

Figure 3.7: Whole animal images of R800 tissue deposition in mouse using NIRF imaging. Images of control and GF120918 treated mice were taken at time 0, 7, and 40 minutes following R800 injection. Mice were positioned on the side for R800 imaging. The arrows indicate accumulation of R800 in peripheral organs including liver (black arrow), intestines (dark gray arrow) and kidney (light gray arrow).

3.4. DISCUSSION

It is well established that the drug efflux transporter, P-gp, plays an important role in the absorption, distribution, and excretion of a number of drugs (Polli et al. 2001, 620-628). Of particular importance is the emerging role that P-gp has in limiting the CNS penetration of drugs (Jonker et al. 1999, 43-50). Given the potential for altered P-gp activity, either through a particular pathological condition, such as epilepsy (Lazarowski et al. 2007, 140-149) or through drug treatment regiments (Loscher and Potschka 2002, 7-14), a non-invasive method for imaging changes in P-gp activity, both quantitatively and spatially, in the BBB would provide an essential research tool. Traditionally, P-gp imaging in both the pre clinical and clinical setting has been done using positron emission tomography (PET) and radiolabeled substrates of P-gp such as [^{11}C] verapamil (Dorner et al. 2009, 6073-6082). While PET imaging is a powerful technique, it requires highly specialized instrumentation and support facilities and can be cost prohibitive, especially in the pre-clinical setting. Thus, there is a need for the development of alternative imaging modalities.

Near infrared fluorescence represents an emerging imaging technology (Zidan et al. 2010, 202-214). The long absorption wavelengths (700-800 nm) in the NIRF region results in reduced background or autofluorescence within tissue. In addition, compared to fluorescence imaging within the visible spectrum that has a tissue penetration depth limited only to 1-2 mm, NIRF can penetrate up to several centimeters (Ntziachristos, Bremer, and Weissleder 2003, 195-208). Furthermore, the ability to utilize NIRF probes from the cellular to whole animal level provides an integrated imaging platform. In the present study we report the initial identification and characterization of the NIRF probe, R800, as a potential imaging agent for assessing P-gp function at both the cellular and whole animal level.

The assessment of P-gp function using NIFR imaging technology required identification of a suitable compound with P-gp activity. Due to their planar ring structure, positive charge, and fluorescent properties, the rhodamine dyes, most notably rhodamine 123, have been utilized for functional assessment of P-gp (Miller et al. 1996, 301-306; Wang et al. 1995, 719-726; Yumoto et al. 1999, 149-155; Fontaine, Elmquist, and Miller 1996, 1521-1531). While the NIRF dye, R800, has some structural similarities to rhodamine 123, interactions of R800 with P-gp or other drug efflux transporters have not been reported. To assess whether R800 was indeed a P-gp substrate a series of *in vitro* studies were performed. Cellular accumulation of R800 was performed using MDCKwt monolayers and MDCK*MDR1* monolayers. The MDCK*MDR1* transfected cell line over-expresses P-gp and the utility of these cells in examining P-gp dependent transporter processes has been well documented (Horio et al. 1989, 14880-14884). There are two lines of evidence that suggest R800 is a substrate for P-gp in the cell accumulation studies. First, R800 had a significantly lower accumulation in the MDCK*MDR1* cells compared to the wild-type cells. Second, treatment with the P-gp inhibitor, GF 120918, was able to bring R800 accumulation in the MDCK*MDR1* cells to the same level as the MDCKwt monolayers.

Additional evidence supporting R800 as a transport substrate for P-gp comes from the bi-directional permeability studies in the MDCK*MDR1* monolayers. Determination of permeability in both the A-B and B-A directions has been extensively utilized to identify compounds with drug efflux transporter liability (Zhang, Bachmeier, and Miller 2003, 31-51). For compounds that are only dependent on passive diffusion processes, permeability across polarized epithelial cells would be expected to be similar in both directions. However, those compounds dependent on transport processes will display bi-directional permeability differences. In the case of P-gp-mediated transport, an increased B-A permeability is observed

(Shaik et al. 2007, 2076-2085). As observed in the present study, R800 permeability in MDCK*MDR1* monolayers was significantly greater in the B-A direction compared to that observed in the A-B direction. This resulted in an efflux ratio for R800 in MDCK*MDR1* monolayers of approximately 3 and indicates that P-gp is expressed selectively on the apical cell surface. This is above the typical cut-off value of 2 used to identify drug efflux transporter liabilities in drug screening assays (International Transporter Consortium et al. 2010, 215-236). Addition of the P-gp inhibitor, GF120918, resulted in a similar permeability of R800 in both the B-A and A-B directions.

Finally, confirmation that R800 is transported by P-gp comes from the membrane ATPase studies. P-glycoprotein-dependent transport requires the binding of the substrate to the transporter and subsequent hydrolysis of ATP via the ATPase portion of the transporter (Zhang, Bachmeier, and Miller 2003, 31-51). Therefore, the screening of prospective substrates or inhibitors of P-gp can be determined by examining the amount of free phosphate generated through the activity of ATPase (Zhang, Bachmeier, and Miller 2003, 31-51). The use of specific membranes that overexpress P-gp enables researchers to look at the interaction between a potential substrate and P-gp transporter without other confounding factors such as other efflux/influx transporters or permeability through an intact cell monolayer that can mask drug efflux transporter activity. In the present study, R800 produced a concentration dependent increase in P-gp ATPase activity. The EC_{50} for R800 in the P-gp ATPase assay was 7 μM. This is similar to the 3 μM EC_{50} values reported previously for rhodamine 123 (Urbatsch, al-Shawi, and Senior 1994, 7069-7076; Bachmeier, Trickler, and Miller 2006, 998-1003). In contrast to the P-gp ATPase membrane assay, no clear concentration dependent response to R800 was observed

in the BCRP or MRP1 ATPase membrane preparations, suggesting that transport through these drug efflux systems is modest at best.

Based on *in vitro* studies demonstrating that R800 was a P-gp substrate, *in vivo* studies were initiated to determine to what extent R800 could be used to image P-gp function. Whole animal imaging of R800 distribution showed marked accumulation in the liver, kidney and intestinal tissue, which was enhanced in the GF 120918 treated mice. This is consistent with the important role that P-gp has in the elimination of compounds in these tissues. In this regard, these whole mouse images are similar to what has been reported previously with P-gp probes using PET (Syvanen et al. 2011, 1). Examination of brain slices from mice following systemic administration of R800 indicated very little penetration of R800 into the brain. Indeed, under normal conditions, the brain region with the greatest R800 retention was the ventricles. However, following blockade of P-gp with GF 120918, there was a significant enhancement in R800 fluorescence in the brain slices (approximately 4-fold). The enhanced R800 accumulation in the brain slices from GF120918-treated mice in the current study is consistent with the approximately 3-fold increase in brain accumulation reported previously for rhodamine 123 following P-gp inhibition in rats using brain microdialysis (Wang et al. 1995, 719-726). While GF 120918 can also inhibit BCRP transporter activity, the absence of effect in the BCRP membrane ATPase assay suggests the increases in fluorescence observed in the brain slices following GF120918 is attributable to P-gp inhibition.

Additional evidence that the enhanced R800 accumulation in the brain following GF120918 is due to inhibition of P-gp at the BBB is the lack of response observed with IRdye 800cw PEG contrast agent. This compound is a near infrared agent used previously to visualize the permeability of leaky or discontinuous vascular endothelium and lymph node mapping

(Tanaka et al. 2006, 1671-1681). The encapsulated portion of the molecule consists of Poly(ethylene glycol) PEG, a synthetic polymer that is commonly used to enhance the retention time or to alter the pharmacokinetics of an agent. The molecular weight of IRDye 800cw PEG is approximately 25 kDa. Based on the physicochemical properties of IRDye 800cw PEG, this imaging agent was selected to evaluate the specificity of the response to the P-gp inhibitor, GF120918. As expected from the physicochemical properties of the imaging agent, systemic administration of IRdye 800cw PEG resulted in little to no detectable accumulation in the brain and the choroid region. In addition, treatment with GF120918 had no effect on the accumulation of IRdye 800cw PEG in brain tissue, indicating the effects observed with GF 120918 in the R800 treated mice was due to inhibition of P-gp-mediated transport at the BBB.

In addition to the brain endothelial cells, P-gp is also expressed in the epithelial cells of the choroid plexus (Urquhart and Kim 2009a, 1063-1070). Bidirectional permeability studies using neonatal rat choroid plexus epithelia along with radiolabeled probes ^{99m}Tc-sestamibi and ^{3}[H]Taxol showed that the permeability of P-gp substrates in the basolateral to apical direction was greater than permeability in the apical to basolateral direction (Rao et al. 1999, 3900-3905). Furthermore the enhanced basolateral to apical permeability was abolished when the choroid plexus epithelial cells were treated with GF120918 (Rao et al. 1999, 3900-3905). The directionality of P-gp transport in the blood-cerebral spinal fluid barrier (BCSFB) is such that P-gp substrates would be concentrated in the cerebral spinal fluid (CSF) of the ventricles while just the opposite occurs in the BBB with the removal of P-gp substrates from the brain extracellular fluid (de Lange 2004, 1793-1809). The apical localization of P-gp in the choroid plexus epithelial cells would account for the strong R800 fluorescence signal observed in the central ventricles following systemic administration of the dye. These findings are in good agreement with

previous studies using PET imaging methods demonstrating a localization of P-gp PET probes in the ventricles (Langer et al. 2007, 1774-1784). Thus, the brain accumulation of R800 observed under control conditions is consistent with the different orientations of P-gp in the BBB and BCSFB. When P-gp was inhibited, by the administration of GF120918, the amount of R800 in the brain was dramatically increased while the fluorescence in the ventricles only increased modestly. This is consistent with inhibition of P-gp in the BBB. The increase in R800 in the ventricles following GF120918 is attributable to diffusion of R800 from the brain extracellular fluid pool to the CSF pool. Such a phenomenon has been shown for doxorubicin brain distribution following P-gp inhibition (Bigotte and Olsson 1984, 55-67). In these studies doxorubicin concentrations were monitored in both the brain cortex and ventricles using brain microdialysis. Thus, the results with the newly identified NIRF imaging agent in the present studies, resembles the more established techniques for assessing P-gp function in the BBB and BCSFB.

Due to its localization within the body, P-gp can influence the bioavailability and tissue distribution of a wide range of compounds. Changes in P-gp activity either due to specific disease states, or a particular drug regimen have the potential to alter pharmacodynamics of P-gp sensitive drug agents (Dombrowski et al. 2001, 1501-1506). Furthermore, transporter-mediated drug-drug interactions are also of growing concern (Lin 2007, 81-92). A non-invasive approach for examining the activity of P-gp would be of value for understanding the role of P-gp in both the above mentioned conditions. While additional studies are required, this initial report suggests NIRF spectroscopy with imaging agents like R800 may provide an additional tool for monitoring changes in P-gp activity and drug distribution in tissues, including the brain.

CHAPTER 4: RAPID AND REVERSIBLE ENHANCEMENT OF BLOOD-BRAIN BARRIER (BBB) PERMEABILITY USING LYSOPHOSPHATIDIC ACID (LPA).

4.1. INTRODUCTION

Lysophosphatidic acid (LPA), also referred to as monoacyl-sn-glycerol-3-phosphate, is a phospholipid found in most cell types including neurons, Schwann cells, adipocytes and fibroblasts (Rivera and Chun 2008, 25-46). It is highly concentrated in platelets and can be detected in bodily fluids including serum, saliva, follicular fluid and malignant effusions (Moolenaar, van Meeteren, and Giepmans 2004, 870-881). Although once considered an inert intermediate in lipid metabolism, the identification of LPA as a major mitogenic component in serum (van Corven et al. 1989, 45-54) provided the first initial evidence of the biological activity of the phospholipid. It is now clearly established that LPA is a bioactive lipid capable of producing a variety of responses in mammalian cells (Moolenaar, van Meeteren, and Giepmans 2004, 870-881). The responses to LPA are initiated through the binding of the phospholipid to LPA receptors on the plasma membrane of the cell (Hecht et al. 1996, 1071-1083). Currently, there are at least 6 different types of LPA receptors (LPAR1-LPAR6) that share the common G-protein coupled receptor (GPCR) structure (Zhao and Natarajan 2009, 367-377; Avendano-Vazquez, Garcia-Caballero, and Garcia-Sainz 2005, 677-684). Consistent with the diversity of GPCR signaling pathways, cellular responses to LPA are considerably diverse ranging from cell migration and survival to neurite retraction and gap junction closure (Moolenaar, van Meeteren, and Giepmans 2004, 870-881). Furthermore, as LPA is released locally in response to inflammation, elevations in LPA have been implicated in the pathogenesis of several conditions including atherosclerosis and myocardial injury (Goetzl et al. 2002, 324-338; Siess 2002, 204-215), cancer (Mills and Moolenaar 2003, 582-591), and neurological disorders (Harrison et al. 2003, 1170-1179).

An important cellular target of LPA is the vascular endothelium where LPA-induced changes in mitogenesis, cell migration (Nitz et al. 2003, 30-40) and permeability have been observed (Schulze et al. 1997, 991-1000; Sarker, Hu, and Fraser 2010, 39-46). The effects of LPA on vascular permeability are a topic of considerable debate with some studies reporting a decrease in endothelial cell permeability following LPA exposure (Alexander et al. 1998, H115-22; English et al. 1999, 627-634), while others support an increase in vascular leakage following LPA exposure (Schulze et al. 1997, 991-1000; Nitz et al. 2003, 30-40; Tigyi et al. 1995, H2048-55). Consistent with LPA-mediated increases in vascular permeability, several studies have reported an induction of stress fiber formation, and focal contact following LPA exposure resulting in the disruption of tight junctions of endothelial cells (Moolenaar 1995, 12949-12952). Studies of LPA on brain microvessel endothelial cell permeability support an enhancement of permeability with increases in both transcellular electrical resistance (TER) and flux of vascular markers observed in primary cultured brain endothelial cell preparations (Schulze et al. 1997, 991-1000; Tigyi et al. 1995, H2048-55). More recent studies indicate increased permeability following localized application of LPA to the cerebral microvasculature (Tigyi et al. 1995, H2048-55).

The brain microvessel endothelial cells forming the blood-brain barrier (BBB) are structurally and functionally different from capillaries found in other organs (Banks 2009, S3; Engelhardt and Sorokin 2009, 497-511; Engelhardt 2003, 119-129). The brain microvessel endothelial cells, with complex tight junctions, adherens junctions, low pinocytic activity and absence of fenestrations, limit the BBB permeability of most hydrophilic solutes (Reese and Karnovsky 1967, 207-217). Furthermore, the expression of numerous uptake and efflux transporters provides additional selectivity with regard to solutes that can penetrate the BBB (Hermann and Bassetti 2007, 128-134; Tamai and Tsuji 2000, 1371-1388). The restrictive nature

of the BBB is important for maintaining the proper extracellular fluid environment within the brain required for neuronal transmission. However, in terms of CNS therapy, an intact BBB presents a formidable obstacle to drug delivery to the brain (Pardridge 1999, 556-569; Pardridge 2010, 157-167). Thus, depending on the magnitude and duration of response, LPA-mediated alterations in BBB permeability could have both pathophysiological and therapeutic implications.

While there are studies supporting LPA-induced increases in cerebral vascular permeability *in vitro*, the effects of LPA on BBB permeability at the whole animal or organ level are still poorly understood. The present studies describe a series of experiments intended to elucidate the effects of LPA on BBB permeability *in vivo*, specifically, examining the time of onset, and the duration of action for LPA-induced changes in cerebral vascular permeability in the mouse. Furthermore, using both magnetic resonance imaging (MRI) and near infrared fluorescence (NIRF) contrast agents, a thorough characterization of the magnitude and extent of BBB disruption produced by LPA exposure was determined. The results demonstrate that LPA-induced increases in BBB permeability occur within minutes of systemic administration. Equally important, BBB integrity was restored within 20-minutes. Finally, increases in BBB permeability were observed for both small and large molecular weight contrast agents indicating that LPA can influence the BBB permeability of a wide range of drug molecules.

4.2. MATERIAL AND METHODS

4.2.1. Materials/Reagents:

Lysophosphatidic acid (LPA) was purchased from Sigma Chemical Company (Oakville, ON). The NIRF imaging agents, IRdye 800cw PEG and rhodamine 800 (R800), were obtained from Licor (Lincoln, NE) and Exciton (Dayton, OH), respectively. Gadolinium diethylenetriamine

pentaacetate (Gad) contrast agent used for MRI of BBB permeability was obtained from Berlex, Canada. Ketamine hydrochloride and xylazine were purchased from Wyeth (Guelph, ON) and Bayer Inc. (Toronto, ON), respectively. All other reagents and chemicals were purchased from Sigma Chemical Company (St. Louis, MO).

4.2.2. Cell Lines:

Human brain microvessel endothelial (HBMEC) cells were purchased from Cell Systems (Kirkland, WA). The cells were grown in Dulbecco's Modified Eagle's Medium (DMEM) supplemented with 10% fetal bovine serum (FBS), 1% penicillin-streptomycin and 1% non-essential amino acids. Cells were expanded in 25 cm^2 culture flasks and seeded onto 6-well culture plates or Transwell® inserts at a density of 50, 000 cells per cm^2 for permeability studies. Cells were grown in a humidified environment of 37°C with 5% CO_2 with media replacement every other day.

4.2.3. LPA Response in Cultured Brain Microvessels:

HBMEC were grown to confluent monolayers on Transwell polycarbonate membrane inserts. Permeability was assessed over a 90 minute period in HBMEC monolayers in the apical to basolateral (A to B) direction. All cells were pre-treated in assay buffer for 30 minutes at 37ºC. Permeability to fluorescence dextran (FDX3000) was assessed in the presence of various concentrations of LPA (0.1 μM, 1.0 μM, and 10 μM) dissolved in 0.25 mg/ml bovine serum albumin (BSA) in phosphate buffer saline (PBS). The control cells were pretreated with 0.25 mg/ml BSA in PBS. The total volume of the apical compartment was 1.5 ml and the volume in the basolateral compartment was 2.5 ml. A 1 μM solution of FDX3000 was applied to the apical (lumenal) side of the HBMEC monolayer at the start of the permeability study. Samples (50 μl) were taken from the apical compartment at the start of the experiment and from the

basolateral (ablumenal) compartment at 0, 30, 60, and 90 minute time points. All samples removed were replaced with an equal volume of assay buffer, and all permeability studies were performed at 37˚C. The amount of FDX3000 was analyzed using a Gene5 fluorescence plate reader at emission and excitation wavelengths of 485 nm and 528 nm, respectively.

4.2.4. LPA Receptor Expression:

LPA receptor expression was examined in both HBMEC as well as in mouse brain, specifically in the brain homogenate and capillary enriched fraction using RT-PCR.

4.2.4.1. Capillary Depletion: Capillary enriched fractions of the mouse brain were collected using the capillary depletion technique described by (Triguero, Buciak, and Pardridge 1990, 1882-1888). Fresh mouse brains were isolated and the meninges removed. Approximately 3-4 mouse brains were weighed and pooled together. Brain Buffer Solution (BBS) (10 mM Hepes, 141 mM NaCl, 4mM KCl, 2.8 mM CaCl2, 1 mM MgSO4, and 1 mM NaH2PO4, 10 mM D-glucose at a physiological pH of 7.4) was added at a volume of 5x the weight of the brain tissue and the brain tissue was homogenized with a glass homogenizer for a total of 8 strokes. An equal volume of 26% dextran solution was added and the resulting homogenate was then centrifuged at 5,400 g for 15 minutes at 4°C. Both the pellet (capillary-enriched fraction) and the supernatant fractions were collected for Real-time polymerase chain reaction (RT-PCR) analysis of LPARs as described below.

4.2.4.2. RT-PCR Analysis: RNA from HBMECs, brain homogenate, and the brain capillary-enriched fraction was isolated using Trizol reagent (GIBCO) according to the manufacturer's instructions. RT- PCR analysis of LPARs (LPAR1-LPAR5) and β-Actin gene expression was carried out using Quantitect Probe RT-PCR SYBR Green Kit (Qiagen). The gene expression measurements

were analyzed quantitatively using Mastercycler ep *realplex* system (Eppendorf). The primers and the hybridization probes were synthesized by Invitrogen (Ontario, Canada, and Qiagen (Massacheusetts, USA) with the following sequences:

LPAR1: FORWARD: TGGTCATGGTGGCAATCTACGTCA
REVERSE: ACTAGGCAAATCCAGCCAAGAAGT

LPAR2: FORWARD: TGGCCTTGAACTCTTGATGGTCCT
REVERSE: TCAGAGTGGAAAGGCTTGCTCTGT

LPAR3: FORWARD: TGAGAGTCCACAGCAACTTGACCA
REVERSE: ATGTTGCAGAGGCAATTCCATCCC

LPAR4: FORWARD: ATGCTCTTCCTCACCTGCATCAGT
REVERSE: CTTCAAAGCAAGTGGTGGTCGCAT

LPAR5: FORWARD: ACCTTGTTGTTCCCTACGATGCCT
REVERSE: TGGAGCACAGAGCTGTTGGTAGAA

4.2.5. LPA Response in vivo:

Adult female Balb/c mice were used to characterize the BBB-disruption profile produced by LPA. Mice were obtained from the University of Manitoba breeding colony and maintained in the Central Animal Care Facility under temperature-controlled environment with 12 hours dark/light cycle and unlimited access to food and water. All animal experiments were approved by the University of Manitoba Animal Care Committee (protocol number 09-049). Quantitative determination of BBB permeability was performed using three different imaging agents and magnetic resonance (MR) and near infrared fluorescence (NIRF) imaging modalities described below.

4.2.5.1. Magnetic Resonance Imaging of BBB Permeability: The onset and duration of LPA-induced alterations in BBB permeability were initially assessed using magnetic resonance imaging (MRI) with Gad contrast agent. Mice were anesthetized and secured in a Bruker

Biospect MR (7 tesla/21 cm) spectrometer with 2.5 x 2.5 cm^2 field of view. A series of T1-weighted images (Rare factor = 8, Echo Time = 11.56 ms, Effective Echo Time = 11.56 ms, Repetition Time = 852 ms, Averages = 6, Total Image Time = 2.40 min) and T2-weighted images (Rare factor = 8, Echo Time = 20 ms, Effective Echo Time = 80 ms, Repetition Time = 1640 ms, Averages = 12, Total Image Time = 10.50 min) of the mouse brain were obtained prior to administration of Gad contrast agent to acquire background images of the mouse brain. To determine the onset of LPA induced BBB disruption, mice were given Gad contrast agent (0.4 mmol/kg) together with LPA (0.1 -10 mg/kg) or LPA vehicle (0.25% BSA in PBS). A series of T1-weighted images was obtained immediately following Gad injection and at 3-minute intervals throughout a 21-minute imaging session. After 21 minutes, a second dose of Gad was administered and T1-weighted images were obtained at 3-minute intervals for an additional 21-minute imaging session. To confirm the BBB disruption period for LPA, a separate group of mice were administered LPA (1 mg/kg) or LPA vehicle at 20 min prior to the first Gad (0.4mmol/kg) injection. Immediately following administration of Gad contrast agent, a series of T1-weighted scans was taken at an interval of 3 minutes for a period of 21 minutes. After the first 21 minutes of scanning, the mice received a second dose of Gad and were imaged for an additional 21 minutes as described above. Assessment of Gad enhancement in the brain images were determined using percent difference images within the Paravision 3.0 software package according to the following formula:

((Post-Gad T1-weighted images – Pre-Gad T1-weighted images) / Pre-Gad T1-weighted images) x 100.

Quantification of Gad enhancement was accomplished by manually outlining regions of interest (ROI) within the coronal brain slices using Marevisi 3.5 software (Institute for Biodiagnostics, National Research Council, Canada).

4.2.5.2. Near Infrared Fluorescence Imaging of BBB Permeability: The LPA-induced changes in the BBB permeability of large molecular weight compounds as well as P-gp sensitive agents was also examined using NIRF. For these studies, mice received either IRdye 800cw (0.01 μmol/kg), a pegylated dye of approximately 25 kD used for assessing macromolecule vascular leakage (Sampath et al. 2007, 1501-1510) or R800 (0.032μmol/kg), a NIRF dye with P-gp substrate properties (On et al. 2011). The NIRF probes were administered either alone or in combination with LPA (1 mg/kg) via tail vein injection. The mice were sacrificed at various times (10-40 minutes) following treatment via cardiac perfusion with 10% formaldehyde solution. The brain and other tissues were removed and the accumulation of NIRF dyes examined *ex vivo* using an Odyssey near infrared imaging system (Licor, Lincoln, NE). Quantitative assessment of fluorescence was performed on ROI in 2 mm thick coronal tissue slices and normalized to fluorescence from blood samples taken at the time of tissue collection. Resulting values are presented as relative fluorescence units per mm^3 of tissue divided by relative fluorescence units per μl blood.

4.2.5.3. Desensitization of LPA-Mediated BBB Disruption: Examination of desensitization to BBB disruption produced by LPA was examined using both MR and NIRF imaging agents. Mice were anesthetized and administered LPA via tail vein injection under three different dosing schedules (A-C). Those mice under dosing schedule A received LPA (1 mg/kg) as a single bolus injection. Mice under dosing schedule B received a second bolus injection of LPA (1 mg/kg) 20

minutes after the first injection. Mice under dosing schedule C received a third bolus injection of LPA (1 mg/kg) 20 minutes after the second injection. All mice were imaged using either Gad contrast agent or IRdye 800cw following the last LPA injection. Quantitative assessment of BBB disruption was determined as described above.

4.2.5.4. LPA-Mediated BBB Permeability to Radiolabelled Methotrexate (Study performed by Dr. Sanjot Savant):

To determine potential application of LPA for enhanced drug delivery to the brain, females mice were administered a bolus injection (ml/kg) of ^{3}H-methotrexate (4μCi total activity) via the tail vein. The radiolabeled methotrexate was given in combination with either LPA (1 mg/kg) or vehicle (0.25 mg/ml BSA in PBS solution). Fifteen minutes after the injection of methotrexate, mice were anesthetized using intraperitoneal injection of ketamine and xylazine and a sample of blood was removed by cardiac puncture. Following the blood sample, mice were sacrificed and the brain was removed for determination of ^{3}H-methotrexate. Blood samples were spun for 8-10 minutes and 100 μL of plasma was collected. The brains were weighed and homogenized with double the volume of tissue solubilizing agent (Scintigest™ , Fisher Scientific). A 200 μL aliquot of the tissue homogenate was used to analyze the tissue samples. The samples were then mixed with Ultima gold™ (Perkin Elmer) scintillation cocktail and analyzed by liquid scintillation counter (Perkin Elmer) to determine the amount of ^{3}H-methotrexate present in the blood and tissue. The distribution of ^{3}H-methotrexate was based on the ratio of radioactivity in the brain versus the radioactivity in the plasma sample.

4.3. RESULTS

4.3.1. In vitro Permeability Studies:

The effects of various concentrations of LPA on the permeability of HBMEC were examined at different time points using FDX3000 as a fluorescence marker. Under normal conditions (control), permeability of HBMEC to FDX3000 from the apical to basolateral (A-B) direction was significantly lower than the LPA treated cells (Figure 4.1). This was observed at all time points of the study. The presence of LPA enhanced the permeability of the cells allowing more FDX3000 to penetrate. The increase of BBB permeability occurred within the first 10 minutes of LPA incubation, and appeared to plateau within 30 minutes (Figure 4.1). The enhancement of BBB permeability due to the presence of LPA occured in a concentration dependent manner, with the lowest LPA concentration (0.1μM) showing a slight increase in permeability after 30 minutes of sampling, while the highest concentration of LPA (10 μM) showed a moderate enhancement of the tight junction permeability. The intermediate LPA concentration (1μM) unexpectedly showed the greatest disruption of endothelial barrier properties and allowed the highest amount of FDX3000 to penetrate.

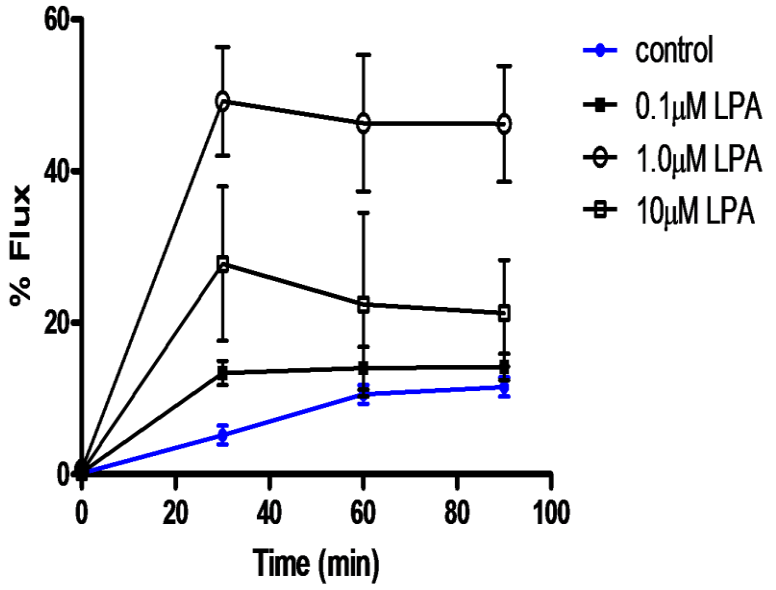

Figure 4.1: Permeability of FDX3000 in HBMEC monolayers. Apical to basolateral permeability of FDX3000 on HBME cells in the presence of various LPA concentrations.

4.3.2. LPA Receptor Expression Profile:

The expression profile of LPA receptors was examined in HBMEC as well as in both mouse brain homogenate and capillary enriched fractions. As shown in Figure 4.2A, LPAR1, LPAR2 and LPAR3 were highly expressed in HBMECs. Examination of LPA receptor expression in brain homogenates indicates the presence of LPAR1-R5 (Figure 4.2B). Expression of LPAR1, LPAR4 and LPAR5 was enriched in the capillary fraction compared to the brain homogenate (Figure 4.2B). In contrast, expression levels of LPAR2 and LPAR3 were lower in the capillary fraction compared to that observed in total brain homogenate (Figure 4.2B).

A.

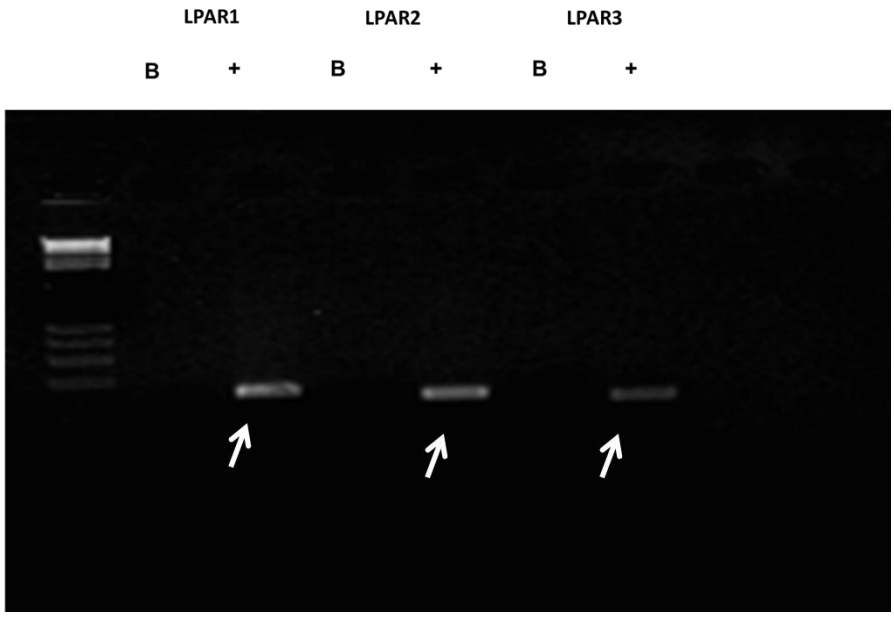

B.

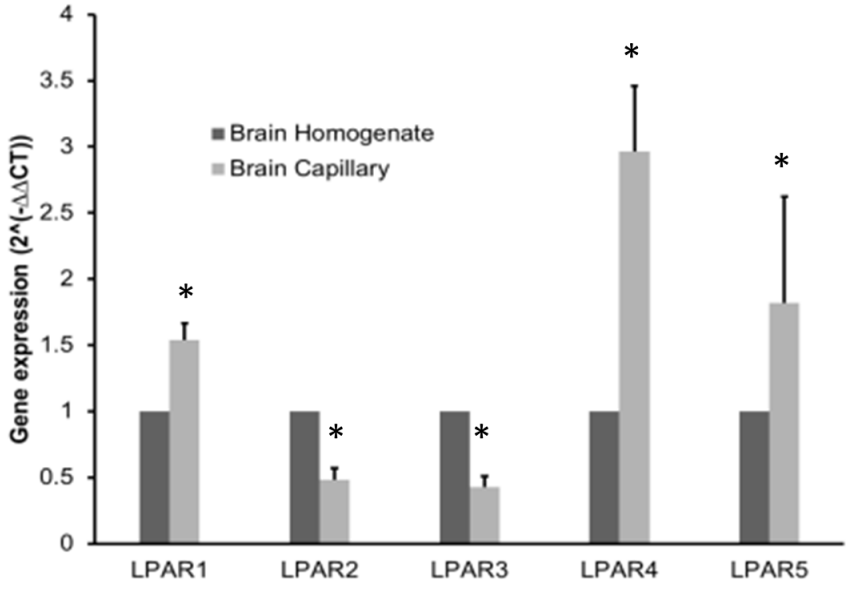

Figure 4.2: The expression of various LPA receptors was examined using RT-PCR in HBMEC lysates (panel A) and RT-PCR from both mouse brain homogenate and capillary enriched fractions (panel B). Arrows indicate band of interest (panel A). Values represent the mean ± sem of 3 trials. * $p < 0.05$ compared brain homogenate.

4.3.3. Rapid and Reversible Disruption of BBB Permeability Following LPA:

The effects of LPA on BBB permeability was initially characterized using Gad contrast enhanced MRI. Figure 4.3 shows a representative series of T1-weighted MR images taken from the posterior, midbrain and anterior brain regions of vehicle (Figures 4.3A and 4.3B) or LPA-treated (Figures 4.3C and 4.3D) mice. Under control conditions, the BBB is intact with negligible Gad enhancement observed, as indicated by the similar Gad enhancement in the brain slices at time 0 (prior to the injection of vehicle solution) and time 6 (6 minutes after vehicle injection) (Figure 4.3A, and 4.3B respectively). Indeed, the only brain region showing appreciable accumulation of Gad contrast agent under normal conditions was the ventricles (Figure 4.3B). In contrast, following the administration of 1mg/kg LPA, the amount of Gad contrast agent accumulating in brain was substantially enhanced compared to time 0 images (prior to LPA injection as shown in Figure 4.3C).

The BBB disruption produced by LPA was dose-dependent with both the 1 mg/kg and 10 mg/kg doses of LPA causing significant increases in Gad accumulation in the brain (Figure 4.4). In contrast, the lowest dose of LPA examined (0.1 mg/kg) had no effect on BBB permeability. Interestingly, the magnitude of BBB disruption produced by 10 mg/kg of LPA was less than that observed with the 1 mg/kg dosage (Figure 4.4). While there were regional differences in Gad intensity observed in both the vehicle and LPA treated mice, increases in Gad distribution to the brain following LPA administration were observed in all regions examined. Quantitative assessment of Gad contrast enhancement in the various brain regions indicated an approximately 5-fold increase in Gad intensity in the LPA treatment group compared to control mice (Figure 4.3 and 4.5). In all brain regions examined, the increase in Gad intensity was rapid, occurring within 3-6 minutes following administration of LPA (Figure 4.5A-C). Furthermore, the

BBB disruption produced by LPA was short in duration with restoration of BBB permeability returning within the 21-minute imaging session. Additional confirmation is provided by the observation that administration of Gad contrast agent 20-minutes following LPA exposure resulted in no additional increases in Gad accumulation in the brain (Figure 4.5 and 4.6).

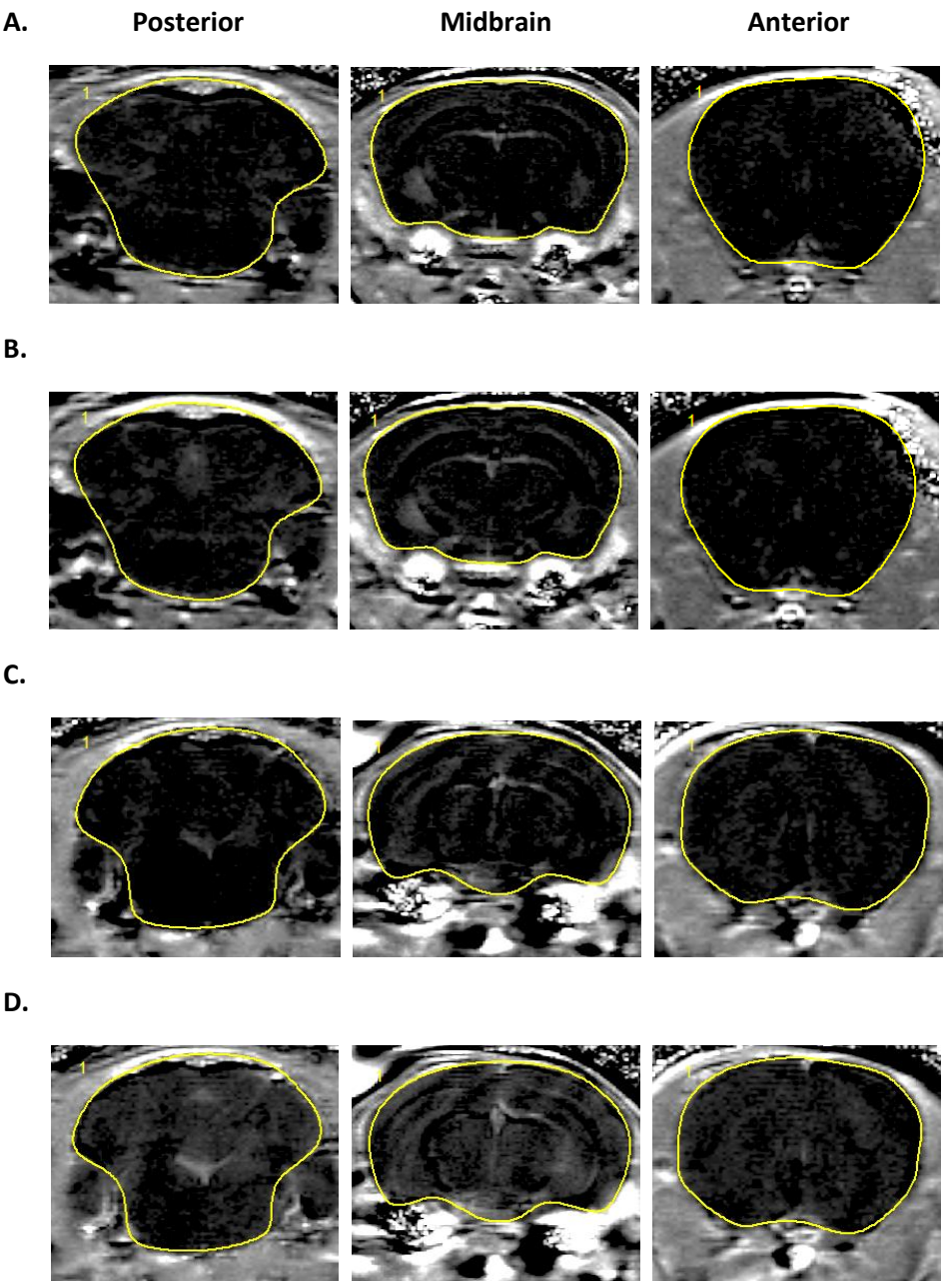

Figure 4.3: Representative % enhancement of Gad of mouse brain at time 0 (A and C) and 6 minutes (B and D) after injection of vehicle solution (A and B) or LPA (C and D).

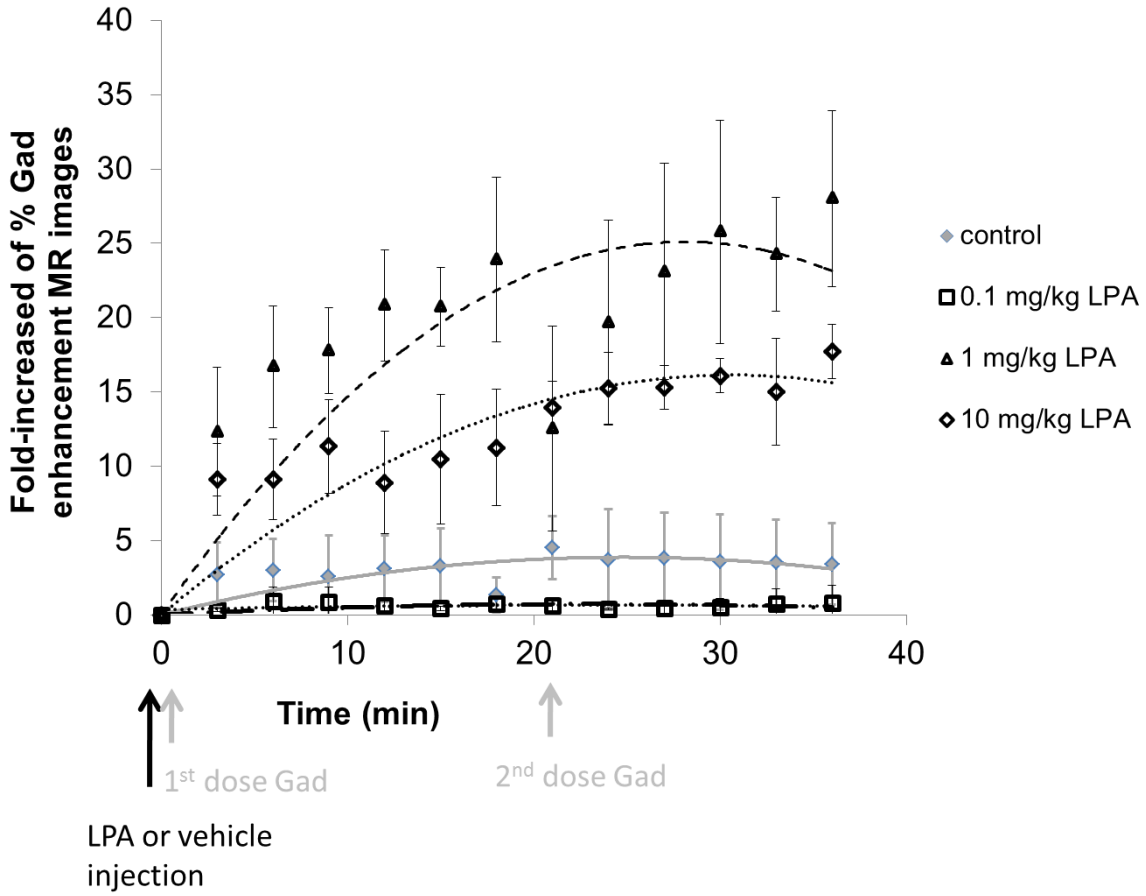

Figure 4.4: Dose dependent effects of LPA on the permeability of Gad in the posterior region of the brain. Mice were randomly assigned to their respective treatment group and the brains were scanned using T1-weighted images with Gad at 3 minute intervals. Quantitative analysis of % enhancement of MR images following Gad injection was determined on posterior brain images. Values represent the mean ± sem of 4 mice per treatment group.

A.

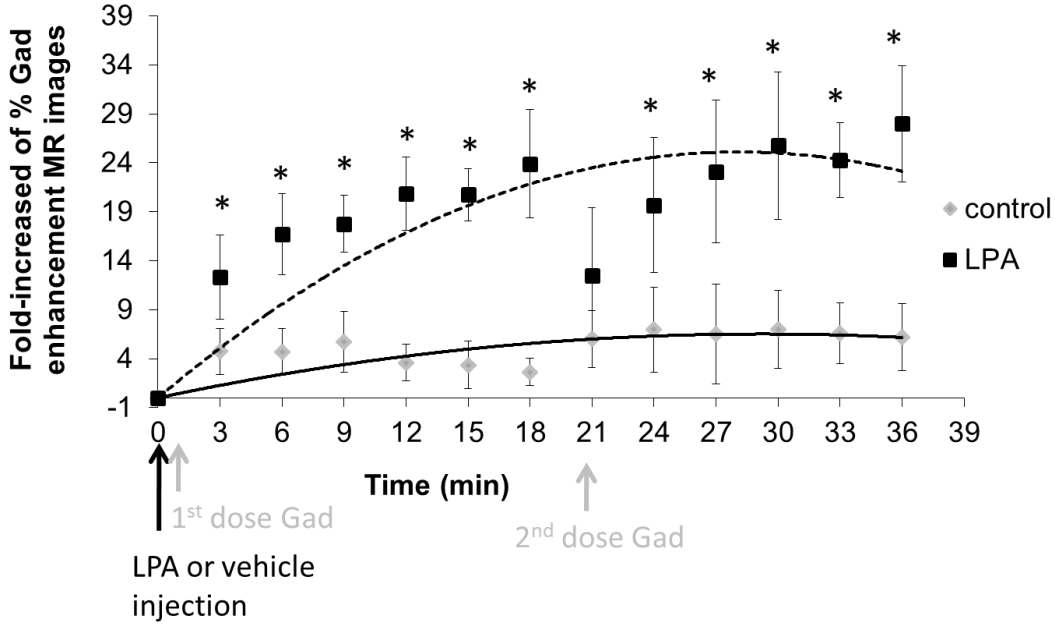
Fold-increased of % Gad enhancement MR images
39
34
29
24
19
14
9
4
-1
0 3 6 9 12 15 18 21 24 27 30 33 36 39
Time (min)
control
LPA
1st dose Gad
2nd dose Gad
LPA or vehicle injection

B.

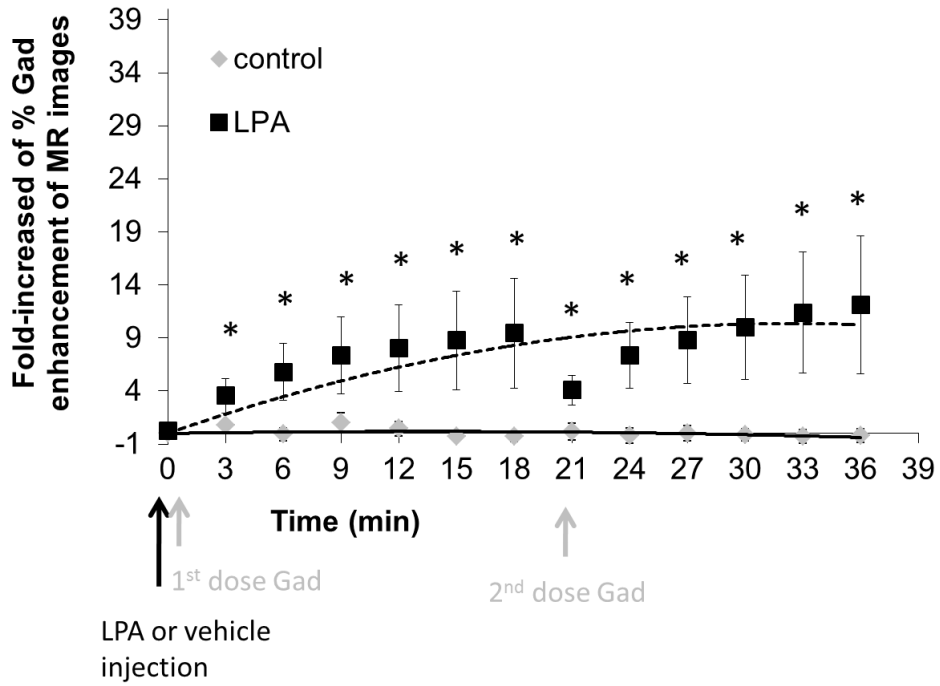
Fold-increased of % Gad enhancement of MR images
39
34
29
24
19
14
9
4
-1
0 3 6 9 12 15 18 21 24 27 30 33 36 39
Time (min)
control
LPA
1st dose Gad
2nd dose Gad
LPA or vehicle injection

C.

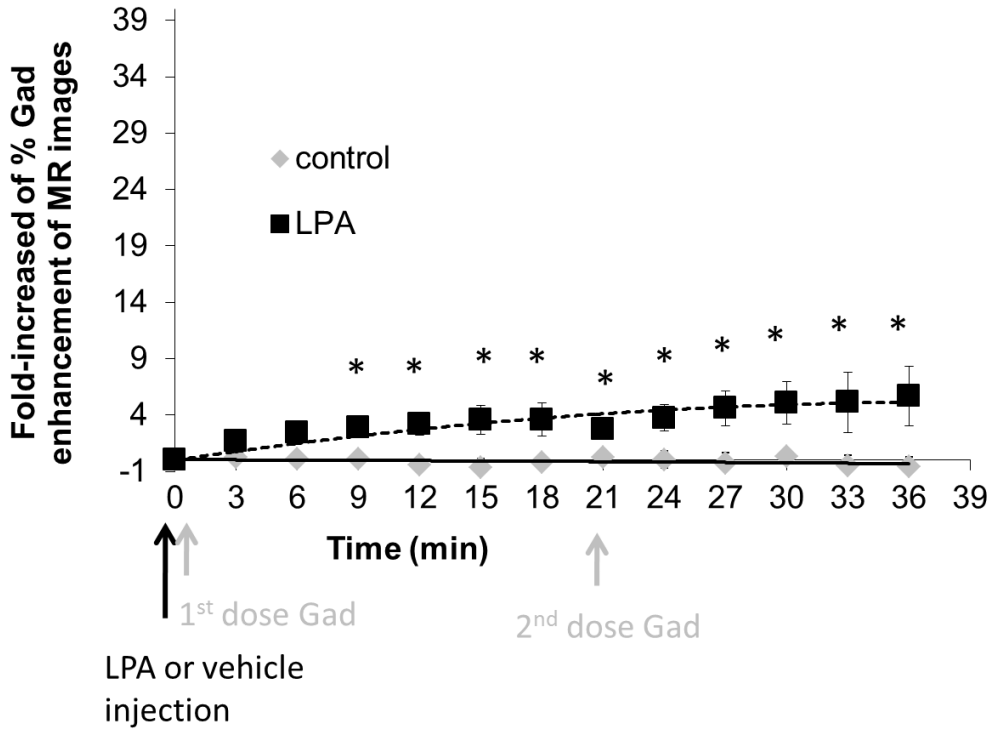

Figure 4.5: Quantitative analysis of % enhancement of MR images following Gad injection was determined in (A) posterior brain images, (B) midbrain images, and (C) anterior brain images in vehicle-treated or LPA-treated mice (1mg/kg). * $p < 0.05$ compared to control mice at the same time point. Values represent the mean ± sem for 5 mice per treatment group.

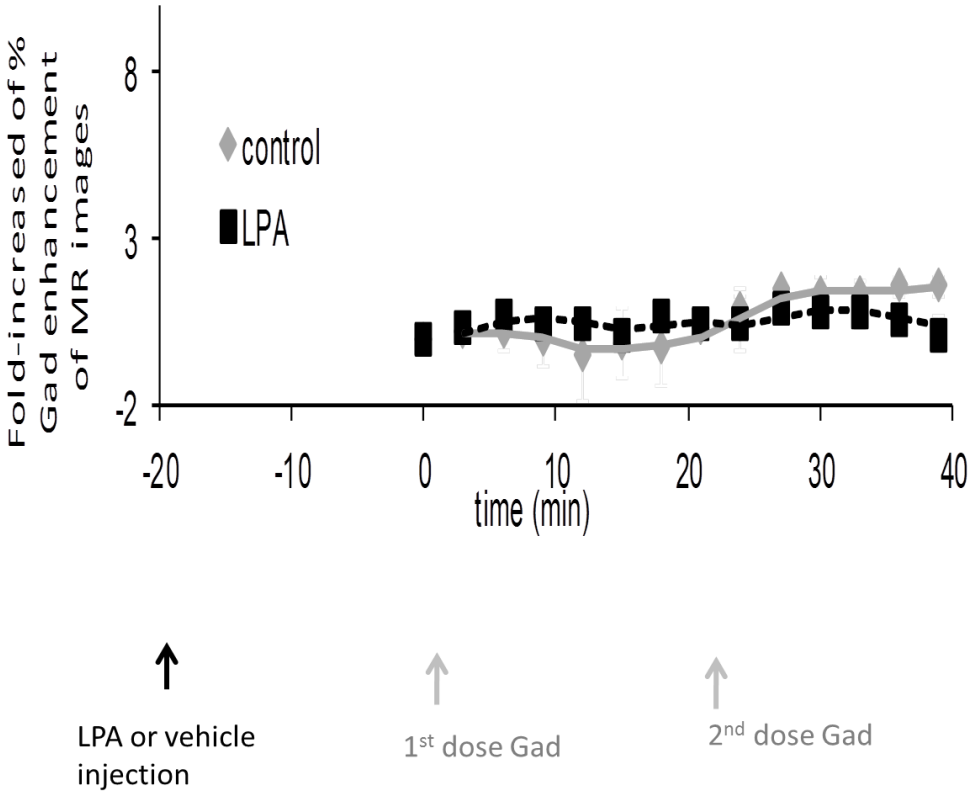

Figure 4.6: Quantitative analysis of % enhancement of MR images following Gad injection in mice at 20-minute exposure to vehicle or LPA (1 mg/kg) solution. Values represent the mean ± sem for 4 mice per treatment group.

4.3.4. Effects of LPA on Macromolecule BBB Permeability:

To determine the extent to which LPA exposure could alter macromolecule permeability in the BBB, studies were performed using IRdye800 cw PEG, a 25kDa near infrared fluorescent permeability marker. Under control conditions, there was little if any appreciable dye accumulation in the brain, with most of the IRdye800 dye remaining within the main vessels of the brain as shown in Figure 4.7B and 4.7D. In contrast, exposure to LPA significantly enhanced the penetration of IRdye800 cw PEG in the brain tissue (Figure 4.7C and 4.7E) both at 20 and 40 minutes post injection of the dye. The time frame for disruption observed with IRdye800 was similar to that with Gad. This is evident at the 20-minute time point, where there was intense fluorescence near and around the area of the vessels, consistent with leakage from the microvasculature (Figure 4.7C). However, by 40-minutes post LPA exposure, fluorescence intensity was reduced around the vasculature as the dye was able to diffuse throughout the entire brain region (Figure 4.7E). One concern regarding the systemic administration of LPA is its effects on the vascular integrity of the pulmonary circulation, specifically the endothelial cells lining blood vessels. It has been shown that increases in endothelial cell permeability through the activation of the Rho GPTase pathway leads to acute respiratory distress syndrome and ischemia-reperfusion injury (Wojciak-Stothard, Tsang, and Haworth 2005, L749-60). However, examination of LPA-induced changes in vascular permeability of IRdye800 cw PEG in the lung indicated no significant alterations in permeability in these organs (Figure 4.8).

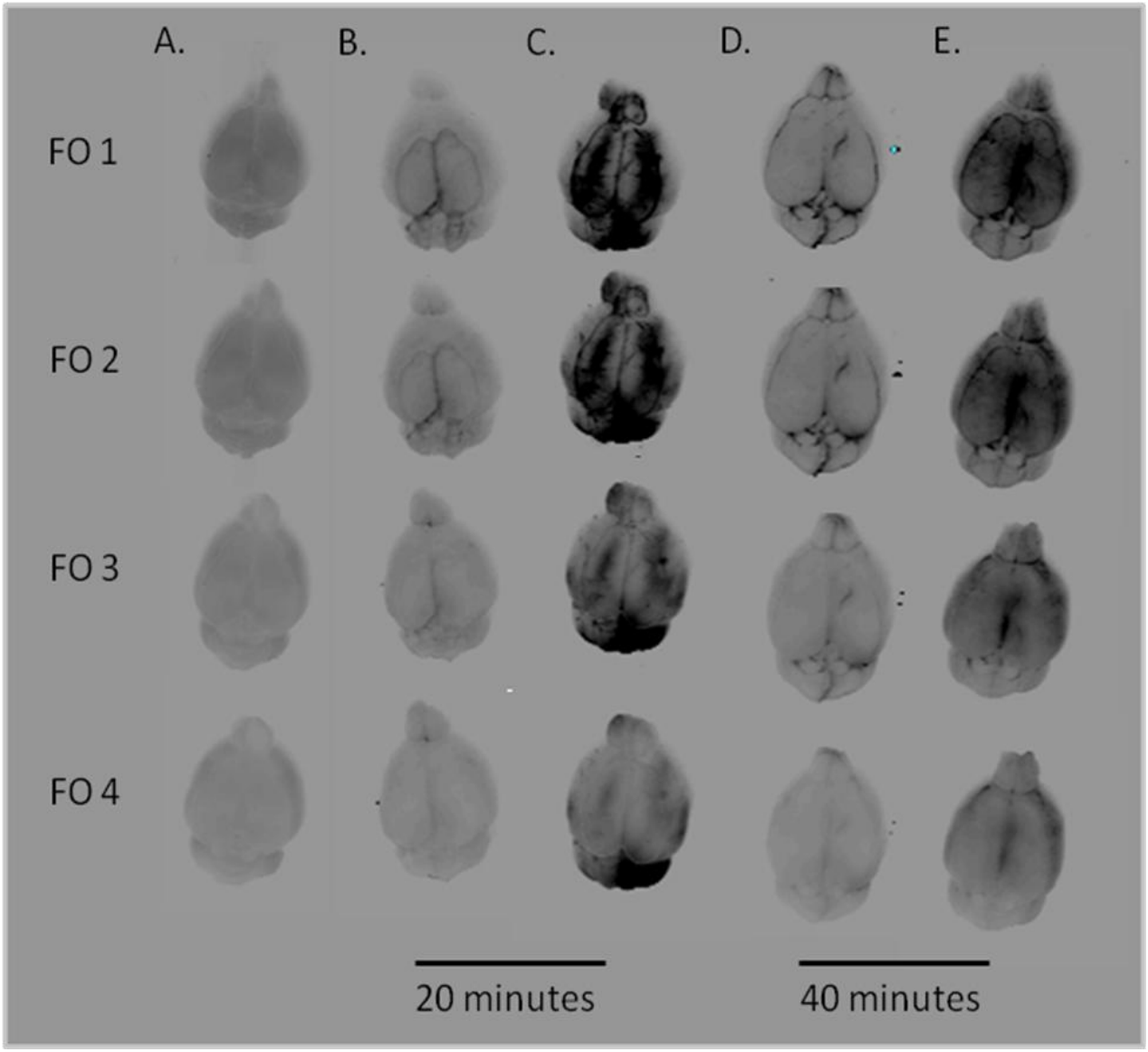

Figure 4.7: The accumulation of IRdye 800cw PEG in whole brain obtained using the Odyssey Near Infrared Imaging system at different focus offset (FO) values for mice receiving no-treatment (A), vehicle-treatment (B and D), and LPA treatment (C and E). The mice were sacrificed at 20 minutes (B and C) and 40 minutes (D and E) following treatment.

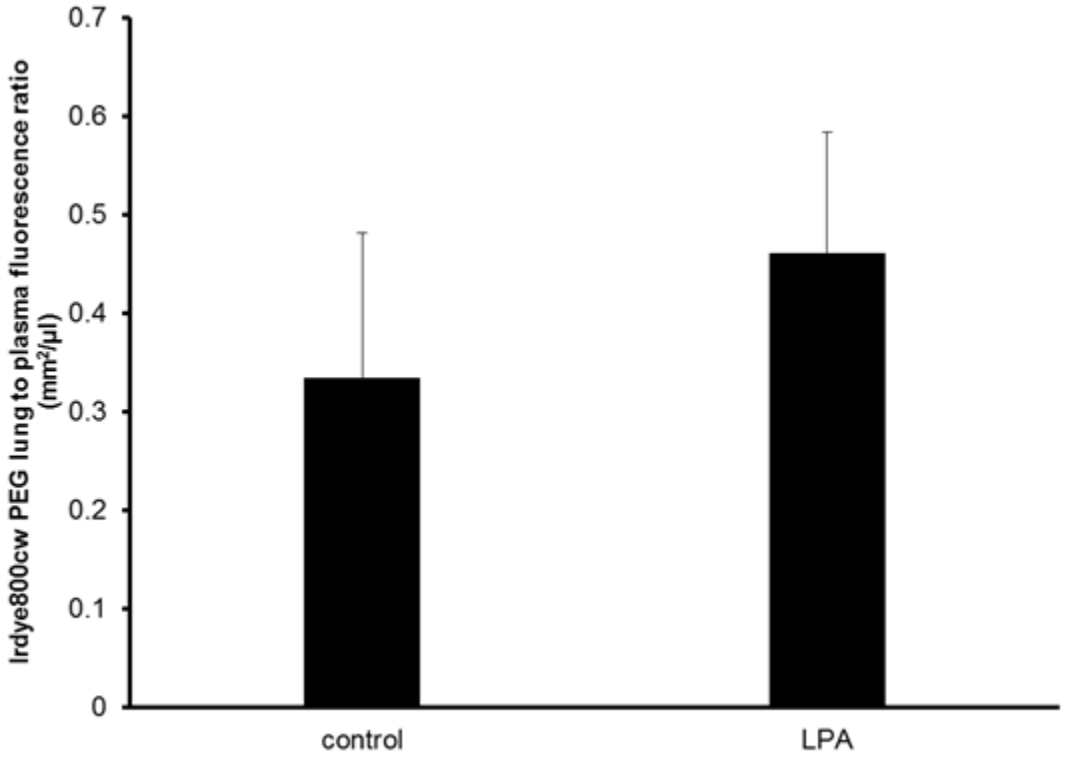

Figure 4.8: Quantitative assessment of IRdye800cw PEG in the lungs following 20 minutes of single i.v. bolus injections of vehicle (0.25% BSA in PBS) or LPA (1mg/kg). Values represent the mean ± sem for 3 mice per treatment group. The student t-test indicated non-significant with $p < 0.05$.

4.3.5. Tachphylaxis to LPA-Induced BBB Disruption:

Tachyphylaxis to LPA-induced BBB disruption was examined using both small (Gad) and large (IRdye800 cw PEG) molecule permeability markers. In the case of Gad contrast agent, BBB disruption following two injections of LPA showed an approximately 5-fold increase in Gad distribution in the brain (Figure 4.9A and 4.9B), similar in magnitude to a single injection of LPA. In the case of IRdye800 cw PEG, there was a significant decrease in the accumulation of IRdye800 cw PEG fluorescence in the brain as the number of LPA injections increased. Indeed, a triple injection of LPA resulted in little to no accumulation of the dye (Figure 4.10C and 4.10D) in

the brain tissue other than the cerebellum when compared to the control mice. The double injections of LPA had more IRdye800 cw PEG penetration than the control group (Figure 4.10A and 4.10B); however, the amount of IRdye800 cw PEG accumulated in the brain was significantly less when compared to the mice receiving only a single injection of 1mg/kg of LPA. Quantitative analysis of the dye revealed significant enhancement of IRdye 800cw PEG accumulation in the LPA treated mice at 20 minutes (Figure 4.11) and 40 minutes (data not shown) post injection of IRdye800 cw PEG when compared to their control counterparts. However, as the number of LPA injections increased, the amount of IRdye800 cw PEG accumulating in the brain tissue decreased, even comparable to the control group as in the case of the triple injections of LPA (Figure 4.11).

A.

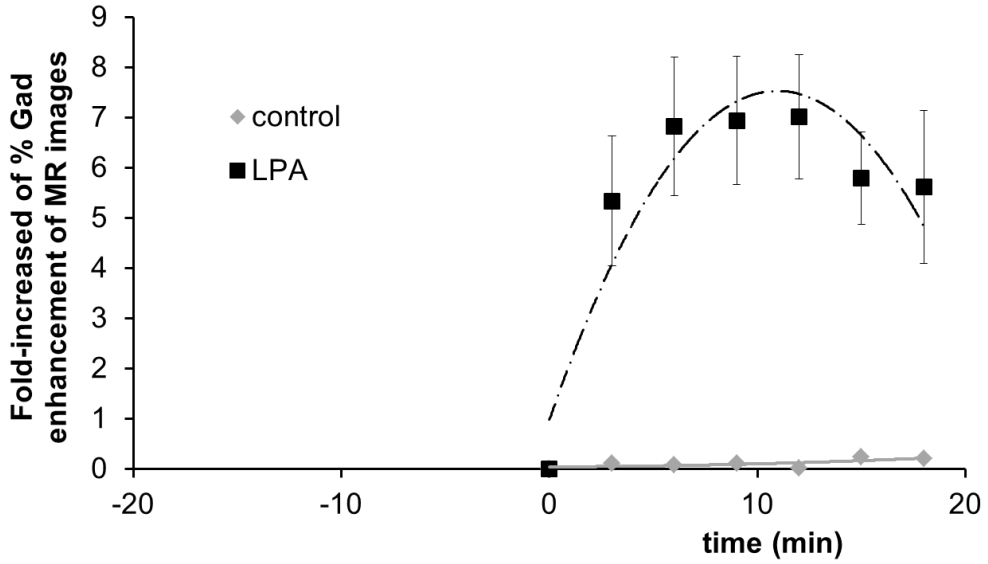

B.

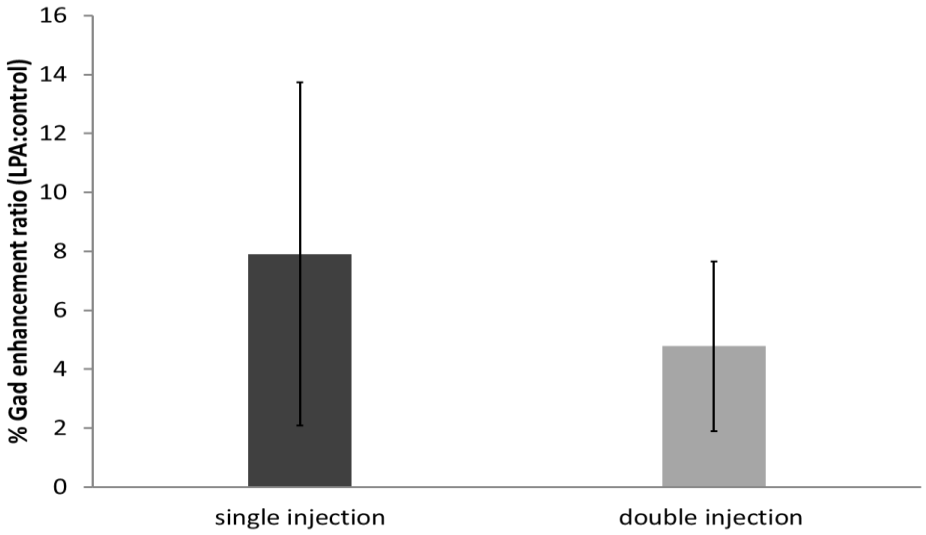

Figure 4.9: (A) Quantitative analysis of % enhancement of MR images following Gad injection in the posterior brain images following multiple injections of either vehicle or LPA (1mg/kg) solutions administered at 20-minute intervals. (B) Determination of maximal BBB permeability increases produced by single and repeated injection of LPA in mice. Values are expressed as the % enhancement Gad in T1-weighted images from posterior brain images following LPA (1mg/kg) exposure compared to vehicle treated mice. Values represent the mean ± sem of 4 mice per treatment group.

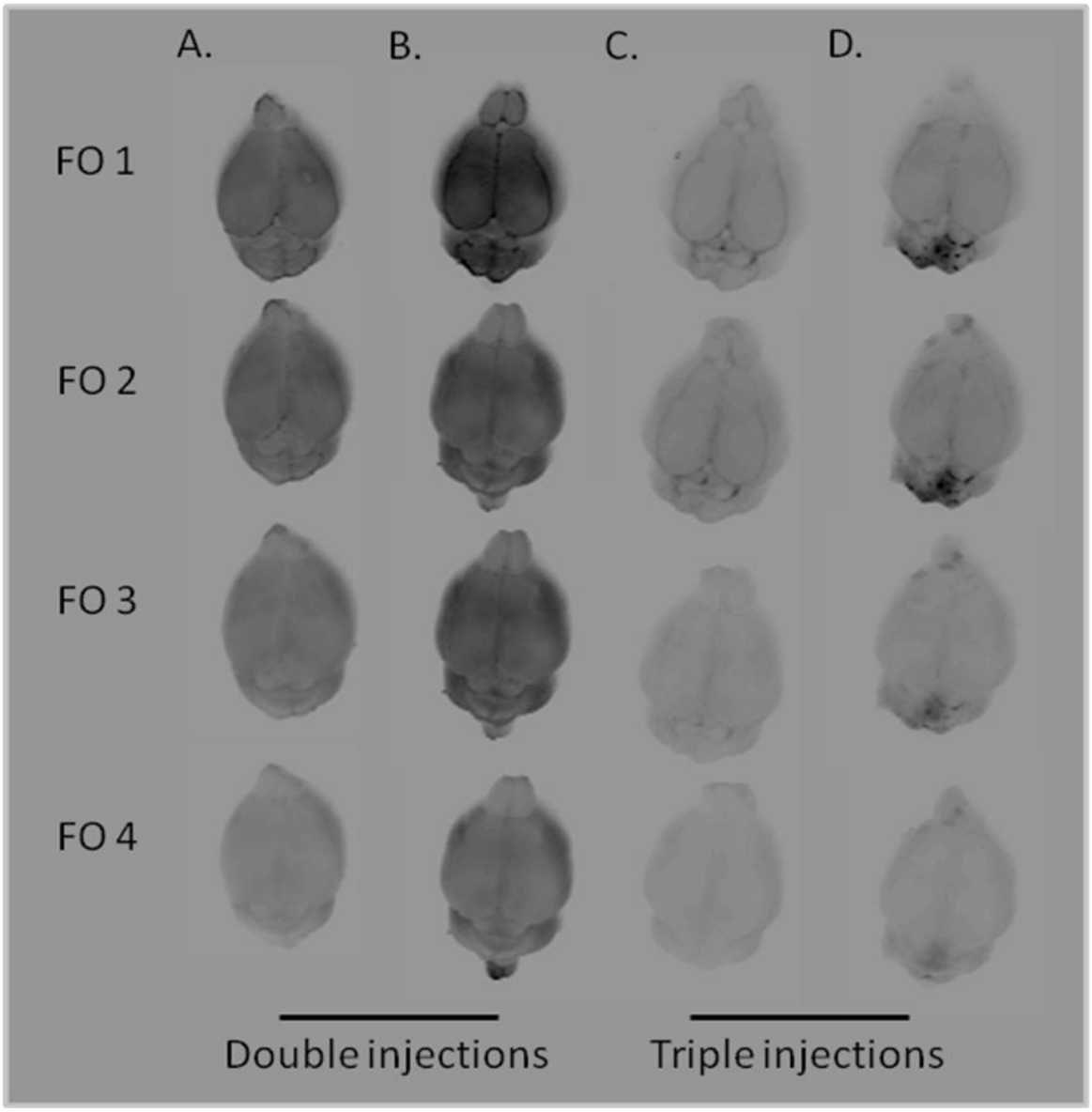

Figure 4.10: The accumulation of IRdye800cw PEG in the brain following a double (A and B) or triple (C and D) dosing sequence of either vehicle (A and C) or LPA (B and D). Mice were euthanized 20 minutes following the i.v. adminstration of IRdye800cw PEG and tissue was perfused with formalin. Whole brain images were obtained using the Odyssey Near Infrared Imaging system scanned using focus offset lengths from 1-4 mm (FO 1-4). Images were taken from a representative of n = 5.

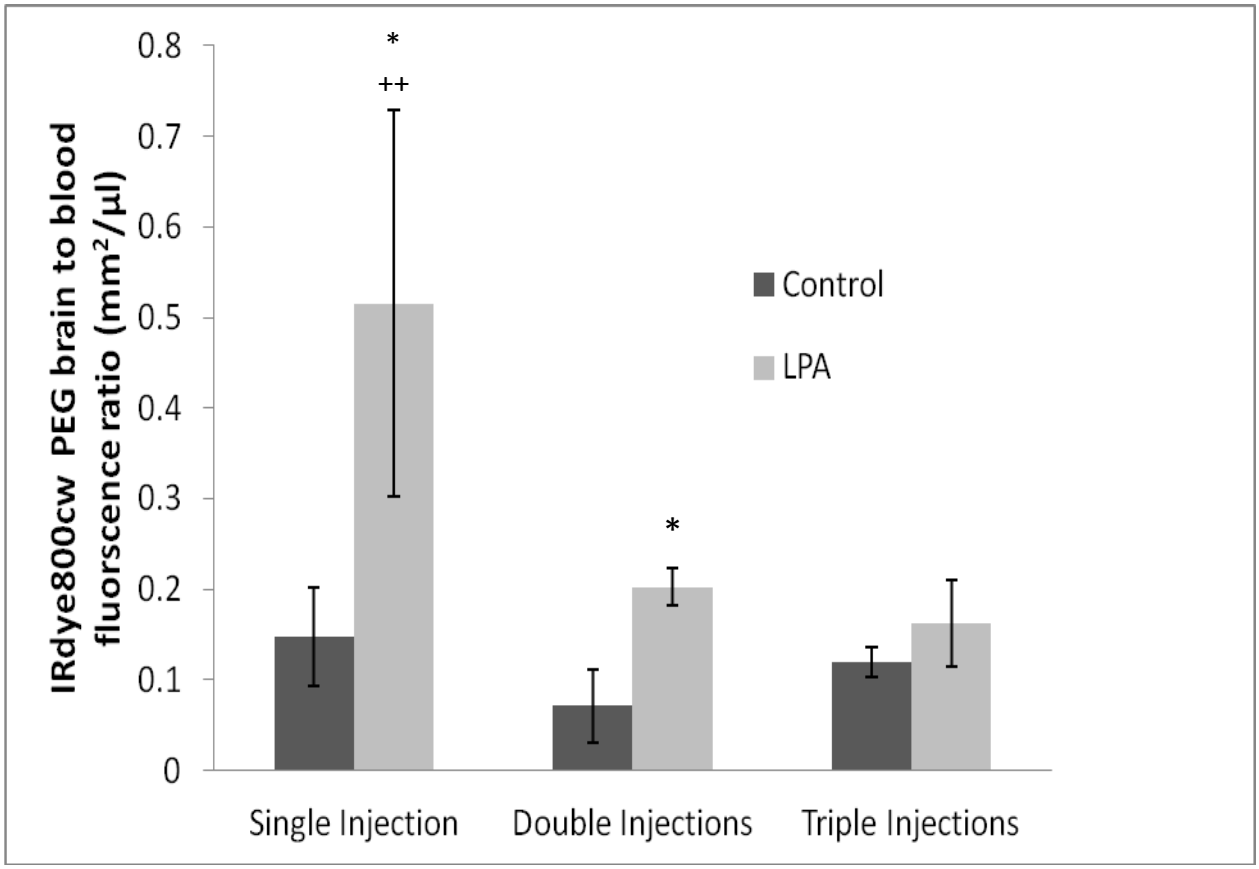

Figure 4.11: Quantitative assessment of IRdye800cw PEG in the brain following single or multiple i.v. bolus injections of vehicle (0.25mg/ml BSA in PBS) or LPA (1mg/kg). 2-way ANOVA was conducted to determine if there is a statistical difference between treatment groups as well as the number of injections. * $p < 0.05$ compared to control mice within the same treatment group. ++ $p<0.05$ compared to LPA treated mice from multiple injection treatment groups. Values represent the mean ± sem with n = 4 per treatment group.

4.3.6. Effects of LPA on R800 Permeability in the BBB:

The accumulation of a P-gp substrate, Rhodamine 800, was also examined under normal conditions and following BBB disruption with LPA. Representative *ex vivo* NIRF images of R800 in the brain are shown in Figure 4.12. Increases in R800 fluorescence were observed in LPA treated mice compared to that in the vehicle treatment group. Quantitative analysis of the brain images showed a 2-fold enhancement of R800 fluorescence in the brains of the LPA treated

mice at 10 minutes post LPA exposure. In contrast, examination of R800 fluorescence 20-minutes post LPA treatment showed no significant enhancement compared to control mice (Figure 4.13).

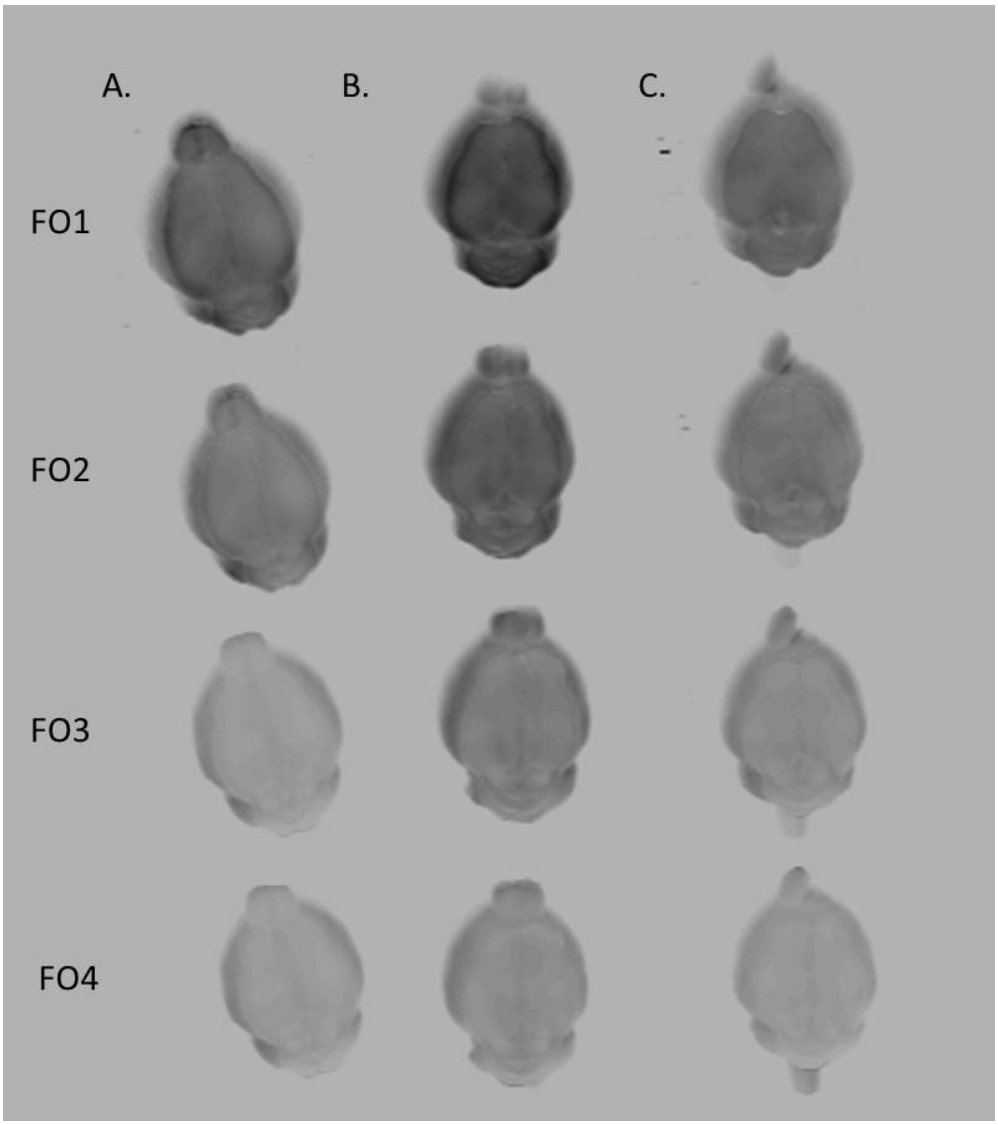

Figure 4.12: The accumulation of R800 in the brain obtained using the Odyssey Near infrared Imaging system scanned at different focus offsets (FO 1-4) for control mouse (A) and LPA treated mice (B and C). The mice were sacrificed at 10 minutes (A and B) and 20 minutes (C) following R800 injection.

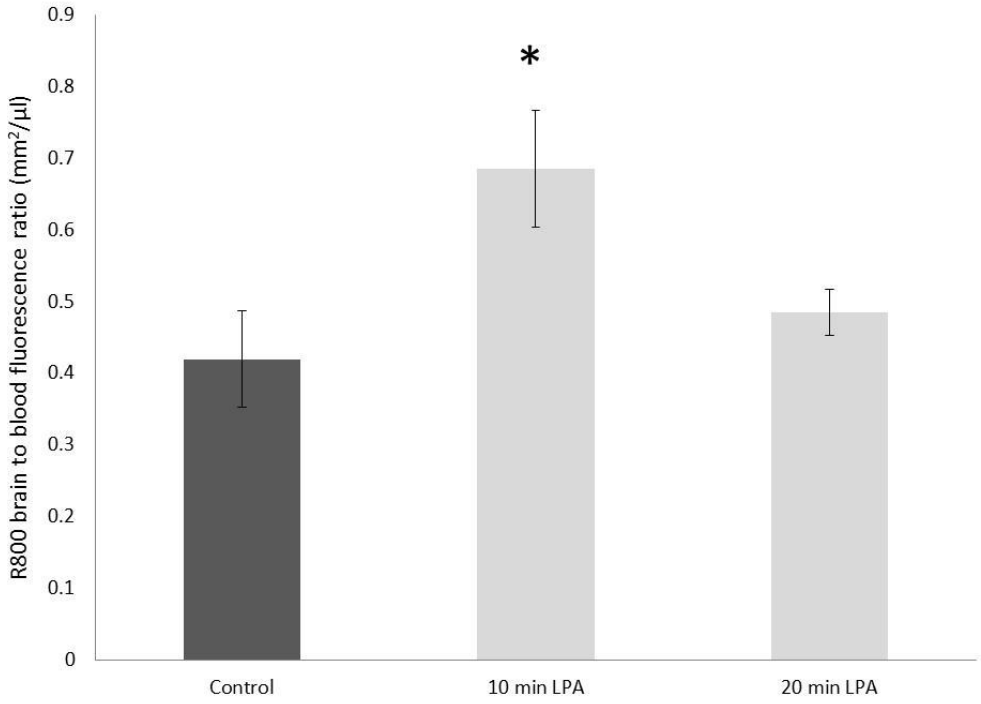

Figure 4.13: Quantitative analysis of R800 accumulation in brain tissue following vehicle or LPA (1mg/kg) exposure. Mice were given R800 via tail vein injection either alone or in combination with LPA (1 mg/kg). The BBB permeability of R800 was expressed as the brain to blood ratio determined at 10 and 20-minutes post treatment. Values represent the mean ± sem for 3 mice per treatment group. ANOVA was conducted to determine statistical significant among the treatment groups. * $p<0.05$ compared to control group.

4.3.7. LPA-Mediated BBB Permeability to Radiolabelled Methotrexate:

As the first step in potential utilization of LPA to transiently disrupt BBB permeability for enhancing drug delivery to the brain, the study also examined the brain accumulation of radiolabeled methotrexate. Under control conditions, the brain penetration of methotrexate was minimal with a brain to plasma ratio of 1-2%. However, following LPA administration, radiolabeled methotrexate reached brain to plasma ratios of over 20%. This represented an almost 20-fold enhancement in radiolabeled methotrexate delivery to the brain following LPA-mediated disruption of the BBB (Figure 4.14).

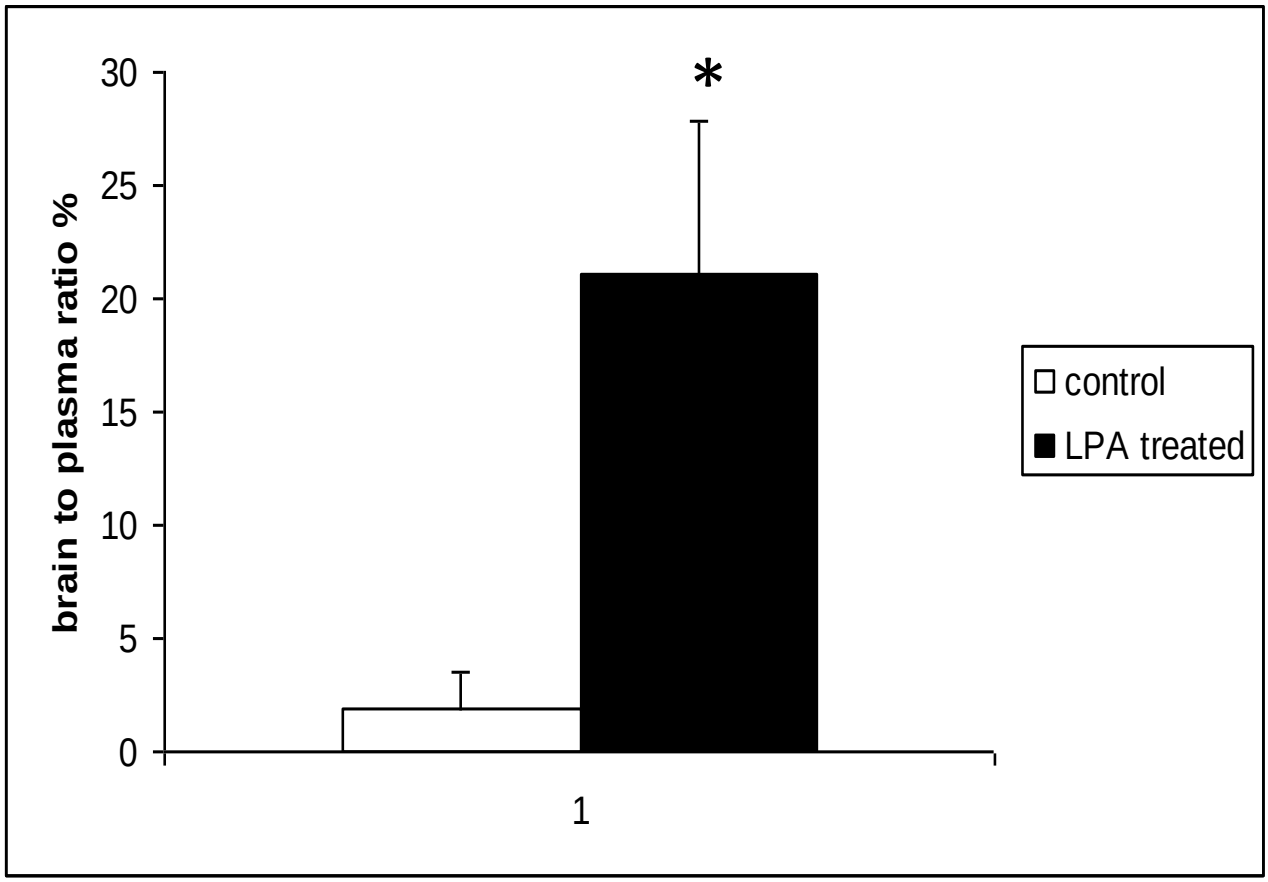

Figure 4.14: Quantitative assessment of radiolabelled methotrexate in the brain following single i.v. bolus injections of vehicle (0.25% BSA in PBS) or LPA (1mg/kg). Values are expressed as the brain to plasma ratio of radioactivity and represent the mean ± sem of 6 mice per treatment group. *$p<0.05$ compared to control mice receiving LPA vehicle injection.

4.4. DISCUSSION

Lysophosphatidic acid is one of the simplest glycerolphospholipids. While originally thought to be an intermediate in lipid metabolism, it is now known to mediate a variety of biological responses depending on the cellular target (Moolenaar, van Meeteren, and Giepmans 2004, 870-881). Biological responses to LPA are initiated through binding of the phospholipid to LPA receptors on the plasma membrane of the cell. Hecht JH *et al* identified LPA as a ligand for ventricular zone-1 (vzg-1) receptor which is a member of the endothelial differentiation gene (EDG) family (Hecht et al. 1996, 1071-1083). There are currently at least 6 different types of LPA receptors (LPAR1-LPAR6) (Zhao and Natarajan 2009, 367-377). Based on amino acid sequence, LPAR1-LPAR3 share 50% homology and belong to the EDG subfamily of G-protein coupled receptors formally known as EDG2, EDG4 and EDG7, respectively. The remaining LPA receptors, including LPAR4 (GPR23), LPAR5 (GPR92), and LPAR6 (GPR87) are structurally distinct from the EDG family and share less than 40% amino acid sequence homology with the conventional LPARs (Zhao and Natarajan 2009, 367-377).

Within the brain, LPAR1 is the most highly expressed, although LPAR2 and LPAR3 are also present (Choi et al. 2010, 157-186). Considering the pleiotropic effects of LPA in the brain along with the upregulation of LPAR1-3 following injury, it was proposed that LPA could regulate essential aspects of cellular organization and play a crucial role in reactive astrogliosis, neural regeneration and axonal regrowth (Goldshmit et al. 2010, 23-32). Little is known about the role of LPAR4 and LPAR5; however, studies by Yanagida K *et al* 2007 reported a high expression of LPAR4 in neuronal cells and indicated that activation of the LPAR4 receptor was associated with morphological changes including cell rounding and N-cadherin-associated cell aggregation (Yanagida et al. 2007, 5814-5824). LPAR5 is highly expressed in the genital organ, skeletal

muscles, as well as brain (Tabata et al. 2007, 861-866). However, the role of LPAR5 within the brain tissue is largely unknown. Within the context of the present study, all known LPARs were expressed at the mRNA level in mouse brain homogenates. Compared to the expression pattern observed in brain homogenate, LPAR1, LPAR4 and LPAR5 had a much higher level of expression in the capillary fraction, suggesting potential enrichment in the brain capillaries. In contrast, LPAR2 and LPAR3 were substantially reduced compared to the brain homogenates suggesting other non-capillary sources for these particular LPA receptors in the brain.

The enriched expression of several LPA receptors within the brain microvasculature is not surprising, given that the vascular endothelium is a major target for LPA with changes in proliferation, angiogenesis and permeability reported following exposure to the phospholipid (Schulze et al. 1997, 991-1000; Brault et al. 2007, R1174-83). In the case of permeability, most studies support an increase in vascular leakage following LPA exposure (Schulze et al. 1997, 991-1000; Tigyi et al. 1995, H2048-55; Goeckeler and Wysolmerski 1995, 613-627; Inoue, Forster, and Epstein 1995, 888-896). However, there are some contradictory reports of LPA-induced reductions in endothelial cell permeability (i.e. barrier enhancing properties) (English et al. 1999, 627-634). The conflicting reports regarding LPA-induced permeability could be dependent on a number of factors including differences in vascular bed, species of the mice or the profile of LPA receptors expressed. In the case of the latter, it should be noted that LPA was able to restore the barrier properties of primary small airway epithelial cells (HSAEpCs) after endotoxin-induced disruption (He et al. 2009, 24123-24132). As LPAR3 is the primary receptor expressed within the lung epithelium (Zhao and Natarajan 2009, 367-377), it is tempting to suggest that activation of LPAR1 and LPAR3 have opposing effects on permeability, and the net effect of LPA on vascular permeability depends on the LPAR involved.

In cultured brain microvessel endothelial cells, LPA exposure has been associated with increases in permeability (Schulze et al. 1997, 991-1000; Nitz et al. 2003, 30-40). Such findings are consistent with the effects of LPA on permeability of primary cultured brain microvessel endothelial cell monolayers observed in the present study. The effects of LPA were concentration dependent and the increases in permeability occurred rapidly within minutes of exposure. Furthermore, LPA-induced increases in BMEC permeability were observed across various species including bovine, mouse and human and were prevented by pre-treatment of the monolayers with toxin C. As toxin C is an inhibitor of the small G protein Rho mediated second messenger system associated with cytoskeletal structure (Borges et al. 2011, 368-379), the permeability increases observed with LPA are likely the result of activation of G protein coupled receptors on the BMECs. Based on the expression levels of LPARs in both the human primary brain endothelial cells and mouse capillary enriched fractions, and the role of LPAR1 in vascular permeability increases observed with LPA in other vascular beds (Sarker, Hu, and Fraser 2010, 39-46), this receptor is likely to be involved in the permeability responses observed in the present study.

In addition to examining the permeability effects of LPA in cultured brain endothelial cells, the present study is the first to demonstrate enhanced BBB permeability following systemic administration of LPA in an *in vivo* model. In adult Balb/c mice, bolus injections of LPA produced dose-dependent disruption of BBB integrity as assessed using Gad contrast agent. While the use of Gad to identify localized cerebral microvascular leakage resulting from brain tumors or stroke is common (Nagaraja *et al*. 2011, 547-558), the present study used Gad contrast enhanced MRI to characterize both the time course and magnitude of BBB disruption following LPA exposure. A unique feature of MRI imaging technology is the fast acquisition time

which allows monitoring of rapid changes in BBB permeability within the same animal. These studies demonstrated significant enhancement of BBB permeability to Gad within 3 minutes of LPA exposure. The BBB disruption produced was both quick in onset and rapid in dissipation with return of BBB function within 20 minutes of LPA exposure.

The rapid onset of LPA action is consistent with a GPCR response which takes place through phosphorylation/dephosphorylation cycles. Phosphorylation of the receptors can attenuate the signaling of G-protein through the recruitment of arrestin, an adaptor protein which can also facilitate the endocytosis of GPCR (Avendano-Vazquez, Garcia-Caballero, and Garcia-Sainz 2005, 677-684). This internalized receptor can be dephosphorylated by membrane phosphatase and be recycled back to the plasma membrane. The rapid dissipation of LPA action can be explained by the metabolism of LPA. Lipid phosphate phosphatase (LPPs) hydrolyzes numerous lipid phosphates including phosphatidate, lysophosphatidate (LPA), sphingosine-1-phosphate (S1P), ceramide-1-phosphate (C1P) and diacylglycerol pyrophosphatate. The extracellular metabolism of LPA and SIP is mediated through the activity of LPPs (Brindley and Pilquil 2009, S225-30). Indeed, increases expression of LPPs resulted in increased dephosphorylation of LPA, SIP and CIP (Jasinska et al. 1999, 677-686). Studies with LPP knockout mice (P*pap*2a$^{tr/tr}$) showed a significant increase in plasma LPA concentration compared to wild-type mice, furthermore, the absence of LPPs in P*pap*2a$^{tr/tr}$ mice also increased the plasma half-life of LPA to 12 minutes as opposed to 3 minutes in control animals (Tomsig et al. 2009, 611-618).

The use of Gad contrast MRI to capture LPA-induced changes in BBB permeability also allowed for examination of regional differences in BBB permeability under both normal conditions and following LPA exposure. Under control conditions, in the absence of LPA

exposure, Gad contrast enhancement was greater in the posterior sections of the brain compared to mid-brain and anterior regions. This suggests a slightly higher BBB permeability in the posterior brain regions. Such regional differences in BBB permeability have been reported previously (Phares et al. 2006, 7666-7675); however, identification is difficult with many of the techniques commonly used for assessing BBB permeability. Regional differences in the magnitude of Gad contrast enhancement were also observed in the LPA treatment group. However, the net increase in BBB permeability to Gad contrast agent following LPA exposure compared to vehicle treated mice was approximately 5 fold throughout all brain regions examined. These findings suggest that cerebral vascular permeability responses to LPA are similar throughout the brain.

The tight junctions formed by the endothelial cells of the BBB limit the penetration of most hydrophilic molecules. In general, hydrophilic solutes greater than 500 Da in size undergo little if any appreciable paracellular diffusion and are considered to be impermeable in the BBB (Banks 2009, S3). This was certainly evident with Gad contrast agent which had little BBB penetration under normal conditions. To fully characterize the extent of BBB disruption produced by LPA, additional imaging studies were performed using the near infrared fluorescence (NIRF) contrast agent, IRdye 800cw PEG. Previous studies have used IRdye 800cw PEG to examine vascular leakage and lymphatic drainage (Sampath et al. 2007, 1501-1510). With a molecular weight of 25 kDa, little dye penetration into the brain was expected following systemic administration. This was certainly the case in the present study, under control conditions, where the IRdye800cw PEG dye was confined to the cerebral vascular space. However, when the dye was administered systemically, in combination with LPA, a substantial enhancement of IRdye 800cw PEG leakage was observed in the brain. The enhanced BBB

permeability observed with IRdye 800cw PEG was lesser in magnitude than that observed with Gad contrast agent. This finding is consistent with LPA-induced disruption of tight junctions within the brain microvessel endothelial cells as such disruption would be expected to have a greater impact on small solutes compared to large macromolecular solutes. These findings indicate that LPA-induced BBB disruption was not limited to only small weight compounds but was also present for larger macromolecules. Furthermore, the intense dye staining around the area of the vessels at 20 minutes compared to the more dispersed dye distribution in the brain observed at 40 minutes post LPA exposure further confirms the BBB disruption produced by the phospholipid was short-acting.

In addition, LPA had also been known to modulate the integrity of endothelial cells lining the pulmonary circulation. Through the activation of Rho kinase pathway, LPA induced an increase pulmonary endothelial permeability for horseradish peroxidase (HRP) (van Nieuw Amerongen, Vermeer, and van Hinsbergh 2000, E127-33). This increase in vascular integrity within the pulmonary circulation contributes to the pathogenesis of pulmonary disorders including asthma, acute respiratory distress syndrome and ischemia-reperfusion injury (Wojciak-Stothard, Tsang, and Haworth 2005, L749-60; van Nieuw Amerongen and van Hinsbergh 2002, 257-272). The disruption of the endothelial barrier may lead to excessive plasma extravasation obstructing the airway passage triggering an asthmatic like symptoms and respiratory distress. However, the current study showed no apparent changes in the pulmonary vascular permeability regardless of the treatment conditions as indicated by similar accumulation of the IRdye800cw PEG in the lungs. This unexpected finding could be explained by the dosage of LPA used. Indeed, a rather high concentration of LPA was necessary to induce endothelial hyperpermeability (van Nieuw Amerongen and van Hinsbergh 2002, 257-272). Perhaps the

dosage of LPA used in the current study was insufficient to cause the systemic vascular disruption.

To confirm that the mechanism of LPA-induced BBB disruption was primarily due to enhanced paracellular diffusion through altered tight junction complexes, additional imaging studies were performed using R800. Rhodamine 800 is a small, lipophilic, NIRF molecule known to be a substrate for P-glycoprotein (P-gp), one of the main efflux transporters found in the BBB (On et al. 2011). Previous BBB permeability studies with R800 showed only minimal brain accumulation of the NIRF agent due to P-gp mediated efflux transport at the BBB (On et al. 2011). Therefore, R800 appeared to be an ideal agent to assess the effects of LPA-mediated BBB disruption on solutes that undergo transcellular route of passage through the BBB. In contrast to both Gad and IRdye 800cw PEG, the brain accumulation of R800 in LPA-treated mice was not significantly greater than vehicle treated mice at 20 minutes following LPA. Examination of R800 fluorescence at 10-minutes post LPA treatment showed significantly greater brain penetration compared to control mice. However, it should be noted that even at this time point enhancement was not as pronounced as that observed with Gad contrast agent. The reduced effects of LPA-mediated BBB disruption on R800 passage into the brain are most likely attributable to the significant transcellular exchange mechanisms that influence R800 permeability in the BBB. Thus, while LPA may increase the paracellular diffusion of R800 into the brain, this is off-set by transcellular diffusion and P-gp mediated transport of the dye from brain tissue back to the blood. Based on these results, it appears that LPA-mediated disruption of the BBB will have the greatest impact on hydrophilic agents whose transcellular permeability in the BBB is limited.

Desensitization due to receptor internalization is a common feature of G-protein coupled receptors (Kelly, Bailey, and Henderson 2008, S379-88). In the classic desensitization model, binding of ligand to GPCR results in the activation of heterotrimeric G-protein which is involved in the exchange of GDP for GTD (Calebiro et al. 2010, 221-228). Repeated exposure to the ligand initiates receptor desensitization by phosphorylating the receptor, thus preventing the coupling of G-protein and a loss of response to receptor activation (Ligeti, Csepanyi-Komi, and Hunyady 2012, 469-478). This phosphorylation process is also linked to GPCR internalization and, as such, impacts on the degradation and/or recycling of receptor (Bohm, Grady, and Bunnett 1997, 1-18). Recent studies have reported tachyphylaxis in regards to the permeability response to LPA (Sarker, Hu, and Fraser 2010, 39-46). Using an *in situ* preparation in which LPA was topically applied to the cerebral microvasculature, continuous infusion of LPA over 10 minutes resulted in reduced permeability to subsequent LPA challenge (Sarker, Hu, and Fraser 2010, 39-46). The potential development of tachyphylaxis to LPA-induced BBB disruption *in vivo* was examined in the present study. While repeated exposure to bolus injections of LPA (at 20 minute intervals) enhanced the BBB permeability of Gad contrast agent to a similar extent, significant reductions in BBB disruption were observed when IRdye 800cw PEG imaging agent was used. As Gad contrast agent is a relatively small molecule (547 Da) compared to IRdye 800cw PEG (approximately 25 kDa), the magnitude of disruption of tight junctions necessary to result in the loss of BBB integrity to small hydrophilic agents is substantially less than that required for larger macromolecules. Thus, desensitization of LPA receptor-mediated permeability responses are likely to be more apparent with large macromolecule imaging agents such as IRdye 800cw PEG. The mechanism by which tachyphylaxis to LPA-mediated BBB disruption occurs remains to be determined; however, since LPAR1 activates different G-

proteins including G_i, G_q, and G_{12}, and given the time frame of desensitization, the decreased response to LPA is likely attributed to the uncoupling of the protein through the phosphorylation of the receptor and subsequent receptor internalization. In support of this, studies by Avendeno-Vazquez and colleagues (Avendano-Vazquez, Garcia-Caballero, and Garcia-Sainz 2005, 677-684) reported rapid internalization of LPAR1 in hepatocytes continuously exposed to LPA.

The effect of LPA on BBB permeability is a topic of debate; furthermore, little is known about the physiological role of LPA, particularly in the brain. Endogenous LPA released during platelet activation has also been implicated in a decrease in endothelial permeability *in vitro*. Indeed, it has been observed that human platelets release factors that decrease the solute permeability of cultured bovine endothelial cells in a rapid and reversible manner (Haselton and Alexander 1992, L670-8). Furthermore, cell-column chromatography measurements of endothelial cell permeability using fluorescence dextran, cyanocobalamine and sodium fluorescein have shown that platelet-derived LPA rapidly reduces the permeability of the bovine aortic and bovine fetal endothelial cells, thus reducing the elution of sodium fluorescein and cyanocobalamine, as well as fluorescein dextran (Alexander et al. 1998, H115-22). The effects of endogenously released LPA are likely to be local and of short duration. This suggests that platelet-derived LPA can also regulate *in vivo* endothelial cell barrier properties in the peripheral system. However, in the case of cultured brain microvessel endothelial cells, LPA exposure has been associated with increases in permeability (Schulze et al. 1997, 991-1000; Nitz et al. 2003, 30-40). Using various imaging technologies including MRI and NIRF, we found that LPA was able to disrupt the BBB allowing both a small molecule such as Gad, as well as a large molecule (IRdye800cw PEG), to penetrate the brain. These findings indicate that LPA can influence the

BBB permeability of a wide range of solutes. The present study examined the effects of LPA on the accumulation of small molecular markers of vascular permeability such as Gad, a large macromolecule solute such as IRdye800cw PEG and the P-gp probe, R800 as a molecule with efflux transport activity. As the first step in potential utilization of LPA to transiently disrupt BBB permeability for enhancing drug delivery to the brain, the study also examined the brain accumulation of radiolabeled methotrexate which has low permeability across the BBB. As expected, under control conditions, the brain penetration of methotrexate was minimal with a brain to plasma ratio of 1-2%. However, following LPA administration, radiolabeled methotrexate reached brain to plasma ratios of over 20%. This represented an almost 20-fold enhancement in radiolabeled methotrexate delivery to the brain following LPA-mediated disruption of the BBB. This is similar in magnitude to the responses reported previously with osmotic disruption and bradykinin receptor activation (Kroll and Neuwelt 1998, 1083-99; discussion 1099-100). The rapid onset of BBB disruption and the rapid restoration of the barrier properties following an administration of LPA suggest LPA may have applications for increasing drug delivery to the brain and the tumor sites.

CHAPTER 5: LYSOPHOSPHATIDIC ACID (LPA)-INDUCED ENHANCEMENT OF BLOOD-BRAIN BARRIER (BBB) PERMEABILITY IN A MOUSE BRAIN TUMOR MODEL.

5.1. INTRODUCTION

Compared to the other therapeutic drug classes, CNS drugs have the lowest probability of success in clinical trials (Wang, Hung, and O'Neill 2011, 159-166). The difficulty in developing therapeutic drugs to treat CNS disorders can be attributed to several factors including the complexity of the brain and consequently brain related disorders, undesired adverse effects of the drugs, and the presence of neuroprotective barriers such as the blood-brain barrier (BBB), and the blood-CSF barrier (BCSFB) that hinder the delivery of drugs to their site of action within the CNS (Neuwelt et al. 2008, 84-96). Given the trend towards larger drug molecules and bioactive macromolecules to treat CNS diseases, achieving sufficient BBB permeability is likely the most important factor limiting the future growth of neurotherapeutics (Pardridge 2005, 3-14).

The BBB is comprised of a continuous layer of endothelial cells, associated astrocyte foot-processes, and scattered pericytes. However, it is the brain microvessel endothelial cells with highly developed tight-junction complexes, low endocytic activity and the absence of fenestrations (Girardin 2006, 311-321) that provide the physical barrier to the passage of most polar and hydrophilic solutes from the blood into the brain. The paracellular diffusion of nutrients and metabolites between the blood and the extracellular compartment of the brain is highly restricted by tight junctions that form between the brain endothelial cells. In addition to restricted paracellular diffusion, the brain microvessel endothelial cells (BMEC) forming the BBB express numerous transporter systems that are essential for maintaining the proper brain microenvironment (Girardin 2006, 311-321; de Boer and Gaillard 2006, 455-462). Consequently, the uptake of essential molecules, such as glucose and amino acids, to meet the metabolic requirements of the brain occurs through specific transporter proteins located on the plasma

membrane of the endothelial cells. In addition to uptake transporters, the endothelial cells also express numerous efflux transporters including breast cancer resistance protein (BCRP), P-glycoprotein (P-gp), and multidrug resistance protein (MRP) (Hermann and Bassetti 2007, 128-134). As members of the ATP-binding cassette (ABC) superfamily of transporter proteins, these efflux transporters are responsible for the active transport of a wide variety of compounds including phospholipids, ions, peptides, steroids, polysaccharides, amino acids, organic anions, bile acids, drugs and other xenobiotic compounds across cellular membranes (Beaulieu et al. 1997, 539-544; Balayssac et al. 2005b, 319-329; Lee et al. 2010, 603-619; Schinkel et al. 1996, 2517-2524; Feng et al. 2008, 268-275; Miller et al. 1996, 301-306). As these transporters utilize energy from ATP hydrolysis, compounds can be removed from the cells against a concentration gradient. Various members of the ABC transporter family are known to play a major role in multidrug resistance of cancer cells (Dean 2009, 3-9) and bacterial cells (Li and Nikaido 2004, 159-204). Although the expression of a variety of drug efflux transporters in the BBB is essential in protecting the brain from the circulating agents and xenobiotic compounds in the blood capable of disturbing neuronal function and maintaining the proper microenvironment necessary for neuronal transmission, from a drug therapy standpoint, the presence of drug efflux transporters within the BBB limits the brain penetration of many agents (Loscher and Potschka 2005, 86-98; Loscher and Potschka 2005, 22-76; Bachmeier, Trickler, and Miller 2006, 998-1003; Miller, Hinton, and Chen 2011, 1633-1638). As the efflux transporters such as P-gp, BCRP and MRP are known to transport a wide variety of chemotherapeutic agents, their presence in the brain endothelial cells can significantly reduce the accumulation of chemotherapeutic drugs in the brain, thereby limiting effectiveness of these agents in treating

brain tumors (Ernst et al. 2010, 540-549; Schinkel et al. 1996, 2517-2524; Callaghan et al. 2008, 365-378; Fontaine, Elmquist, and Miller 1996, 1521-1531).

The restrictive nature of the BBB and the localization of P-gp present formidable obstacle to the delivery of drugs to the brain. This is the case even in those conditions where BBB permeability is presumed to be compromised, such as in brain tumors (Siegal et al. 2000, 599-605; Kroll and Neuwelt 1998, 1083-99; discussion 1099-100). Recent studies from our laboratory with a murine brain tumor model indicate that the BBB remains largely intact early during tumor development with significant loss of BBB integrity only occurring during late stages of tumor progression (Chapter 2). This is consistent with previous studies by Zhang et al., indicating the BBB is intact in the early stages of brain tumor growth in nude mice, when diagnosis is most critical (Zhang et al. 1992, 1115-1124). Using a mouse metastatic brain tumor model, it was observed that the blood-brain barrier remained intact in and around tumors smaller than 0.5 mm in diameter, but was leaky in larger metastases (Fidler et al. 2002a, 53-57). Furthermore, recent studies suggest that while alterations in BBB and blood-tumor barrier (BTB) permeability may occur with brain metastases, the extent of this disruption is insufficient to achieve optimal therapeutic levels of drug in the tumor regions (Lockman et al. 2010, 5664-5678). Additional evidence of the role of the BBB in the limited brain tumor responses to chemotherapeutic agents is the effectiveness of these same agents when the tumor is located outside of the CNS (Weiss 1980, 51-81; Lockman et al. 2010, 5664-5678). These findings highlight the need for new strategies that would enhance chemotherapeutic penetration into the CNS and brain tumor.

One method that has been used clinically to enhance drug delivery to the brain is transient BBB opening. Disruption of the BBB has been achieved through both receptor-

mediated (bradykinin receptor agonists) and non-receptor-mediated (osmotic agents) mechanisms. Osmotic disruption of the BBB by systemic infusion of hypertonic solutions of osmotic agents, such as mannitol, causes the shrinkage of endothelial cells and thus disruption of tight junctions (Kemper et al. 2004, 415-423). The breakdown of the tight junction complexes within the brain microvessel endothelial cells results in enhanced paracellular diffusion of solutes from the blood to the brain. While osmotic disruption of the BBB has been used clinically to increase delivery of chemotherapeutic agents in treating brain tumors, the major drawback of osmotic disruption is the long recovery period (up to several hours) required for restoration of BBB integrity (Siegal et al. 2000, 599-605). The prolonged period of BBB opening allows the entry of plasma proteins such as albumin and pathogens, which can result in major side effects such as seizures, neuropathological changes, and neurological toxicity (Kemper et al. 2004, 415-423).

Administration of histamine, bradykinin or bradykinin analogues have also been used to open the BBB by activating the bradykinin B2 receptor located on the endothelial cells (Patel et al. 2009, 35-58) resulting in second messenger mediated disruption of tight junctions formed between the endothelial cells of the BBB. In contrast to osmotic disruption, the opening of the BBB mediated by this receptor system within the cerebral microvasculature is shorter in duration (Kemper et al. 2004, 415-423). However, despite reports of effectiveness in rodent models, clinical trials with the bradykinin analogue, Cereport^{TM}, have failed to produce the desired response (Prados et al. 2003, 96-103). One possible explanation for the failure of Cereport^{TM} can be attributed to a varying level of bradykinin B2 receptor expression in glioma patients eliciting varying amount of BBB and blood-tumor barrier (BTB) disruption (Black and Ningaraj 2004, 165-173). Alternatively, the negative results can also be due to the sub-optimal

dosage of Cereport™ and/or the differences between the properties of BTB models in glioma patients and the model used in preclinical trials (Kemper et al. 2004, 415-423). Together these studies point to the need for a more controlled method of transient BBB disruption that can influence permeability within both tumor and non-tumor regions of the brain.

Recently our laboratory reported on the BBB permeability modulating effects of the phospholipid, lysophosphatidic acid (LPA) (Chapter 4). In these studies, LPA induced a rapid and concentration dependent increase in vascular permeability in both *in vitro* and *in vivo* BBB models. The BBB disruption produced by systemic LPA administration was also short in duration. One of the simplest glycerolphospholipids, LPA is known to exist endogenously at concentrations of 2-20 μM and can function as an intracellular signaling molecule to produce a broad range of biological responses (Moolenaar, van Meeteren, and Giepmans 2004, 870-881) including cell migration and proliferation, smooth muscle contraction, the assembly of focal adhesion, and stress fiber formation. Pretreatment of LPA on porcine endothelial cells has shown a significant reduction (up to 3-fold decrease compared to control values) in the transcellular electrical resistance (TER) values which reflects on the increase in tight junction permeability (Schulze et al. 1997, 991-1000) allowing 2-3 fold increase flux of sucrose across the monolayer. Furthermore, our laboratory also showed that inhibiting P-gp activity with GF120918 can also enhances the accumulation of their substrates in the brain by at least 4-fold (Chapter 3). Together these studies suggest LPA and other similar molecules along with GF might provide an alternative method for enhancing the delivery of drugs to the brain and the tumor sites.

The present studies describe a series of experiments intended to provide proof-of-concept for the use of LPA to transiently modulate BBB for the purposes of enhancing drug delivery to the brain. To explore the potential utility of LPA modulation of BBB in a brain tumor

model, tumor bearing mice were examined at day 7 when the BBB is intact, and at day 12 when the BBB is compromised. Using both magnetic resonance imaging (MRI) and near infrared fluorescence (NIRF) contrast agents, the magnitude of BBB disruption produced by LPA exposure was determined in both the tumor region and non-tumor region to a variety of molecules with different physico-chemical properties. Furthermore, we also examine the response of tumor mice to paclitaxel under various conditions including with taxol alone, taxol with LPA, taxol with GF120918, or taxol with combination of both LPA and GF120918. The results indicate that LPA-induced increases in BBB permeability occur within minutes of administration at both day 7 and day 12 of tumor growth. Within non-tumor regions of the brain, treatment with LPA modulated BBB permeability to both small and large molecular weight contrast agents. Within the tumor region, the disruptive effect of LPA on BBB permeability was observed during the early stages of tumor growth. However, by day 12 of tumor growth, vascular permeability within the tumor region was already compromised and no further enhancement of BBB permeability within the tumor was observed. Furthermore, the presence of GF120918 do not have a significant impact on paracellular markers including Gad and IRdye800cw PEG, however, the presence of GF120918 significantly enhances the accumulation of R800 in the brain and the tumor region at both day 7 and day 12 post tumor implantation. The presence of LPA and GF120918 also extend the survival time frame of tumor mice treated with paclitaxel.

5.2. MATERIALS AND METHODS

5.2.1. Materials/Reagents:

Lysophosphadidic acid (LPA) was purchased from Sigma Chemical Company (Oakville, ON). The NIRF imaging agents, IRdye 800cw PEG and rhodamine 800 (R800), were obtained from Licor (Lincoln, NE) and Exciton (Dayton, OH), respectively. Gadolinium diethylenetriamine

pentaacetate (Gad) contrast agent used for MRI of BBB permeability was obtained from Berlex, Canada. Ketamine hydrochloride and xylazine were purchased from Wyeth (Guelph, ON) and Bayer Inc. (Toronto, ON) respectively. All other reagents and chemicals were purchased from Sigma Chemical Company (St. Louis, MO).

5.2.2. Tumor Model:

Female inbred Balb/c mice were used for the brain tumor model. Adult Balb/c mice were obtained from the University of Manitoba breeding colony and maintained in the Central Animal Care Facility under temperature-controlled environment with 12 hours dark/light cycle and unlimited access to food and water. Mice were anesthetized and placed in a stereotaxic apparatus (Kopf instruments) for intracerebral implantation of the 3LL tumor cells. A total of 5000 3LL cells were suspended in 7.5 µl of buffer and injected slowly over a 3-minute period into the right hemisphere at a depth of 4 mm, 2 mm posterior of the bregma and 1 mm lateral of the coronal suture using a 25 µl Hamilton syringe fitted with a 30½-gauge beveled needle. Mice were allowed to recover from anesthesia undisturbed before being returned to their respective cages. All animal experiments were approved by the University of Manitoba Animal Care Committee (protocol number 11-073).

5.2.3. LPA Response in Brain Tumor Mice:

The qualitative and quantitative determination of BBB permeability in the mouse brain tumor model following systemic administration of LPA and GF120918 was determined using three different imaging agents and magnetic resonance (MR) and near infrared fluorescence (NIRF) imaging modalities described below.

5.2.3.1. Magnetic Resonance Imaging of BBB Permeability in Metastatic Brain Tumor:

LPA-induced alterations in BBB permeability were assessed at day 7 and day 12 post tumor cell implantation using magnetic resonance imaging (MRI) with Gad contrast agent. Mice were anesthetized and secured in a Bruker Biospect MR (7 tesla/21 cm) spectrometer with 2.5 x 2.5 cm^2 field of view. A series of T2-weighted images were obtained (Rare factor = 8, Echo Time = 20 ms, Effective Echo Time = 80 ms, Repetition Time = 1640 ms, Averages = 12, Total Image Time = 10.50 min) to identify tumor regions within the brain. In addition, T1-weighted images (Rare factor = 8, Echo Time = 11.56 ms, Effective Echo Time = 11.56 ms, Repetition Time = 852 ms, Averages = 6, Total Image Time = 2.40 min) of the brain were acquired prior to administration of Gad contrast agent to obtain the background images of the brain. To determine the effect of LPA induced BBB disruption in the tumor bearing mice, Gad contrast agent (0.4 mmol/kg) together with either vehicle (0.25mg/ml BSA in PBS), LPA (1mg/kg) or combination of LPA (1mg/kg) and GF120918 (9mg/kg) was administered via tail vein. A series of T1-weighted images were obtained immediately following Gad injection at 3-minute intervals throughout a 21-minute imaging session. Regions of interest within the T1-weighted images were captured using Marevisi 3.5 software (Institute for Biodiagnostics, National Research Council, Canada). The intensity of Gad contrast agent within specific regions of interest were quantitatively assessed by obtaining the percent difference images according to the following formula using Paravision 3.0 software:

((Post-Gad T1-weighted images – Pre-Gad T1-weighted images) / Pre-Gad T1-weighted images) x 100.

5.2.3.2. Near Infrared Fluorescence Imaging of BBB Permeability in Tumor Mice: The

LPA-induced changes in BBB permeability of large molecular weight compounds as well as P-gp sensitive agents was also examined in tumor mice at day 7 and day 12 post tumor implantation using NIRF. For these studies, both pegylated IRdye800cw and Rhodamine800 (R800) were used as NIRF probes. As previously described, IRdye800cw PEG is a pegylated molecule with molecular weight of 25kDa used to monitor vascular leakage (Sampath et al. 2007, 1501-1510). R800 is a recently established NIRF dye with P-gp substrate properties (On et al. 2011). The NIRF probes were administered with either vehicle solution (0.25mg/ml BSA in PBS), LPA (1 mg/kg), GF120918 (9 mg/kg) or the combination of GF120918 (9 mg/kg) and LPA (1 mg/kg) via tail vein injection. Mice were sacrificed at 20 minutes following treatment via cardiac perfusion with 10% formaldehyde solution. The brain and other tissues were removed and the accumulation of NIRF dyes examined ex vivo using an Odyssey near infrared imaging system. Quantitative assessment of fluorescence was performed on regions of interest (ROI) in 2 mm thick tissue slices and normalized to fluorescence from blood samples taken at the time of tissue collection. Resulting values are presented as the brain to blood ratio of NIRF activity.

5.2.4. Response of Tumor Mice to Paclitaxel:

Tumor mice were induced as previous described in section 5.2.2. Mice were randomly assigned to different treatment groups which consists control (no taxol), taxol (4mg/kg) alone, taxol (4mg/kg) with LPA (1mg/kg), taxol (4mg/kg) with GF120918 (9mg/kg) or taxol (4mg/kg) with both LPA (1mg/kg) and GF120918 (9mg/kg). Treatment commenced at day 7 post tumor injection and continued every other 4 days until the mice meet the criteria for sacrifice, which included a 25% weight lost, hunchback posture, and a lost of movement.

5.3. RESULTS

5.3.1. Tumor Progression:

All mice injected with 3LL cells developed brain tumors with weight loss (< 10% body weight) being the earliest outward sign of tumor burden typically occurring within 10 days post-innoculation. This was followed by a period of 1 - 4 days of further weight loss, and diminished locomotor activity. As shown in Figure 5.1, the developing tumor is confined to the right hemisphere of the brain and is predominantly located within the midbrain region. Assessment of tumor volume indicated roughly 2.0 mm^3 and 30 mm^3 for day 7 and day 12 tumor mice, respectively, in both control and LPA animals (Figure 5.2).

A.

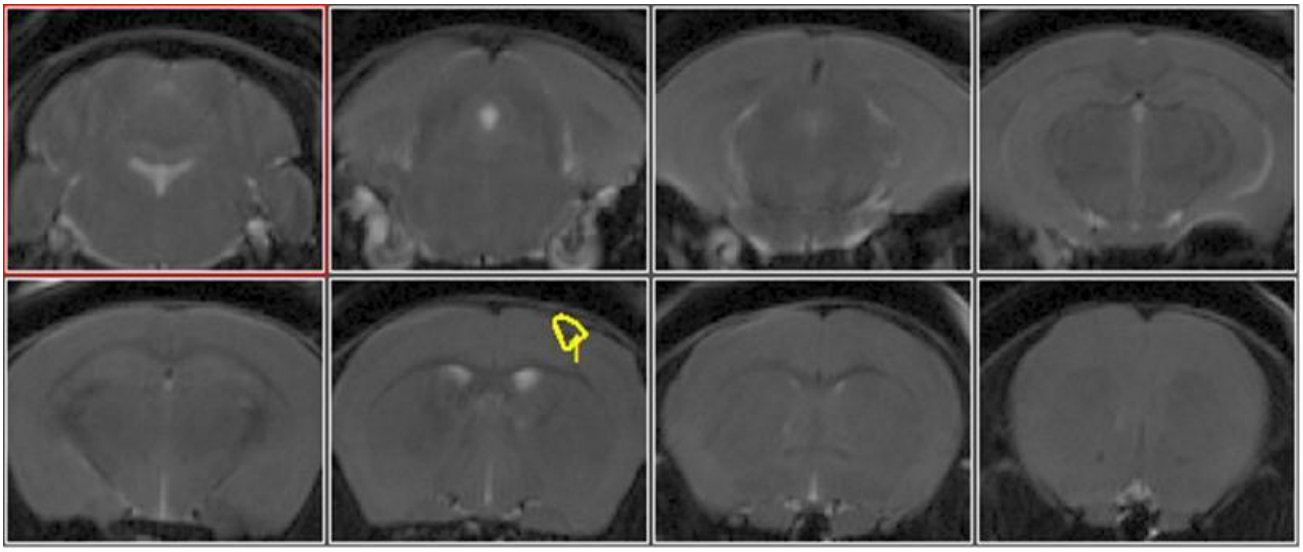

B.

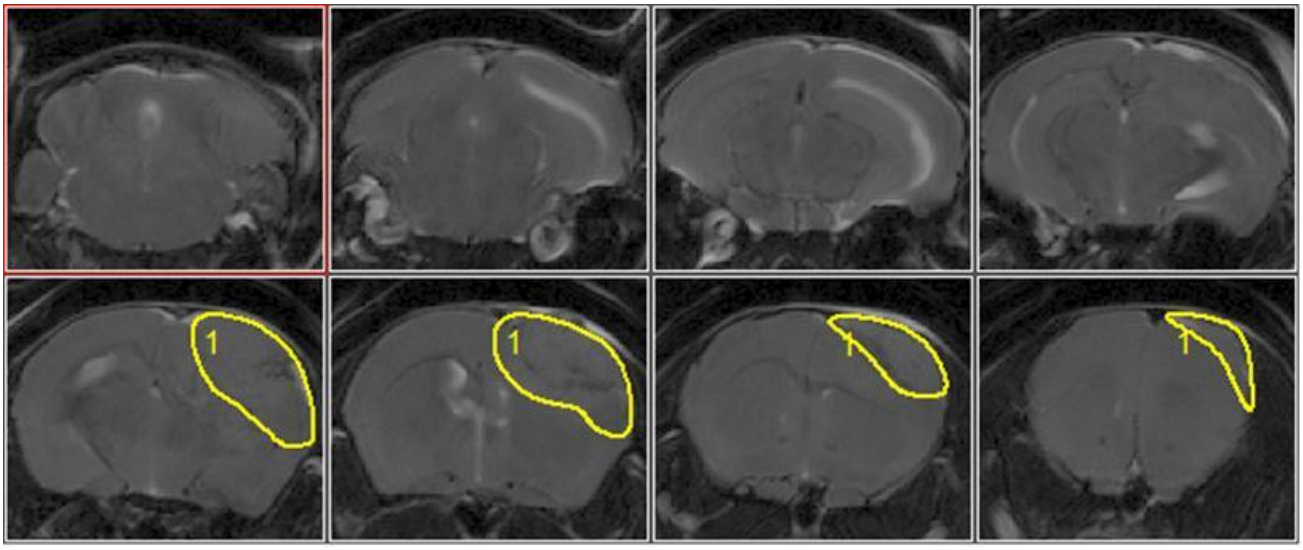

Figure 5.1: Series of T2-weighted images of mouse brain at (A) day 7 and (B) day 12 post tumor implantation. The images were taken from the posterior to anterior region of the brain. The tumor region is outlined in yellow.

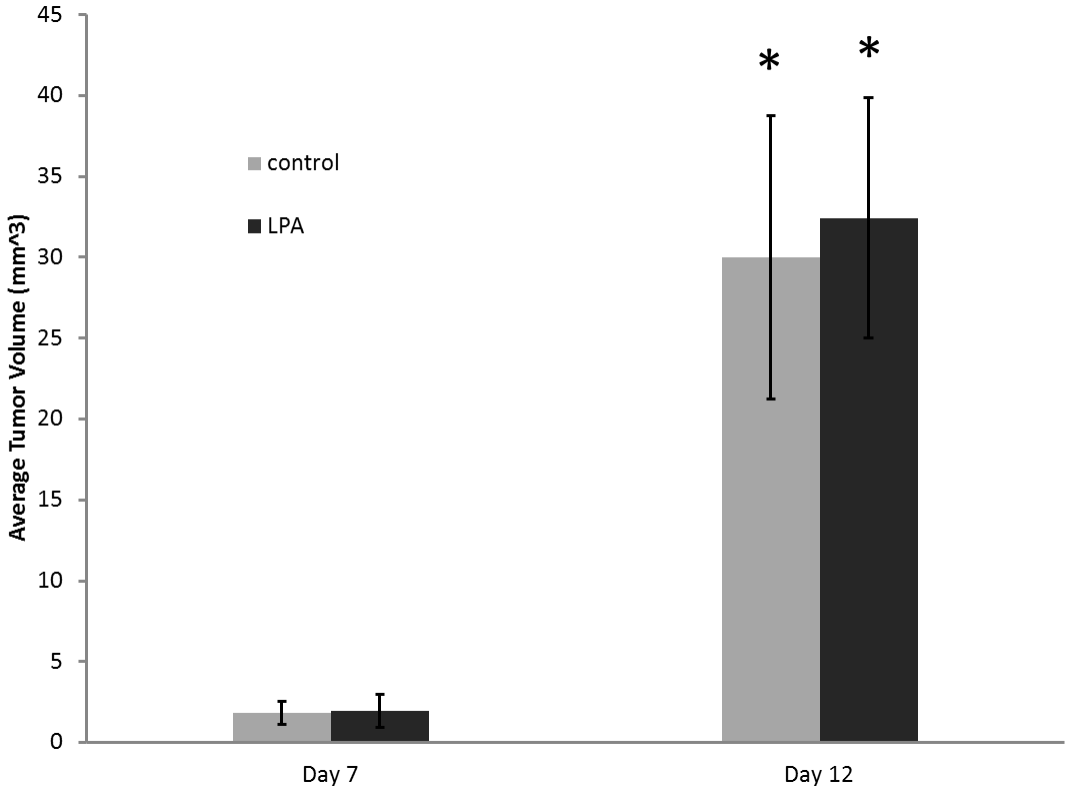

Figure 5.2: Tumor volume on day 7 and 12 post 3-LL tumor cell injection in control and LPA-treated mice. * p <0.05 compared to day 7 tumor mice within the same treatment group. The data is represented as mean ± sem, n=3 for each time point.

5.3.2. Effects of LPA and GF120918 on Brain Tumor Mice:

5.3.2.1. BBB Permeability in Tumor Mice Following LPA Exposure: Alterations in BBB permeability were examined in tumor-bearing mice using Gad contrast enhancement MRI. For these studies, accumulation of Gad contrast agent in the brain was examined at various time points in mice under control conditions and following treatment with either LPA or LPA with GF120918 (Figure 5.3). Quantitative analysis of Gad penetration revealed significant brain enhancement in tumor mice receiving either LPA or LPA with GF120918 compared to vehicle treated controls (Figure 5.4, 5.5). The magnitude of Gad enhancement in mice receiving LPA varied depending on brain region with as much as 15 and 19 fold enhancement observed at day

7 and day 12 post tumor cell implantation, respectively (Figure 5.4, 5.5). As tumors were confined to the mid-brain region, a more detailed examination of Gad enhancement was performed on the mid-brain sections to assess changes in tumor and non-tumor regions of the brain. At early stages of tumor development (i.e. 7 day post tumor cell implantation), the BBB was largely intact in both the tumor and non-tumor regions of the brain. This was evident by the similar Gad enhancement in the brain slices at time 0 (prior to the injection of vehicle solution) and time 6 (6 minutes after vehicle injection) (Figure 5.6A). Similarly, BBB integrity in non-tumor regions was unaffected in the later stages of tumor development (i.e. 12 day post tumor cell implantation). However, there was significant Gad enhancement within the tumor site in 12 day tumor mice (Figure 5.6B). Treatment of mice with LPA, either alone or in combination with GF120918, resulted in significant increases in BBB permeability to Gad contrast agent in both tumor and non-tumor regions at the early stage of tumor development (Figure 5.6). In contrast, in the later stages of tumor development, while LPA treatment resulted in significant Gad enhancement in non-tumor regions, there was no significant enhancement over vehicle treatment within the tumor region (Figure 5.6B).

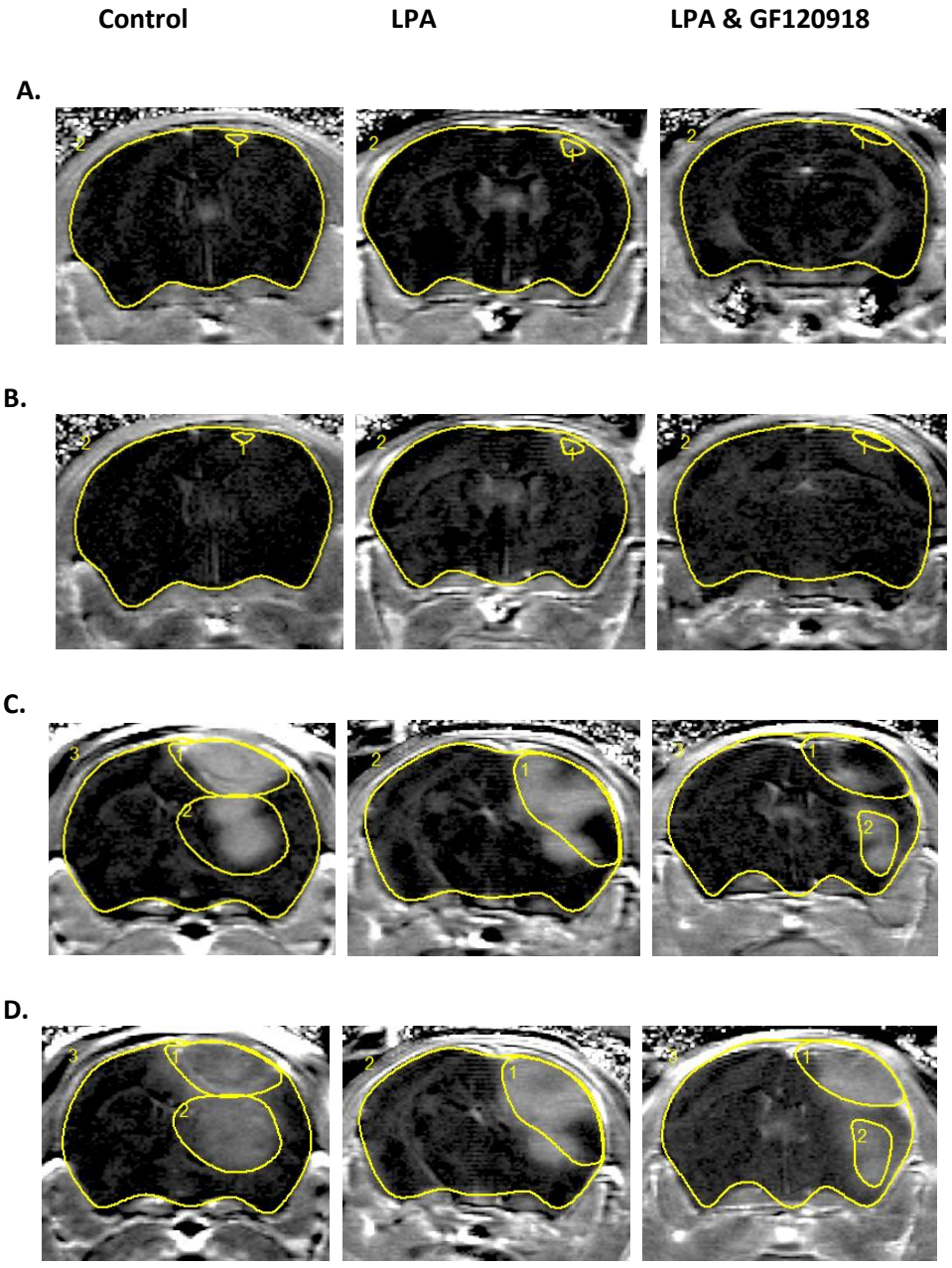

Figure 5.3: Representative of % Gad enhancement MR images of mouse following an injection of vehicle solution (control), LPA, and LPA with GF120918 at time 0 (A and C) and 6 minutes (B and D) during day 7 (A and B) and day 12 post tumor implantation (C and D). #1 and #2 indicate the tumor region, and #3 indicates brain region.

A.

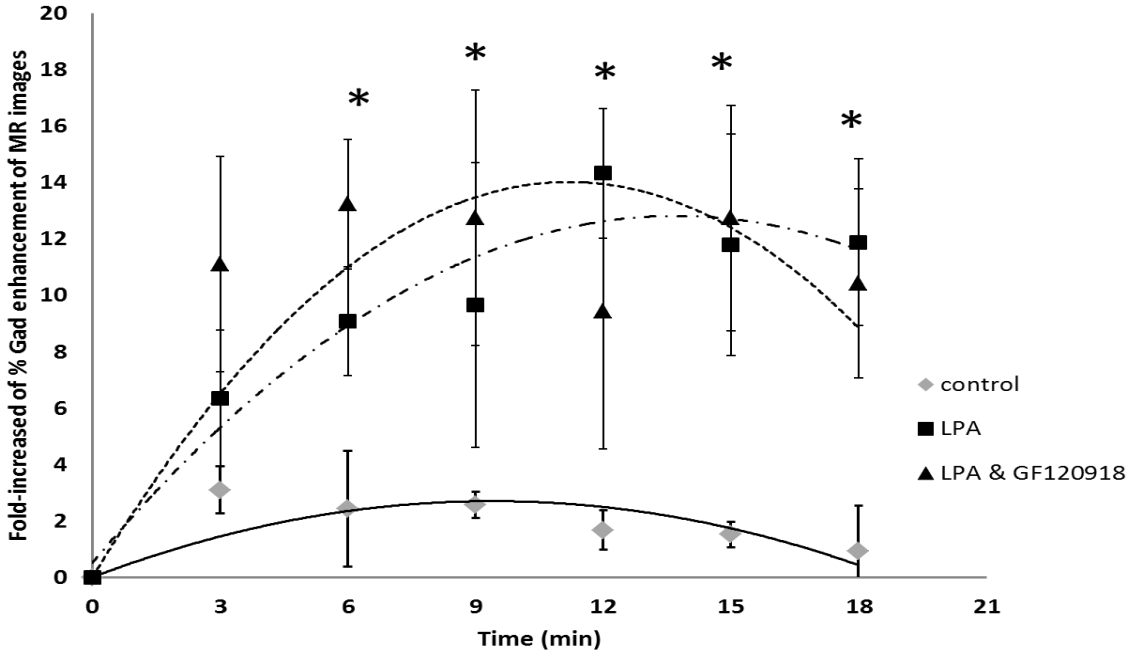
Fold-increased of % Gad enhancement of MR images
Time (min)
control
LPA
LPA & GF120918

B.

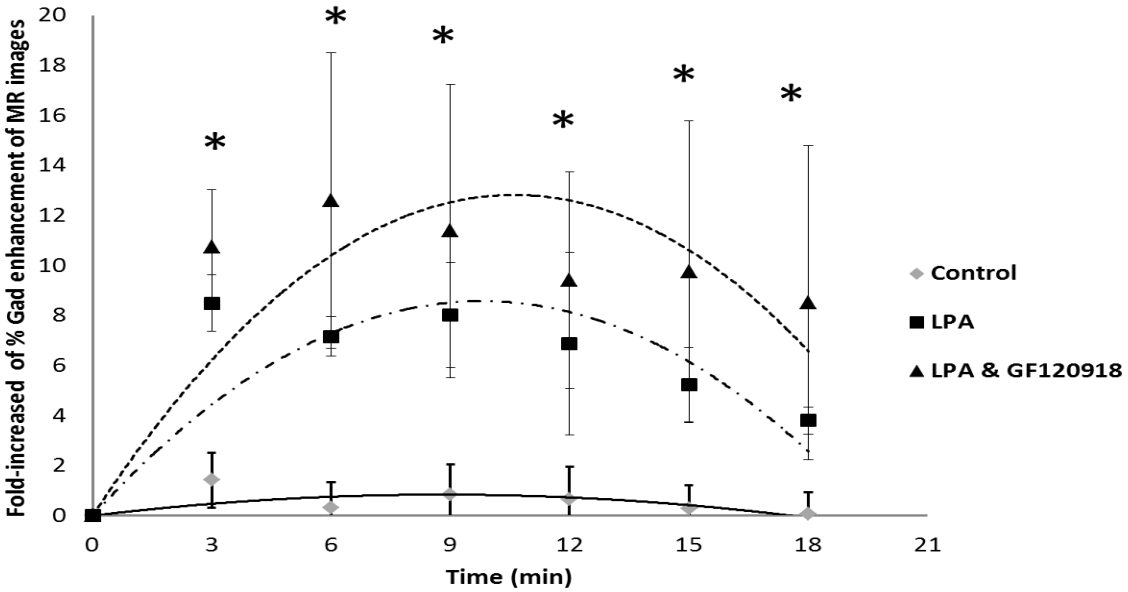
Fold-increased of % Gad enhancement of MR images
Time (min)
Control
LPA
LPA & GF120918

C.

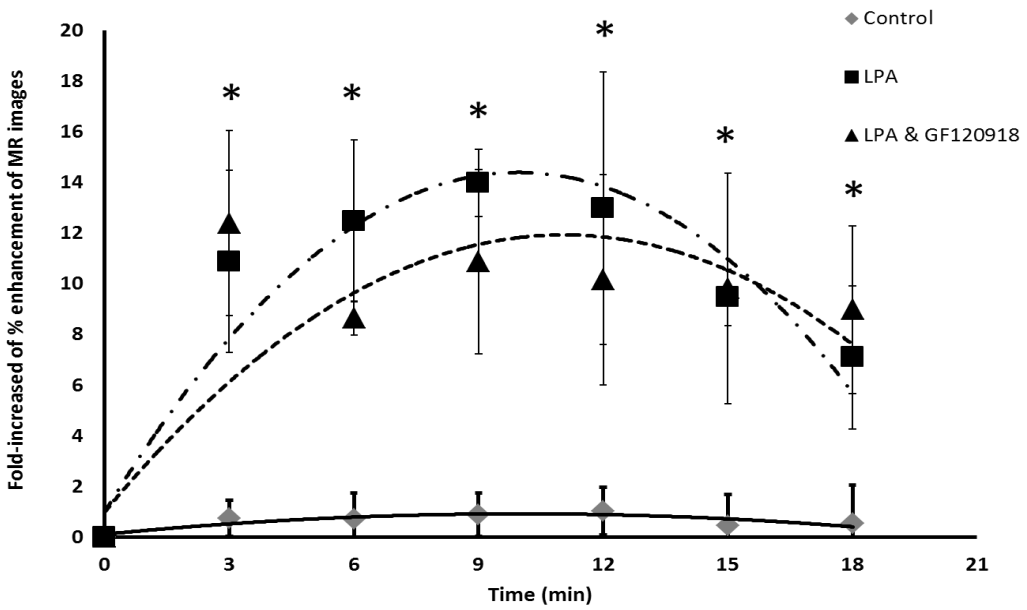

Figure 5.4: Quantitative analysis of % enhancement of MR images following Gad injection in tumor brain images at day 7 post tumor implantation in (A) posterior brain images, (B) midbrain images, and (C) anterior brain images in control, LPA-treated, and LPA with GF120918 treated mice. ANOVE was conducted to determined statistical difference between the treatment groups in their respective time. * $p < 0.05$ compared to control mice at the same time point for both LPA and LPA with GF120918 groups. Values represent the mean ± sem for 5 mice per treatment group.

A.

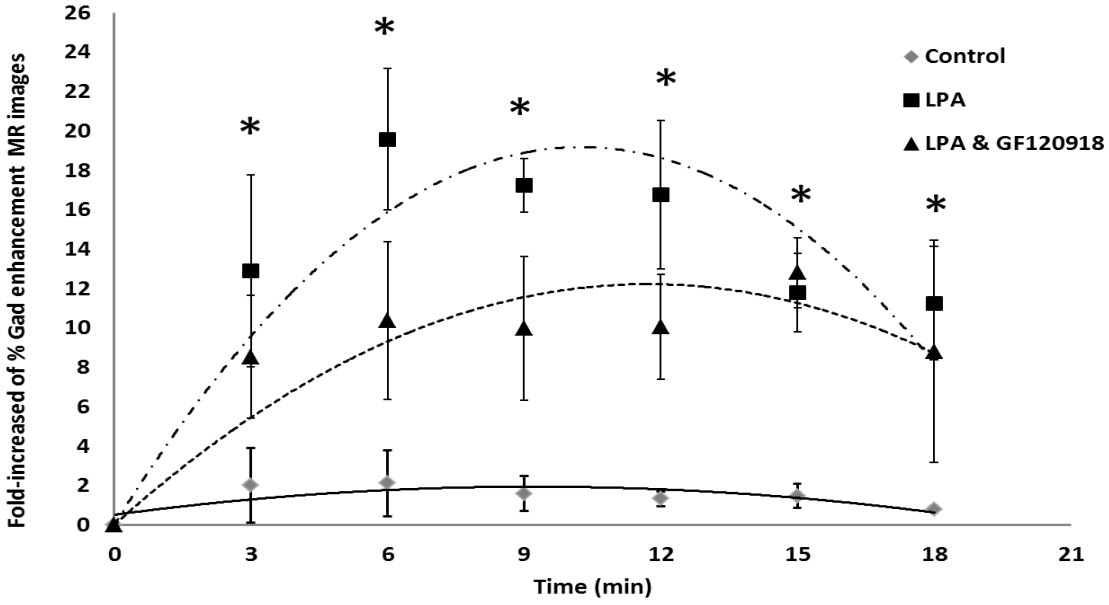
Fold-increased of % Gad enhancement MR images
Time (min)
Control
LPA
LPA & GF120918
0
2
4
6
8
10
12
14
16
18
20
22
24
26
0
3
6
9
12
15
18
21
*

B.

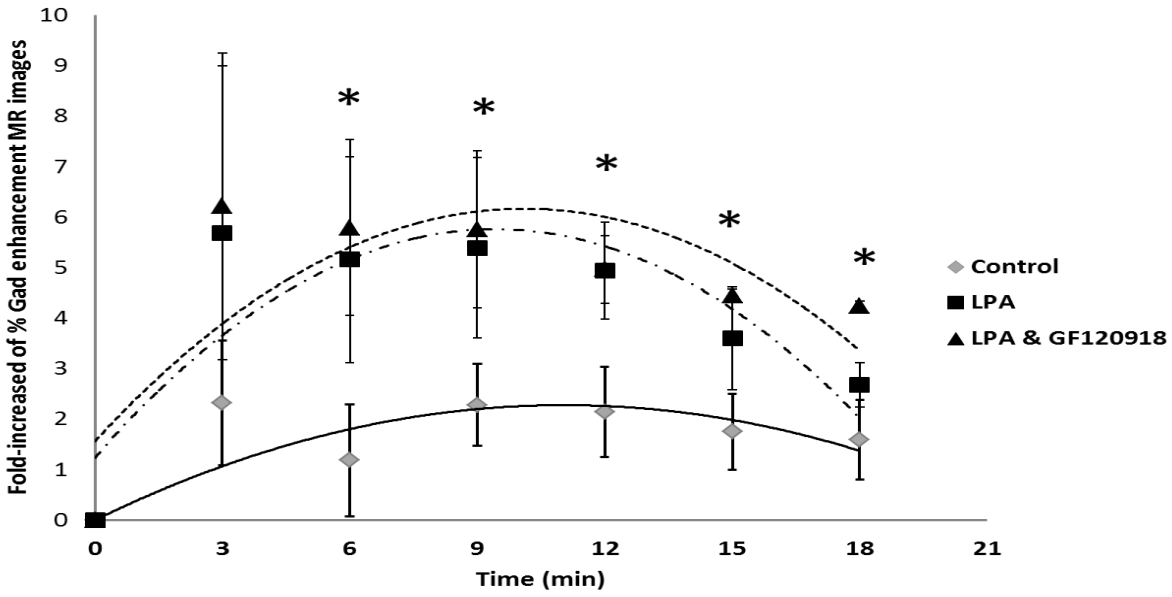
Fold-increased of % Gad enhancement MR images
Time (min)
Control
LPA
LPA & GF120918
0
1
2
3
4
5
6
7
8
9
10
0
3
6
9
12
15
18
21
*

C.

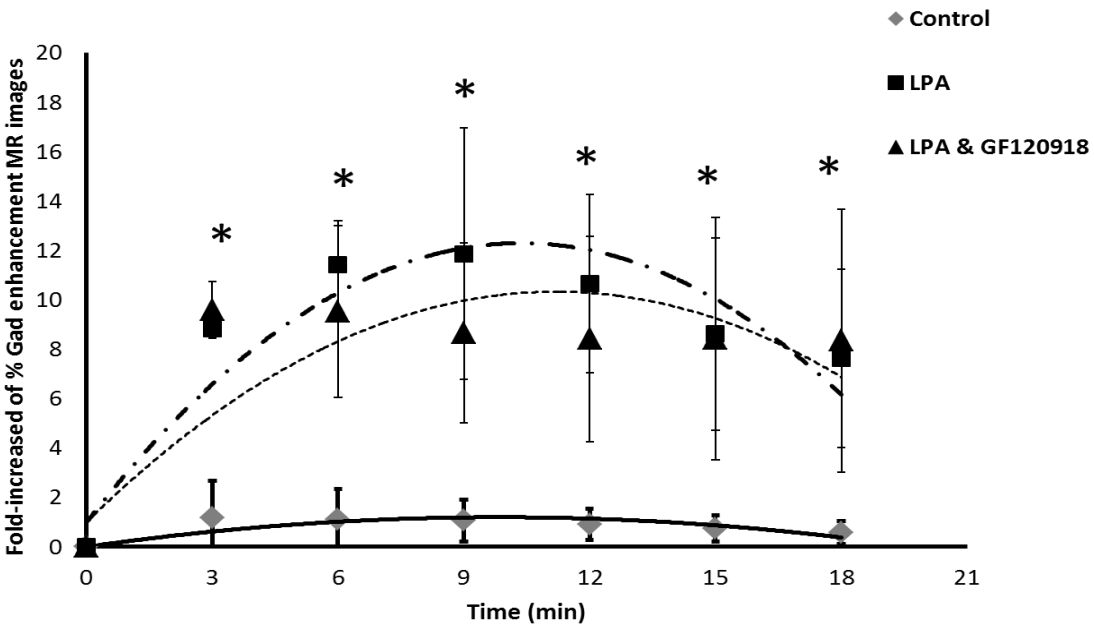

Figure 5.5: Quantitative analysis of % enhancement of MR images following Gad injection in tumor brain images at day at day 12 post tumor implantation in (A) posterior brain region, (B) midbrain region, and (C) anterior brain region in control, LPA-treated, and LPA with GF120918 treated mice. ANOVE was conducted to determined statistical difference between the treatment groups in their respective time. * $p < 0.05$ compared to control mice at the same time point for both LPA and LPA with GF120918 groups. Values represent the mean ± sem for 5 mice per treatment group.

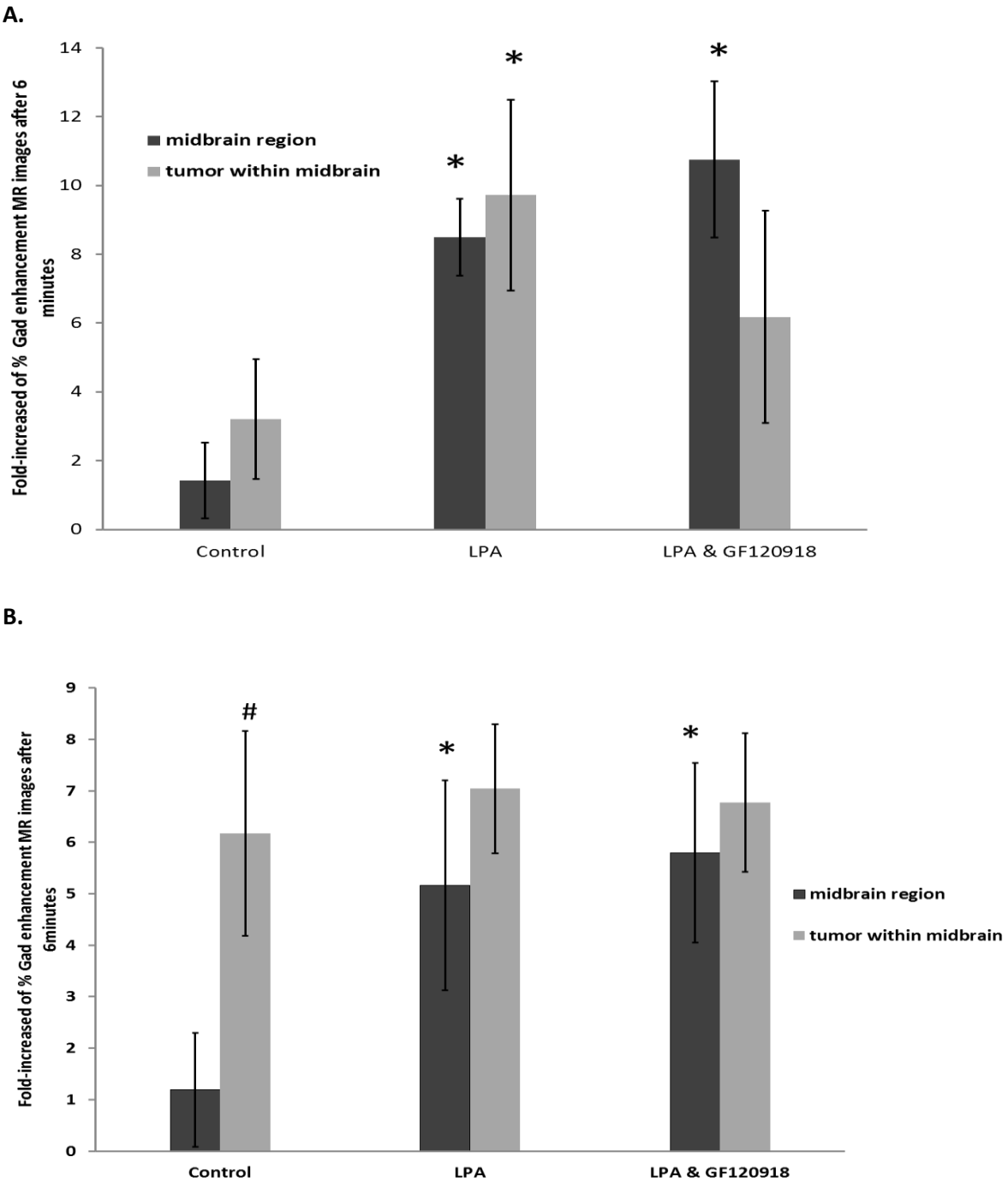

Figure 5.6: Quantitative analysis of % enhancement of MR images after 6 minutes of Gad injection in tumor brain images at (A) day 7 and (B) day 12 post tumor implantation. 2-way ANOVA was conducted to determine statistical significance between treatment groups and within different regions. * $p < 0.05$ compared to control mice within the same region. # $p < 0.05$ compared to non-tumor region within the same animal.

5.3.2.2. Near Infrared Fluorescence Imaging of BBB Permeability in Tumor Mice: The effects of LPA and GF120918 on the permeability of both a large macromolecule as well as a molecule with P-gp activity were examined at different stages of brain tumor development using pegylated IRdye800cw and R800 respectively. In day 7 tumor mice receiving no LPA or GF120918, there was little penetration of either R800 or pegylated IRdye800cw in brain tissue (Figure 5.7A and 5.7B respectively). By day 12 of tumor development, the impairment of the BBB was evident by the appearance of the pegylated IRdye800cw in the tumor region of the control mice as shown in Figure 5.8B. However, the permeability of R800 in the vehicle injected mice was minimal at both day 7 and day 12 post tumor implantation (Figure 5.7A and 5.8A respectively). The LPA injected mice had a higher amount of pegylated IRdye800cw accumulation compared to control mice at both day 7 and day 12 (Figure 5.7B and 5.8B. In contrast, the administration of LPA alone had no effect on R800 brain accumulation in tumor and non-tumor sites during the early stages of tumor growth (Figure 5.7A). However, accumulation of R800 in both tumor and non-tumor sites following treatment with LPA was enhanced during the late stage of tumor development (Day 12) (Figure 5.8A). Furthermore, the presenceof GF120918 had no effect on the paracellular diffusion of IRdye800cw PEG at both day 7 and day 12 post tumor implantation, but it enhanced the accumulation of R800 in tumor and non-tumore region of the brain at both day 7 and day 12 post tumor injection. Quantitative analysis of the dye revealed significant enhancement of IRdye 800cw accumulation following administration of either LPA or LPA and GF120918 at day 7 (Figure 5.9A) and day 12 (Figure 5.9B) of tumor injection, but the administration of GF120918 had no affect on the permeability of IRdye800cw PEG. Furthermore, the integrity of the BBB was severely disrupted by day 12 of tumor implantation resulting in significant enhancement of the dye in the tumor region

compared to non-tumor region, even for the vehicle treated mice (Figure 5.9B). Quantitative analysis of the P-gp probe, R800, within the brain revealed significant enhancement of the dye accumulation only in those mice receiving either GF120918 or LPA in combination with GF120918 (Figure 5.10A). Administration of LPA alone at 7 days post tumor cell implantation had no significant effect on the accumulation of R800 in either tumor or non-tumor regions (Figure 5.10A). However, by day 12 of tumor growth, LPA exposure either alone or in combination with GF120918 resulted in a significant increase in R800 accumulation in both tumor and non-tumor regions of the mouse brain (Figure 5.10B).

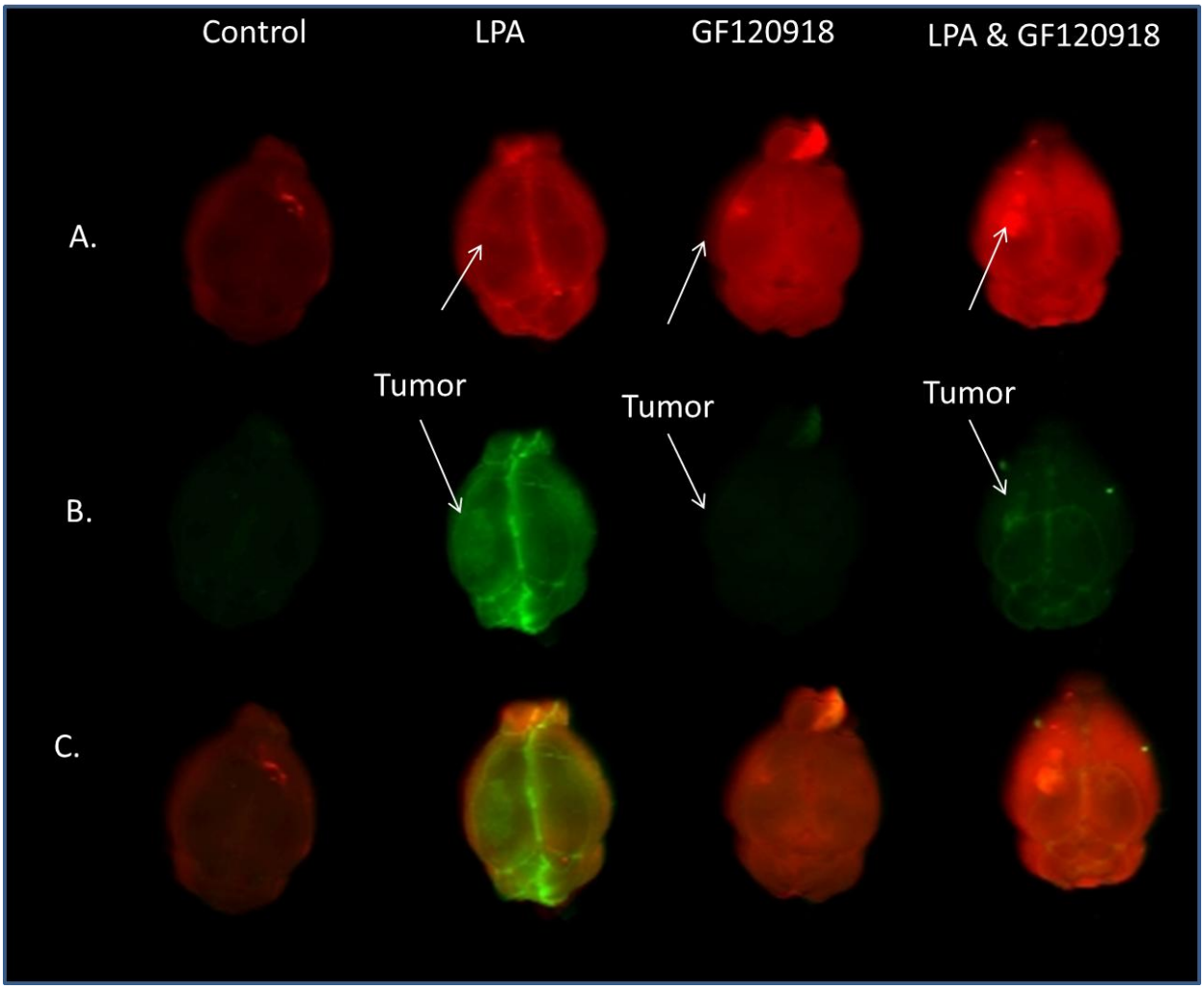

Figure 5.7: The accumulation of (A) R800, (B) IRdye800cw PEG and (C) combination of both in tumor mice at day 7 post tumor implantation obtained using the Odyssey Near Infrared Imaging at focus offsets 3 (FO3) for control mouse (vehicle injected), LPA treated mouse, GF120918 treated mouse and LPA with GF120918 mouse with a representative of n = 5 in each treatment group.

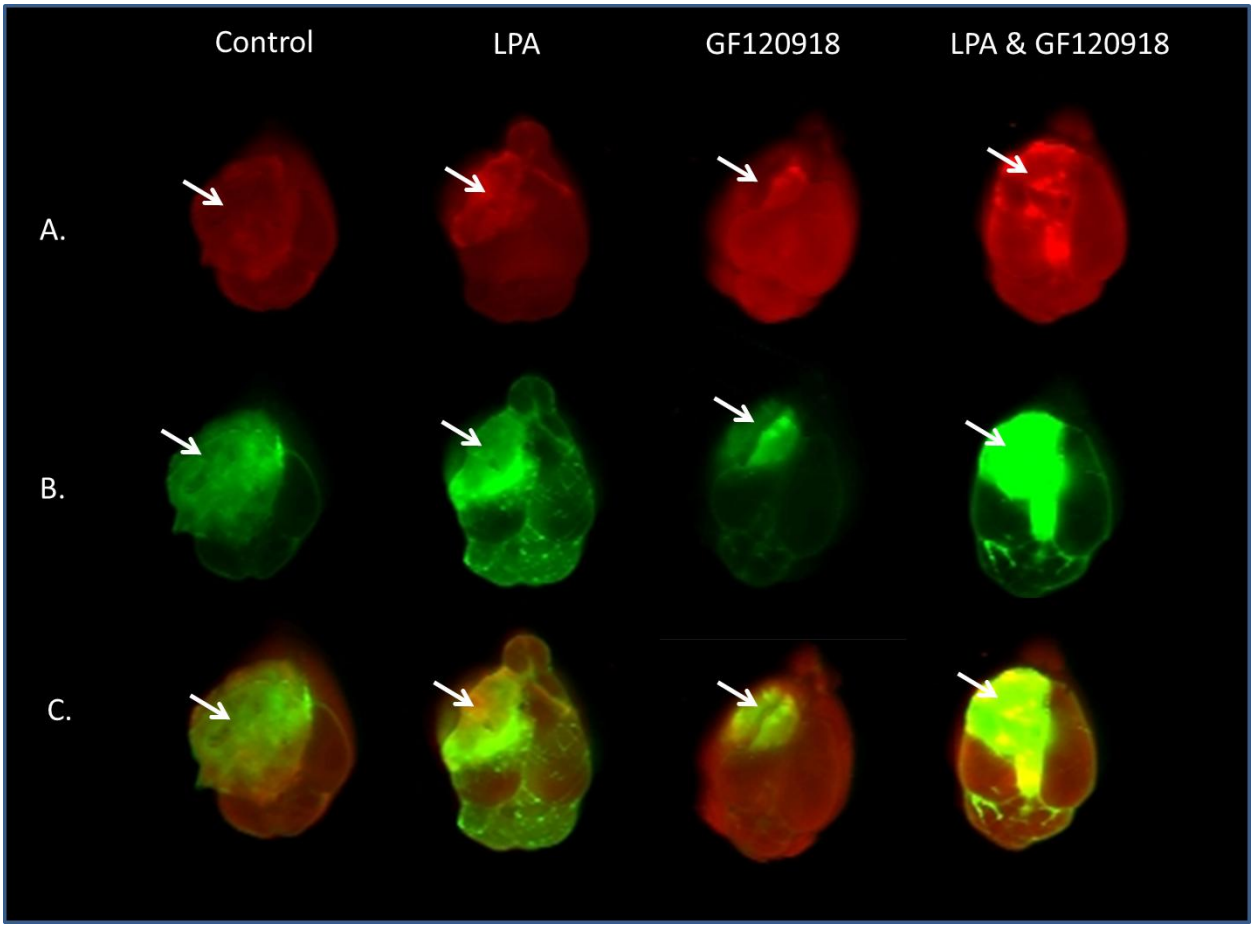

Figure 5.8: The accumulation of (A) R800, (B) IRdye800cw PEG and (C) combination of both in tumor mice at day 12 post tumor implantation obtained using the Odyssey Near Infrared Imaging at focus offsets 3 (FO3) for control mouse (vehicle injected), LPA treated mouse, GF120918 treated mouse and LPA with GF120918 mouse with a representative of n = 5 in each treatment group.

A.

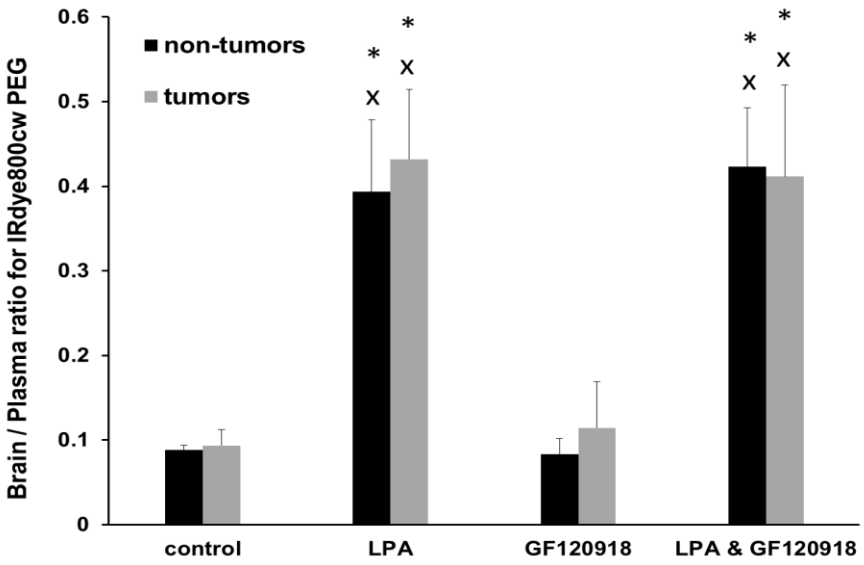

B.

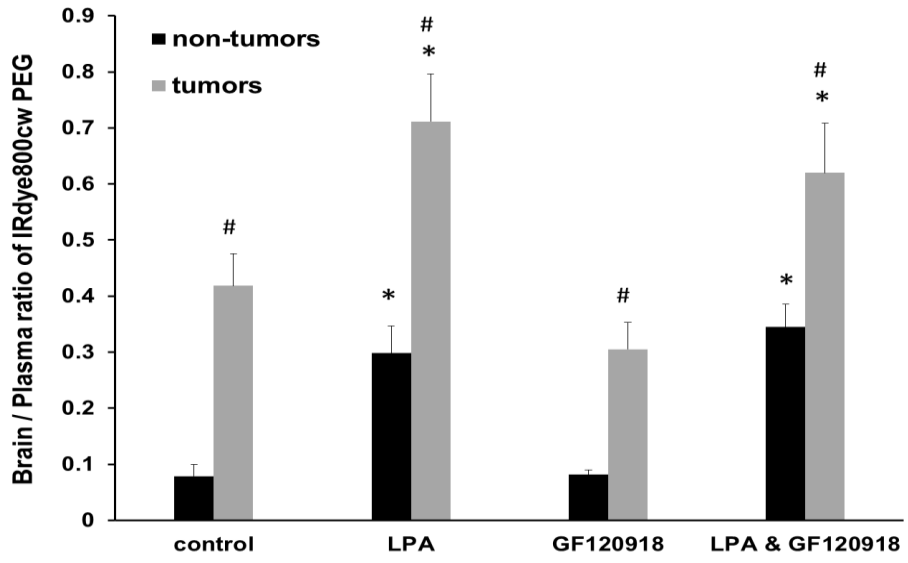

Figure 5.9: Quantification of IRdye800cw PEG in the tumor and non-tumor regions of mice under various treatments at (A) day 7 and (B) day 12 post tumor implantation. 2-way ANOVA was conducted to determine statistical significance between treatment groups and within different brain regions * $p < 0.05$ compared to control mice within the same region. x $p<0.05$ compared to GF120918 treated mice within the same region. # $p<0.05$ compared to non-tumor region within the same animal. The data is represented as mean ± sem with n = 5 each treatment group.

A.

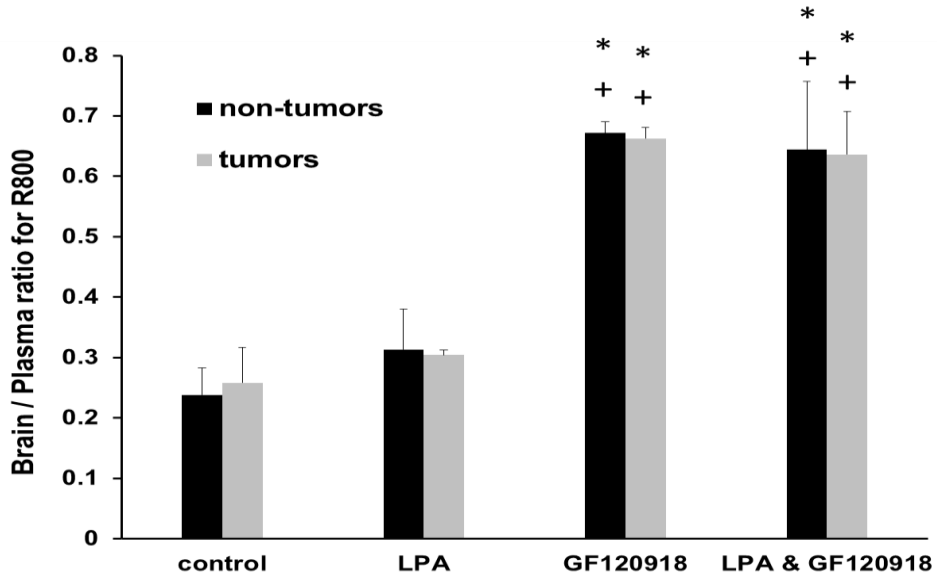

B.

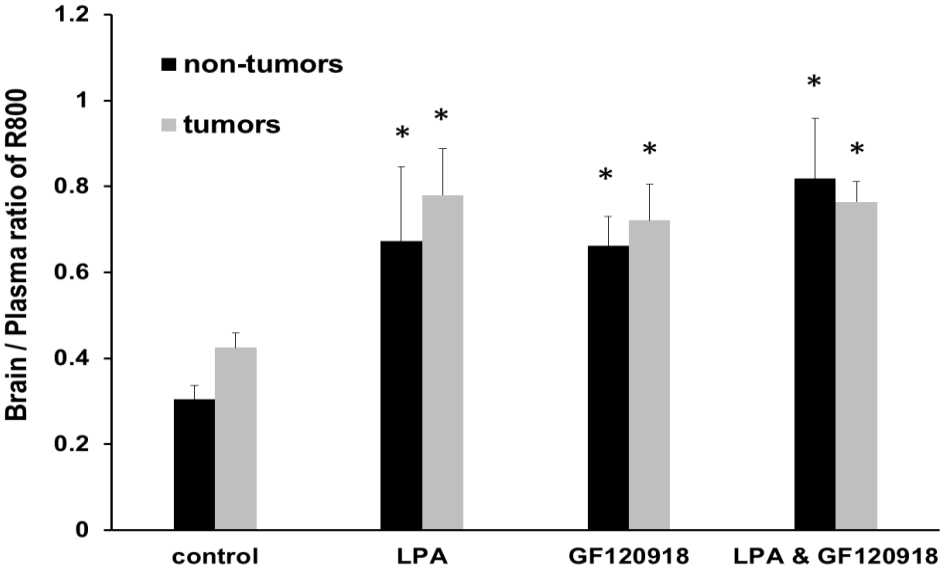

Figure 5.10: Quantification of R800 in the tumor and non-tumor regions of mice under various treatments at (A) day 7 and (B) day 12 post tumor implantation. 2-way ANOVA was conducted to determine statistical significance between treatment groups and within different brain regions * $p < 0.05$ compared to control mice within the same region. + $p < 0.05$ compared to LPA-treated mice within the same region. The data is represented as mean ± sem with n = 5 for each treatment group.

5.3.3. Response of brain tumor mice to paclitaxel:

The response of brain tumor mice to a chemotherapeutic agent (paclitaxel) was examined under the conditions with LPA, GF120918 or combination of both LPA and GF120918. All mice injected with 3LL cells developed brain tumors as previously described in chapter 2. Treament began at the initial stages of tumor development (day 7) when the tumor size is small and the BBB is still intact and continued every 4 days until the mice meet the end point criteria for sacrifice. Based survival curve shown Figure 5.11, under either control or taxol treated conditions alone; the median survival time frame of tumor mice was 15 days with no mice survived past day 16 post injection. Administration of either LPA or GF120918 in combination of taxol significant enhances the survival time of tumor mice up to 21 days; furthermore, the combination of both GF120918 and LPA together with taxol can further extend the survival time frame of tumor mice to 25 days before they meet the sacrificing criteria.

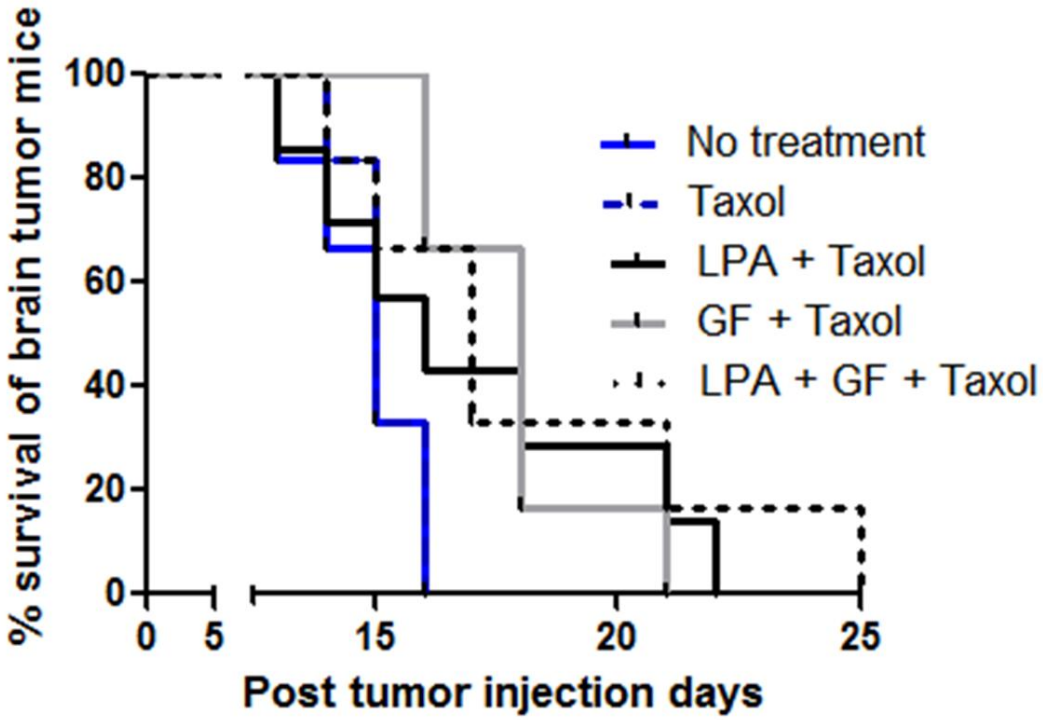

Figure 5.11: The response of tumor mice to taxol in the presence of LPA, GF120918, or combination of both LPA and GF120918 with n = 8 per each treatment group.

5.4. DISCUSSION

The discovery and development of new pharmacological therapies to treat CNS disorders remains one of the most challenging aspects in the drug industry. Despite aggressive efforts, many new compounds targeting the CNS are not effective in achieving a safe and efficacious dose in the brain (Stewart 1994, 121-139; Reichel 2009, 2030-2049). The approval rate for drugs to treat CNS disorders including stroke, Alzheimer's disease, multiple sclerosis, and brain tumors is low compared to other therapeutic classes (Stewart 1994, 121-139). Part of the reason for the failure of CNS agents can be attributed to the complexity of CNS disorders and the insufficient knowledge of the underlying pathophysiology of CNS diseases. However, an often under-appreciated problem in CNS drug development is drug permeability across

protective barriers such as the blood-brain barrier (BBB) and the blood-CSF barrier (BCSFB). Given the complexities of CNS disorders and the increasing interest in macromolecule therapies, issues of drug penetration across the BBB and BCSFB will continue to dominate.

While often considered a static barrier, alterations in BBB permeability are involved in various physiological and pathophysiological responses. Several endogenous hormones including maternal glucocorticoid (Sadowska, Malaeb, and Stonestreet 2010, H179-88) and cytokines such as tumor necrosis factor and interleukin-1β (Trickler, Mayhan, and Miller 2005, 24-31; McColl, Rothwell, and Allan 2008, 9451-9462) have been shown to cause increases in BBB permeability. In addition, disruption of the BBB has also been observed in several pathological conditions including hypertension, hypoxia, and ischemia (Bidros and Vogelbaum 2009, 539-546). Thus, one method that has been explored to enhance drug delivery to the brain involves the reversible disruption of the BBB. The challenge of this approach from a drug delivery standpoint has been to control the magnitude and duration of BBB disruption while minimizing side effects. In this regard, osmotic disruption of the BBB has been the most extensively studied approach. The method involves infusion of a hyperosmotic agent such as mannitol that causes fluid to diffuse rapidly out of the cells resulting in shrinkage of endothelium and subsequently disruption of the anatomical tight junctions of the BBB (Bidros and Vogelbaum 2009, 539-546). Animal studies demonstrate that the administration of high dose mannitol along with chemotherapeutic agents including carboplatin and etoposide significantly enhance drug delivery to the brain (Williams et al. 1995, 17-27; discussion 27-8). However, when this technique was applied to human patients with either primary or metastatic brain tumors, the results were disappointing (Kemper et al. 2004, 415-423). This is partly due to issues related to intracranial pressure caused by tumor burden, and the further exacerbation of this by the

infusion of large amounts of mannitol (Williams et al. 1995, 17-27; discussion 27-8). Furthermore, the long recovery period associated with hyperosmotic disruption can cause an influx of pathogens and proteins into the brain tissues causing major side effects including seizures, neuropathological changes and neurotoxicity (Kemper et al. 2004, 415-423; Williams et al. 1995, 17-27; discussion 27-8; Neuwelt et al. 1983, 5278-5285).

Another alternative to osmotic disruption of the BBB is the use of inflammatory mediators including leukotrienes, histamine, and bradykinin to enhance the vascular permeability in brain tumors. It has been observed that these compounds stimulate receptors that are present at the BBB to initiate second messenger systems, resulting in the disruption of tight junctions (Kemper et al. 2004, 415-423). In contrast to osmotic opening, receptor-mediated disruption is shorter in duration, lasting approximately 20 minutes. Furthermore, animal studies using Cereport^{TM} (bradykinin analogue) resulted in a significant increase of carboplatin in rat brain tissue by 30-80% (Elliott et al. 1996, 3998-4005). Similarly, significant responses were achieved compared to control group when carboplatin was administered in combination with Cereport^{TM} in the RG2 rat glioma model (Inamura et al. 1994, 752-758). However, phase II clinical trials with glioma patients reported no significant improvement in response when chemotherapy was given with Cereport^{TM} (Ford et al. 1998, 1807-1811). These negative results were attributed to the differences in the tumor characteristics between the animal glioma model and human glioma (Kemper et al. 2004, 415-423). In this regard it was suggested that the blood-tumor barrier (BTB) in the rodent was more leaky and did not sufficiently model the BTB characteristics in human patients (Kemper et al. 2004, 415-423).

Given the limitations with both the osmotic and bradykinin receptor-mediated BBB disruption, the present study explored the use of the phospholipid, LPA, to transiently enhance

BBB permeability in a mouse brain tumor model. These proof-of-principle studies were based on previous work demonstrating LPA-induced enhancement of permeability in brain microvessel endothelial cells using both *in vitro* cell culture models ((Schulze et al. 1997, 991-1000; Nitz et al. 2003, 30-40; Tigyi et al. 1995, H2048-55; Wojciak-Stothard, Tsang, and Haworth 2005, L749-60; van Nieuw Amerongen, Vermeer, and van Hinsbergh 2000, E127-33) and *in vivo* preparations (Chapter 4). In regards to the *in vivo* studies demonstrating LPA-mediated disruption of the BBB, there were three primary observations of particular importance. One was the rapidity of onset of BBB disruption in response to systemic administration of LPA. Second was the relatively short period required for restoration of BBB integrity following LPA exposure in the mouse (Chapter 4). Third was the scope of the effects of LPA on the cerebral microvasculature with significant disruption of BBB permeability occurring for both small molecule (Gad contrast agent) and large molecule (pegylated IRdye800) permeability markers throughout all regions of the brain examined. These same basic characteristics regarding LPA-mediated disruption of BBB permeability were also found in the present study using a murine brain tumor model. Based on Gad contrast enhanced MRI of BBB integrity, significant increases in cerebral vascular permeability were observed within 3-6 minutes of LPA administration with maximal response being achieved within 10-15 minutes. Furthermore, BBB integrity was restored within 20 minutes following the injection of LPA in tumor bearing mice.

An additional finding of importance for LPA-mediated modulation of BBB for chemotherapeutic applications is the observation that BBB permeability was enhanced in both the tumor and the non-tumor regions of the brain. The ability to alter drug distribution to both the tumor and non-tumor regions of the brain is critical to achieve optimal chemotherapeutic response. The spatial heterogeneity of BBB permeability associated with brain tumors

establishes a concentration gradient of drugs. The higher drug concentration in the tumor than the surrounding brain tissue will result in rapid equilibration into normal brain tissues resulting in subtherapeutic concentrations of drugs at the tumor sites (the sink effect) (Robinson and Rapoport 1990, 153-161). Uniformly disrupting the BBB will provide a higher and more uniform delivery of drugs to the whole CNS, thereby, decreasing the rate at which drugs diffuse away from the tumor, resulting in prolonged tumor exposure to a higher concentration of drug (Kemper et al. 2004, 415-423). As seen in the present study, the increased permeability in the non-tumor regions of the brain was observed for the early stages as well as the later stages of tumor growth. This is important in light of the fact that BBB integrity is mostly intact when the tumor burden is small and most responsive to therapeutic interventions (Zhang et al. 1992, 1115-1124). An intact BBB would be a formidable obstacle for the entry of chemotherapeutic substances to the brain and the tumor sites. The current studies support the potential use of LPA as part of the treatment regiment to achieve greater accumulation of chemotherapeutic agents in tumor and non-tumor sites within the brain, thus, enhancing the treatment response.

The failure of chemotherapeutic agents in treating brain tumors is due in part to the poor BBB permeability of most anticancer agents (Stewart 1994, 121-139). In the case of hydrophilic drugs, paracellular diffusion is limited with agents greater than 500 Daltons having little BBB penetration (Banks 2009, S3). As a result, there is restricted BBB permeability for a wide variety of anticancer agents including both small molecule compounds such as cisplatin and large macromolecules such as bevacizumab (Avastin^{TM}) (Tfayli et al. 1999, 73-77; Thompson, Frenkel, and Neuwelt 2011, 87-93). Thus, the fact that LPA exposure was able to increase the BBB permeability of even the large molecular contrast agent, pegylated IRdye800cw, suggests

that LPA could be effective at increasing the delivery of the newer anti-cancer agents such as biological response modifiers and monoclonal antibodies.

The endothelial cells that form the BBB also express numerous influx and efflux transporters which can influence the permeability of a variety of compounds (Hermann and Bassetti 2007, 128-134). In the case of drugs that are substrates of efflux or influx transporters, accumulation within the brain can be affected by the activity of the transporters, either reduced in the case of efflux transporters or enhanced for influx transporters. For many chemotherapeutic agents, potential interactions with drug efflux transporters expressed in the BBB can limit brain accumulation. Therefore, the present study also examined the effects of LPA and GF120918 (P-gp inhibitor) on the BBB permeability of R800, a known substrate for P-gp, the main efflux transporters within the BBB (On et al. 2011). Based on these studies, LPA alone had no effect on the diffusion of R800 during the early stages of tumor growth (day 7) while the presence of GF120918 enhances the permeability of R800 in brain and tumor regions at both day 7 and day 12 post tumor development. This confirms the previous study from chapter 3 concerning the role of P-gp on the accumulation of drugs in the brain and brain tumors. By combining LPA with GF120918, the accumulation of R800 was significantly enhanced by 3-fold in both the tumor and non-tumor region. Such results are consistent with previous findings in non-tumor mice in which LPA exposure had little effect on R800 permeability (Chapter 4), and suggest LPA-mediated disruption of the BBB to improve drug delivery of P-gp dependent chemotherapeutics may be less than optimal. However, it should be noted that LPA alone was able to enhance the accumulation of the R800 in both the tumor and non-tumor region of the brain in day 12 tumor mice. While previous studies showed P-gp expression within the BBB in this particular brain tumor model was similar throughout all stages of tumor development

(Chapter 2), perhaps the increased R800 accumulation following LPA administration can be explained by tumor-induced changes in P-gp efflux transporter activity in the BBB. At 12-day post tumor implantation there are significant changes in BBB permeability observed within the tumor site. Thus, there is a possibility that alterations in the integrity of the BBB may influence P-gp transporter activity. Studies performed by Gallo and colleagues (2003) suggest that during certain CNS pathologies, such as brain tumors, the activity of P-gp is significantly diminished. The role of P-gp in limiting the distribution of their substrates in the brain and even with the tumor vasculature was evidence by examining the distribution of paclitaxel (PAC) in various regions of the brain in wild-type and P-gp knock-out tumor mice (Kemper et al. 2003, 2849-2855; Gallo et al. 2003, 5114-5117). Furthermore, it was also noted that P-gp activity within the tumor site was less compared to normal brain tissue. This decrease in P-gp activity was attributed to the leaky vasculature of the tumor, and suggests that P-gp transporter activity may be influenced by the tumor (Gallo et al. 2003, 5114-5117).

The potential utiltization of LPA and GF120918 to enhance drug delivery to the brain was also examined by evaluating the response of tumor mice to paclitaxel. Paclitaxel was choosen due to their high cytotoxicity against 3LL cells; furthermore, taxol is also a known P-gp substrate. The survival time frame of tumor mice following an injection of taxol alone was very similar to the control treated (no taxol) mice. Indeed, the median survival time for these mice was roughly 15 days. The combination of either LPA or GF120918 with taxol significantly enhanced the survival time frame of tumor mice by at least 7 days. The presence of both LPA and GF120918 with taxol enables the mice to survive up to 25 days, which is significantly higher compared to control or taxol treated mice. These studies conclusively indicated that the permeability of taxol is minimal under normal condition when the BBB property and P-gp

function is unaltered. However, by disrupting the tight junction with LPA or by inhibiting P-gp function with GF120918, or combination of both allowing more taxol to be accumulated in both the brain and tumor region, thus resulted in a positive tumor response.

It is well established that the presence of the BBB hinders the accumulation of drugs to the brain which contributes to the ineffective treatment of CNS disorders. However, it is also known that the barrier properties can be modulated using various compounds including high concentration of mannitol, bradykinin, and recently lipid mediators such as LPA. *In vitro* studies have shown an increase in vascular leakage following LPA exposure (Schulze et al. 1997, 991-1000; Nitz et al. 2003, 30-40; Tigyi et al. 1995, H2048-55; Wojciak-Stothard, Tsang, and Haworth 2005, L749-60; van Nieuw Amerongen, Vermeer, and van Hinsbergh 2000, E127-33). The increase vascular permeability of LPA *in vivo* has also been well characterized in our laboratory. This particular study examined the vascular effects of LPA in brain tumor mice. Similar to our previous findings in normal mice, LPA enhanced BBB permeability to a wide range of compounds in a murine brain tumor model. The effects of LPA-mediated BBB disruption was most apparent for hydrophilic agents; however, enhanced brain distribution of the P-gp probe R800 was also observed at the later stages of tumor development. Applications involving delivery of P-gp sensitive agents to the brain tumor may require the addition of a P-gp inhibitor to achieve optimal brain penetration. While further studies are required, the use of LPA to transiently open the BBB may have promise in the future treatment of brain tumors and other CNS disorders.

CHAPTER 6: CONCLUDING REMARKS

6.1. CONCLUSIONS

According to the Canadian Cancer Society, the incidence of brain tumors is significantly lower than other forms of cancer including breast, lung, and prostate. However, the overall survival rate for brain tumor patients is also among the lowest compared to other forms of cancer. Even choosing the best cohort, those with controlled systemic disease, early detection and 65 years-old or younger, the median survival for those with brain metastases is only 7 months. Furthermore, the likelihood of increased incidence of metastatic disease due to the improvements in treating cancer at the primary site, highlights the urgent need for improved treatment strategies to enhance not only survival time but also the quality of life of patients with metastatic brain tumors.

One reason for the low survival rate of brain tumors is the limited therapeutic drug treatment options available to tumors located within the CNS. The difficulty in developing therapeutic drugs to treat CNS disorders can be attributed to several factors including the complexity of the brain and brain related disorders, undesired adverse effects of the drugs, and the presence of neuroprotective barriers such as the blood-brain barrier (BBB), and the blood-CSF barrier (BCSFB). The presence of the BBB is essential for normal brain function due to its protective role against pathogens and xenobiotic substances. However under CNS pathological conditions including brain tumors, the BBB prevents obtaining therapeutically relevant levels of drugs in the brain. Thus, improved treatment of brain tumors must focus not only on the therapeutic target, but also methods for ensuring adequate delivery of the agents to sites within the brain.

In the mouse metastatic brain tumor model used, implantation of 3LL cells into the brains of Balb/c mice resulted in a rapidly progressing tumor with a median survival time of 17

days. Examination of BBB permeability during various stages of tumor progression using radiolabelled mannitol and Gad contrast enhanced MRI demonstrated that the BBB remained largely intact during the early stages of tumor progression with significant disruption only occurring during intermediate and late stages of tumor growth. Furthermore, although alterations in BBB permeability within the tumor were observed, non-tumor portions of the brain were not affected. This is an important point, as an intact BBB in areas around the tumor would potentially limit chemotherapeutic levels at the tumor periphery. Finally, there was no significant difference in P-gp expression in the tumor-bearing and non-tumor bearing cerebral vascular samples at any time point examined. As was observed in Chapter 3, the presence of P-gp in the BBB can significantly reduce the accumulation of P-gp substrates in the brain by at least 4-fold. Together these findings suggest that modification of BBB permeability either through barrier disruption techniques or pharmacological inhibition of drug efflux transporters could be an effective way to enhance the delivery of chemotherapeutic agents to the brain and the tumor regions.

One potential modulator of BBB is LPA. Within the context of the present study, LPA increased vascular leakage in both tumor and normal brain tissue. The enhancement of BBB permeability occured within 3 minutes of LPA exposure and dissipated within 20 minutes. The rapid onset of BBB disruption and the rapid restoration of the barrier properties following administration of LPA suggest LPA may have applications for increasing drug delivery to the brain and the tumor sites. Furthermore, the BBB disruption produced by LPA was not only limited to small molecular weight (Gad) compounds but was also present for larger macromolecules (Irdye800cw PEG) suggesting that LPA can influence the BBB permeability of a wide range of solutes. Similar findings were observed when LPA was administered to the brain

tumor-bearing mice. Increased permeability was observed in both non-tumor and tumor regions of the brain even at the early stages as well as the later stages of tumor growth. The use of LPA to transiently open the BBB may have promise in the future treatment of brain tumors and other CNS disorders. The current studies support the potential use of LPA as part of the treatment regiment to achieve greater accumulation of chemotherapeutic agents in tumor and non-tumor sites within the brain, thus enhancing the treatment response.

6.2. FUTURE DIRECTIONS

The findings from this project can have great potential for improving CNS drug delivery. Since the administration of LPA and P-gp inhibitor, GF120918, resulted in significant enhancement of BBB permeability in both the brain and the tumor region. The next logical step is to examine the response of tumor mice to selected chemotherapeutic drugs in the presence/absence of LPA, GF120918 or combination of both. Based on preliminary results, an injection of either LPA (1mg/kg) or GF120918 (9mg/kg) in combination with paclitaxel (4mg/kg) extended the survival time of tumor mice beyond the typical average of 17 days

These studies are the first to demonstrate LPA-mediated modulation of BBB permeability following systemic administration of the phospholipid in the whole animal. However, the effects of LPA on BBB permeability are not fully elucidated. For instance, it is not known which LPA receptors cause alterations in BBB permeability. The current literature supports the involvement of LPAR1 as the likely player in the BBB permeability effects observed. Our results indicate that there are at least 5 different types of LPA receptors distributed between the homogenates and the capillary-enriched fractions of the brain. It would be interesting to identify the role of each LPA receptor in the brain and how their respective activation can modulate BBB permeability. Furthermore, it has been shown that other

phospholipids such as sphingosine-1-phosphate (S1P) also modulates the blood brain barrier integrity, but in an antagonistic manner to LPA. Instead of the enhancing property observed with LPA, S1P has been shown to tighten the barrier property and restrict the paracellular diffusion of compounds. Another potential research question would be to explore the BBB permeability in the presence of both LPA and S1P, as this would provide true modulation of BBB permeability.

The present study also developed a method for examining P-gp activity in the BBB using near infrared fluorescence (NIRF) imaging techniques. P-gp, the main efflux transporter found in numerous organs including the BBB, is an important transporter that influences the absorption, distribution and elimination of a wide variety of drugs. From a drug delivery standpoint, it would be appealing to observe the activity of P-gp through non-invasive imaging in the whole animal. While the present study identified an acceptable NIRF probe and the initial time course and dosing required, imaging within the brain was limited due in part to autofluorescence from the hair follicles. One way to eliminate the background signals from the hair follicles is through the use of hairless mice. In this regard it would be noteworthy to utilize these mice in combination with NIRF imaging technique to simultaneously monitor the activity of P-gp and integrity of the barrier systems within the brain or peripheral organs of the animal over a period of time.

THE END

REFERENCES

Abbott, N. J. 2002. Astrocyte-endothelial interactions and blood-brain barrier permeability. *Journal of Anatomy* 200 (6) (Jun): 629-38.

Abbott, N. J., A. A. Patabendige, D. E. Dolman, S. R. Yusof, and D. J. Begley. 2010. Structure and function of the blood-brain barrier. *Neurobiology of Disease* 37 (1) (Jan): 13-25.

Alexander, J. S., W. F. Patton, B. W. Christman, L. L. Cuiper, and F. R. Haselton. 1998. Platelet-derived lysophosphatidic acid decreases endothelial permeability in vitro. *The American Journal of Physiology* 274 (1 Pt 2) (Jan): H115-22.

Aoki, K., N. Saso, S. Kato, Y. Sugiyama, and H. Sato. 2008. Nitric oxide and peroxynitrite regulate transporter transcription in rat liver slices. *Biological & Pharmaceutical Bulletin* 31 (10) (Oct): 1882-7.

Au, K. K., E. Liong, J. Y. Li, P. S. Li, C. C. Liew, T. T. Kwok, Y. M. Choy, C. Y. Lee, and K. P. Fung. 1997. Increases in mRNA levels of glucose transporters types 1 and 3 in ehrlich ascites tumor cells during tumor development. *Journal of Cellular Biochemistry* 67 (1) (Oct 1): 131-5.

Avendano-Vazquez, S. E., A. Garcia-Caballero, and J. A. Garcia-Sainz. 2005. Phosphorylation and desensitization of the lysophosphatidic acid receptor LPA1. *The Biochemical Journal* 385 (Pt 3) (Feb 1): 677-84.

Bachmeier, C. J., T. J. Spitzenberger, W. F. Elmquist, and D. W. Miller. 2005. Quantitative assessment of HIV-1 protease inhibitor interactions with drug efflux transporters in the blood-brain barrier. *Pharmaceutical Research* 22 (8) (Aug): 1259-68.

Bachmeier, C. J., W. J. Trickler, and D. W. Miller. 2006. Comparison of drug efflux transport kinetics in various blood-brain barrier models. *Drug Metabolism and Disposition: The Biological Fate of Chemicals* 34 (6) (Jun): 998-1003.

Baeten, K. M., and K. Akassoglou. 2011. Extracellular matrix and matrix receptors in blood-brain barrier formation and stroke. *Developmental Neurobiology* (Jul 20).

Balabanov, R., and P. Dore-Duffy. 1998. Role of the CNS microvascular pericyte in the blood-brain barrier. *Journal of Neuroscience Research* 53 (6) (Sep 15): 637-44.

Balayssac, D., N. Authier, A. Cayre, and F. Coudore. 2005. Does inhibition of P-glycoprotein lead to drug-drug interactions? *Toxicology Letters* 156 (3) (Apr 28): 319-29.

Banks, W. A. 2009. Characteristics of compounds that cross the blood-brain barrier. *BMC Neurology* 9 Suppl 1 (Jun 12): S3.

Bart, J., H. J. Groen, N. H. Hendrikse, W. T. van der Graaf, W. Vaalburg, and E. G. de Vries. 2000. The blood-brain barrier and oncology: New insights into function and modulation. *Cancer Treatment Reviews* 26 (6) (Dec): 449-62.

Bauer, F., C. Kuntner, J. P. Bankstahl, T. Wanek, M. Bankstahl, J. Stanek, S. Mairinger, et al. 2010. Synthesis and in vivo evaluation of [11C]tariquidar, a positron emission tomography radiotracer based on a third-generation P-glycoprotein inhibitor. *Bioorganic & Medicinal Chemistry* 18 (15) (Aug 1): 5489-97.

Beaulieu, E., M. Demeule, L. Ghitescu, and R. Beliveau. 1997. P-glycoprotein is strongly expressed in the luminal membranes of the endothelium of blood vessels in the brain. *The Biochemical Journal* 326 (Pt 2) (Pt 2) (Sep 1): 539-44.

Bendayan, R., P. T. Ronaldson, D. Gingras, and M. Bendayan. 2006. In situ localization of P-glycoprotein (ABCB1) in human and rat brain. *The Journal of Histochemistry and Cytochemistry : Official Journal of the Histochemistry Society* 54 (10) (Oct): 1159-67.

Bertalanffy, A., K. Roessler, O. Koperek, E. Gelpi, D. Prayer, M. Neuner, and E. Knosp. 2006. Intraventricular meningiomas: A report of 16 cases. *Neurosurgical Review* 29 (1) (Jan): 30-5.

Bidros, D. S., and M. A. Vogelbaum. 2009. Novel drug delivery strategies in neuro-oncology. *Neurotherapeutics : The Journal of the American Society for Experimental NeuroTherapeutics* 6 (3) (Jul): 539-46.

Bigotte, L., and Y. Olsson. 1984. Cytotoxic effects of adriamycin on the central nervous system of the mouse--cytofluorescence and electron-microscopic observations after various modes of administration. *Acta Neurologica Scandinavica.Supplementum* 100 : 55-67.

Birnbaum, M. J., H. C. Haspel, and O. M. Rosen. 1986. Cloning and characterization of a cDNA encoding the rat brain glucose-transporter protein. *Proceedings of the National Academy of Sciences of the United States of America* 83 (16) (Aug): 5784-8.

Black, K. L., and N. S. Ningaraj. 2004. Modulation of brain tumor capillaries for enhanced drug delivery selectively to brain tumor. *Cancer Control : Journal of the Moffitt Cancer Center* 11 (3) (May-Jun): 165-73.

Bohm, S. K., E. F. Grady, and N. W. Bunnett. 1997. Regulatory mechanisms that modulate signalling by G-protein-coupled receptors. *The Biochemical Journal* 322 (Pt 1) (Pt 1) (Feb 15): 1-18.

Bondy, C. A., W. H. Lee, and J. Zhou. 1992. Ontogeny and cellular distribution of brain glucose transporter gene expression. *Molecular and Cellular Neurosciences* 3 (4) (Aug): 305-14.

Borges, R. M., M. L. Lamers, F. L. Forti, M. F. Santos, and C. Y. Yan. 2011. Rho signaling pathway and apical constriction in the early lens placode. *Genesis (New York, N.Y.: 2000)* 49 (5) (May): 368-79.

Bouzier-Sore, A. K., M. Merle, P. J. Magistretti, and L. Pellerin. 2002. Feeding active neurons: (re)emergence of a nursing role for astrocytes. *Journal of Physiology, Paris* 96 (3-4) (Apr-Jun): 273-82.

Brandoni, A., N. Anzai, Y. Kanai, H. Endou, and A. M. Torres. 2006. Renal elimination of p-aminohippurate (PAH) in response to three days of biliary obstruction in the rat. the role of OAT1 and OAT3. *Biochimica Et Biophysica Acta* 1762 (7) (Jul): 673-82.

Brault, S., F. Gobeil Jr, A. Fortier, J. C. Honore, J. S. Joyal, P. S. Sapieha, A. Kooli, et al. 2007. Lysophosphatidic acid induces endothelial cell death by modulating the redox environment. *American Journal of Physiology.Regulatory, Integrative and Comparative Physiology* 292 (3) (Mar): R1174-83.

Brindley, D. N., and C. Pilquil. 2009. Lipid phosphate phosphatases and signaling. *Journal of Lipid Research* 50 Suppl (Apr): S225-30.

Buist, S. C., N. J. Cherrington, S. Choudhuri, D. P. Hartley, and C. D. Klaassen. 2002. Gender-specific and developmental influences on the expression of rat organic anion transporters. *The Journal of Pharmacology and Experimental Therapeutics* 301 (1) (Apr): 145-51.

Burckhardt, G., and B. C. Burckhardt. 2011. In vitro and in vivo evidence of the importance of organic anion transporters (OATs) in drug therapy. *Handbook of Experimental Pharmacology* (201) (201): 29-104.

Calebiro, D., V. O. Nikolaev, L. Persani, and M. J. Lohse. 2010. Signaling by internalized G-protein-coupled receptors. *Trends in Pharmacological Sciences* 31 (5) (May): 221-8.

Callaghan, R., E. Crowley, S. Potter, and I. D. Kerr. 2008. P-glycoprotein: So many ways to turn it on. *Journal of Clinical Pharmacology* 48 (3) (Mar): 365-78.

Carrubba, C. J., and T. W. Vitaz. 2009. Factors affecting the outcome after treatment for metastatic melanoma to the brain. *Surgical Neurology* 72 (6) (Dec): 707-11.

Chan, A. W., and J. S. Loeffler. 2001. Controversies in the management of patients with brain metastases. *Cancer Journal (Sudbury, Mass.)* 7 (2) (Mar-Apr): 105-7.

Chang, X. B. 2007. A molecular understanding of ATP-dependent solute transport by multidrug resistance-associated protein MRP1. *Cancer Metastasis Reviews* 26 (1) (Mar): 15-37.

Choi, J. W., D. R. Herr, K. Noguchi, Y. C. Yung, C. W. Lee, T. Mutoh, M. E. Lin, et al. 2010. LPA receptors: Subtypes and biological actions. ***Annual Review of Pharmacology and Toxicology*** **50 : 157-86.**

Choy, G., P. Choyke, and S. K. Libutti. 2003. Current advances in molecular imaging: Noninvasive in vivo bioluminescent and fluorescent optical imaging in cancer research. ***Molecular Imaging : Official Journal of the Society for Molecular Imaging*** **2 (4) (Oct): 303-12.**

Cohen, M. H., and M. J. Matthews. 1978. Small cell bronchogenic carcinoma: A distinct clinicopathologic entity. ***Seminars in Oncology*** **5 (3) (Sep): 234-43.**

Cole, S. P., G. Bhardwaj, J. H. Gerlach, J. E. Mackie, C. E. Grant, K. C. Almquist, A. J. Stewart, E. U. Kurz, A. M. Duncan, and R. G. Deeley. 1992. Overexpression of a transporter gene in a multidrug-resistant human lung cancer cell line. ***Science (New York, N.Y.)*** **258 (5088) (Dec 4): 1650-4.**

Cranmer, L. D., K. T. Trevor, S. Bandlamuri, and E. M. Hersh. 2005a. Rodent models of brain metastasis in melanoma. ***Melanoma Research*** **15 (5) (Oct): 325-56.**

Cruz-Munoz, W., and R. S. Kerbel. 2011. Preclinical approaches to study the biology and treatment of brain metastases. ***Seminars in Cancer Biology*** **21 (2) (Apr): 123-30.**

Dantzig, A. H., D. P. de Alwis, and M. Burgess. 2003. Considerations in the design and development of transport inhibitors as adjuncts to drug therapy. ***Advanced Drug Delivery Reviews*** **55 (1) (Jan 21): 133-50.**

de Boer, A. G., and P. J. Gaillard. 2006. Blood-brain barrier dysfunction and recovery. ***Journal of Neural Transmission (Vienna, Austria : 1996)*** **113 (4) (Apr): 455-62.**

de Lange, E. C. 2004. Potential role of ABC transporters as a detoxification system at the blood-CSF barrier. ***Advanced Drug Delivery Reviews*** **56 (12) (Oct 14): 1793-809.**

de Vries, N. A., J. H. Beijnen, W. Boogerd, and O. van Tellingen. 2006. Blood-brain barrier and chemotherapeutic treatment of brain tumors. ***Expert Review of Neurotherapeutics*** **6 (8) (Aug): 1199-209.**

Dean, M. 2009. ABC transporters, drug resistance, and cancer stem cells. ***Journal of Mammary Gland Biology and Neoplasia*** **14 (1) (Mar): 3-9.**

DeAngelis LM. 2001. Brain tumors. ***The New England Journal of Medicine*** **344 (2): 114.**

Deeken, J. F., and W. Loscher. 2007. The blood-brain barrier and cancer: Transporters, treatment, and trojan horses. ***Clinical Cancer Research : An Official Journal of the American Association for Cancer Research*** **13 (6) (Mar 15): 1663-74.**

Dombrowski, S. M., S. Y. Desai, M. Marroni, L. Cucullo, K. Goodrich, W. Bingaman, M. R. Mayberg, L. Bengez, and D. Janigro. 2001. Overexpression of multiple drug resistance genes in endothelial cells from patients with refractory epilepsy. *Epilepsia* 42 (12) (Dec): 1501-6.

Donelli, M. G., M. Zucchetti, and M. D'Incalci. 1992. Do anticancer agents reach the tumor target in the human brain? *Cancer Chemotherapy and Pharmacology* 30 (4): 251-60.

Dorner, B., C. Kuntner, J. P. Bankstahl, M. Bankstahl, J. Stanek, T. Wanek, G. Stundner, et al. 2009. Synthesis and small-animal positron emission tomography evaluation of [11C]-elacridar as a radiotracer to assess the distribution of P-glycoprotein at the blood-brain barrier. *Journal of Medicinal Chemistry* 52 (19) (Oct 8): 6073-82.

Ehrlich Paul. 1885. Das sauerstaff: Bedurfris des organismus. : 69-72.

Elaimy, A. L., A. R. Mackay, W. T. Lamoreaux, R. K. Fairbanks, J. J. Demakas, B. S. Cooke, B. J. Peressini, J. T. Holbrook, and C. M. Lee. 2011. Multimodality treatment of brain metastases: An institutional survival analysis of 275 patients. *World Journal of Surgical Oncology* 9 (Jul 5): 69.

Elliott, P. J., N. J. Hayward, R. L. Dean, D. G. Blunt, and R. T. Bartus. 1996. Intravenous RMP-7 selectively increases uptake of carboplatin into rat brain tumors. *Cancer Research* 56 (17) (Sep 1): 3998-4005.

Emerich, D. F., R. L. Dean, C. Osborn, and R. T. Bartus. 2001. The development of the bradykinin agonist labradimil as a means to increase the permeability of the blood-brain barrier: From concept to clinical evaluation. *Clinical Pharmacokinetics* 40 (2): 105-23.

Engelhardt, B. 2003. Development of the blood-brain barrier. *Cell and Tissue Research* 314 (1) (Oct): 119-29.

Engelhardt, B., and L. Sorokin. 2009. The blood-brain and the blood-cerebrospinal fluid barriers: Function and dysfunction. *Seminars in Immunopathology* 31 (4) (Nov): 497-511.

English, D., A. T. Kovala, Z. Welch, K. A. Harvey, R. A. Siddiqui, D. N. Brindley, and J. G. Garcia. 1999. Induction of endothelial cell chemotaxis by sphingosine 1-phosphate and stabilization of endothelial monolayer barrier function by lysophosphatidic acid, potential mediators of hematopoietic angiogenesis. *Journal of Hematotherapy & Stem Cell Research* 8 (6) (Dec): 627-34.

Ernst, R., P. Kueppers, J. Stindt, K. Kuchler, and L. Schmitt. 2010. Multidrug efflux pumps: Substrate selection in ATP-binding cassette multidrug efflux pumps--first come, first served? *The FEBS Journal* 277 (3) (Feb): 540-9.

Essig, M., M. A. Weber, H. von Tengg-Kobligk, M. V. Knopp, W. T. Yuh, and F. L. Giesel. 2006. Contrast-enhanced magnetic resonance imaging of central nervous system tumors:

Agents, mechanisms, and applications. *Topics in Magnetic Resonance Imaging : TMRI* 17 (2) (Apr): 89-106.

Farrell, C. L., J. Yang, and W. M. Pardridge. 1992. GLUT-1 glucose transporter is present within apical and basolateral membranes of brain epithelial interfaces and in microvascular endothelia with and without tight junctions. *The Journal of Histochemistry and Cytochemistry : Official Journal of the Histochemistry Society* 40 (2) (Feb): 193-9.

Fathallah-Shaykh, H. M., L. J. Zhao, A. I. Kafrouni, G. M. Smith, and J. Forman. 2000. Gene transfer of IFN-gamma into established brain tumors represses growth by antiangiogenesis. *Journal of Immunology (Baltimore, Md.: 1950)* 164 (1) (Jan 1): 217-22.

Fellner, S., B. Bauer, D. S. Miller, M. Schaffrik, M. Fankhanel, T. Spruss, G. Bernhardt, et al. 2002. Transport of paclitaxel (taxol) across the blood-brain barrier in vitro and in vivo. *The Journal of Clinical Investigation* 110 (9) (Nov): 1309-18.

Feng, B., J. B. Mills, R. E. Davidson, R. J. Mireles, J. S. Janiszewski, M. D. Troutman, and S. M. de Morais. 2008. In vitro P-glycoprotein assays to predict the in vivo interactions of P-glycoprotein with drugs in the central nervous system. *Drug Metabolism and Disposition: The Biological Fate of Chemicals* 36 (2) (Feb): 268-75.

Fidler, I. J., S. Yano, R. D. Zhang, T. Fujimaki, and C. D. Bucana. 2002a. The seed and soil hypothesis: Vascularisation and brain metastases. *The Lancet Oncology* 3 (1) (Jan): 53-7.

Fontaine, M., W. F. Elmquist, and D. W. Miller. 1996. Use of rhodamine 123 to examine the functional activity of P-glycoprotein in primary cultured brain microvessel endothelial cell monolayers. *Life Sciences* 59 (18): 1521-31.

Ford, J., C. Osborn, T. Barton, and N. M. Bleehen. 1998. A phase I study of intravenous RMP-7 with carboplatin in patients with progression of malignant glioma. *European Journal of Cancer (Oxford, England : 1990)* 34 (11) (Oct): 1807-11.

Friesema, E. C., S. Ganguly, A. Abdalla, J. E. Manning Fox, A. P. Halestrap, and T. J. Visser. 2003. Identification of monocarboxylate transporter 8 as a specific thyroid hormone transporter. *The Journal of Biological Chemistry* 278 (41) (Oct 10): 40128-35.

Gallo, J. M., S. Li, P. Guo, K. Reed, and J. Ma. 2003. The effect of P-glycoprotein on paclitaxel brain and brain tumor distribution in mice. *Cancer Research* 63 (16) (Aug 15): 5114-7.

Gao, B., B. Stieger, B. Noe, J. M. Fritschy, and P. J. Meier. 1999. Localization of the organic anion transporting polypeptide 2 (Oatp2) in capillary endothelium and choroid plexus epithelium of rat brain. *The Journal of Histochemistry and Cytochemistry : Official Journal of the Histochemistry Society* 47 (10) (Oct): 1255-64.

Gaspar, L., C. Scott, M. Rotman, S. Asbell, T. Phillips, T. Wasserman, W. G. McKenna, and R. Byhardt. 1997. Recursive partitioning analysis (RPA) of prognostic factors in three

radiation therapy oncology group (RTOG) brain metastases trials. ***International Journal of Radiation Oncology, Biology, Physics*** **37 (4) (Mar 1): 745-51.**

Giglio, P., and M. R. Gilbert. 2010. Neurologic complications of cancer and its treatment. ***Current Oncology Reports*** **12 (1) (Jan): 50-9.**

Ginguene, C., J. Champier, S. Maallem, N. Strazielle, A. Jouvet, M. Fevre-Montange, and J. F. Ghersi-Egea. 2010. P-glycoprotein (ABCB1) and breast cancer resistance protein (ABCG2) localize in the microvessels forming the blood-tumor barrier in ependymomas. ***Brain Pathology (Zurich, Switzerland)*** **20 (5) (Sep): 926-35.**

Girardin, F. 2006. Membrane transporter proteins: A challenge for CNS drug development. ***Dialogues in Clinical Neuroscience*** **8 (3): 311-21.**

Gjedde, A., and C. Crone. 1975. Induction processes in blood-brain transfer of ketone bodies during starvation. ***The American Journal of Physiology*** **229 (5) (Nov): 1165-9.**

Goeckeler, Z. M., and R. B. Wysolmerski. 1995. Myosin light chain kinase-regulated endothelial cell contraction: The relationship between isometric tension, actin polymerization, and myosin phosphorylation. ***The Journal of Cell Biology*** **130 (3) (Aug): 613-27.**

Goetzl, E. J., M. Graeler, M. C. Huang, and G. Shankar. 2002. Lysophospholipid growth factors and their G protein-coupled receptors in immunity, coronary artery disease, and cancer. ***TheScientificWorldJournal*** **2 (Feb 6): 324-38.**

Goldmann EE. 1909. Die aussere und innere skretion des genden und gekranken organismus im licht der vitalen farbung. 64 : 192-265.

Goldshmit, Y., K. Munro, S. Y. Leong, A. Pebay, and A. M. Turnley. 2010. LPA receptor expression in the central nervous system in health and following injury. ***Cell and Tissue Research*** **341 (1) (Jul): 23-32.**

Goldstein, G. W., and A. L. Betz. 1986. The blood-brain barrier. ***Scientific American*** **255 (3) (Sep): 74-83.**

Graesser, D., A. Solowiej, M. Bruckner, E. Osterweil, A. Juedes, S. Davis, N. H. Ruddle, B. Engelhardt, and J. A. Madri. 2002. Altered vascular permeability and early onset of experimental autoimmune encephalomyelitis in PECAM-1-deficient mice. ***The Journal of Clinical Investigation*** **109 (3) (Feb): 383-92.**

Hagenbuch, B., and P. J. Meier. 2004. Organic anion transporting polypeptides of the OATP/ SLC21 family: Phylogenetic classification as OATP/ SLCO superfamily, new nomenclature and molecular/functional properties. ***Pflugers Archiv : European Journal of Physiology*** **447 (5) (Feb): 653-65.**

Hahnova-Cygalova, L., M. Ceckova, and F. Staud. 2011. Fetoprotective activity of breast cancer resistance protein (BCRP, ABCG2): Expression and function throughout pregnancy. *Drug Metabolism Reviews* 43 (1) (Feb): 53-68.

Hall, W. A., N. D. Doolittle, M. Daman, P. K. Bruns, L. Muldoon, D. Fortin, and E. A. Neuwelt. 2006. Osmotic blood-brain barrier disruption chemotherapy for diffuse pontine gliomas. *Journal of Neuro-Oncology* 77 (3) (May): 279-84.

Harrison, S. M., C. Reavill, G. Brown, J. T. Brown, J. E. Cluderay, B. Crook, C. H. Davies, et al. 2003. LPA1 receptor-deficient mice have phenotypic changes observed in psychiatric disease. *Molecular and Cellular Neurosciences* 24 (4) (Dec): 1170-9.

Hasegawa, H., Y. Ushio, T. Hayakawa, K. Yamada, and H. Mogami. 1983. Changes of the blood-brain barrier in experimental metastatic brain tumors. *Journal of Neurosurgery* 59 (2) (Aug): 304-10.

Haseloff, R. F., I. E. Blasig, H. C. Bauer, and H. Bauer. 2005. In search of the astrocytic factor(s) modulating blood-brain barrier functions in brain capillary endothelial cells in vitro. *Cellular and Molecular Neurobiology* 25 (1) (Feb): 25-39.

Haselton, F. R., and J. S. Alexander. 1992. Platelets and a platelet-released factor enhance endothelial barrier. *The American Journal of Physiology* 263 (6 Pt 1) (Dec): L670-8.

Haslam, I. S., K. Jones, T. Coleman, and N. L. Simmons. 2008. Rifampin and digoxin induction of MDR1 expression and function in human intestinal (T84) epithelial cells. *British Journal of Pharmacology* 154 (1) (May): 246-55.

Hawkins, B. T., and T. P. Davis. 2005. The blood-brain barrier/neurovascular unit in health and disease. *Pharmacological Reviews* 57 (2) (Jun): 173-85.

Hawkins, R. A., A. M. Mans, and D. W. Davis. 1986. Regional ketone body utilization by rat brain in starvation and diabetes. *The American Journal of Physiology* 250 (2 Pt 1) (Feb): E169-78.

He, D., Y. Su, P. V. Usatyuk, E. W. Spannhake, P. Kogut, J. Solway, V. Natarajan, and Y. Zhao. 2009. Lysophosphatidic acid enhances pulmonary epithelial barrier integrity and protects endotoxin-induced epithelial barrier disruption and lung injury. *The Journal of Biological Chemistry* 284 (36) (Sep 4): 24123-32.

Hecht, J. H., J. A. Weiner, S. R. Post, and J. Chun. 1996. Ventricular zone gene-1 (vzg-1) encodes a lysophosphatidic acid receptor expressed in neurogenic regions of the developing cerebral cortex. *The Journal of Cell Biology* 135 (4) (Nov): 1071-83.

Henson, J. W., C. Cordon-Cardo, and J. B. Posner. 1992. P-glycoprotein expression in brain tumors. *Journal of Neuro-Oncology* 14 (1) (Sep): 37-43.

Hermann, D. M., and C. L. Bassetti. 2007. Implications of ATP-binding cassette transporters for brain pharmacotherapies. *Trends in Pharmacological Sciences* 28 (3) (Mar): 128-34.

Hilderbrand, S. A., and R. Weissleder. 2010. Near-infrared fluorescence: Application to in vivo molecular imaging. *Current Opinion in Chemical Biology* 14 (1) (Feb): 71-9.

Hollo, Z., L. Homolya, T. Hegedus, and B. Sarkadi. 1996. Transport properties of the multidrug resistance-associated protein (MRP) in human tumour cells. *FEBS Letters* 383 (1-2) (Mar 25): 99-104.

Horio, M., K. V. Chin, S. J. Currier, S. Goldenberg, C. Williams, I. Pastan, M. M. Gottesman, and J. Handler. 1989. Transepithelial transport of drugs by the multidrug transporter in cultured madin-darby canine kidney cell epithelia. *The Journal of Biological Chemistry* 264 (25) (Sep 5): 14880-4.

Imai, Y., S. Asada, S. Tsukahara, E. Ishikawa, T. Tsuruo, and Y. Sugimoto. 2003. Breast cancer resistance protein exports sulfated estrogens but not free estrogens. *Molecular Pharmacology* 64 (3) (Sep): 610-8.

Inamura, T., T. Nomura, R. T. Bartus, and K. L. Black. 1994. Intracarotid infusion of RMP-7, a bradykinin analog: A method for selective drug delivery to brain tumors. *Journal of Neurosurgery* 81 (5) (Nov): 752-8.

Inoue, C. N., H. G. Forster, and M. Epstein. 1995. Effects of lysophosphatidic acid, a novel lipid mediator, on cytosolic Ca2+ and contractility in cultured rat mesangial cells. *Circulation Research* 77 (5) (Nov): 888-96.

International Transporter Consortium, K. M. Giacomini, S. M. Huang, D. J. Tweedie, L. Z. Benet, K. L. Brouwer, X. Chu, et al. 2010. Membrane transporters in drug development. *Nature Reviews.Drug Discovery* 9 (3) (Mar): 215-36.

Isakov, N., M. Feldman, and S. Segal. 1982. An immune response against the alloantigens of the 3LL lewis lung carcinoma prevents the growth of lung metastases, but not of local allografts. *Invasion & Metastasis* 2 (1): 12-32.

Jasinska, R., Q. X. Zhang, C. Pilquil, I. Singh, J. Xu, J. Dewald, D. A. Dillon, et al. 1999. Lipid phosphate phosphohydrolase-1 degrades exogenous glycerolipid and sphingolipid phosphate esters. *The Biochemical Journal* 340 (Pt 3) (Pt 3) (Jun 15): 677-86.

Jonker, J. W., E. Wagenaar, L. van Deemter, R. Gottschlich, H. M. Bender, J. Dasenbrock, and A. H. Schinkel. 1999. Role of blood-brain barrier P-glycoprotein in limiting brain accumulation and sedative side-effects of asimadoline, a peripherally acting analgaesic drug. *British Journal of Pharmacology* 127 (1) (May): 43-50.

Juliano, R. L., and V. Ling. 1976. A surface glycoprotein modulating drug permeability in chinese hamster ovary cell mutants. *Biochimica Et Biophysica Acta* 455 (1) (Nov 11): 152-62.

Kaijzel, E. L., G. van der Pluijm, and C. W. Lowik. 2007. Whole-body optical imaging in animal models to assess cancer development and progression. *Clinical Cancer Research : An Official Journal of the American Association for Cancer Research* 13 (12) (Jun 15): 3490-7.

Kaler, G., D. M. Truong, D. E. Sweeney, D. W. Logan, M. Nagle, W. Wu, S. A. Eraly, and S. K. Nigam. 2006. Olfactory mucosa-expressed organic anion transporter, Oat6, manifests high affinity interactions with odorant organic anions. *Biochemical and Biophysical Research Communications* 351 (4) (Dec 29): 872-6.

Kalliokoski, A., and M. Niemi. 2009. Impact of OATP transporters on pharmacokinetics. *British Journal of Pharmacology* 158 (3) (Oct): 693-705.

Kamar, F. G., and J. B. Posner. 2010. Brain metastases. *Seminars in Neurology* 30 (3) (Jul): 217-35.

Kamouchi, M., T. Ago, J. Kuroda, and T. Kitazono. 2011. The possible roles of brain pericytes in brain ischemia and stroke. *Cellular and Molecular Neurobiology* (Aug 10).

Kania, K. D., H. C. Wijesuriya, S. B. Hladky, and M. A. Barrand. 2011. Beta amyloid effects on expression of multidrug efflux transporters in brain endothelial cells. *Brain Research* 1418 (Oct 18): 1-11.

Kelly, E., C. P. Bailey, and G. Henderson. 2008. Agonist-selective mechanisms of GPCR desensitization. *British Journal of Pharmacology* 153 Suppl 1 (Mar): S379-88.

Kemper, E. M., W. Boogerd, I. Thuis, J. H. Beijnen, and O. van Tellingen. 2004. Modulation of the blood-brain barrier in oncology: Therapeutic opportunities for the treatment of brain tumours? *Cancer Treatment Reviews* 30 (5) (Aug): 415-23.

Kemper, E. M., A. E. van Zandbergen, C. Cleypool, H. A. Mos, W. Boogerd, J. H. Beijnen, and O. van Tellingen. 2003. Increased penetration of paclitaxel into the brain by inhibition of P-glycoprotein. *Clinical Cancer Research : An Official Journal of the American Association for Cancer Research* 9 (7) (Jul): 2849-55.

Keppler, D. 2011. Multidrug resistance proteins (MRPs, ABCCs): Importance for pathophysiology and drug therapy. *Handbook of Experimental Pharmacology* (201) (201): 299-323.

Kikuchi, R., H. Kusuhara, D. Sugiyama, and Y. Sugiyama. 2003. Contribution of organic anion transporter 3 (Slc22a8) to the elimination of p-aminohippuric acid and benzylpenicillin across the blood-brain barrier. *The Journal of Pharmacology and Experimental Therapeutics* 306 (1) (Jul): 51-8.

Kim, K. H., J. Lee, J. I. Lee, H. Nam do, D. S. Kong, Y. C. Ahn, H. C. Park, et al. 2010. Can upfront systemic chemotherapy replace stereotactic radiosurgery or whole brain radiotherapy in the treatment of non-small cell lung cancer patients with asymptomatic brain metastases? *Lung Cancer (Amsterdam, Netherlands)* 68 (2) (May): 258-63.

Klip, A., T. Tsakiridis, A. Marette, and P. A. Ortiz. 1994. Regulation of expression of glucose transporters by glucose: A review of studies in vivo and in cell cultures. *FASEB Journal : Official Publication of the Federation of American Societies for Experimental Biology* 8 (1) (Jan): 43-53.

Klohs, J., A. Wunder, and K. Licha. 2008. Near-infrared fluorescent probes for imaging vascular pathophysiology. *Basic Research in Cardiology* 103 (2) (Mar): 144-51.

Kroll, R. A., and E. A. Neuwelt. 1998. Outwitting the blood-brain barrier for therapeutic purposes: Osmotic opening and other means. *Neurosurgery* 42 (5) (May): 1083,99; discussion 1099-100.

Kullak-Ublick, G. A., B. Hagenbuch, B. Stieger, C. D. Schteingart, A. F. Hofmann, A. W. Wolkoff, and P. J. Meier. 1995. Molecular and functional characterization of an organic anion transporting polypeptide cloned from human liver. *Gastroenterology* 109 (4) (Oct): 1274-82.

Langer, O., M. Bauer, A. Hammers, R. Karch, E. Pataraia, M. J. Koepp, A. Abrahim, et al. 2007. Pharmacoresistance in epilepsy: A pilot PET study with the P-glycoprotein substrate R-[(11)C]verapamil. *Epilepsia* 48 (9) (Sep): 1774-84.

Lazarowski, A., L. Czornyj, F. Lubienieki, E. Girardi, S. Vazquez, and C. D'Giano. 2007. ABC transporters during epilepsy and mechanisms underlying multidrug resistance in refractory epilepsy. *Epilepsia* 48 Suppl 5 : 140-9.

Lee, C. A., J. A. Cook, E. L. Reyner, and D. A. Smith. 2010. P-glycoprotein related drug interactions: Clinical importance and a consideration of disease states. *Expert Opinion on Drug Metabolism & Toxicology* 6 (5) (May): 603-19.

Leino, R. L., D. Z. Gerhart, and L. R. Drewes. 1999. Monocarboxylate transporter (MCT1) abundance in brains of suckling and adult rats: A quantitative electron microscopic immunogold study. *Brain Research.Developmental Brain Research* 113 (1-2) (Mar 12): 47-54.

Li, X. Z., and H. Nikaido. 2004. Efflux-mediated drug resistance in bacteria. *Drugs* 64 (2): 159-204.

Ligeti, E., R. Csepanyi-Komi, and L. Hunyady. 2012. Physiological mechanisms of signal termination in biological systems. *Acta Physiologica (Oxford, England)* 204 (4) (Apr): 469-78.

Lin, J. H. 2007. Transporter-mediated drug interactions: Clinical implications and in vitro assessment. *Expert Opinion on Drug Metabolism & Toxicology* 3 (1) (Feb): 81-92.

Lin, J. H., and M. Yamazaki. 2003. Role of P-glycoprotein in pharmacokinetics: Clinical implications. *Clinical Pharmacokinetics* 42 (1): 59-98.

Lockman, P. R., R. K. Mittapalli, K. S. Taskar, V. Rudraraju, B. Gril, K. A. Bohn, C. E. Adkins, et al. 2010. Heterogeneous blood-tumor barrier permeability determines drug efficacy in experimental brain metastases of breast cancer. *Clinical Cancer Research : An Official Journal of the American Association for Cancer Research* 16 (23) (Dec 1): 5664-78.

Loe, D. W., R. G. Deeley, and S. P. Cole. 1998. Characterization of vincristine transport by the M(r) 190,000 multidrug resistance protein (MRP): Evidence for cotransport with reduced glutathione. *Cancer Research* 58 (22) (Nov 15): 5130-6.

Loscher, W., and H. Potschka. 2005. Blood-brain barrier active efflux transporters: ATP-binding cassette gene family. *NeuroRx : The Journal of the American Society for Experimental NeuroTherapeutics* 2 (1) (Jan): 86-98.

———. 2005. Role of drug efflux transporters in the brain for drug disposition and treatment of brain diseases. *Progress in Neurobiology* 76 (1) (May): 22-76.

———. 2002. Role of multidrug transporters in pharmacoresistance to antiepileptic drugs. *The Journal of Pharmacology and Experimental Therapeutics* 301 (1) (Apr): 7-14.

Madsen, S. J., and H. Hirschberg. 2010. Site-specific opening of the blood-brain barrier. *Journal of Biophotonics* 3 (5-6) (Jun): 356-67.

Maher, F. 1995. Immunolocalization of GLUT1 and GLUT3 glucose transporters in primary cultured neurons and glia. *Journal of Neuroscience Research* 42 (4) (Nov 1): 459-69.

Martin, C., G. Berridge, C. F. Higgins, and R. Callaghan. 1997. The multi-drug resistance reversal agent SR33557 and modulation of vinca alkaloid binding to P-glycoprotein by an allosteric interaction. *British Journal of Pharmacology* 122 (4) (Oct): 765-71.

Matsuoka, Y., M. Okazaki, Y. Kitamura, and T. Taniguchi. 1999. Developmental expression of P-glycoprotein (multidrug resistance gene product) in the rat brain. *Journal of Neurobiology* 39 (3) (Jun 5): 383-92.

Mawrin, C., and A. Perry. 2010. Pathological classification and molecular genetics of meningiomas. *Journal of Neuro-Oncology* 99 (3) (Sep): 379-91.

McColl, B. W., N. J. Rothwell, and S. M. Allan. 2008. Systemic inflammation alters the kinetics of cerebrovascular tight junction disruption after experimental stroke in mice. *The Journal of Neuroscience : The Official Journal of the Society for Neuroscience* 28 (38) (Sep 17): 9451-62.

Meairs, S., and A. Alonso. 2007. Ultrasound, microbubbles and the blood-brain barrier. *Progress in Biophysics and Molecular Biology* 93 (1-3) (Jan-Apr): 354-62.

Meier-Abt, F., Y. Mokrab, and K. Mizuguchi. 2005. Organic anion transporting polypeptides of the OATP/SLCO superfamily: Identification of new members in nonmammalian species, comparative modeling and a potential transport mode. *The Journal of Membrane Biology* 208 (3) (Dec): 213-27.

Mendoza, M., and C. Khanna. 2009. Revisiting the seed and soil in cancer metastasis. *The International Journal of Biochemistry & Cell Biology* 41 (7) (Jul): 1452-62.

Miller, D. S., C. Graeff, L. Droulle, S. Fricker, and G. Fricker. 2002. Xenobiotic efflux pumps in isolated fish brain capillaries. *American Journal of Physiology.Regulatory, Integrative and Comparative Physiology* 282 (1) (Jan): R191-8.

Miller, D. W., M. Fontain, C. Kolar, and T. Lawson. 1996. The expression of multidrug resistance-associated protein (MRP) in pancreatic adenocarcinoma cell lines. *Cancer Letters* 107 (2) (Oct 22): 301-6.

Miller, D. W., M. Hinton, and F. Chen. 2011. Evaluation of drug efflux transporter liabilities of darifenacin in cell culture models of the blood-brain and blood-ocular barriers. *Neurourology and Urodynamics* 30 (8) (Nov): 1633-8.

Mills, G. B., and W. H. Moolenaar. 2003. The emerging role of lysophosphatidic acid in cancer. *Nature Reviews.Cancer* 3 (8) (Aug): 582-91.

Mogi, M., J. Yang, J. F. Lambert, G. A. Colvin, I. Shiojima, C. Skurk, R. Summer, A. Fine, P. J. Quesenberry, and K. Walsh. 2003. Akt signaling regulates side population cell phenotype via Bcrp1 translocation. *The Journal of Biological Chemistry* 278 (40) (Oct 3): 39068-75.

Moolenaar, W. H. 1995. Lysophosphatidic acid, a multifunctional phospholipid messenger. *The Journal of Biological Chemistry* 270 (22) (Jun 2): 12949-52.

Moolenaar, W. H., L. A. van Meeteren, and B. N. Giepmans. 2004. The ins and outs of lysophosphatidic acid signaling. *BioEssays : News and Reviews in Molecular, Cellular and Developmental Biology* 26 (8) (Aug): 870-81.

Morgello, S., R. R. Uson, E. J. Schwartz, and R. S. Haber. 1995. The human blood-brain barrier glucose transporter (GLUT1) is a glucose transporter of gray matter astrocytes. *Glia* 14 (1) (May): 43-54.

Motl, S., Y. Zhuang, C. M. Waters, and C. F. Stewart. 2006. Pharmacokinetic considerations in the treatment of CNS tumours. *Clinical Pharmacokinetics* 45 (9): 871-903.

Muldoon, L. L., C. Soussain, K. Jahnke, C. Johanson, T. Siegal, Q. R. Smith, W. A. Hall, et al. 2007. Chemotherapy delivery issues in central nervous system malignancy: A reality

check. *Journal of Clinical Oncology : Official Journal of the American Society of Clinical Oncology* 25 (16) (Jun 1): 2295-305.

Nagaraja, T. N., J. R. Ewing, K. Karki, P. E. Jacobs, G. W. Divine, J. D. Fenstermacher, C. S. Patlak, and R. A. Knight. 2011. MRI and quantitative autoradiographic studies following bolus injections of unlabeled and (14)C-labeled gadolinium-diethylenetriaminepentaacetic acid in a rat model of stroke yield similar distribution volumes and blood-to-brain influx rate constants. *NMR in Biomedicine* 24 (5) (Jun): 547-58.

Nakamura, T., R. Saito, S. Sugiyama, Y. Sonoda, T. Kumabe, and T. Tominaga. 2011. Local convection-enhanced delivery of chemotherapeutic agent transiently opens blood-brain barrier and improves efficacy of systemic chemotherapy in intracranial xenograft tumor model. *Cancer Letters* 310 (1) (Nov 1): 77-83.

Nayak, L., E. Q. Lee, and P. Y. Wen. 2012. Epidemiology of brain metastases. *Current Oncology Reports* 14 (1) (Feb): 48-54.

Neuwelt, E., N. J. Abbott, L. Abrey, W. A. Banks, B. Blakley, T. Davis, B. Engelhardt, et al. 2008. Strategies to advance translational research into brain barriers. *Lancet Neurology* 7 (1) (Jan): 84-96.

Neuwelt, E. A., P. A. Barnett, M. Glasberg, and E. P. Frenkel. 1983. Pharmacology and neurotoxicity of cis-diamminedichloroplatinum, bleomycin, 5-fluorouracil, and cyclophosphamide administration following osmotic blood-brain barrier modification. *Cancer Research* 43 (11) (Nov): 5278-85.

Nicolazzo, J. A., and K. Katneni. 2009. Drug transport across the blood-brain barrier and the impact of breast cancer resistance protein (ABCG2). *Current Topics in Medicinal Chemistry* 9 (2): 130-47.

Nies, A. T., G. Jedlitschky, J. Konig, C. Herold-Mende, H. H. Steiner, H. P. Schmitt, and D. Keppler. 2004. Expression and immunolocalization of the multidrug resistance proteins, MRP1-MRP6 (ABCC1-ABCC6), in human brain. *Neuroscience* 129 (2): 349-60.

Nitz, T., T. Eisenblatter, K. Psathaki, and H. J. Galla. 2003. Serum-derived factors weaken the barrier properties of cultured porcine brain capillary endothelial cells in vitro. *Brain Research* 981 (1-2) (Aug 15): 30-40.

Ntziachristos, V., C. Bremer, and R. Weissleder. 2003. Fluorescence imaging with near-infrared light: New technological advances that enable in vivo molecular imaging. *European Radiology* 13 (1) (Jan): 195-208.

Nybo, L., and N. H. Secher. 2004. Cerebral perturbations provoked by prolonged exercise. *Progress in Neurobiology* 72 (4) (Mar): 223-61.

On, N. H., F. Chen, M. Hinton, and D. W. Miller. 2011. Assessment of P-glycoprotein activity in the blood-brain barrier (BBB) using near infrared fluorescence (NIRF) imaging techniques. *Pharmaceutical Research* (May 20).

Ose, A., H. Kusuhara, C. Endo, K. Tohyama, M. Miyajima, S. Kitamura, and Y. Sugiyama. 2010. Functional characterization of mouse organic anion transporting peptide 1a4 in the uptake and efflux of drugs across the blood-brain barrier. *Drug Metabolism and Disposition: The Biological Fate of Chemicals* 38 (1) (Jan): 168-76.

Ozvegy, C., T. Litman, G. Szakacs, Z. Nagy, S. Bates, A. Varadi, and B. Sarkadi. 2001. Functional characterization of the human multidrug transporter, ABCG2, expressed in insect cells. *Biochemical and Biophysical Research Communications* 285 (1) (Jul 6): 111-7.

Pajouhesh, H., and G. R. Lenz. 2005. Medicinal chemical properties of successful central nervous system drugs. *NeuroRx : The Journal of the American Society for Experimental NeuroTherapeutics* 2 (4) (Oct): 541-53.

Pardridge, W. M. 2010. Biopharmaceutical drug targeting to the brain. *Journal of Drug Targeting* 18 (3) (Apr): 157-67.

———. 2005. The blood-brain barrier: Bottleneck in brain drug development. *NeuroRx : The Journal of the American Society for Experimental NeuroTherapeutics* 2 (1) (Jan): 3-14.

———. 1999. Blood-brain barrier biology and methodology. *Journal of Neurovirology* 5 (6) (Dec): 556-69.

Pardridge, W. M., R. J. Boado, and C. R. Farrell. 1990. Brain-type glucose transporter (GLUT-1) is selectively localized to the blood-brain barrier. studies with quantitative western blotting and in situ hybridization. *The Journal of Biological Chemistry* 265 (29) (Oct 15): 18035-40.

Patel, M. M., B. R. Goyal, S. V. Bhadada, J. S. Bhatt, and A. F. Amin. 2009. Getting into the brain: Approaches to enhance brain drug delivery. *CNS Drugs* 23 (1): 35-58.

Peereboom, D. M. 2005. Chemotherapy in brain metastases. *Neurosurgery* 57 (5 Suppl) (Nov): S54,65; discusssion S1-4.

Pekcec, A., B. Unkruer, V. Stein, J. P. Bankstahl, J. Soerensen, A. Tipold, W. Baumgartner, and H. Potschka. 2009. Over-expression of P-glycoprotein in the canine brain following spontaneous status epilepticus. *Epilepsy Research* 83 (2-3) (Feb): 144-51.

Pellerin, L. 2003. Lactate as a pivotal element in neuron-glia metabolic cooperation. *Neurochemistry International* 43 (4-5) (Sep-Oct): 331-8.

Pfister, S., C. Hartmann, and A. Korshunov. 2009. Histology and molecular pathology of pediatric brain tumors. *Journal of Child Neurology* 24 (11) (Nov): 1375-86.

Phares, T. W., R. B. Kean, T. Mikheeva, and D. C. Hooper. 2006. Regional differences in blood-brain barrier permeability changes and inflammation in the apathogenic clearance of virus from the central nervous system. *Journal of Immunology (Baltimore, Md.: 1950)* 176 (12) (Jun 15): 7666-75.

Pierre, K., and L. Pellerin. 2005. Monocarboxylate transporters in the central nervous system: Distribution, regulation and function. *Journal of Neurochemistry* 94 (1) (Jul): 1-14.

Pierre, K., L. Pellerin, R. Debernardi, B. M. Riederer, and P. J. Magistretti. 2000. Cell-specific localization of monocarboxylate transporters, MCT1 and MCT2, in the adult mouse brain revealed by double immunohistochemical labeling and confocal microscopy. *Neuroscience* 100 (3): 617-27.

Polli, J. W., S. A. Wring, J. E. Humphreys, L. Huang, J. B. Morgan, L. O. Webster, and C. S. Serabjit-Singh. 2001. Rational use of in vitro P-glycoprotein assays in drug discovery. *The Journal of Pharmacology and Experimental Therapeutics* 299 (2) (Nov): 620-8.

Popowski, K., J. J. Eloranta, M. Saborowski, M. Fried, P. J. Meier, and G. A. Kullak-Ublick. 2005. The human organic anion transporter 2 gene is transactivated by hepatocyte nuclear factor-4 alpha and suppressed by bile acids. *Molecular Pharmacology* 67 (5) (May): 1629-38.

Postmus, P. E., and E. F. Smit. 1999. Chemotherapy for brain metastases of lung cancer: A review. *Annals of Oncology : Official Journal of the European Society for Medical Oncology / ESMO* 10 (7) (Jul): 753-9.

Potschka, H. 2010. Targeting regulation of ABC efflux transporters in brain diseases: A novel therapeutic approach. *Pharmacology & Therapeutics* 125 (1) (Jan): 118-27.

Prados, M. D., S. C. Schold SC JR, H. A. Fine, K. Jaeckle, F. Hochberg, L. Mechtler, M. R. Fetell, et al. 2003. A randomized, double-blind, placebo-controlled, phase 2 study of RMP-7 in combination with carboplatin administered intravenously for the treatment of recurrent malignant glioma. *Neuro-Oncology* 5 (2) (Apr): 96-103.

Preusser, M., S. de Ribaupierre, A. Wohrer, S. C. Erridge, M. Hegi, M. Weller, and R. Stupp. 2011. Current concepts and management of glioblastoma. *Annals of Neurology* 70 (1) (Jul): 9-21.

Rao, V. V., J. L. Dahlheimer, M. E. Bardgett, A. Z. Snyder, R. A. Finch, A. C. Sartorelli, and D. Piwnica-Worms. 1999. Choroid plexus epithelial expression of MDR1 P glycoprotein and multidrug resistance-associated protein contribute to the blood-cerebrospinal-fluid drug-permeability barrier. *Proceedings of the National Academy of Sciences of the United States of America* 96 (7) (Mar 30): 3900-5.

Reese, T. S., and M. J. Karnovsky. 1967. Fine structural localization of a blood-brain barrier to exogenous peroxidase. *The Journal of Cell Biology* 34 (1) (Jul): 207-17.

Regina, A., M. Demeule, A. Laplante, J. Jodoin, C. Dagenais, F. Berthelet, A. Moghrabi, and R. Beliveau. 2001. Multidrug resistance in brain tumors: Roles of the blood-brain barrier. *Cancer Metastasis Reviews* 20 (1-2): 13-25.

Reichel, A. 2009. Addressing central nervous system (CNS) penetration in drug discovery: Basics and implications of the evolving new concept. *Chemistry & Biodiversity* 6 (11) (Nov): 2030-49.

Rice, A., M. L. Michaelis, G. Georg, Y. Liu, B. Turunen, and K. L. Audus. 2003. Overcoming the blood-brain barrier to taxane delivery for neurodegenerative diseases and brain tumors. *Journal of Molecular Neuroscience : MN* 20 (3): 339-43.

Rivera, R., and J. Chun. 2008. Biological effects of lysophospholipids. *Reviews of Physiology, Biochemistry and Pharmacology* 160 : 25-46.

Roberts, L. M., D. S. Black, C. Raman, K. Woodford, M. Zhou, J. E. Haggerty, A. T. Yan, S. E. Cwirla, and K. K. Grindstaff. 2008. Subcellular localization of transporters along the rat blood-brain barrier and blood-cerebral-spinal fluid barrier by in vivo biotinylation. *Neuroscience* 155 (2) (Aug 13): 423-38.

Robey, R. W., K. K. To, O. Polgar, M. Dohse, P. Fetsch, M. Dean, and S. E. Bates. 2009. ABCG2: A perspective. *Advanced Drug Delivery Reviews* 61 (1) (Jan 31): 3-13.

Robinson, P. J., and S. I. Rapoport. 1990. Model for drug uptake by brain tumors: Effects of osmotic treatment and of diffusion in brain. *Journal of Cerebral Blood Flow and Metabolism : Official Journal of the International Society of Cerebral Blood Flow and Metabolism* 10 (2) (Mar): 153-61.

Sadowska, G. B., S. N. Malaeb, and B. S. Stonestreet. 2010. Maternal glucocorticoid exposure alters tight junction protein expression in the brain of fetal sheep. *American Journal of Physiology.Heart and Circulatory Physiology* 298 (1) (Jan): H179-88.

Sakata, S., M. Fujiwara, K. Ohtsuka, H. Kamma, M. Nagane, A. Sakamoto, and Y. Fujioka. 2011. ATP-binding cassette transporters in primary central nervous system lymphoma: Decreased expression of MDR1 P-glycoprotein and breast cancer resistance protein in tumor capillary endothelial cells. *Oncology Reports* 25 (2) (Feb): 333-9.

Sampath, L., S. Kwon, S. Ke, W. Wang, R. Schiff, M. E. Mawad, and E. M. Sevick-Muraca. 2007. Dual-labeled trastuzumab-based imaging agent for the detection of human epidermal growth factor receptor 2 overexpression in breast cancer. *Journal of Nuclear Medicine : Official Publication, Society of Nuclear Medicine* 48 (9) (Sep): 1501-10.

Sarker, M. H., D. E. Hu, and P. A. Fraser. 2010. Regulation of cerebromicrovascular permeability by lysophosphatidic acid. *Microcirculation (New York, N.Y.: 1994)* 17 (1) (Jan): 39-46.

Sato, S., T. Kawase, S. Harada, H. Takayama, and S. Suga. 1998. Effect of hyperosmotic solutions on human brain tumour vasculature. *Acta Neurochirurgica* 140 (11): 1135,41; disc 1141-2.

Schinkel, A. H., E. Wagenaar, C. A. Mol, and L. van Deemter. 1996. P-glycoprotein in the blood-brain barrier of mice influences the brain penetration and pharmacological activity of many drugs. *The Journal of Clinical Investigation* 97 (11) (Jun 1): 2517-24.

Schuette, W. 2004. Treatment of brain metastases from lung cancer: Chemotherapy. *Lung Cancer (Amsterdam, Netherlands)* 45 Suppl 2 (Aug): S253-7.

Schulze, C., C. Smales, L. L. Rubin, and J. M. Staddon. 1997. Lysophosphatidic acid increases tight junction permeability in cultured brain endothelial cells. *Journal of Neurochemistry* 68 (3) (Mar): 991-1000.

Seelig, A., and E. Landwojtowicz. 2000. Structure-activity relationship of P-glycoprotein substrates and modifiers. *European Journal of Pharmaceutical Sciences : Official Journal of the European Federation for Pharmaceutical Sciences* 12 (1) (Nov): 31-40.

Seetharaman, S., M. A. Barrand, L. Maskell, and R. J. Scheper. 1998. Multidrug resistance-related transport proteins in isolated human brain microvessels and in cells cultured from these isolates. *Journal of Neurochemistry* 70 (3) (Mar): 1151-9.

Shaik, N., N. Giri, G. Pan, and W. F. Elmquist. 2007. P-glycoprotein-mediated active efflux of the anti-HIV1 nucleoside abacavir limits cellular accumulation and brain distribution. *Drug Metabolism and Disposition: The Biological Fate of Chemicals* 35 (11) (Nov): 2076-85.

Siegal, T., R. Rubinstein, F. Bokstein, A. Schwartz, A. Lossos, E. Shalom, R. Chisin, and J. M. Gomori. 2000. In vivo assessment of the window of barrier opening after osmotic blood-brain barrier disruption in humans. *Journal of Neurosurgery* 92 (4) (Apr): 599-605.

Siess, W. 2002. Athero- and thrombogenic actions of lysophosphatidic acid and sphingosine-1-phosphate. *Biochimica Et Biophysica Acta* 1582 (1-3) (May 23): 204-15.

Simpson, I. A., A. Carruthers, and S. J. Vannucci. 2007. Supply and demand in cerebral energy metabolism: The role of nutrient transporters. *Journal of Cerebral Blood Flow and Metabolism : Official Journal of the International Society of Cerebral Blood Flow and Metabolism* 27 (11) (Nov): 1766-91.

Steeg, P. S., and D. Theodorescu. 2008. Metastasis: A therapeutic target for cancer. *Nature Clinical Practice.Oncology* 5 (4) (Apr): 206-19.

Stern L. and Gautier R. 1921. Rapports entre le liquide cephalo-rachidien et la circulation sanguine. 17 : 138-92.

Stewart, D. J. 1994. A critique of the role of the blood-brain barrier in the chemotherapy of human brain tumors. *Journal of Neuro-Oncology* 20 (2): 121-39.

Stewart, P. A., K. Hayakawa, C. L. Farrell, and R. F. Del Maestro. 1987a. Quantitative study of microvessel ultrastructure in human peritumoral brain tissue. evidence for a blood-brain barrier defect. *Journal of Neurosurgery* 67 (5) (Nov): 697-705.

Stewart, P. A., and M. J. Wiley. 1981. Developing nervous tissue induces formation of blood-brain barrier characteristics in invading endothelial cells: A study using quail--chick transplantation chimeras. *Developmental Biology* 84 (1) (May): 183-92.

Suzuki, M., H. Suzuki, Y. Sugimoto, and Y. Sugiyama. 2003. ABCG2 transports sulfated conjugates of steroids and xenobiotics. *The Journal of Biological Chemistry* 278 (25) (Jun 20): 22644-9.

Syvanen, S., G. Luurtsema, C. F. Molthoff, A. D. Windhorst, M. C. Huisman, A. A. Lammertsma, R. A. Voskuyl, and E. C. de Lange. 2011. (R)-[11C]verapamil PET studies to assess changes in P-glycoprotein expression and functionality in rat blood-brain barrier after exposure to kainate-induced status epilepticus. *BMC Medical Imaging* 11 (Jan 3): 1.

Tabata, K., K. Baba, A. Shiraishi, M. Ito, and N. Fujita. 2007. The orphan GPCR GPR87 was deorphanized and shown to be a lysophosphatidic acid receptor. *Biochemical and Biophysical Research Communications* 363 (3) (Nov 23): 861-6.

Tai, L. M., P. S. Reddy, M. A. Lopez-Ramirez, H. A. Davies, D. K. Male, A. J. Loughlin, and I. A. Romero. 2009. Polarized P-glycoprotein expression by the immortalised human brain endothelial cell line, hCMEC/D3, restricts apical-to-basolateral permeability to rhodamine 123. *Brain Research* 1292 (Oct 6): 14-24.

Taimur, S., and M. J. Edelman. 2003. Treatment options for brain metastases in patients with non-small-cell lung cancer. *Current Oncology Reports* 5 (4) (Jul): 342-6.

Takada, T., H. Suzuki, Y. Gotoh, and Y. Sugiyama. 2005. Regulation of the cell surface expression of human BCRP/ABCG2 by the phosphorylation state of akt in polarized cells. *Drug Metabolism and Disposition: The Biological Fate of Chemicals* 33 (7) (Jul): 905-9.

Talmadge, J. E., and I. J. Fidler. 1982. Enhanced metastatic potential of tumor cells harvested from spontaneous metastases of heterogeneous murine tumors. *Journal of the National Cancer Institute* 69 (4) (Oct): 975-80.

Tamai, I., and A. Tsuji. 2000. Transporter-mediated permeation of drugs across the blood-brain barrier. *Journal of Pharmaceutical Sciences* 89 (11) (Nov): 1371-88.

Tanaka, E., H. S. Choi, H. Fujii, M. G. Bawendi, and J. V. Frangioni. 2006. Image-guided oncologic surgery using invisible light: Completed pre-clinical development for sentinel lymph node mapping. *Annals of Surgical Oncology* 13 (12) (Dec): 1671-81.

Tatsuta, T., M. Naito, T. Oh-hara, I. Sugawara, and T. Tsuruo. 1992. Functional involvement of P-glycoprotein in blood-brain barrier. *The Journal of Biological Chemistry* 267 (28) (Oct 5): 20383-91.

Tfayli, A., P. Hentschel, S. Madajewicz, J. Manzione, N. Chowhan, R. Davis, P. Roche, et al. 1999. Toxicities related to intraarterial infusion of cisplatin and etoposide in patients with brain tumors. *Journal of Neuro-Oncology* 42 (1) (Mar): 73-7.

Thompson, E. M., E. P. Frenkel, and E. A. Neuwelt. 2011. The paradoxical effect of bevacizumab in the therapy of malignant gliomas. *Neurology* 76 (1) (Jan 4): 87-93.

Tigyi, G., L. Hong, M. Yakubu, H. Parfenova, M. Shibata, and C. W. Leffler. 1995. Lysophosphatidic acid alters cerebrovascular reactivity in piglets. *The American Journal of Physiology* 268 (5 Pt 2) (May): H2048-55.

Timpl, R. 1989. Structure and biological activity of basement membrane proteins. *European Journal of Biochemistry / FEBS* 180 (3) (Apr 1): 487-502.

Tomsig, J. L., A. H. Snyder, E. V. Berdyshev, A. Skobeleva, C. Mataya, V. Natarajan, D. N. Brindley, and K. R. Lynch. 2009. Lipid phosphate phosphohydrolase type 1 (LPP1) degrades extracellular lysophosphatidic acid in vivo. *The Biochemical Journal* 419 (3) (May 1): 611-8.

Trickler, W. J., W. G. Mayhan, and D. W. Miller. 2005. Brain microvessel endothelial cell responses to tumor necrosis factor-alpha involve a nuclear factor kappa B (NF-kappaB) signal transduction pathway. *Brain Research* 1048 (1-2) (Jun 28): 24-31.

Triguero, D., J. Buciak, and W. M. Pardridge. 1990. Capillary depletion method for quantification of blood-brain barrier transport of circulating peptides and plasma proteins. *Journal of Neurochemistry* 54 (6) (Jun): 1882-8.

Ueda, K., Y. Taguchi, and M. Morishima. 1997. How does P-glycoprotein recognize its substrates? *Seminars in Cancer Biology* 8 (3) (Jun): 151-9.

Ueno, M. 2007. Molecular anatomy of the brain endothelial barrier: An overview of the distributional features. *Current Medicinal Chemistry* 14 (11): 1199-206.

Urbatsch, I. L., M. K. al-Shawi, and A. E. Senior. 1994. Characterization of the ATPase activity of purified chinese hamster P-glycoprotein. *Biochemistry* 33 (23) (Jun 14): 7069-76.

Urquhart, B. L., and R. B. Kim. 2009. Blood-brain barrier transporters and response to CNS-active drugs. *European Journal of Clinical Pharmacology* 65 (11) (Nov): 1063-70.

van Corven, E. J., A. Groenink, K. Jalink, T. Eichholtz, and W. H. Moolenaar. 1989. Lysophosphatidate-induced cell proliferation: Identification and dissection of signaling pathways mediated by G proteins. *Cell* 59 (1) (Oct 6): 45-54.

van Nieuw Amerongen, G. P., and V. W. van Hinsbergh. 2002. Targets for pharmacological intervention of endothelial hyperpermeability and barrier function. *Vascular Pharmacology* 39 (4-5) (Nov): 257-72.

van Nieuw Amerongen, G. P., M. A. Vermeer, and V. W. van Hinsbergh. 2000. Role of RhoA and rho kinase in lysophosphatidic acid-induced endothelial barrier dysfunction. *Arteriosclerosis, Thrombosis, and Vascular Biology* 20 (12) (Dec): E127-33.

Vannucci, S. J., F. Maher, and I. A. Simpson. 1997. Glucose transporter proteins in brain: Delivery of glucose to neurons and glia. *Glia* 21 (1) (Sep): 2-21.

Vannucci, S. J., and I. A. Simpson. 2003. Developmental switch in brain nutrient transporter expression in the rat. *American Journal of Physiology.Endocrinology and Metabolism* 285 (5) (Nov): E1127-34.

Vargo, M. 2011. Brain tumor rehabilitation. *American Journal of Physical Medicine & Rehabilitation / Association of Academic Physiatrists* 90 (5 Suppl 1) (May): S50-62.

Vemula, S., K. E. Roder, T. Yang, G. J. Bhat, T. J. Thekkumkara, and T. J. Abbruscato. 2009. A functional role for sodium-dependent glucose transport across the blood-brain barrier during oxygen glucose deprivation. *The Journal of Pharmacology and Experimental Therapeutics* 328 (2) (Feb): 487-95.

Viani, G. A., M. S. Castilho, J. V. Salvajoli, A. C. Pellizzon, P. E. Novaes, F. S. Guimaraes, M. A. Conte, and R. C. Fogaroli. 2007. Whole brain radiotherapy for brain metastases from breast cancer: Estimation of survival using two stratification systems. *BMC Cancer* 7 (Mar 26): 53.

Villar, S. R., A. Brandoni, N. Anzai, H. Endou, and A. M. Torres. 2005. Altered expression of rat renal cortical OAT1 and OAT3 in response to bilateral ureteral obstruction. *Kidney International* 68 (6) (Dec): 2704-13.

Virgintino, D., D. Robertson, M. Errede, V. Benagiano, F. Girolamo, E. Maiorano, L. Roncali, and M. Bertossi. 2002. Expression of P-glycoprotein in human cerebral cortex microvessels. *The Journal of Histochemistry and Cytochemistry : Official Journal of the Histochemistry Society* 50 (12) (Dec): 1671-6.

Vogel, H., and G. N. Fuller. 2003. Primitive neuroectodermal tumors, embryonal tumors, and other small cell and poorly differentiated malignant neoplasms of the central and peripheral nervous systems. *Annals of Diagnostic Pathology* 7 (6) (Dec): 387-98.

Vogelbaum, M. A., T. Masaryk, P. Mazzone, T. Mekhail, V. Fazio, S. McCartney, N. Marchi, A. Kanner, and D. Janigro. 2005. S100beta as a predictor of brain metastases: Brain versus cerebrovascular damage. *Cancer* 104 (4) (Aug 15): 817-24.

Vorbrodt, A. W., and D. H. Dobrogowska. 2003. Molecular anatomy of intercellular junctions in brain endothelial and epithelial barriers: Electron microscopist's view. *Brain Research.Brain Research Reviews* 42 (3) (Jun): 221-42.

Walbert, T., and M. R. Gilbert. 2009. The role of chemotherapy in the treatment of patients with brain metastases from solid tumors. *International Journal of Clinical Oncology / Japan Society of Clinical Oncology* 14 (4) (Aug): 299-306.

Wang, Q., H. Yang, D. W. Miller, and W. F. Elmquist. 1995. Effect of the p-glycoprotein inhibitor, cyclosporin A, on the distribution of rhodamine-123 to the brain: An in vivo microdialysis study in freely moving rats. *Biochemical and Biophysical Research Communications* 211 (3) (Jun 26): 719-26.

Wang, S. J., H. M. Hung, and R. O'Neill. 2011. Adaptive design clinical trials and trial logistics models in CNS drug development. *European Neuropsychopharmacology : The Journal of the European College of Neuropsychopharmacology* 21 (2) (Feb): 159-66.

Waniewski, R. A., and D. L. Martin. 2004. Astrocytes and synaptosomes transport and metabolize lactate and acetate differently. *Neurochemical Research* 29 (1) (Jan): 209-17.

Weiss, L. 1980. Metastasis: Differences between cancer cells in primary and secondary tumors. *Pathobiology Annual* 10 : 51-81.

Wijesuriya, H. C., J. Y. Bullock, R. L. Faull, S. B. Hladky, and M. A. Barrand. 2010. ABC efflux transporters in brain vasculature of alzheimer's subjects. *Brain Research* 1358 (Oct 28): 228-38.

Wilhelm, I., C. Fazakas, and I. A. Krizbai. 2011. In vitro models of the blood-brain barrier. *Acta Neurobiologiae Experimentalis* 71 (1): 113-28.

Williams, P. C., W. D. Henner, S. Roman-Goldstein, S. A. Dahlborg, R. E. Brummett, M. Tableman, B. W. Dana, and E. A. Neuwelt. 1995. Toxicity and efficacy of carboplatin and etoposide in conjunction with disruption of the blood-brain tumor barrier in the treatment of intracranial neoplasms. *Neurosurgery* 37 (1) (Jul): 17,27; discussion 27-8.

Wiranowska, M., A. A. Gonzalvo, S. Saporta, O. R. Gonzalez, and L. D. Prockop. 1992. Evaluation of blood-brain barrier permeability and the effect of interferon in mouse glioma model. *Journal of Neuro-Oncology* 14 (3) (Nov): 225-36.

Wojciak-Stothard, B., L. Y. Tsang, and S. G. Haworth. 2005. Rac and rho play opposing roles in the regulation of hypoxia/reoxygenation-induced permeability changes in pulmonary artery endothelial cells. *American Journal of Physiology.Lung Cellular and Molecular Physiology* 288 (4) (Apr): L749-60.

Wolburg, H., and W. Paulus. 2010. Choroid plexus: Biology and pathology. *Acta Neuropathologica* 119 (1) (Jan): 75-88.

Wolburg, H., K. Wolburg-Buchholz, J. Kraus, G. Rascher-Eggstein, S. Liebner, S. Hamm, F. Duffner, E. H. Grote, W. Risau, and B. Engelhardt. 2003. Localization of claudin-3 in tight junctions of the blood-brain barrier is selectively lost during experimental autoimmune encephalomyelitis and human glioblastoma multiforme. *Acta Neuropathologica* 105 (6) (Jun): 586-92.

Wolff, J. E., T. Trilling, G. Molenkamp, R. M. Egeler, and H. Jurgens. 1999. Chemosensitivity of glioma cells in vitro: A meta analysis. *Journal of Cancer Research and Clinical Oncology* 125 (8-9) (Aug-Sep): 481-6.

Wong, E. T., and A. Berkenblit. 2004. The role of topotecan in the treatment of brain metastases. *The Oncologist* 9 (1): 68-79.

Yanagida, K., S. Ishii, F. Hamano, K. Noguchi, and T. Shimizu. 2007. LPA4/p2y9/GPR23 mediates rho-dependent morphological changes in a rat neuronal cell line. *The Journal of Biological Chemistry* 282 (8) (Feb 23): 5814-24.

Yumoto, R., T. Murakami, Y. Nakamoto, R. Hasegawa, J. Nagai, and M. Takano. 1999. Transport of rhodamine 123, a P-glycoprotein substrate, across rat intestine and caco-2 cell monolayers in the presence of cytochrome P-450 3A-related compounds. *The Journal of Pharmacology and Experimental Therapeutics* 289 (1) (Apr): 149-55.

Zhang, R. D., J. E. Price, T. Fujimaki, C. D. Bucana, and I. J. Fidler. 1992. Differential permeability of the blood-brain barrier in experimental brain metastases produced by human neoplasms implanted into nude mice. *The American Journal of Pathology* 141 (5) (Nov): 1115-24.

Zhang, Y., C. Bachmeier, and D. W. Miller. 2003. In vitro and in vivo models for assessing drug efflux transporter activity. *Advanced Drug Delivery Reviews* 55 (1) (Jan 21): 31-51.

Zhang, Y., J. D. Schuetz, W. F. Elmquist, and D. W. Miller. 2004. Plasma membrane localization of multidrug resistance-associated protein homologs in brain capillary endothelial cells. *The Journal of Pharmacology and Experimental Therapeutics* 311 (2) (Nov): 449-55.

Zhao, Y., and V. Natarajan. 2009. Lysophosphatidic acid signaling in airway epithelium: Role in airway inflammation and remodeling. *Cellular Signalling* 21 (3) (Mar): 367-77.

Zidan, A. S., C. Spinks, J. Fortunak, M. Habib, and M. A. Khan. 2010. Near-infrared investigations of novel anti-HIV tenofovir liposomes. *The AAPS Journal* 12 (2) (Jun): 202-14.